

AD-762 935

LOW-POWER TURBOPROPULSION COMBUSTOR
EXHAUST EMISSIONS. VOLUME I. THEORETI-
CAL FORMULATION AND DESIGN ASSESSMENT

Stanley A. Mosier, et al

Pratt and Whitney Aircraft

Prepared for:

Air Force Aero Propulsion Laboratory

June 1973

DISTRIBUTED BY:

NTIS

National Technical Information Service
U. S. DEPARTMENT OF COMMERCE
5285 Port Royal Road, Springfield Va. 22151

**Best
Available
Copy**

AD 762935

LOW-POWER TURBOPROPULSION COMBUSTOR EXHAUST EMISSIONS

VOLUME I. THEORETICAL FORMULATION AND DESIGN ASSESSMENT

Stanley A. Mosier
Richard Roberts

Pratt & Whitney Aircraft
Division of United Aircraft Corporation

Technical Report AFAPL-TR-73-36, Volume I

June 1973

Approved for Public Release; Distribution Unlimited

Air Force Aero Propulsion Laboratory
Air Force System Command
Wright-Patterson Air Force Base, Ohio

Reproduced by
NATIONAL TECHNICAL
INFORMATION SERVICE
U S Department of Commerce
Springfield VA 22151

NOTICE

A

When Government drawings, specifications, or other data are used for any purpose other than in connection with a definitely related Government procurement operation, the United States Government thereby incurs no responsibility nor any obligation whatsoever; and the fact that the Government may have formulated, furnished, or in any way supplied the said drawings, specifications, or other data, is not to be regarded by implication or otherwise as in any manner licensing the holder or any other person or corporation, or conveying any rights or permission to manufacture, use, or sell any patented invention that may in any way be related thereto.

Copies of this report should not be returned unless return is required by security considerations, contractual obligations, or notice on a specific document.

UNCLASSIFIED

Security Classification

DOCUMENT CONTROL DATA - R & D

(Security classification of title, body of abstract and indexing annotation must be entered when the overall report is classified)

1. ORIGINATING ACTIVITY (Corporate author) Pratt & Whitney Aircraft Division of United Aircraft Corporation West Palm Beach, Florida 33402		2a. REPORT SECURITY CLASSIFICATION Unclassified	
		2b. GROUP	
3. REPORT TITLE Low-Power Turbopropulsion Combustor Exhaust Emissions			
4. DESCRIPTIVE NOTES (Type of report and inclusive dates) Technical Report Vol. 1 30 June 1971 through 30 November 1972			
5. AUTHOR(S) (First name, middle initial, last name) Stanley A. Mosier Richard Roberts			
6. REPORT DATE June 1973		7a. TOTAL NO. OF PAGES 330	7b. NO. OF REFS 31
8a. CONTRACT OR GRANT NO. F33615-71-C-1870		9a. ORIGINATOR'S REPORT NUMBER(S) FR-5415	
b. PROJECT NO. 3066			
c. Task No. 306605		9b. OTHER REPORT NO(S) (Any other numbers that may be assigned this report) AFAPL-TR-73-36 Vol. I	
d.			
10. DISTRIBUTION STATEMENT Approved for public release; distribution unlimited			
11. SUPPLEMENTARY NOTES This report is Volume I of the final report for Contract No. F33615-71-C-1870		12. SPONSORING MILITARY ACTIVITY Air Force Aero Propulsion Laboratory Air Force Systems Command Wright-Patterson AFB, Ohio	
13. ABSTRACT An exploratory development program was undertaken to formulate and develop a computerized, theoretical model to predict emissions characteristics of gas turbine engine combustors. In support of the model development, a number of experimental studies were conducted to provide information for structuring the formulation and for guiding its refinement. Direct support was provided by three laboratory test programs and a burner survey test program. The laboratory programs were incorporated to provide data, unavailable in the combustion literature, on reaction rates under realistic burner operating conditions. The survey program was incorporated to provide baseline emissions characteristics for a number of existing gas turbine engine burners against which the generality of the model could be assessed. Indirect support of the model was provided by a comprehensive test program in which component design techniques for reducing low-power emissions by controlling the primary-zone equivalence ratio were evaluated using a research combustor. Control means included air-staging, fuel-staging, and premixing of fuel and air prior to their being introduced into the combustor. Low values of UHC concentrations were obtained when air staging was used; CO concentrations, however, remained relatively high. When fuel staging was used both UHC and CO concentrations remained high. However, very low concentrations of UHC and CO were achieved when fuel and air were premixed prior to their being injected into the combustor.			

DD FORM 1473
1 NOV 65UNCLASSIFIED
Security Classification

14 KEY WORDS	LINK A		LINK B		LINK C	
	ROLE	WT	ROLE	WT	ROLE	WT
Low-Power Emissions Combustor Emissions Exhaust Emissions Air Pollution Analytical Model Computer Model Reaction Kinetics Turbulent Flame Studies Premixing Combustor Aerothermodynamic Model Emission Reduction Techniques Pollution Measurement Techniques Hydrocarbon Combustion Studies Gas Turbine Engine Combustion Air Staging Combustor Fuel Staging Combustor						

i-a

FOREWORD

This report was prepared by the Pratt & Whitney Aircraft Division of United Aircraft Corporation under Contract F33615-71-C-1870, "Low-Power Turbopropulsion Combustor Exhaust Emissions." It is Volume I of the final report, which encompasses work associated with the accomplishment of Phases I and II of the subject contract from 30 June 1971 through 30 November 1972. The originator's report number is FR-5415.


The Pratt & Whitney Aircraft Program Manager is Mr. Stanley A. Mosier of the Florida Research and Development Center, West Palm Beach, Florida 33402; the Deputy Program Manager is Dr. Richard Roberts of the Connecticut Operations, East Hartford, Connecticut 06108.

Contract F33615-71-C-1870 is being sponsored by the Air Force Aero Propulsion Laboratory, Air Force Systems Command, United States Air Force, Wright-Patterson Air Force Base, Ohio, under Project 306605. The Air Force Project Engineer is Lt. Dennis E. Walsh.

This report was submitted by the authors in March 1973.

The program managers wish to acknowledge the valuable contributions made to this exploratory development program by personnel from the Air Force Aero Propulsion Laboratory and from Pratt & Whitney Aircraft's Experimental Engineering Department. They wish to acknowledge specifically the following: Mr. R. E. Henderson, AFAPL/TBC for his direction and suggestions on all phases of the program; Mr. R. J. Mador of the Combustion T&R Group for his efforts in the programming and development of the analytical combustor model; Dr. R. Kollrack and Mr. L. D. Aceto of the Scientific Analysis Group for their development of the hydrocarbon chemical kinetics mechanism; Mr. E. D. Taback and Dr. A. Vranos of the Combustion T&R Group for the conduct of the Laboratory Test Programs; Mr. R. M. Pierce of the Applied Research Combustion Group for his conceiving and developing analytical tools and concepts used in accomplishing the design assessment effort; Mr. P. W. Smith and Dr. W. R. Kaminski, formerly of the Applied Research Combustion Group, for their execution of the design, fabrication, and experimental portions of the assessment effort; Mr. W. J. B. Purvis of the Applied Research Combustion Group for his development and operation of the on-line emission analysis system; and to Messrs. E. R. Robertson of the Applied Research Combustion Group and R. Taber of the Instrumentation Laboratory for their support of the engineering operations.

Publication of this report does not constitute Air Force approval of the report's findings or conclusions. It is published only for the exchange and stimulation of ideas.


Ernest C. Simpson
Director, Turbine Engine Division
Air Force Aero Propulsion Laboratory

ABSTRACT

An exploratory development program was undertaken to formulate and develop a computerized, theoretical model to predict emissions characteristics of gas turbine engine combustors. In support of the model development, a number of experimental studies were conducted to provide information for structuring the formulation and for guiding its refinement. Direct support was provided by three laboratory test programs and a burner survey test program. The laboratory programs were incorporated to provide data, unavailable in the combustion literature, on reaction rates under realistic burner operating conditions. The survey program was incorporated to provide baseline emissions characteristics for a number of existing gas turbine engine burners against which the generality of the model could be assessed. Indirect support of the model was provided by a comprehensive test program in which component design techniques for reducing low-power emissions by controlling the primary-zone equivalence ratio were evaluated using a research combustor. Control means included air-staging, fuel-staging, and premixing of fuel and air prior to their being introduced into the combustor. Low values of unburned hydrocarbon (UHC) concentrations were obtained when air staging was used; carbon monoxide (CO) concentrations, however, remained relatively high. When fuel staging was used both UHC and CO concentrations remained high. However, very low concentrations of UHC and CO were achieved when fuel and air were premixed prior to their being injected into the combustor.

CONTENTS

SECTION		PAGE
	ILLUSTRATIONS	vii
	TABLES	xix
	SYMBOLS	xx
I	GENERAL SUMMARY	1
II	INTRODUCTION AND PROBLEM DEFINITION	3
III	PHASE I - THEORETICAL FORMULATION	5
	A. Summary	5
	1. Streamtube Combustor Model Development	5
	2. Low-Power Emissions Research Studies	5
	3. Presentation of Predicted Results	6
	B. Preliminary Combustor Model	6
	1. General	6
	2. Description	6
	3. Phase II Predictions	10
	C. Streamtube Combustor Model	14
	1. Conceptual Approach	14
	2. Description of the Combustor Model	15
	3. Application of the Streamtube Model	27
	4. Computational Procedures	27
	D. Survey Testing	29
	1. General	29
	2. Discussion	32
	E. Laboratory Test Program	32
	1. General	32
	2. JT8D Burner Probing Studies	33
	3. Turbulent Flame Studies	44
	4. Low-Temperature Hydrocarbon Kinetics Studies	60
IV	PHASE II - DESIGN ASSESSMENT	70
	A. Summary	70
	B. Discussion	71
	1. Objective and Approach	71
	2. Constraints and Qualifications	72
	3. Experimental Combustors	74
	4. Test Rig and Stand	80
	5. Traverse and Sample-Gas Transfer Systems	80

CONTENTS (Continued)

SECTION	PAGE
IV B	
6. Exhaust Gas Analysis System	87
7. Concept Evaluation	93
8. Test Classification	95
9. Combustor A Test Program	95
10. Combustor B Test Program	137
V	
COMPARISON OF PREDICTED AND MEASURED EMISSION CONCENTRATIONS	175
A. General	175
B. JT8D Probing Studies	175
C. Phase II - Combustor A	182
D. Phase II - Combustor B	182
E. Parametric Study	187
F. Discussion of the Model Predictions	188
VI	
NOMENCLATURE FOR TEST DATA SUMMARY	194
APPENDIX I - JT8D Combustor Concentration and Fuel-Air Ratio Profiles	195
APPENDIX II - Combustion Efficiency and Tem- perature Profiles	207
APPENDIX III - Procedure for Calculating Re- action Rates for Fuel and CO	215
APPENDIX IV - FA, X ₁ , and pH Test Data	219
APPENDIX V - Test Data Flowpath	225
APPENDIX VI - Controlled and Measured Test Data	242
APPENDIX VII - Sample - Gas Transfer Line Tem- perature Data	248
APPENDIX VIII - Measured Test Data	255
APPENDIX IX - UHC Emission Concentration Data	261
APPENDIX X - CO Emission Concentration Data	267
APPENDIX XI - Nitrogen Oxide Emission Con- centration Data	273
APPENDIX XII - CO ₂ Emission Concentration Data	280
APPENDIX XIII - H ₂ O Emission Concentration Data	295
APPENDIX XIV - Performance Parameters	301
REFERENCES	307

ILLUSTRATIONS

FIGURE		PAGE
1	Schematic Diagram of Aerodynamic Model	7
2	Comparison of Measured and Predicted UHC Concentration with Fuel-Air Ratio.	11
3	Comparison of Measured and Predicted CO Concentration with Fuel-Air Ratio.	12
4	Comparison of Measured and Predicted NO _x Concentration with Fuel-Air Ratio.	13
5	Primary-Zone Flow Pattern Observed in Can-Type Combustor (Reference 2).	15
6	Schematic Diagram of Internal Flowfield Streamtube Model for Can-Type Combustor	16
7	Transverse - Jet Penetration Model	20
8	Variation in Species Concentration with Time (Stoichiometric Equivalence Ratio, P = 2 atm, T _{in} = 100°K)	24
9	Flow Chart for Low-Power Emissions Computer Program	28
10	Analysis of a Bluff-Body-Stabilized Can Burner at Idle	30
11	Cold-Flow Analysis of a Bluff-Body-Stabilized Can Burner	31
12	Schematic Diagram of JT8D Burner Probing Rig	34
13	Sampling Probe Locations	35
14	JT8D Sampling Probes	36
15	JT8D Sampling Probe and Traverse Mechanism	36
16	JT8D Burner Probing Sampling Train	37
17	(Upper) View of Gas-Sampling Probe Before Testing; (Lower) View of Gas-Sampling Probe Tip Showing Plugging.	39
18	Variation in Local CO Concentration with Local FA at Simulated Idle Operating Conditions	40
19	Variation in Local CO Concentration with Local FA at Simulated Approach Operating Conditions.	41
20	Schematic Diagram of Turbulent Flame Study Rig	45
21	Test Section for Turbulent Flame Studies	46
22	Test Rig for Turbulent Flame Studies	47
23	Sampling Probe for the Turbulent Flame Study Test Rig.	48

ILLUSTRATIONS (Continued)

FIGURE		PAGE
24	Variation in Combustion Product Concentration with Lateral Position 3 in. Downstream of Flameholder ($\phi = 1.0$, $T = 245^\circ\text{F}$)	50
25	Variation in Combustion Product Concentrations with Lateral Position 5 in. Downstream of Flameholder ($\phi = 1.0$, $T = 240^\circ\text{F}$)	51
26	Variation in Combustion Product Concentrations with Lateral Position 5 in. Downstream of Flameholder ($\phi = 1.2$, $T = 243^\circ\text{F}$)	52
27	Variation in Combustion Product Concentration with Lateral Position 5 in. Downstream of Flameholder ($\phi = 1.2$, $T = 665^\circ\text{F}$)	53
28	Variation in CO Concentration with Axial Distance from Flameholder and Temperature Along Rig Centerline (Equivalence Ratio = 1.2)	54
29	Variation in CO Concentration with Axial Distance from Flameholder and Equivalence Ratio Along Rig Centerline ($T = 240^\circ\text{F}$)	54
30	Variation in UHC Concentration with Axial Distance from Flameholder and Temperature Along Rig Centerline (Equivalence Ratio = 1.2)	55
31	Variation in UHC Concentration with Axial Distance from Flameholder and Equivalence Ratio Along Rig Centerline ($T = 240^\circ\text{F}$)	55
32	Variation in Fuel Reaction Rate with Axial Distance, Temperature, and Equivalence Ratio	56
33	Variation in CO Reaction Rate with Axial Distance, Temperature, and Equivalence Ratio	56
34	Variation in Correlating Parameter with Time and Test Conditions	59
35	Comparison of the Variation in Actual and Measured Reaction Rates.	60
36	Schematic Diagram of Hydrocarbon Kinetics Rig	61
37	Hydrocarbon Kinetics Rig	62
38	Test Section Installation for the Adiabatic Reactor	63
39	Burn-Off Area	64
40	Sampling and Temperature Measurement Probe for Adiabatic Reactor Rig	65

ILLUSTRATIONS (Continued)

FIGURE		PAGE
41	Variation in CO Concentration with Temperature (15.3% O ₂ , $\phi = 4.9$, Residence Time = 75 msec)	66
42	Variation in CO Concentration with Axial Location and Test Conditions	67
43	Comparison of Calculated and Actual Reaction Rates for CO	69
44	Combustor A Prior to Installation in Rig Case.	75
45	Research Combustor Arrangement	76
46	Combustor A Modified for Scheme 4-1A Arrangement	77
47	Schematic Diagram of Combustor B	78
48	Carburetion Tube Assembly	78
49	Carburetion Tube Assembly Prior to Test	79
50	Schematic Diagram of Test Stand and Rig	81
51	Schematic Diagram of Traverse Probe Configuration	82
52	Traverse Probe System During Assembly	83
53	Sample Gas Inlet Ports on Rake Arm	83
54	Schematic Diagram of Original Sample - Gas Transfer System	84
55	Schematic Diagram of Modified Gas - Transfer System	86
56	Combustor Gas Sample Transfer System Arrangement	87
57	Variation in Sample Gas Temperature with Length for Original System	88
58	Variation in Sample Gas Temperature with Length for Modified System	89
59	Schematic Diagram of Instrumentation Measure- ment System	89
60	Instrumentation Measurement System	90
61	Typical Vendor Certification for NO Calibration Gas	91
62	Typical Vendor Certification for NO ₂ Calibration Gas.	92
63	Research Combustor Nomenclature	93
64	Summary Sheet for Combustor A Schemes 1-1A and 1-1B.	97

ILLUSTRATIONS (Continued)

FIGURE		PAGE
65	Variation in Fuel Flowrate and FA with Pressure Drop	98
66	Variation in Combustion Efficiency with Fuel-Air Ratio for Tests with Combustor Schemes 1-1A and 1-1B.	100
67	Variation in UHC Concentration with Fuel-Air Ratio for Tests with Combustor Schemes 1-1A and 1-1B.	100
68	Variation in CO Concentration with Fuel-Air Ratio for Tests with Combustor Schemes 1-1A and 1-1B.	101
69	Variation in NO Concentration with Fuel-Air Ratio for Tests with Combustor Schemes 1-1A and 1-1B.	102
70	Variation in NO ₂ Concentration with Fuel-Air Ratio for Tests with Combustor Schemes 1-1A and 1-1B.	103
71	Variation in NO _x Concentration with Fuel-Air Ratio for Test with Combustor Schemes 1-1A and 1-1B.	103
72	Summary Sheet for Combustor A Scheme 2-1A	105
73	Summary Sheet for Combustor A Scheme 3-1A	105
74	Summary Sheet for Combustor A Scheme 4-1A	106
75	Comparison of Variations in Combustion Efficiency with Fuel-Air Ratio for Tests Conducted with Combustor Schemes 1-1B, 2-1A, 3-1A, and 4-1A	107
76	Comparison of Variations in UHC Concentration with Fuel-Air Ratio for Tests Conducted with Combustor Schemes 1-1B, 2-1A, 3-1A, and 4-1A	108
77	Comparison of Variations in CO Concentration with Fuel-Air Ratio for Tests Conducted with Combustor Schemes 1-1B, 2-1A, 3-1A, and 4-1A	109
78	Comparison of Variations in NO Concentration with Fuel-Air Ratio for Tests Conducted with Combustor Schemes 1-1B, 2-1A, 3-1A, and 4-1A	110
79	Comparison of Variations in NO ₂ Concentration with Fuel-Air Ratio for Tests Conducted with Combustor Schemes 1-1B, 2-1A, 3-1A, and 4-1A	110

ILLUSTRATIONS (Continued)

FIGURE		PAGE
80	Comparison of Variations in NO _x Concentration with Fuel-Air Ratio for Tests Conducted with Combustor Schemes 1-1B, 2-1A, 3-1A, and 4-1A	111
81	Variation in UHC Concentration with PSAR and FA for Tests with Combustor Schemes 1-1B, 2-1A, 3-1A, and 4-1A	111
92	Variation in CO Concentration with PSAR and FA for Tests with Combustor Schemes 1-1B, 2-1A, 3-1A, and 4-1A	112
83	Variation in NO _x Concentration with PSAR and FA for Tests with Combustor Schemes 1-1B, 2-1A, 3-1A, and 4-1A	112
84	Variation in Sauter Mean Diameter with Air Differential Pressure and Fuel Flow	114
85	Comparison of Variations in UHC Concentration with FA and PHIP for Tests Conducted with Combustor Schemes 4-1A and 1-1B.	115
86	Comparison of Variations in CO Concentration with FA and PHIP for Tests Conducted with Combustor Schemes 4-1A and 1-1B.	116
87	Comparison of Variations in NO _x Concentration with FA and PHIP for Tests Conducted with Combustor Schemes 4-1A and 1-1B.	117
88	Comparison of Variations in Combustion Efficiency with FA and PHIP for Tests Conducted with Combustor Schemes 4-1A and 1-1B.	118
89	Comparison of Variations in UHC Concentration with FA and PHIP for Tests Conducted with Combustor Schemes 4-1A and 2-1B.	119
90	Comparison of Variations in CO Concentration with FA and PHIP for Tests Conducted with Combustor Schemes 4-1A and 2-1B.	119
91	Comparison of Variations in NO _x Concentration with FA and PHIP for Tests Conducted with Combustor Schemes 4-1A and 2-1B.	120
92	Comparison of Variations in Combustion Efficiency with FA and PHIP for Tests Conducted with Combustor Schemes 4-1A and 2-1B.	120
93	Variation in UHC Concentration with Reference Velocity and Inlet Temperature for Tests Conducted with Combustor Scheme 1-1B	123

ILLUSTRATIONS (Continued)

FIGURE		PAGE
94	Variation in CO Concentration with Reference Velocity and Inlet Temperature for Tests Conducted with Combustor Scheme 1-1B.	123
95	Variation in NO _x Concentration with Reference Velocity and Inlet Temperature for Tests Conducted with Combustor Scheme 1-1B.	124
96	Comparison of Variations in UHC Concentration with Fuel-Air Ratio for Tests Conducted with Combustor Schemes 2-3A and 2-1A.	126
97	Comparison of Variations in CO Concentration with Fuel-Air Ratio for Tests Conducted with Combustor Schemes 2-3A and 2-1A.	127
98	Comparison of Variations in Combustion Efficiency with Fuel-Air Ratio for Tests Conducted with Combustor Schemes 2-3A and 2-1A.	127
99	Comparison of Variations in NO _x Concentration with Fuel-Air Ratio for Tests Conducted with Combustor Schemes 2-3A and 2-1A.	129
100	Variation in UHC Concentration with Fuel-Air Ratio for the Circumferential Fuel-Staging Tests Conducted with Combustor Scheme 1-1B.	130
101	Variation in UHC Concentration with Circumferential Location for the Circumferential Fuel-Staging Tests Conducted with Combustor Scheme 1-1B at a Nominal Fuel-Air Ratio of 0.008 (Fuel Nozzle Status and Location Shown).	131
102	Variation in CO Concentration with Fuel-Air Ratio for the Circumferential Fuel-Staging Tests Conducted with Combustor Scheme 1-1B.	131
103	Variation in CO Concentration with Circumferential Location for the Circumferential Fuel-Staging Tests Conducted with Combustor Scheme 1-1B at a Nominal Fuel-Air Ratio of 0.008 (Fuel Nozzle Status and Location Shown).	133
104	Variation in NO _x Concentration with Fuel Air Ratio for the Circumferential Fuel-Staging Tests Conducted with Combustor Scheme 1-1B.	133
105	Comparison of Variations in UHC Concentration with Fuel-Air Ratio for Tests Conducted with Combustor Schemes 2-2A and 2-1A.	135
106	Comparison of Variations in CO Concentration with Fuel-Air Ratio for Tests Conducted with Combustor Schemes 2-2A and 2-1A.	135

ILLUSTRATIONS (Continued)

FIGURE		PAGE
107	Comparison of Variations in NO _x Concentration with Fuel-Air Ratio for Tests Conducted with Combustor Schemes 2-2A and 2-1A.	136
108	Comparison of Variations in Combustion Efficiency with Fuel-Air Ratio for Tests Conducted with Combustor Schemes 2-2A and 2-1A.	137
109	Summary Sheet for Combustor B Scheme 5-1B	140
110	Comparison of Variations in UHC Concentration with Fuel-Air Ratio for Tests Conducted with Combustor Schemes 5-1B and 4-1A.	141
111	Comparison of Variations in CO Concentration with Fuel-Air Ratio for Tests Conducted with Combustor Schemes 5-1B and 4-1A.	142
112	Comparison of Variations in NO _x Concentration with Fuel-Air Ratio for Tests Conducted with Combustor Schemes 5-1B and 4-1A.	142
113	Comparison of Variations in Combustion Efficiency with Fuel-Air Ratio for Tests Conducted with Combustor Schemes 5-1B and 4-1A.	143
114	Combustor Scheme 6-1A	144
115	Summary Sheet for Combustor B Scheme 5-1A	145
116	Comparison of Variations in UHC Concentration with Fuel-Air Ratio for Tests Conducted with Combustor Schemes 5-1A and 5-1B.	146
117	Comparison of Variations in CO Concentration with Fuel-Air Ratio for Tests Conducted with Combustor Schemes 5-1A and 5-1B.	147
118	Comparison of Variations in NO _x Concentration with Fuel-Air Ratio for Tests Conducted with Combustor Schemes 5-1A and 5-1B.	148
119	Comparison of Variations in Combustion Efficiency with Fuel-Air Ratio for Tests Conducted with Combustor Schemes 5-1A and 5-1B.	149
120	Summary Sheet for Combustor B Scheme 5-2A	149
121	Summary Sheet for Combustor B Scheme 5-3A	150
122	Summary Sheet for Combustor B Scheme 5-4A	150
123	Comparison of Variations in UHC Concentration with Fuel-Air Ratio for Tests Conducted with Combustor Schemes 5-1A, 5-2A, 5-3A, and 5-4A.	151

ILLUSTRATIONS (Continued)

FIGURE		PAGE
124	Comparison of Variations in CO Concentration with Fuel-Air Ratio for Tests Conducted with Combustor Schemes 5-1A, 5-2A, 5-3A, and 5-4A	152
125	Comparison of Variations in NO _x Concentration with Fuel-Air Ratio for Tests Conducted with Combustor Schemes 5-1A, 5-2A, 5-3A, and 5-4A	153
126	Summary Sheet for Combustor B Scheme 5-5A	156
127	Summary Sheet for Combustor B Scheme 5-7A	156
128	Variation in UHC Concentration with Fuel-Air Ratio for Tests Conducted with Combustor Schemes 5-5A and 5-7A.	157
129	Variation in CO Concentration with Fuel-Air Ratio for Tests Conducted with Combustor Schemes 5-3A, 5-5A, and 5-7A	158
130	Variation in NO _x Concentration with Fuel-Air Ratio for Tests Conducted with Combustor Scheme 5-5A	159
131	Variation in Combustion Efficiency with Fuel-Air Ratio for Tests Conducted with Combustor Schemes 5-5A and 5-7A.	159
132	Variation in UHC Concentration with Fuel-Air Ratio for the Circumferential Fuel-Staging Tests Conducted with Combustor Scheme 5-7A	162
133	Variation in UHC Concentration with Circumferential Location for the Circumferential Fuel-Staging Tests Conducted with Combustor Scheme 5-7A at a Nominal Fuel-Air Ratio of 0.008 (Fuel Nozzle Status and Location Shown).	162
134	Variation in CO Concentration with Fuel-Air Ratio for the Circumferential Fuel-Staging Tests Conducted with Combustor Scheme 5-7A	163
135	Variation in CO Concentration with Circumferential Location for the Circumferential Fuel-Staging Tests Conducted with Combustor Scheme 5-7A at a Nominal Fuel-Air Ratio of 0.008 (Fuel Nozzle Status and Location Shown).	163
136	Variation in Combustion Efficiency with Fuel-Air Ratio for the Circumferential Fuel-Staging Tests Conducted with Combustor Scheme 5-7A.	164
137	Summary Sheet for Combustor B Scheme 5-8A	165

ILLUSTRATIONS (Continued)

FIGURE		PAGE
138	Comparison of Variations in UHC Concentration with Fuel-Air Ratio for Tests Conducted with Combustor Schemes 5-8A and 1-1B.	166
139	Comparison of Variations in CO Concentration with Fuel-Air Ratio for Tests Conducted with Combustor Schemes 5-8A and 1-1B.	167
140	Comparison of Variations in NO _x Concentration with Fuel-Air Ratio for Tests Conducted with Combustor Schemes 5-8A and 1-1B.	167
141	Comparison of Variations in Combustion Efficiency with Fuel-Air Ratio for Tests Conducted with Combustor Schemes 5-8A and 1-1B.	168
142	Combustor Rig Case Showing Blockage.	170
143	Variation in UHC and CO Concentrations with Circumferential Location for Tests with Blockage	171
144	Variation in UHC and CO Concentrations with Circumferential Location for Tests with No Blockage	171
145	Comparison of Variations in UHC Concentration with Fuel-Air Ratio for Tests with Blockage and No Blockage.	172
146	Comparison of Variations in CO Concentration with Fuel-Air Ratio for Tests with Blockage and No Blockage.	172
147	Comparison of Variations in NO _x Concentration with Fuel-Air Ratio for Tests with Blockage and No Blockage.	173
148	Variation in pH with FA for Full-Traversal Tests of Combustors A and B	174
149	Variation in Predicted and Measured CO Concentrations within JT8D Burner (Idle Operation).	176
150	Variation in Predicted and Measured UHC Concentrations within JT8D Burner (Idle Operation)	177
151	Variation in Predicted and Measured FA within JT8D Burner (Idle Operation).	178
152	Variation in Predicted and Measured CO Concentrations within JT8D Burner (Approach Operation).	179
153	Variation in Predicted and Measured UHC Concentrations within JT8D Burner (Approach Operation).	180
154	Variation in Predicted and Measured FA within JT8D Burner (Approach Operation)	181

ILLUSTRATIONS (Continued)

FIGURE		PAGE
155	Comparison of Predicted and Measured Variations in CO Concentration with FA for Air-Staging Tests	183
156	Comparison of Predicted and Measured Variations in UHC Concentration with FA for Air-Staging Tests . . .	183
157	Comparison of Predicted and Measured Variations in CO Concentration with FA for Fuel-Staging Tests (Scheme 2-1A)	184
158	Comparison of Predicted and Measured Variations in UHC Concentration with FA for Fuel-Staging Tests (Scheme 2-1A, 4 gph Fuel Nozzles in Primary and Secondary)	184
159	Comparison of Predicted and Measured Variations in CO Concentration with FA Fuel-Staging Tests (Schemes 4-1A, 4 gph Fuel Nozzles in Primary and Secondary)	185
160	Comparison of Predicted and Measured Variations in UHC Concentration with FA for Fuel-Staging Tests (Scheme 4-1A, 4 gph Fuel Nozzles in Primary, Air Blast Nozzles in Secondary)	185
161	Comparison of Predicted and Measured Variations in CO Concentration with FA for Scheme 5-1A Tests . . .	186
162	Comparison of Predicted and Measured Variations in UHC Concentration with FA for Scheme 5-1A Tests . .	186
163	Comparison of Predicted and Measured Variations in CO Concentration with Inlet Air Temperature (Scheme 1-1B, FA = 0.0082, Reference Velocity = 100 fps)	189
164	Comparison of Predicted and Measured Variations in UHC Concentration with Inlet Air Temperature (Scheme 1-1B, FA = 0.0082, Reference Velocity = 100 fps)	189
165	Comparison of Predicted and Measured Variations in CO Concentration with Inlet Air Pressure (Scheme 1-1B, FA = 0.0082, Reference Velocity = 100 fps)	190
166	Comparison of Predicted and Measured Variations in UHC Concentration with Inlet Air Pressure (Scheme 1-1B, FA = 0.0082, Reference Velocity = 100 fps)	190
167	Comparison of Predicted and Measured Variations in CO Concentration with Reference Velocity (Scheme 1-1B, FA = 0.0082, Inlet Air Temp = 400°F)	191

ILLUSTRATIONS (Continued)

FIGURE		PAGE
168	Comparison of Predicted and Measured Variations in UHC Concentration with Reference Velocity (Scheme 1-1B, FA = 0.0082, Reference Velocity = 100 fps)	191
169	Comparison of Predicted and Measured Variations in CO Concentration with FA for Pressure-Atomizing and Air-Blast Fuel Nozzles	192
170	Comparison of Predicted and Measured UHC Concentration with FA for Pressure-Atomizing and Air-Blast Fuel Nozzles	192
171	Comparison of Predicted and Measured CO Concentration with FA for Tests Demonstrating the Effect of Dome Cooling	193
172	Comparison of Predicted and Measured UHC Concentration with FA for Tests Demonstrating the Effect of Dome Cooling	193
173	Variation in FA and Concentration of Combustion Products with Diametral Position (Position 1B, Idle Operation).	195
174	Variation in FA and Concentration of Combustion Products with Diametral Position (Position 2A, Idle Operation).	196
175	Variation in UHC Concentrations with Diametral Position (Position 2A, Idle Operation)	197
176	Variation in FA and Concentration of Combustion Products with Diametral Position (Position 2B, Idle Operation).	198
177	Variation in UHC Concentrations with Diametral Position (Position 2B, Idle Operation)	199
178	Variation in FA and Concentrations of Combustion Products with Diametral Position (Position 3A, Idle Operation).	200
179	Variation in UHC Concentrations with Diametral Position (Position 3A, Idle Operation)	201
180	Variation in FA and Concentrations of Combustion Products with Diametral Position (Position 3B, Idle Operation).	202
181	Variation in FA and Concentrations of Combustion Products with Spanwise Position (Exhaust Location, Idle Operation).	203

ILLUSTRATIONS (Continued)

FIGURE		PAGE
182	Variation in FA and Concentrations of Combustion Products with Diametral Position (Position 2B, Approach Operation)	204
183	Variation in FA and Concentrations of Combustion Products with Diametral Position (Position 3B, Approach Operation)	205
184	Variation in FA and Concentrations of Combustion Products with Spanwise Position (Exhaust Location, Approach Operation)	206
185	Variation in Combustion Efficiency and Temperature with Diametral Position (Probe Location 1B, Idle Operation)	207
186	Variation in Combustion Efficiency and Temperature with Diametral Position (Probe Location 2A, Idle Operation)	208
187	Variation in Combustion Efficiency and Temperature with Diametral Position (Probe Location 2B, Idle Operation)	209
188	Variation in Combustion Efficiency and Temperature with Diametral Position (Probe Location 3A, Idle Operation)	210
189	Variation in Combustion Efficiency and Temperature with Diametral Position (Probe Location 3B, Idle Operation)	211
190	Variation in Combustion Efficiency and Temperature with Diametral Position (Probe Location 2B, Approach Operation)	212
191	Variation in Combustion Efficiency and Temperature with Diametral Position (Probe Location 3B, Approach Operation)	213
192	Variation in Combustion Efficiency and Temperature with Position at the Combustor Exit (Idle and Approach Operations)	214
193	Schematic Diagram Showing Sampling Plane and Coordinate System for Turbulent Flame Rig	216
194	Test Data Flowpath.	226

TABLES

TABLE		PAGE
I	Preliminary Hydrocarbon Kinetics System	9
II	Reactions Constituting the Hydrocarbon Oxidation Kinetics System	22
III	Reduced Hydrocarbon Oxidation System	26
IV	Test Matrix for JT8D Probing Tests	38
V	Operating Conditions for Simulation of Engine Idle and Approach.	38
VI	Test Matrix for Turbulent Flame Probing Studies	49
VII	Test Matrix for Adiabatic Reactor Program	67
VIII	Predicted Droplet Diameters	98
IX	Air-Staging Design-Point Parameters	104
X	Summary of Selected Data for Tests Conducted Using Combustor Schemes 1-1A, 1-1B, and 4-1A.	122
XI	Combustor B Basic Design Features	139
XII	Comparison of Predicted and Measured JT8D Probing Data	182
XIII	FA, X, and pH Test Data.	220
XIV	Combustor Rig Test Results.	227
XV	Controlled and Measured Test Data	243
XVI	Sample-Gas Transfer Line Temperature Data	249
XVII	Measured Test Data	256
XVIII	UHC Emission Concentration Data	262
XIX	CO Emission Concentration Data.	268
XX	Nitrogen Oxide Emission Concentration Data.	274
XXI	CO ₂ Emission Concentration Data	290
XXII	H ₂ O Emission Concentration Data	296
XXIII	Performance Parameters	302

SYMBOLS

Symbol	Description
A	Area
$\overline{C_8H_{16}}$	Partial equilibrium products of combustion (CO_2 excluded) corresponding to temperature, pressure and fuel-air ratio
C_D	Aerodynamic drag coefficient
C_p	Specific heat
D_c	Diameter of combustion air jet entry hole
D_d	Diameter of liquid fuel droplet
FA	Fuel-air ratio
i	Stoichiometric oxygen-fuel weight ratio
L	Heat of vaporization of the fuel
\dot{m}_f	Rate of mass vaporization from liquid fuel droplet
Nd	Fuel droplet number density
P	Static gas pressure
Q	Heat of combustion of the fuel
\dot{Q}	Rate of combustion heat release
R	Streamtube radius
r	Streamtube radius
T	Static gas temperature
T_o	Total gas temperature
T_f	Fuel droplet surface temperature
U	Axial velocity component
V	Tangential velocity component
w_e	External mass addition flowrate
w_r	Recirculation mass flowrate

SYMBOLS (Continued)

Symbol	Description
w_t	Rate of turbulent mass exchange between adjacent streamtubes
WCO	Mass flowrate of carbon monoxide
WHC	Mass flowrate of unburned hydrocarbons
WUV	Mass flowrate of unburned vapor fuel
\bar{W}	Mass flowrate of partial equilibrium products of combustion, C_8H_{16}
x	Axial coordinate direction
Δx	Axial distance downstream of air addition site
Y	Transverse air jet penetration distance
Y_{O_2}	Weight fraction of oxygen in ambient gas
α_j	Fraction of recirculation mass flow entering or leaving the jth streamtube
β_0	Angle of jet entry
λ	Thermal conductivity
μ	Viscosity
ρ	Density
ϕ	Equivalence ratio, local FA/stoichiometric FA
Subscripts	
B	Bulk gas parameters
c	Air addition jet parameters
d	Fuel droplet parameters
eq	Equilibrium
g	Local gas parameters
j	Identifying the jth streamtube
l	Liquid fuel parameters

SECTION I

GENERAL SUMMARY

The first two phases of work specified under Air Force Contract F33615-71-C-1870 have been completed. In the first phase, a generalized, theoretical combustor model was developed for predicting concentrations and distributions of objectionable exhaust emissions from and within gas turbine engine combustors. The basic model has been formulated and is currently applicable for predicting emissions generated during low-power operation. The model was developed using a building block philosophy wherein three portions of the overall analysis were developed separately and were then combined into a single model structure adaptable to the spectrum of current and advanced burners. The modules composing the general analytical system are a two-dimensional stream-tube flowfield calculation procedure, a hydrocarbon combustion kinetics treatment, and a physical combustion formulation.

To facilitate development of the general model, three categories of laboratory tests were conducted as a part of the first phase of the program. These tests provided information concerning fundamental hydrocarbon combustion mechanisms directly applicable to the main burner environment. The first test program involved detailed probing in the primary zone of a swirl-stabilized JT9D burner can to obtain axial and radial distributions of unburned hydrocarbons, carbon monoxide, and local fuel-air ratios to assist in determining the validity of the overall model arrangement and in guiding model refinements where required. The second experimental program involved turbulent flow reactor tests to provide realistic reaction rate data for hydrocarbons and carbon monoxide under conditions of temperature, concentration, and turbulence level comparable to those found in combustors during low-power operation. The third experimental investigation involved low-temperature hydrocarbon kinetics tests, conducted in a flow reactor, to provide information about hydrocarbon oxidation under overall mixture conditions where strong exothermic effects are excluded.

Under the second phase, a comprehensive experimental component investigation was conducted to define and assess combustor design techniques for increasing combustion efficiency during low-power operation, consequently, reducing the concentrations of objectionable emissions. The first and second phases of work were conducted concurrently; continuous interchange of information between the two enhanced the accomplishment of each. The objective of the three basic design techniques examined during the second phase was to control the primary-zone equivalence ratio of the combustor over a wide range of overall fuel-air ratios. Variable airflow (air staging), variable fuel flow (axial and circumferential fuel staging), and fuel-air premixing concepts were examined experimentally to assess their capabilities for reducing the quantity of undesirable exhaust emissions. Low concentrations of unburned hydrocarbons were obtained with combustor configurations incorporating the air staging, circumferential fuel staging, and premixing concepts. However, low concentrations of carbon monoxide were achieved only

with those in which the air-staging and premixing concepts were used. Of the burners employing these two concepts, the premixing configuration was superior, producing but a fraction of the carbon monoxide generated by the best of the air staging arrangements.

SECTION II

INTRODUCTION AND PROBLEM DEFINITION

During the past several years, significant technological advances have been realized in gas turbine engine combustion system design and performance. Advanced and future primary combustors should have the operational flexibility to accept wide variations in compressor discharge pressure, temperature, and air-flow with minimum pressure loss and good design-point combustion efficiency while providing an acceptable exhaust gas temperature profile into the turbine. More recently, however, an additional requirement has been imposed: to reduce objectionable exhaust emissions.

Increased citizen awareness of environmental issues, coupled with the visible smoke emissions from aircraft powerplants, has brought substantial public attention to aircraft-contributed pollution. Although smoke by itself may not be harmful, its presence focused attention on the gas turbine engine as a potential source of additional pollutants: the undesirable gaseous emissions carbon monoxide (CO); unburned hydrocarbons, UHC; and oxides of nitrogen, NO_x. Even though turbine engine-powered aircraft contribute but a small amount to the overall air pollution problem, these aircraft can become significant contributors in and around high-traffic airports and military air installations.

Of particular concern are the relatively high levels of invisible emissions produced during part-power or low-power (idle/taxi) engine operation. These invisible emissions are principally UHC and CO. Both are nonequilibrium by-products of the combustion process between engine fuel and air. Under ideal thermodynamic conditions, neither should be present as combustion products; however, under low-power operating conditions, the efficiency of current gas turbine engine combustors tends to be low. Consequently, thermodynamic equilibrium is not attained during the combustion process and objectionable exhaust emissions are produced. Minimizing turbine engine exhaust pollution requires that emission control and abatement techniques become a major consideration in the design and development of future combustion systems.

To provide effective emission control without compromising required aerothermodynamic performance of the combustor, two basic approaches may be considered. One approach is to conduct an extensive experimental combustor development program involving the evaluation of many design changes and variations addressed to reducing pollutant concentrations without incurring system performance degradation. Unfortunately, this approach is often very costly and time-consuming and generally requires, ultimately, some system performance compromises and penalties. Another approach is to develop a generalized, analytical combustor model that realistically describes the coupled physical and chemical processes occurring within the combustor and predicts the exhaust product concentration and distribution produced by the combustion system as a function of combustor design, aerothermodynamics, and general operating conditions. Such a model could then become a vital engineering tool, permitting the designer to assess the impact of design changes for exhaust emission control of component performance prior to initiating costly development testing.

An exploratory development program was therefore undertaken to formulate and develop a computerized theoretical model to predict emissions characteristics of gas turbine engine combustors. In support of the model development, a number of experimental studies were conducted to provide information for structuring the formulation and for guiding its refinement. Direct support was provided by three laboratory test programs and a burner survey test program. The laboratory programs were incorporated to provide data, unavailable in the combustion literature, on reaction rates under realistic burner operating conditions. The survey program provided baseline emissions characteristics for a number of existing gas turbine engine burners, permitting the generality of the model to be assessed. Indirect support of the model was provided by a test program in which design techniques for reducing pollutant emission levels from an annular research burner were defined and assessed. Data from this program served as a guide for refining the model.

A detailed discussion of the model development, laboratory tests, and survey tests is presented in Section III. The annular burner test program for evaluating design techniques is presented in Section IV. A comparison of the exhaust concentrations predicted for the combustor configurations examined in Phase II with the actual data obtained during the experimental evaluation is presented in Section V.

This report has been physically arranged such that figures and tables relating to a particular section or subsection will be found as closely as possible to the written portion of the section or subsection in question.

An exploratory development program was therefore undertaken to formulate and develop a computerized theoretical model to predict emissions characteristics of gas turbine engine combustors. In support of the model development, a number of experimental studies were conducted to provide information for structuring the formulation and for guiding its refinement. Direct support was provided by three laboratory test programs and a burner survey test program. The laboratory programs were incorporated to provide data, unavailable in the combustion literature, on reaction rates under realistic burner operating conditions. The survey program provided baseline emissions characteristics for a number of existing gas turbine engine burners, permitting the generality of the model to be assessed. Indirect support of the model was provided by a test program in which design techniques for reducing pollutant emission levels from an annular research burner were defined and assessed. Data from this program served as a guide for refining the model.

A detailed discussion of the model development, laboratory tests, and survey tests is presented in Section III. The annular burner test program for evaluating design techniques is presented in Section IV. A comparison of the exhaust concentrations predicted for the combustor configurations examined in Phase II with the actual data obtained during the experimental evaluation is presented in Section V.

This report has been physically arranged such that figures and tables relating to a particular section or subsection will be found as closely as possible to the written portion of the section or subsection in question.

SECTION III

PHASE I - THEORETICAL FORMULATION

A. SUMMARY

Work under Phase I of Contract F33615-71-C-1870 has been completed. This was an analytical and experimental effort to establish a theoretical combustion model for predicting low-power exhaust emissions of unburned hydrocarbons and carbon monoxide from gas turbine engine main burners. The items of work that were accomplished under Phase I are outlined in the following paragraphs.

1. Streamtube Combustor Model Development

A preliminary low-power emissions concentration prediction model was formulated on the basis of an existing combustor model. This model was used to predict emissions levels for the proposed Phase II Combustor A test program.

A more comprehensive analytical model for predicting concentrations of unburned hydrocarbons and carbon monoxide during low-power operation was formulated, programmed for solution on a digital computer, and developed to functional status. The principal components of this model include a multistreamtube internal flowfield model, a treatment of the physical combustion process, and a treatment of hydrocarbon oxidation kinetics.

Exhaust plane emissions survey measurements were obtained from advanced premixing and piloted swirl combustor rigs.

A parametric study was conducted using the streamtube combustor model to predict the influence of combustor inlet temperature, pressure, reference velocity, fuel injector type, and wall cooling layer on exhaust emission concentrations.

2. Low-Power Emissions Research Studies

Chemical species concentration profiles were measured at three stations within the primary zone and at the exhaust of a JT8D can-type combustor at simulated idle and approach power settings. The corresponding gas temperature and combustion efficiency profiles were generated from these data.

Unburned fuel and carbon monoxide concentration profiles were measured in a turbulent flame reactor test rig. Test conditions were chosen to represent combustion in a gas turbine engine burner at idle and approach power settings. Measured values of combustion rate were used to generate an expression for turbulent mixing-controlled combustion rate as a function of fuel-air ratio and inlet temperature.

A series of tests was conducted in an adiabatic reactor test rig to investigate possible hydrocarbon oxidation reactions under relatively cool, fuel-rich conditions, representative of wall quenching regions. No significant reactions were found to occur.

3. Presentation of Predicted Results

Carbon monoxide and unburned hydrocarbon concentration levels have been predicted using the streamtube model for a series of combustor configurations. Comparisons of predicted and experimental values are presented in Section V for the following:

1. JT8D Probing Tests
2. Phase II, Combustor A
3. Phase II, Combustor B
4. Parametric Study.

B. PRELIMINARY COMBUSTOR MODEL

1. General

The complexity of the generalized combustor model, in particular the flow field calculation procedure, prevented developing a functional computer program in time for application to the early Phase II testing. Therefore, a preliminary combustor model was developed for use until the generalized model was functional. In addition, the preliminary model served as a test vehicle for development of the physical and chemical combustion mechanisms prior to incorporation into the streamtube combustor model.

2. Description

The preliminary low-power emissions model was constructed by modifying an existing three-zone combustor model developed by Pratt & Whitney Aircraft for NO_x prediction (Reference 1). The principal modification was to replace the existing equilibrium hydrocarbon chemistry with a simplified hydrocarbon kinetics treatment, combining kinetic and equilibrium features. Also, the input to the three-zone model was modified to accept fuel injection at multiple axial stations.

The principal elements of the analysis are a combustor internal flow field model, a fuel droplet dynamics and vaporization model, and a treatment of finite-rate hydrocarbon oxidation chemistry. The combustor flow field model is shown schematically in figure 1. The primary zone consists of a central recirculation zone (Region I), characterized by reversed flow and high levels of turbulence and temperature, and an outer streamtube of reacting flow (Region II). The dilution zone is modeled as a single streamtube in which chemical reaction may occur. The division between primary and secondary zones occurs at the first row of liner penetration jet holes, in accordance with experiment (Reference 2). By considering the primary zone to be divided into two parallel flowpaths, a combination of one-dimensional analyses is used to represent the salient two-dimensional features. This flow field treatment is applicable to conventional swirl-stabilized can or annular combustor designs. Chamber geometry, inlet air temperature and pressure, inlet fuel flow, and axial airflow distribution are input quantities.

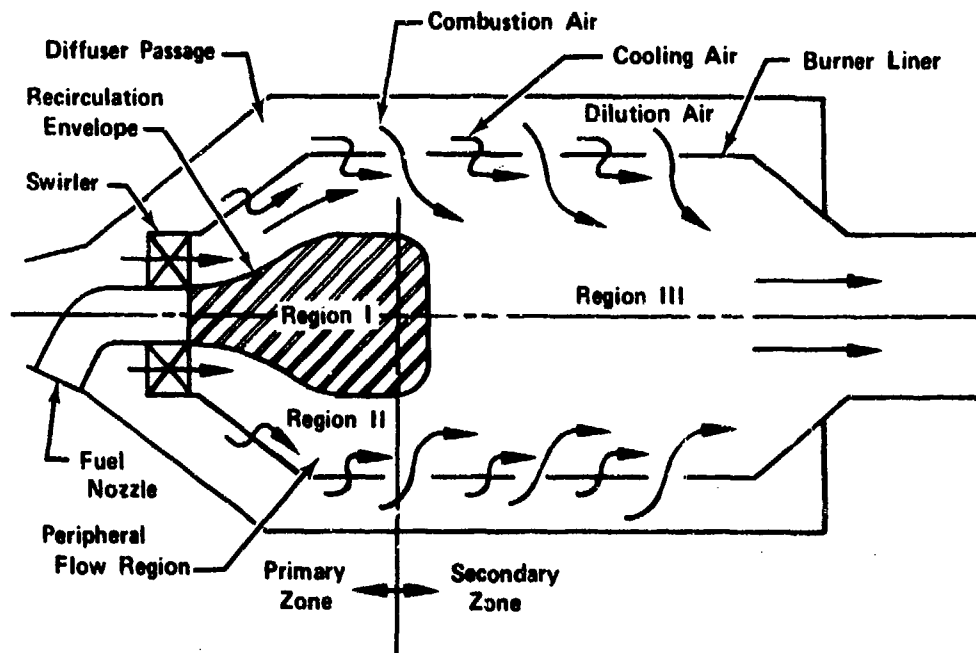


Figure 1. Schematic Diagram of Aerodynamic Model FD 68873

The recirculation zone boundary is determined by use of the semiempirical relationship developed in Reference 3:

$$R_r = f \left[\frac{M_{ang}^2 r_w^2}{\rho_g V^2} \right] \quad (1)$$

where

R_r the ratio of recirculation zone boundary radius to combustor radius, r_r/r_w

M_{ang} axial flux of angular momentum leaving the swirler

ρ_g local gas density

V axial volumetric flowrate

$f[]$ denotes a functional relationship

The independent parameter contained within brackets in equation (1) may be expressed in terms of geometric parameters as follows:

$$\frac{M_{ang} r_w}{\rho_g V^2} = \frac{2 r_w}{3 A_{sw}^2 C V_{sw}} \tan \theta [r_2^3 - r_1^3] \quad (2)$$

where

A_{sw} = swirler flow area

CV_{sw} = swirler discharge coefficient

θ = swirler vane turning angle

r_1 = swirler inner radius

r_2 = swirler outer radius

Once the recirculation region has been defined, the area between its boundary and the chamber wall defines the streamtube region (Region II).

It is assumed that unburned combustion jet air and a fraction of the Region II mixture enter the recirculation zone (Region I) at the downstream boundary of the primary zone. The quantity of mixture entering the upstream flow region is determined from an empirical correlation. All flow recirculating upstream in Region I is assumed to enter Region II at the swirler face. The combustion products from Region I are assumed to mix instantaneously with the unburned air entering Region II. Other than these discrete input flow adjustments that account for mass transfer between regions, there is no interaction between the primary-zone flow regions. Subscribing to the one-dimensional nature of the flow field treatment, air that is added to the combustor through liner holes is assumed to mix instantaneously with the fluid within.

Except for Region I, the combustible mixture preparation rate is assumed to be governed by the rate of fuel droplet vaporization in the presence of diffusive burning. It is further assumed that (1) the fuel spray is uniformly distributed across the Region II streamtube; (2) interaction between burning droplets is insignificant; (3) vaporized fuel mixes instantaneously with the surrounding gas-phase mixture, and (4) the spray can be adequately characterized by a single value of the Sauter mean diameter (SMD). Fuel that enters Region I is assumed to be fully vaporized and perfectly mixed with the airflow within Region I.

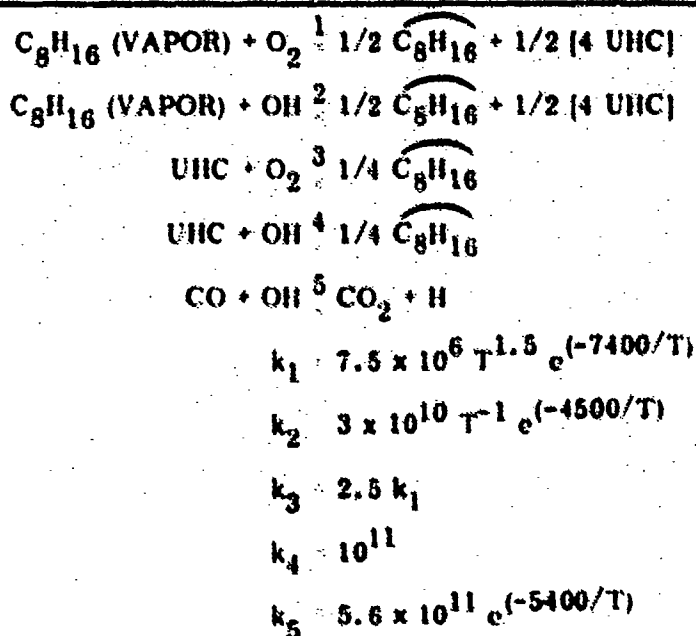
The fuel droplet vaporization rate in Regions I and II is calculated from an expression due to Wood, Lovell, Rosser, and Wise (References 4 and 5), based on local fuel and gas properties. The calculation procedure is essentially identical to that described in paragraph C, Streamtube Combustor Model, and will not be described here. The quantity of fuel vapor that is produced in an increment of combustor length, when fresh vapor is mixed with the products of combustion resulting from reaction between the preexisting vaporized fuel-air mixture, is available for combustion. In the preliminary model, it is assumed that combustion occurs at local bulk mixture strength, corresponding to complete mixing of all vaporized fuel and air available at each axial location in the combustor.

Chemical reaction of the hydrocarbon fuel and air determines the gas temperature and the concentration of active combustion species. The hydrocarbon chemistry treatment contained in the preliminary model was evolved from examination of a series of one-dimensional streamtube calculations using the hydrocarbon

oxidation kinetics system presented in paragraph C (table II). Conditions comprising equivalence ratios from 0.5 to 2.0, over an inlet temperature range of 800°K (1400°R) to 2000°K (3600°R) at a pressure of 2 atm have been studied with the emphasis on the final spectrum of products. Examination of these results showed that the UHC, excluding raw fuel, could be represented by the single species C₂H₂. Examination of the predicted CO concentrations indicated that, in the primary zone, the levels were close to equilibrium values.

Using these conclusions, the detailed hydrocarbon reaction system was reduced to that given in table I. As shown in this table, the preliminary hydrocarbon system consists of rate-limiting steps between raw fuel and equilibrium combustion products, with CO concentrations assumed to be either at equilibrium or frozen. Rates of the first two reactions, representing fuel breakdown for both lean and rich mixtures by O₂ and OH reactions, are the same as those of the full kinetics treatment. A portion of the reaction products are immediately equilibrated, whereas the remainder are identified as UHC. The proportioning has been adjusted to be consistent with the kinetic studies and experimental evidence. The third and fourth reactions represent the family of UHC oxidation reactions and also result in equilibrium products of combustion. These reactions have global rates representing the C₂H₂ system as contained in the full kinetics system. The equilibrium hydrocarbon thermochemistry calculations are based on procedures due to Brinkley (References 6 and 7). Simultaneous checks of the kinetic rate of change of CO concentration are then made. When the kinetic rate drops below that required to maintain equilibrium, the CO concentration is considered to be frozen.

Table I. Preliminary Hydrocarbon Kinetics System



NOTES:

1. Temperature, T, in °K
2. Reaction rate constant, k, in cm³/mole-sec

Table I. Preliminary Hydrocarbon Kinetics System (Continued)

3. $\overline{C_8H_{16}}$ represents equilibrium products of combustion at the local value of FA
4. Sudden freezing criteria:

$$\text{If } \frac{d[CO]}{dt} > \frac{d[CO]_{\text{equil}}}{dt}, [CO]_{t + \Delta t} = [CO]_{\text{equil}, t + \Delta t}$$

$$\text{If } \frac{d[CO]}{dt} < \frac{d[CO]_{\text{equil}}}{dt}, [CO]_{t + \Delta t} = [CO]_t$$
5. UHC is assumed to be C_2H_2 in the preceding chemical equations.

3. Phase II Predictions

The preliminary low-power emissions model represented a first-pass attempt at a prediction model for CO and UHC. In addition to support of the Phase II test program, it served the purpose of identifying those areas where model improvement was needed. The preliminary model was used to predict UHC and CO emissions for all configurations proposed for Phase II combustor A testing. Agreement between predicted and experimental values was not uniformly good, although major trends were predicted correctly.

A comparison of predicted and measured pollutant concentrations with fuel-air ratio is presented for Scheme 1-1A of combustor A to demonstrate the capability of the extended, preliminary model. A description of the Scheme 1-1A burner and test series is presented later in Section IV.

Figure 2 compares predicted and measured concentrations for UHC. A similarity in the rate of change of UHC concentration with fuel-air ratio, FA, is evident in this figure. However, if the predicted curve were shifted to the left by an FA increment of approximately 0.004, much better agreement would be obtained; the measured and predicted curves would nearly coincide.

A possible justification exists for shifting the predicted curve toward the left. The preliminary combustor model predicts that the Scheme 1-1A combustor will not remain lit below an FA of 0.005. In actual rig testing, this combustor had a lean blowout FA, LBO, of 0.0014. The difference between the predicted and measured lean blowout fuel-air ratios is approximately 0.004. The difference in operational limits suggests that the model is simulating a combustion process with an unrealistically low local FA in the primary zone. Indeed, it would not be possible for the combustor to operate at values of FA approaching 0.004 if local values of equivalence ratio corresponding to those predicted by the model did, in fact, exist. Consideration of the fuel vapor-air mixing mechanism incorporated in the preliminary model supports this proposition.

In the preliminary model, it was assumed that vaporized fuel mixed instantaneously with all of the air that was admitted to the primary zone. This is not especially realistic. A more plausible situation, which is incorporated in the general combustor model, considers conditions in the primary zone to be largely

nonhomogeneous, with regions of very high and very low fuel concentrations in evidence. The heterogeneous conditions provide local equivalence ratios sufficiently high to sustain combustion at low overall values of FA.

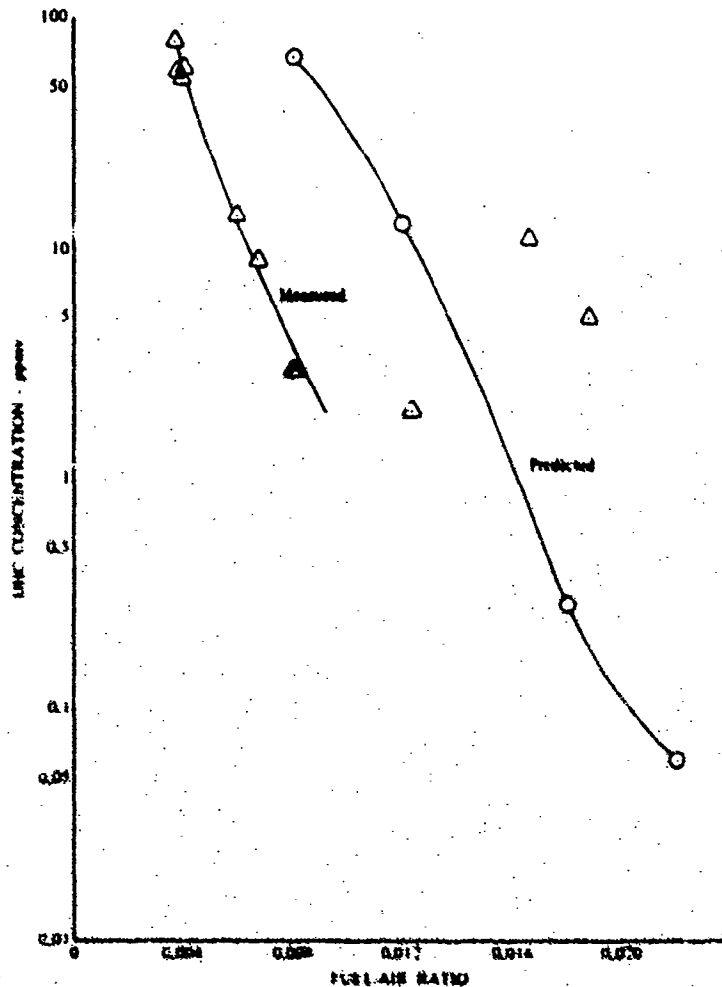


Figure 2. Comparison of Measured and Predicted UHC Concentration with Fuel-Air Ratio DF 96043

Figure 3 compares the variations in measured and predicted concentrations of CO with FA. The general shapes of the two curves are similar, and as observed for UHC, the predicted curve is displaced to the right of the measured data by a difference in FA of approximately 0.004. In addition, the predicted concentrations are approximately one order of magnitude greater than the measured. The predicted curve appears to be in error because the values of combustion efficiency that would result if the CO data were correct would be well below the values of combustion efficiency actually measured.

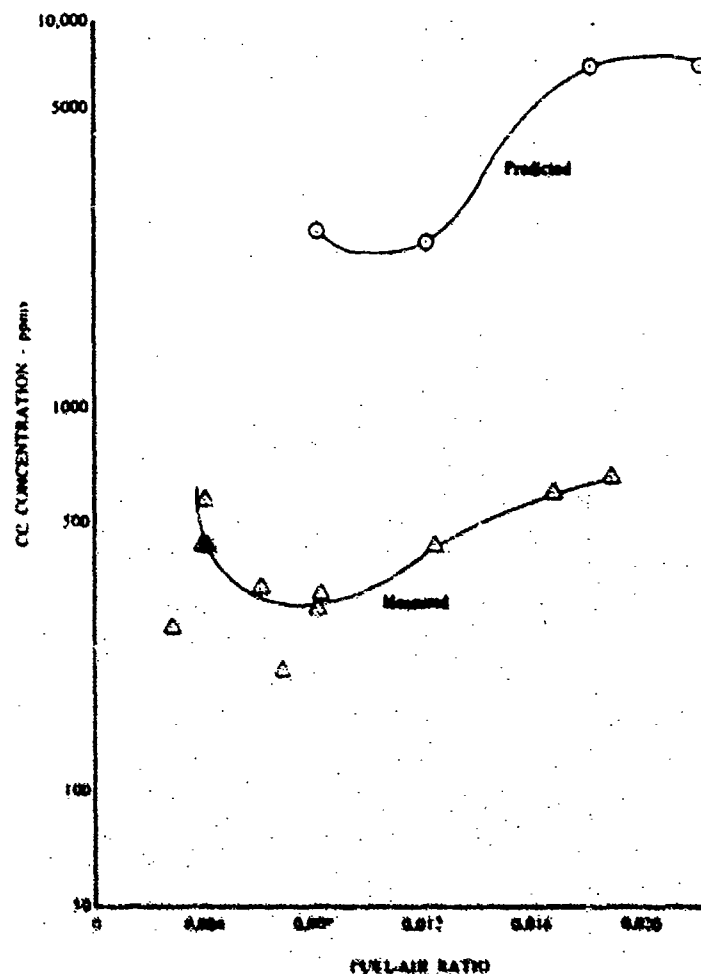


Figure 3. Comparison of Measured and Predicted CO Concentration with Fuel-Air Ratio DF 96044

A possible explanation for the high levels of CO concentration involves the sudden freezing criterion that has been imposed as an assumption in the preliminary combustor model. (See table 1.) In the preliminary model no change in CO concentration is permitted when the kinetic rate of reaction drops below that required to maintain an equilibrium concentration of CO. Experience gained in working with the preliminary model has shown that this assumption leads to unrealistic results. For example, for the test points presented in figure 3, the model predicts sudden freezing of CO concentration immediately downstream of the primary zone. In three of the four cases examined using the preliminary model to simulate Combustor Scheme 1-1A (at fuel-air ratios of 0.008, 0.012, and 0.018), this frozen condition was maintained for the entire length of the combustor, with the frozen concentration serving as the predicted concentration of CO at the combustor exhaust plane. In the fourth case (at a fuel-air ratio of 0.022), however, the kinetic rate of reaction rose above that required to maintain equilibrium at a location only 1.5 in. from the exhaust plane of the combustor. According to the freezing criterion, the CO concentration immediately becomes that corresponding to equilibrium conditions. The equilibrium concentration, however, has declined steadily with length to a level near zero at the aft end of the combustor. The preliminary model, therefore, predicts that the CO concentration drops from 7,500 ppmv to 0.01 ppmv at the

exit of the combustor. This value of 0.01 ppmv, however, is an equilibrium value and is not comparable to the frozen concentrations of 2835, 2690, and 7653 ppmv predicted for values of fuel-air ratio of 0.008, 0.012, and 0.018, respectively. Realistic exit concentrations probably lie somewhere between the frozen and equilibrium values. Therefore, for consistency, all predicted data presented in figure 3 represent frozen CO concentrations. For the data point at a fuel-air ratio of 0.022, the frozen concentration shown was predicted by the model for a location 1.5 in. upstream of the combustor exit plane.

Figure 4 compares the predicted and measured variations in NO_x concentration with fuel-air ratio over the range of conditions investigated. The shapes of the predicted and measured curves are similar. However, as observed for the UHC and CO cases, the predicted curve is shifted well to the right of the measured. And in contrast to the UHC and CO cases, the predicted NO_x concentrations are less than those that were measured. An explanation for this could be forwarded based upon the existence of nonuniform fuel-air ratios throughout the combustor, as opposed to the uniform fuel-air ratio profile assumed by the preliminary model. The amount of NO_x formed in a nonuniform system will certainly exceed that formed in a uniform one.

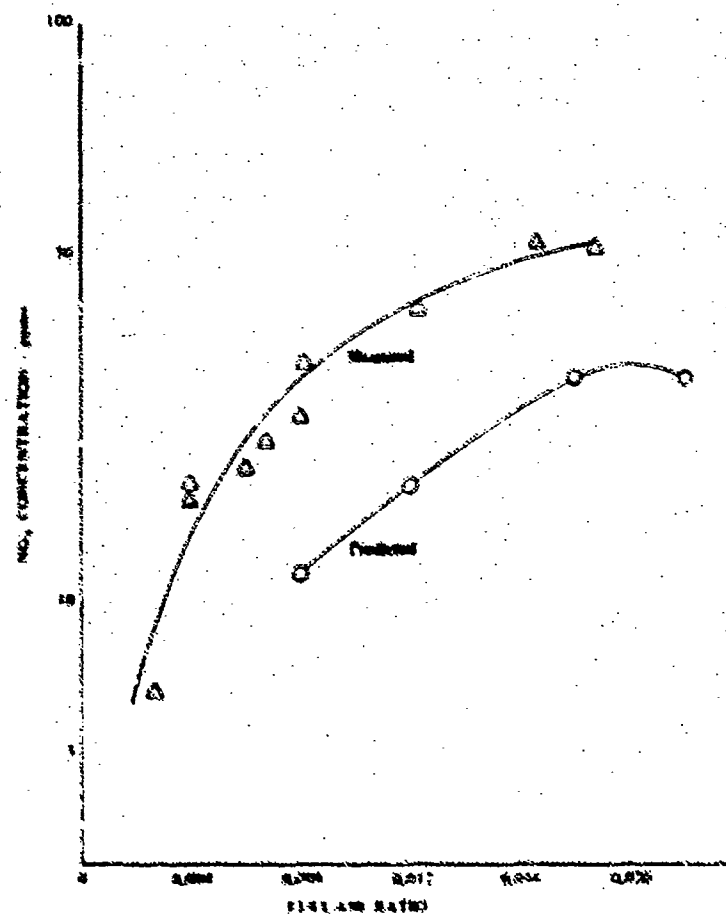


Figure 4. Comparison of Measured and Predicted NO_x Concentration with Fuel-Air Ratio

DF 96045

The principal reasons for lack of agreement in particular cases were the absence of a wall-quenching layer and the discontinuous CO characteristic provided by the freezing criterion. In an actual combustor, the wall film cooling layer freezes partially reacted species that enter the layer. In general, the preliminary model tended to predict very low exhaust concentrations of CO and particularly UHC, despite high primary zone concentrations. This indicates that bulk gas quenching is not a significant factor in low-power emissions of CO and UHC, and emphasizes the need for a cooling layer quench mechanism as included in the streamtube model. The CO mechanism incorporated in the preliminary model produced order of magnitude variation in CO concentration as the freezing criterion alternated between the frozen and nonfrozen states. As a result of this behavior, a mechanism providing kinetic conversion from CO to CO₂ was developed for the streamtube model.

C. STREAMTUBE COMBUSTOR MODEL

1. Conceptual Approach

Although the preliminary combustor model represents a significant step toward a realistic emissions prediction model, several inherent deficiencies make the prediction of CO and UHC, in particular, difficult. The need for a more localized treatment of the internal aerodynamic flowfield and for a sequence of chemical species between raw fuel and equilibrium combustion products becomes apparent. The streamtube combustor model was formulated with the specific intent of remedying these deficiencies.

The approach taken in the development of the low-power emissions combustor model has been to formulate mathematical treatments for principal physical and chemical mechanisms that influence the combustion process, and to integrate these mechanisms through a sequence of thermodynamic states obtained from the coupling of these mechanisms with the physical combustor flowfield. The simultaneous solution of the combustion rate mechanisms and the fluid dynamics provides the gas temperature, flow velocity, and chemical species concentrations as a function of position within the combustor, which, in turn, influence subsequent combustion. The principal elements of the analysis are a combustor internal flowfield model, a physical combustion model, and a treatment of hydrocarbon-air chemical kinetics.

The primary objective of the modeling effort was to develop an engineering tool to assist in the design and development of low-emission combustor hardware. For this reason, the analysis must include sufficient detail to draw a correspondence between the combustion process and combustor geometry, fuel injection characteristics, and engine operating conditions. Development of individual sub-models and combination in modular fashion allowed the requisite detail to be incorporated in a tractable mathematical analysis. A necessary constraint on the degree of complexity, however, was that the resulting analytical model must be practical in terms of computer time required for routine engineering use.

2. Description of the Combustor Model

a. Internal Flowfield Model

The combustor flowfield model, with input quantities of chamber area as a function of axial distance, inlet air temperature, pressure, and axial location of air addition sites defines the physical system upon which the gas dynamic and combustion rate calculations were based. The experimentally determined internal flowfield for a conventional swirl-stabilized, can-type combustor is shown in figure 5. The flowfield is seen to include a region of highly turbulent, reversed flow in the front of the chamber, surrounded by a region of relatively uniform downstream flow. The forward region including the recirculating flow is designated the primary zone and the downstream region, the secondary or dilution zone. The primary zone serves the purpose of stabilizing the combustion process. Liquid fuel is conditioned for burning and combustion is largely completed in this zone. The mixture of high-temperature combustion products and reactants leaving the primary zone continues to burn and subsequently is mixed with dilution air in the secondary zone to provide a suitable temperature profile for entrance to the turbine.

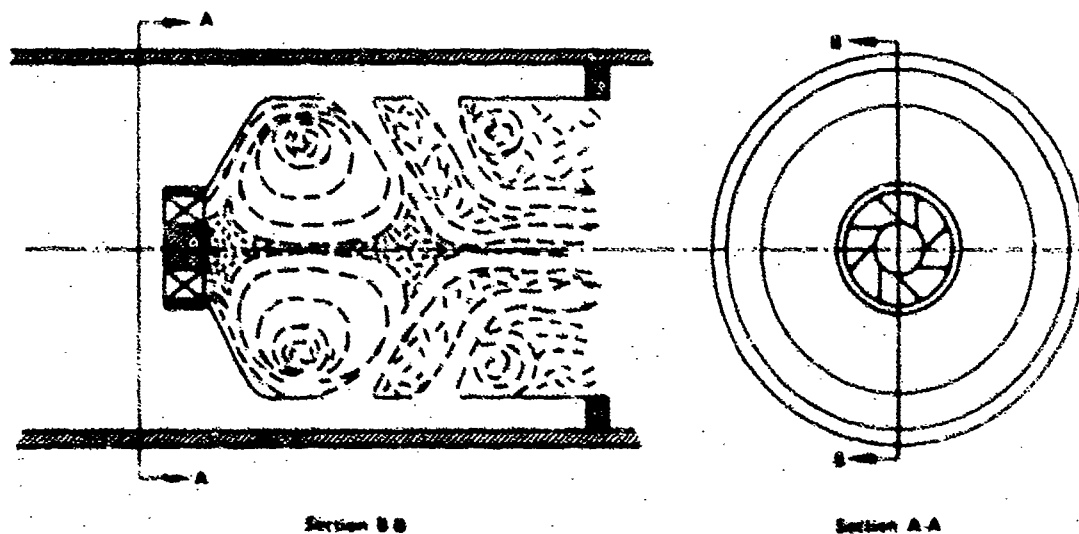


Figure 5. Primary-Zone Flow Pattern Observed in Can-Type Combustor (Reference 2) FD 66733A

The combustor flowfield model employed in the present analysis is shown schematically in figure 6 for the case of a can-type combustor. The two-dimensional internal flowfield has been approximated by a set of coannular, one-dimensional reacting streamtubes. The recirculation zone boundary, enclosing region \textcircled{D} , defines the location and size of a zero net flow, one-dimensional streamtube representing the recirculating flow. The recirculation zone boundary has the physical significance of separating the net upstream and downstream portions of the primary-zone airflow. Air entering the front of the combustor is assigned to the main flow streamtubes on an equal basis. Downstream combustion and dilution jet air is apportioned to the streamtubes by means of a jet penetration

and mixing model described later. All wall cooling air is assigned to the outer streamtube that begins at the first cooling air addition site. The airflow distribution to combustion and cooling holes is specified as model input. The streamtube boundaries are defined by inner and outer radii and are computed as dependent variables. The outermost streamtube is bounded by the location of the chamber wall, which is provided as input.

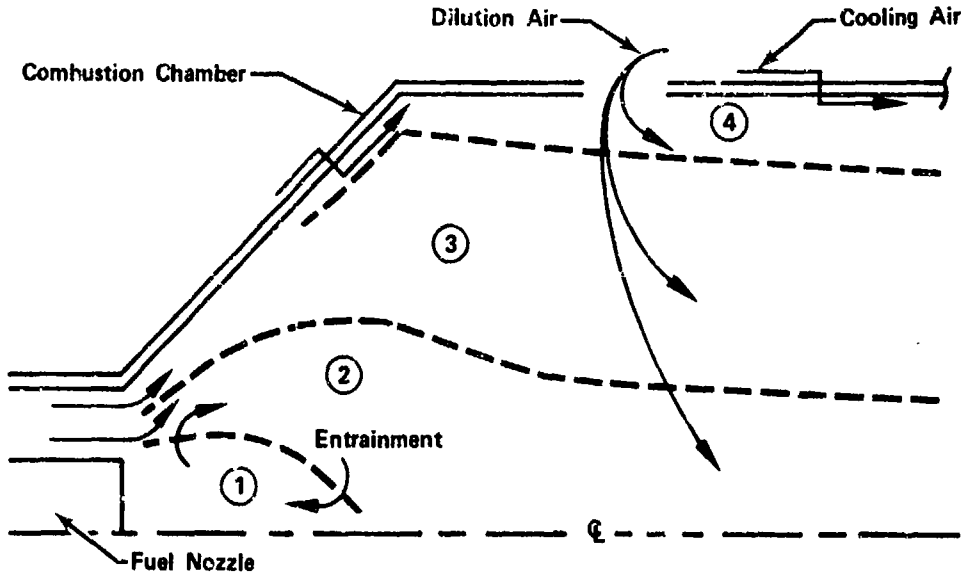


Figure 6. Schematic Diagram of Internal Flowfield Streamtube Model for Can-Type Combustor FD 66734A

The applicability of the model to particular combustor types is determined by the flowfield analysis, and includes can and annular configurations that are adequately described by a radial array of one-dimensional, coaxial streamtubes, symmetric about the geometric combustor axis. The recirculation region(s) may either be symmetric about the combustor axis or be symmetric about individual, regularly spaced axes themselves symmetrically arranged about the combustor axis. In the latter case, transition to the annular streamtube arrangement is made at the end of the recirculation region. The can and annular versions of the model are currently limited to four and seven streamtubes, respectively.

The steady-state, one-dimensional analysis of the flow in a streamtube for the downstream direction, x , is obtained by solving the equations for conservation of mass, momentum, and energy. It is assumed that wall friction, drag of internal bodies, gravity forces, and external heat exchange are negligible. With these assumptions, and considering the list of symbols, presented at the beginning of this report, the differential equations for continuity and linear momentum for the j th streamtube bounded by R_j and R_{j-1} , may be written as shown in equations 3 and 4.

$$\frac{d}{dx} (\rho_j U_j A_j) = \frac{dw_c}{dx} \Big|_j \quad (3)$$

$$\frac{d}{dx} (\rho_j U_j^2 A_j) = - \frac{d}{dx} (P_j A_j) + 2\pi P_{j+1} R_j \frac{dR_j}{dx} - \quad (4)$$

$$- 2\pi P_{j-1} R_{j-1} \frac{dR_{j-1}}{dx} + \frac{dw_t}{dx} \Big|_{j-1, j} (U_{j-1} - U_j) + \frac{dw_t}{dx} \Big|_{j, j+1} (U_{j+1} - U_j)$$

The equation of state, $\rho = P/RT$, is employed to express $d\rho/dx$ in terms of dP/dx and dT/dx in equation 3. In the case of a nonswirling flowfield, static pressure is uniform in the radial direction. For nonzero inlet swirl, additional conservation equations for angular momentum and radial equilibrium are written for the j th streamtube. They are shown, respectively, as equations 5 and 6.

$$\frac{d}{dx} (\rho_j U_j A_j C_{pj} T_{0j}) = \rho_j U_j A_j \dot{Q}_j + \frac{dw_t}{dx} \Big|_{j-1, j} (C_{pj-1} T_{0j-1} - C_{pj} T_{0j}) + \quad (5)$$

$$+ \frac{dw_t}{dx} \Big|_{j, j+1} (C_{pj+1} T_{0j+1} - C_{pj} T_{0j})$$

$$\frac{d}{dx} \left[\rho_j U_j A_j V_j \frac{(R_j + R_{j-1})}{2} \right] = \frac{dw_t}{dx} \Big|_{j-1, j} \cdot \quad (6)$$

$$\cdot \left(V_{j-1} \frac{(R_{j-1} + R_{j-2})}{2} - V_j \frac{(R_j + R_{j-1})}{2} \right) +$$

$$+ \frac{dw_t}{dx} \Big|_{j, j+1} \left(V_{j+1} \frac{(R_{j+1} + R_j)}{2} - V_j \frac{(R_j + R_{j-1})}{2} \right)$$

In the structuring of the computational procedure, the requirements for conservation of energy are realized through a series of species conservation equations that together specify the enthalpy of combustion. Because of the nature of the hydrocarbon thermochemistry model, combustion enthalpy is determined by the quantity of fuel that has reacted to form partial equilibrium products of combustion. This reacted fuel flow is expressed in terms of the local streamtube FA , as shown in equation 7.

$$(\rho_j U_j A_j) \frac{dFA}{dx} \Big|_j = \frac{d\widehat{W}_j}{dt} + \frac{dw_t}{dx} \Big|_{j-1, j} (FA_{j-1} - FA_j) + \frac{dw_t}{dx} \Big|_{j, j+1} \cdot \quad (7)$$

$$\cdot (FA_{j+1} - FA_j) - FA_j \frac{dw_c}{dx} \Big|_j$$

where W_j represents fuel mass that has reacted to partial equilibrium products of combustion at the local fuel-air ratio, and $FA_j = W_j/(\rho_j U_j A_j)$. Additional equations for the conservation of unburned fuel vapor (WUV), unburned hydrocarbons (WHC), and carbon monoxide (WCO) mass flow complete the specification of combustion enthalpy at each streamtube location x :

$$\left. \frac{dWUV}{dx} \right|_j = \frac{dWUV_j}{dt} - \frac{d\widehat{W}_j}{dt} - \frac{dWHC_j}{dt} + \left. \frac{dw_t}{dx} \right|_{j-1,j} \left(\frac{WUV_{j-1}}{(\rho_{j-1} U_{j-1} A_{j-1})} - \frac{WUV_j}{(\rho_j U_j A_j)} \right) + \quad (8)$$

$$+ \left. \frac{dw_t}{dx} \right|_{j,j+1} \left(\frac{WUV_{j+1}}{(\rho_{j+1} U_{j+1} A_{j+1})} - \frac{WUV_j}{(\rho_j U_j A_j)} \right)$$

$$\left. \frac{dWHC}{dx} \right|_j = \frac{dWHC_j}{dt} + \left. \frac{dw_t}{dx} \right|_{j-1,j} \left(\frac{WHC_{j-1}}{(\rho_{j-1} U_{j-1} A_{j-1})} - \frac{WHC_j}{(\rho_j U_j A_j)} \right) + \quad (9)$$

$$+ \left. \frac{dw_t}{dx} \right|_{j,j+1} \left(\frac{WHC_{j+1}}{(\rho_{j+1} U_{j+1} A_{j+1})} - \frac{WHC_j}{(\rho_j U_j A_j)} \right)$$

$$\left. \frac{dWCO}{dx} \right|_j = \frac{dWCO_j}{dt} + \left. \frac{dw_t}{dx} \right|_{j-1,j} \left(\frac{WCO_{j-1}}{(\rho_{j-1} U_{j-1} A_{j-1})} - \frac{WCO_j}{(\rho_j U_j A_j)} \right) + \quad (10)$$

$$+ \left. \frac{dw_t}{dx} \right|_{j,j+1} \left(\frac{WCO_{j+1}}{(\rho_{j+1} U_{j+1} A_{j+1})} - \frac{WCO_j}{(\rho_j U_j A_j)} \right)$$

The rate of change of WUV with time is determined from the fuel droplet vaporization rate expression discussed later. The time derivatives of the species W, WHC and WCO are obtained from the hydrocarbon thermochemistry system, which is described in detail later.

A calculation procedure has been devised to determine the rate of transfer of mass, momentum, and energy between the recirculation zone and the outer streamtubes. With the definition of a mass flowrate, w_r , representing entrainment flow entering or leaving the recirculation region, the conservation equations (continuity, linear momentum, and energy) for region ① may be written as follows:

$$\frac{d}{dx} (\rho_1 U_1 A_1) \frac{dw_r}{dx} \quad (11)$$

$$\frac{d}{dx} (\rho_1 U_1^2 A_1) = - \frac{d}{dx} (P_1 A_1) + 2\pi P_2 R_1 \frac{dR_1}{dx} + \begin{cases} U_1 \frac{dw_r}{dx} & w_r < 0 \\ \sum_{j=2} \alpha_j U_j \frac{dw_r}{dx} & w_r > 0 \end{cases} \quad (12)$$

$$\frac{dFA_1}{dx} = 0 \quad (13)$$

where w_r has been defined to be positive for mass entering the recirculation zone and $\alpha_j dw_r/dx$ defines the fractional exchange rate with streamtube j . Entrainment exchange with the outer streamtubes requires that terms including dw_r/dx in equations 11 and 12 be applied to equations 3, 4 and 7 in the proportion α_j such that total entrainment mass flow is conserved. Experience has shown that satisfactory results are obtained when entrainment flow is uniformly exchanged with all outer streamtubes, with the exception of the wall cooling streamtube(s). The current recirculation zone model gives the most satisfactory results when a constant, stoichiometric fuel-air ratio is assumed for region ①, as expressed by equation 13.

Specification of the recirculation boundary, $R_1(x)$, allows the computation of w_r as an additional dependent variable. However, for arbitrary recirculation zone size, the computed entrainment flow may not be consistent with the required boundary conditions that the recirculation zone contain zero net mass flow and that the axial recirculation velocity, U_1 , approach zero at the upstream and downstream limits of the recirculation zone envelope. By expressing the recirculation zone boundary in functional form, $R_1 = f(x)$, it is possible to iterate on zone length until the boundary conditions are satisfied. Satisfactory results have been obtained employing elliptical zone contours following the work of Reference 8. With this treatment of recirculation entrainment, both recirculation zone size and magnitude of recirculation flow may be computed as dependent variables.

Turbulent mixing between adjacent streamtubes may be expressed in terms of a rate of mass exchange between the streamtubes, w_t . The change in momentum resulting from this mass exchange may be related to the Reynolds shear stress acting at the boundary between the streamtubes

$$\tau A = (U_j - U_{j-1}) w_t,$$

where $A = 2\pi R_{j-1} dx$. The Reynolds stress may be expressed in terms of the turbulent eddy viscosity coefficient, μ_t , such that

$$\tau = \mu_t (\partial U / \partial R) \cong \mu_t (U_j - U_{j-1}) (r_j - r_{j-1})^{-1},$$

where r_j , r_{j-1} are internal streamtube radii corresponding to the "half-jet" approximation. μ_t may be related to local flow quantities by an expression of the form

$$\mu_t = \rho k b |U_{\max} - U_{\min}|$$

where k is an empirical constant fitted to experimental mixing data for two-dimensional turbulent jets, and b is proportional to the width of the mixing region (Reference 9). With appropriate selection of the eddy viscosity model, the rate of mass exchange between adjacent streamtubes is written:

$$\frac{dw_t}{dx} \Big|_{j-1,j} = \frac{2\pi R_{j-1}}{40} \left| \rho_j (U_j^2 + V_j^2)^{1/2} - \rho_{j-1} (U_{j-1}^2 + V_{j-1}^2)^{1/2} \right| \quad (14)$$

The rate of external air addition to the streamtubes defining the internal flowfield, w_c , is determined from a jet penetration and mixing model. With reference to figure 7, a transverse jet is assumed to enter the combustor with negligible momentum in the streamwise direction. In the process of mixing with the streamtube flow, the jet is turned in the downstream direction and is accelerated up to the local stream velocity. The trajectory of the jet centerline at the point of uniform velocity defines the jet penetration. An empirical correlation is used to express the penetration of a single transverse jet in terms of local jet and main-stream flow properties (Reference 10):

$$Y = 0.87 D_c \left(\frac{U_c}{U_B} \right)^{0.85} \left(\frac{\rho_c}{\rho_B} \right)^{0.47} \sin \beta_o \left(\frac{\Delta x}{D_c} \right)^{0.32} \quad (15)$$

where the subscript B denotes bulk-averaged streamtube velocity and density. The jet cross-sectional area is computed with the assumption that jet pressure is equal to the local stream pressure. If the shape of the fully developed jet cross-section is assumed to be an ellipse with ratio of major to minor axes of 5:1 (Reference 11), the jet cross-section is located with respect to the streamtube boundaries by the local value of penetration distance, $Y(\Delta x)$. Jet air addition to the j th streamtube is proportional to that fraction of the jet cross-sectional area intersected by the streamtube boundaries located at R_{j-1} and R_j . The jet is assumed to be fully mixed with the respective streamtube flows at a position $\Delta x = 10 D_c$ downstream of the air-addition site, following the assumption of full penetration in that distance. Jet air addition rate is specified as a sine function of axial distance over the mixing length, as shown in equation 16:

$$w_c(x) = \frac{\pi}{2} \frac{w_c}{10D_c} \sin \left(\frac{\Delta x}{10D_c} \cdot \frac{\pi}{2} \right) \quad (16)$$

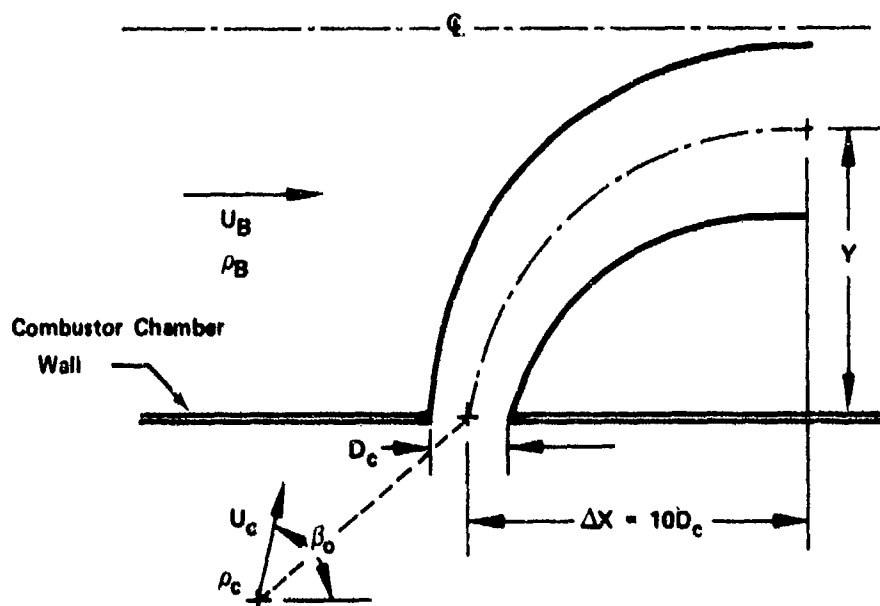


Figure 7. Transverse - Jet Penetration Model

FD 66736A

b. Physical Combustion Model

The rate of combustion of liquid fuel is governed by the respective rates of fuel-droplet vaporization and mixing of vaporized fuel and air in the presence of diffusive burning. It is assumed that fuel droplets are uniformly distributed within a streamtube, that interaction between burning droplets is insignificant, and that the fuel droplets within a given streamtube are adequately described by a single value of Sauter mean diameter (SMD). The fuel droplet vaporization rate for burning droplets, $dWUV/dt$, is calculated from the following expression due to Wood, Lovell, Rosser, and Wise (References 4 and 5):

$$\frac{dWUV}{dt} = \frac{2\pi D_d \lambda_g}{C_{Pg}} \ln \left[1 + \frac{Q_{Y_{O_2}}}{Li} - \frac{C_{Pg}}{L} (T_l - T_g) \right] \frac{N_d}{U_d} \quad (17)$$

Equation 17 is based on assumptions of spherical symmetry, steady-state conditions, independence of transport properties on temperature and composition, and negligible radiation effects. The liquid surface temperature, T_l , is taken to be the ASTM 50% distillation point in accordance with the conclusions reached in Reference 5 for multicomponent fuel blends. Equation 17 is multiplied by

$$1.0 + 0.276 \text{Re}^{1/2} \text{Pr}^{1/3}$$

where the Reynolds number is given by

$$\text{Re} = |U_g - U_d| D_d \rho_g / \mu_g$$

and the Prandtl number by

$$\text{Pr} = C_{Pg} \mu_g / \lambda_g$$

to account for convection (Reference 12).

Since the fuel-droplet velocity typically differs from that of the streamtube flow, acceleration or deceleration of the droplet because of aerodynamic drag must be included. This is accomplished by including a drag force term in the droplet momentum equation. The resulting differential equation for droplet velocity is:

$$\frac{dU_d}{dx} = \frac{1}{U_d} \left(\frac{3C_D \rho_g}{4D\rho_l} \right) |U_g - U_d| \cdot (U_g - U_d) \quad (18)$$

The drag coefficient is calculated from one of the following equations, depending on Reynolds number (Reference 13):

$$\left. \begin{aligned} C_D &= 27 \text{Re}^{-0.84}; 0 < \text{Re} \leq 80 \\ C_D &= 0.271 \text{Re}^{0.217}; 80 < \text{Re} \leq 10^4 \\ C_D &= 2.0; 10^4 < \text{Re} \end{aligned} \right\} \quad (19)$$

Initial values of mean droplet size and injection velocity are determined from fuel-injector characteristics. Initial fuel mass distribution among the streamtubes is specified as model input. Separate droplet vaporization equa-

tions were written for each streamtube containing liquid fuel. Fuel that enters the recirculation zone is assumed to be fully vaporized and mixed with the region ① airflow.

In keeping with the physical droplet burning model represented by equation 17, fuel, once vaporized, is assumed to react in stoichiometric proportion with the surrounding air in the streamtube. The computation of streamtube aerodynamic parameters, however, is based on bulk-mixture conditions at all times. In the case of premixed fuel and air, combustion occurs at the injected mixture proportions. Combustion of injected fuel vapor or partially evaporated fuel droplets is assumed to occur on a stoichiometric basis as above.

c. Hydrocarbon Thermochemistry Model

The quantity of fuel vapor produced in an increment of combustor length, when added to the preexisting fuel-air combustion product vapor mixture at that axial station, is available for combustion. Chemical reaction of the hydrocarbon fuel and air determines the gas temperature and concentration of active combustion species. The degree of completion of the combustion reactions determines the exhaust concentration of CO and UHC. The number of possible reactions involved in the breakdown of hydrocarbon fuels is extremely large, and few have been investigated with respect to their rates. It is, therefore, convenient to assume that fuel breakdown to elemental species occurs in a small number of global steps. The hydrocarbon kinetics system investigated in the present study is shown in table II. As represented by this mechanism, the complex oxidation of hydrocarbon fuel is viewed as occurring in three broad stages. The first stage, represented by global reactions (1) through (3), produces light, unburned, partially oxidized hydrocarbons. The rate constants for these reactions have been adjusted to fit experimental ignition delay data following the approach of Edelman and Fortune (Reference 14). The hypothetical aldehyde intermediate (C_4H_8O) is introduced for computational convenience. The subsequent sequence of reactions, comprising the second stage of combustion, includes the principal exothermic reactions and produces large amounts of H_2O and CO . The particular reactions included in the current system are considered to represent families of intermediate species of similar character. The final stage of combustion is characterized by the conversion of CO to CO_2 via reaction (19). The reaction rate constants have been taken from References 14 through 22 as indicated in table II, with the exception of reaction (7), where the rate has been deduced from results presented in References 15 through 18 and 22. JP-5 fuel is represented chemically by the formulation C_8H_{16} , although it is not meant to be a true olefin. The thermodynamic properties (specific heat, heat of formation) for C_8H_{16} are consistent with those of JP-5.

Table II. Reactions Constituting the Hydrocarbon Oxidation Kinetics System

	Reaction	Rate Constant, $cm^3 \cdot mole^{-1} \cdot sec^{-1}$	Reference Source
(1)	$C_8H_{16} + O_2 \rightarrow 2C_4H_8O$	$k_1 = 7.5 \times 10^6 T^{1.5} e^{-7900/T}$	See Text
(2)	$C_4H_8O + O_2 \rightarrow HO_2 + CO + CH_3 + C_2H_4$	$k_2 = 10^{11} T^{1.5} e^{-10000/T}$	See Text
(3)	$C_8H_{16} + OH \rightarrow H_2CO + CH_3 + 3C_2H_4$	$k_3 = 3 \times 10^{10} T e^{-4500/T}$	See Text

Table II. Reactions Constituting the Hydrocarbon Oxidation Kinetics System
(Continued)

Reaction	Rate Constant, $\text{cm}^3\text{-mole}^{-1}\text{-sec}^{-1}$	Reference Source
(4) $\text{CH}_3 + \text{O} = \text{H}_2\text{CO} + \text{H}$	$k_4 = 2 \times 10^{13}$	15
(5) $\text{CH}_3 + \text{O}_2 = \text{H}_2\text{CO} + \text{OH}$	$k_5 = 10^{12}$	16
(6) $\text{H}_2\text{CO} + \text{OH} = \text{H}_2\text{O} + \text{CO} + \text{H}$	$k_6 = 10^{14} e^{-4000/T}$	15
(7) $\text{C}_2\text{H}_4 + \text{O}_2 = 2\text{H}_2\text{CO}$	$k_7 = 3 \times 10^2 T^{2.5}$	See Text
(8) $\text{C}_2\text{H}_4 + \text{OH} = \text{CH}_3 + \text{H}_2\text{CO}$	$k_8 = 5 \times 10^{13} e^{-3000/T}$	17
(9) $\text{CH}_3 + \text{H}_2 = \text{CH}_4 + \text{H}$	$k_9 = 6 \times 10^{11} e^{-5500/T}$	18
(10) $\text{C}_2\text{H}_4 = \text{C}_2\text{H}_2 + \text{H}_2$	$k_{10} = 7 \times 10^8 e^{-23250/T}$	19
(11) $\text{C}_2\text{H}_2 + \text{OH} = \text{CH}_3 + \text{CO}$	$k_{11} = 10^{13} \times e^{-3500/T}$	16
(12) $2\text{H} + \text{M} = \text{H}_2 + \text{M}$	$k_{12} = 2 \times 10^{18} T^{-1}$	14, 19
(13) $2\text{O} + \text{M} = \text{O}_2 + \text{M}$	$k_{13} = 10^{17} T^{-1}$	16, 20
(14) $\text{OH} + \text{H} + \text{M} = \text{H}_2\text{O} + \text{M}$	$k_{14} = 7 \times 10^{19} T^{-1}$	20, 21
(15) $\text{H} + \text{O}_2 = \text{OH} + \text{O}$	$k_{15} = 2.24 \times 10^{14} e^{-8400/T}$	21
(16) $\text{O} + \text{H}_2 = \text{OH} + \text{H}$	$k_{16} = 1.74 \times 10^{13} e^{-4730/T}$	21
(17) $\text{H} + \text{H}_2\text{O} = \text{H}_2 + \text{OH}$	$k_{17} = 8.41 \times 10^{13} e^{-10050/T}$	21
(18) $\text{O} + \text{H}_2\text{O} = 2\text{OH}$	$k_{18} = 5.75 \times 10^{13} e^{-9000/T}$	21
(19) $\text{CO} + \text{OH} = \text{CO}_2 + \text{H}$	$k_{19} = 5.6 \times 10^{11} e^{-540/T}$	21
(20) $\text{HO}_2 + \text{M} = \text{H} + \text{O}_2 + \text{M}$	$k_{20} = 2.4 \times 10^{15} e^{-22950/T}$	21
(21) $\text{HO}_2 + \text{H} = 2\text{OH}$	$k_{21} = 6 \times 10^{13}$	20, 22

While it is felt that the kinetic mechanism presented in table II offers an adequate representation of the detailed hydrocarbon process, the simultaneous solution of the system of equations does not lend itself to coupling with the stream-tube flowfield model. In particular, computational step size must be very small as species equilibrium is approached resulting in excessively long computation time. The approach taken in the development of the model was to replace the full kinetic mechanism with a reduced kinetic-partial equilibrium system capable of predicting those aspects of the full system behavior that are important to the determination of exhaust emissions.

The kinetic mechanism, presented in table II, is readily solved for the plug-flow combustion of premixed fuel and air. The computed behavior of selected intermediate species is shown in figure 8 for the case of a stoichiometric mixture at a pressure of 2 atm and an initial temperature of 1000°K. The combustion is characterized by a period of abrupt change in species concentration corresponding to rapid temperature rise, followed by a period of relatively slow approach to equilibrium. From the point of view of emissions modeling, the relatively slow post-flame reactions are most significant, representing the reaction of intermediates on a time scale comparable to the combustor residence time. The time spent in the transitory, rapid temperature rise period is an order to magnitude less than typical values of combustor residence time. In addition, the ignition delay period for raw fuel can be significant at lower mixture temperatures. Thus, a reduced system, which provides the ignition delay and post-flame behavior of the full hydrocarbon kinetics mechanism, will adequately predict the influence of the chemical combustion rate on exhaust emissions.

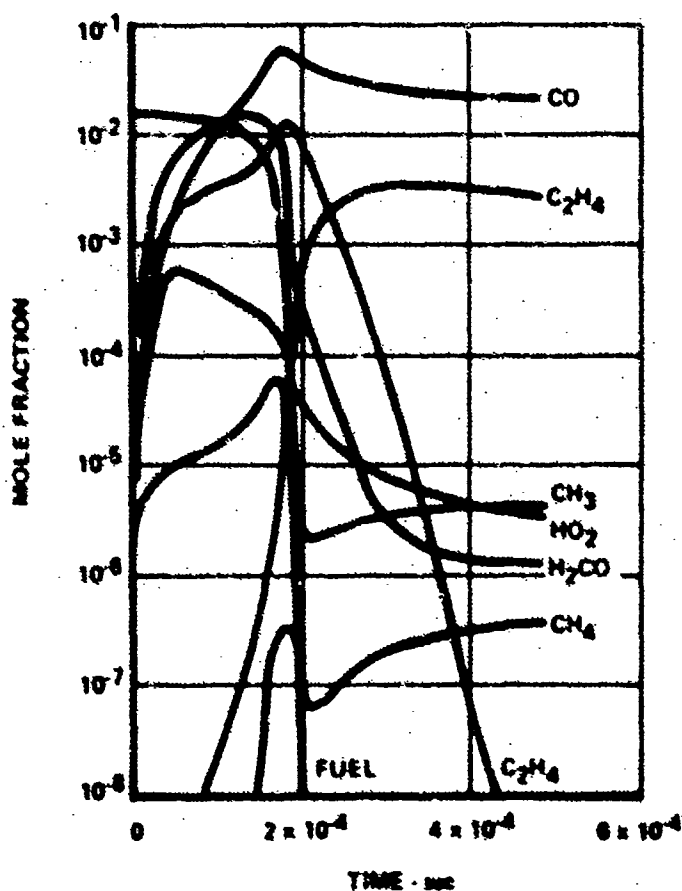


Figure 8. Variation in Species Concentration with Time (Stoichiometric Equivalence Ratio, $P = 2$ atm, $T_{in} = 1000^{\circ}\text{K}$)

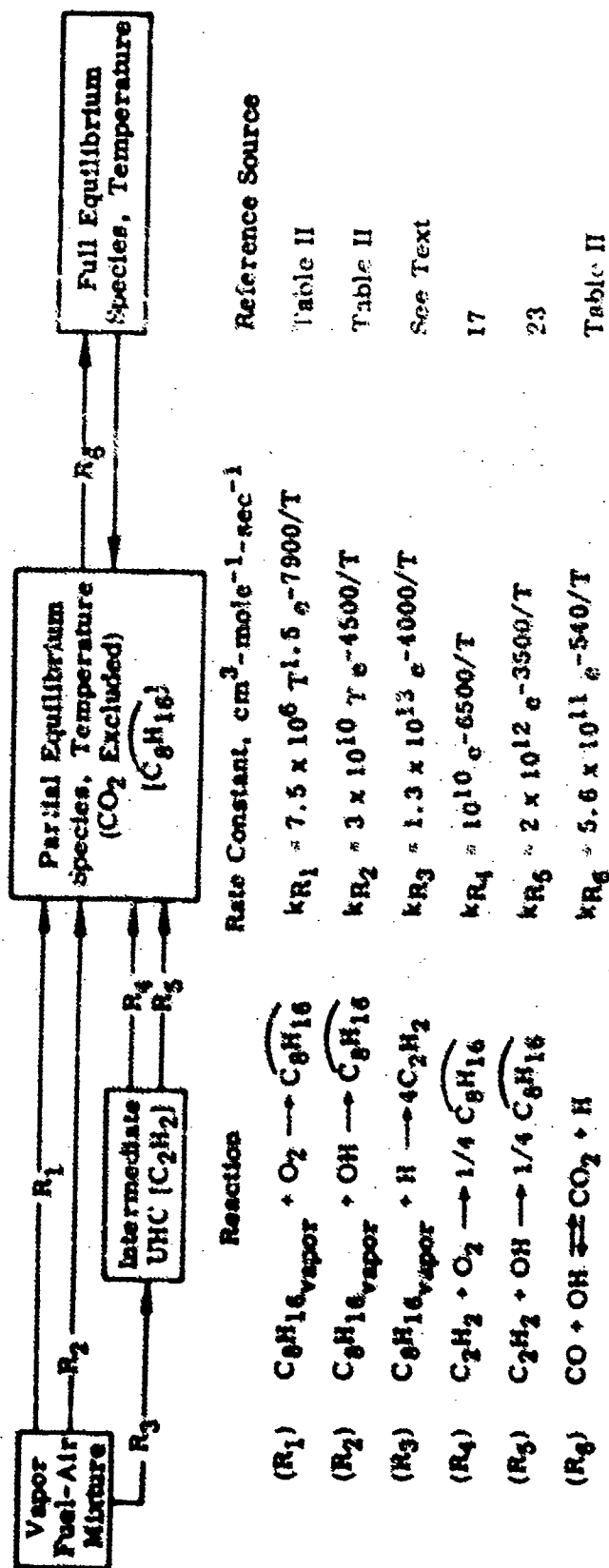
FD 66735A

The behavior of the full kinetics mechanism was documented by performing plug-flow computations for a range of initial temperatures, pressures, and FA. This behavior was then fitted with the reduced kinetic-partial equilibrium mechanism shown in table III. This system provides for the rate-controlled conversion of raw fuel-air mixtures to partial equilibrium products, both directly (R_1 and R_2) and via an unburned hydrocarbon intermediate (R_3 through R_5). CO_2 has been removed as an allowable species in the partial equilibrium state. Subsequent conversion to full equilibrium products is controlled by reaction (R_6). The combustion product temperature and species concentrations are determined by interpolation between the partial and full equilibrium states based on $[CO_2]/[CO_2]$ eq. It should be noted that this treatment of hydrocarbon combustion kinetics requires only that carbon atoms be conserved. Therefore, with the exception of reaction (R_6), only the characteristic reaction products are stated and no reverse reaction is provided. The reaction rate constants for reactions (R_1), (R_2), and (R_6) correspond to those given in table II for the same reactions.

Reaction (R_3) represents direct formation of light, intermediate, unburned hydrocarbons typified by C_2H_2 . Examination of results obtained from the full-kinetic system indicated that intermediate UHC appear in significant quantities after about half the original fuel is consumed. Furthermore, the dependence of UHC concentration on FA and inlet temperature was not simply related to either the O_2 or CO_2 equilibrium concentration. The qualitative behavior of the intermediate unburned hydrocarbons was fitted best by relating the formation to [III] eq. This reaction has no chemical significance, representing only a fit to the observed behavior. The rate indicated in table III has, likewise, been fitted to the observed behavior of the full system. Reactions (R_4) and (R_5) represent reaction of the intermediate UHC with HO_2 and OH to partial-equilibrium products. The rates indicated in table III are representative values for reactions involving light, intermediate hydrocarbons, obtained from References 17 and 23, respectively. Since the species $[HO_2]$ eq is not provided by the equilibrium chemistry computation, reaction (R_4) has been written in terms of $[O_2]$ eq, with the assumption that $[O_2]$ eq is two orders of magnitude greater than $[HO_2]$ eq for the conditions of interest. The calculation subroutine employed for the equilibrium hydrocarbon thermochemistry is based on procedures of Brinkley (References 6 and 7).

Application of the combustion model to a computational procedure that guarantees energy conservation requires conservation of the contributing species' mass flowrates, as expressed in equations 7 through 10. Liquid fuel droplets are vaporized at a rate dWV/dt , determined from equations 17 through 19, to form fuel vapor, WV ($C_{11}H_{16}$ vapor). The rate of formation of partial equilibrium products of combustion $\overline{C_{11}H_{16}}$, dW/dt in equation 7, is governed by reactions (R_1), (R_2), (R_4), and (R_5). The net rate of unburned hydrocarbon formation, or depletion, $dWHC/dt$ in equation 9, is governed by reactions (R_3), production, and (R_4) and (R_5), depletion. Consequently, the net rate of change of unburned fuel vapor in equation 8 is $dWV/dt - dW/dt - dWHC/dt$. The rate of formation of CO from combusting fuel is proportional to dW/dt , while the rate of depletion is governed by reaction (R_6). These competing reactions determine the net chemical rate of change of WCO , $dWCO/dt$ in equation 10. The local CO concentration determined from equation 10, relative to the equilibrium level, specifies the local state of partial equilibrium of the burning mixture, and, thus, the local streamtube gas temperature.

Table III. Reduced Hydrocarbon Oxidation System



3. Application of the Streamtube Model

The applicability of the model to particular combustor types is determined by the formulation of the streamtube flowfield analysis. The streamtube model is capable of treating three basic combustor configurations: (1) a can-type combustor with single axisymmetric recirculation zone, either bluff-body or swirl stabilized; (2) an annular-type combustor with annular, bluff-body induced recirculation zone; and (3) an annular-type combustor with multiple discrete, swirl or bluff-body induced recirculation zones, symmetric about individual, regularly spaced axes themselves symmetrically arranged about the combustor axis.

These combustor configurations are treated by permutation of two basic flow-field models, corresponding to configurations (1) and (2) in the preceding discussion. Combustor type (3) is treated by applying model (1) on a single recirculation zone basis to the forward portion of the combustor and applying model (2) to the aft portion. In the case of bluff-body stabilized recirculation, transition between models occurs at the end of the recirculation zone. In the case of swirl-stabilized recirculation, transition occurs when the tangential velocity about the swirler axis has become insignificant. Interaction between adjacent recirculation zones is assumed to be negligible. In this manner, the preparation of two basic computational procedures permits the treatment of a wide variety of geometric configurations.

The can combustor streamtube analysis consists of four coaxial streamtubes, arranged as shown in figure 6. Flow in the outer three streamtubes may be treated with or without a swirl velocity component depending on the type of recirculation zone employed (swirl or bluff-body induced). Fuel injection is limited to a single source located at the recirculation zone axis. Any type of fuel injection is permitted, including prevaporized and gaseous fuels.

The annular combustor streamtube analysis consists of seven coaxial streamtubes, symmetric about the geometric combustor axis. Swirling flow is not treated in the annular system. Primary-zone fuel injection is treated as continuous in the circumferential direction, coincident with the location of the annular recirculation zone. Secondary, or downstream fuel injection transverse to the streamtube flow direction is also permitted in the annular version of the model.

4. Computational Procedures

The streamtube conservation equations and the physical and chemical combustion models have been programmed for solution on a digital computer. A simplified flow chart of the low-power emissions prediction computer program is shown in figure 9.

Input to the computer program includes specification of combustor type, chamber area as a function of axial distance, inlet air temperature, pressure, axial location of air addition sites, and fuel injector parameters. Initial values of the independent and dependent variables in each streamtube are determined from combustor geometry and input conditions. Prior to beginning the calculation, a table of gas temperature and chemical species concentrations for partial equilibrium (CO_2 excluded) and fuel equilibrium combustion is generated as a function of F/A . This information is stored in subroutine TEMP. Interpolated values of gas temperature and chemical species concentration are retrieved during the course of the calculation.

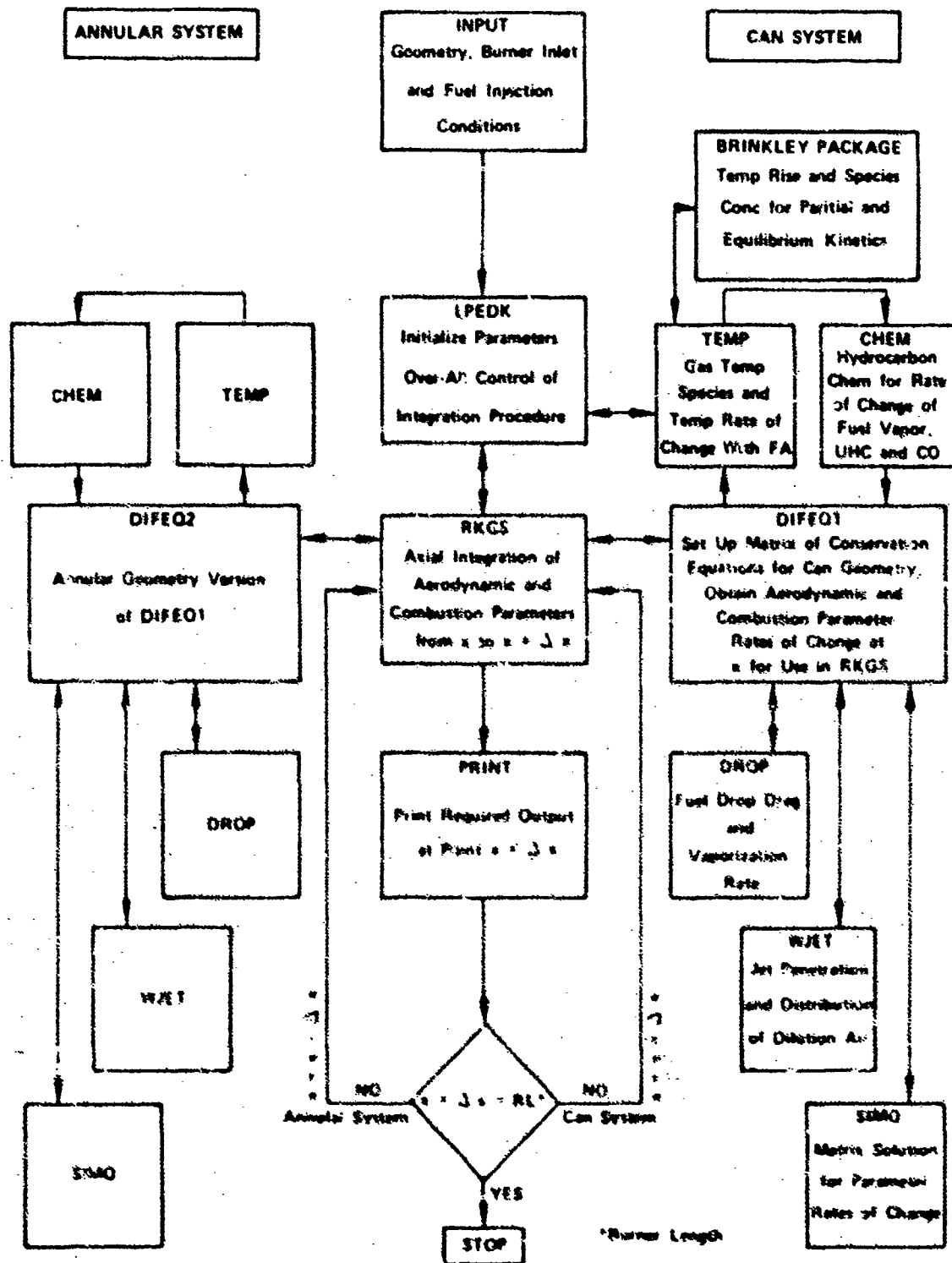


Figure 9. Flow Chart for Low-Power Emissions Computer Program

FD 71967

The aerodynamic equations of motion are written in differential form for each streamtube. These equations, when coupled with an equation describing the recirculation-zone boundary and arranged in matrix form, constitute a set of linear differential equations that may be solved simultaneously for parametric derivatives with respect to x . These differentials are numerically integrated over the interval Δx using a Runge-Kutta procedure to obtain values of parameters at $x + \Delta x$. Integrated values of parameters at $x + \Delta x$ are then used to obtain new derivatives which are integrated to yield values of parameters at $x + 2\Delta x$; this procedure is repeated until the exit plane is reached.

Production of vaporized fuel, chemical reaction of fuel and air, external air addition and turbulent exchange between streamtubes are evaluated in subroutines external to the streamtube equation matrix. Updated values of derivatives with respect to x are provided at the end of each computational step for integration in the next step. For this approach to succeed, it is necessary that variation in parameters not included as dependent variables in the differential equation matrix be small across the computational step. This arrangement of the computational procedure permits concentrations and flow properties of combustion product species to be calculated as a function of position along the individual streamtubes for fairly arbitrary specification of the physical and chemical combustion models.

With reference to the program flow chart (figure 9), the matrix of differential equations is set up in subroutine DIFEQ1 for the can system and DIFEQ2 for the annular system. The matrix is then solved simultaneously in SIMQ for the x -derivatives at each point x . Control of the numerical integration procedure is embodied in subroutine RKGS. However, transfer from the can system to the annular system as well as transfer from the primary zone (four or seven streamtubes) to the secondary zone (three or six streamtubes) is made in LPEDK, in which overall control of the calculation rests. Subroutines CHEM, TEMP, DROP, WJET, SIMQ, RKGS and PRINT are common to both the can and annular systems.

At each point x , streamtube gas velocity, pressure, temperature, air flowrate, FA, recirculation zone entrainment flowrate, fuel droplet size and velocity, and the mass flowrates of unburned vapor, reacted fuel, UHC, CO, and CO₂ are available for printout. Typical computed values of pressure, velocity and stream temperature are shown in figures 10 and 11 for a can-type combustor with zero inlet swirl.

D. SURVEY TESTING

1. General

The theoretical combustor model development effort included a series of exit plane emissions survey tests that were to be conducted in three types of advanced combustors: a high-performance, swirl-stabilized combustor; a pre-mixed combustor; and a pilot-swirl combustor. The purpose of these tests was to establish baseline exhaust emission characteristics for divergent combustor types, and to assist in evaluating the generality of the theoretical model.

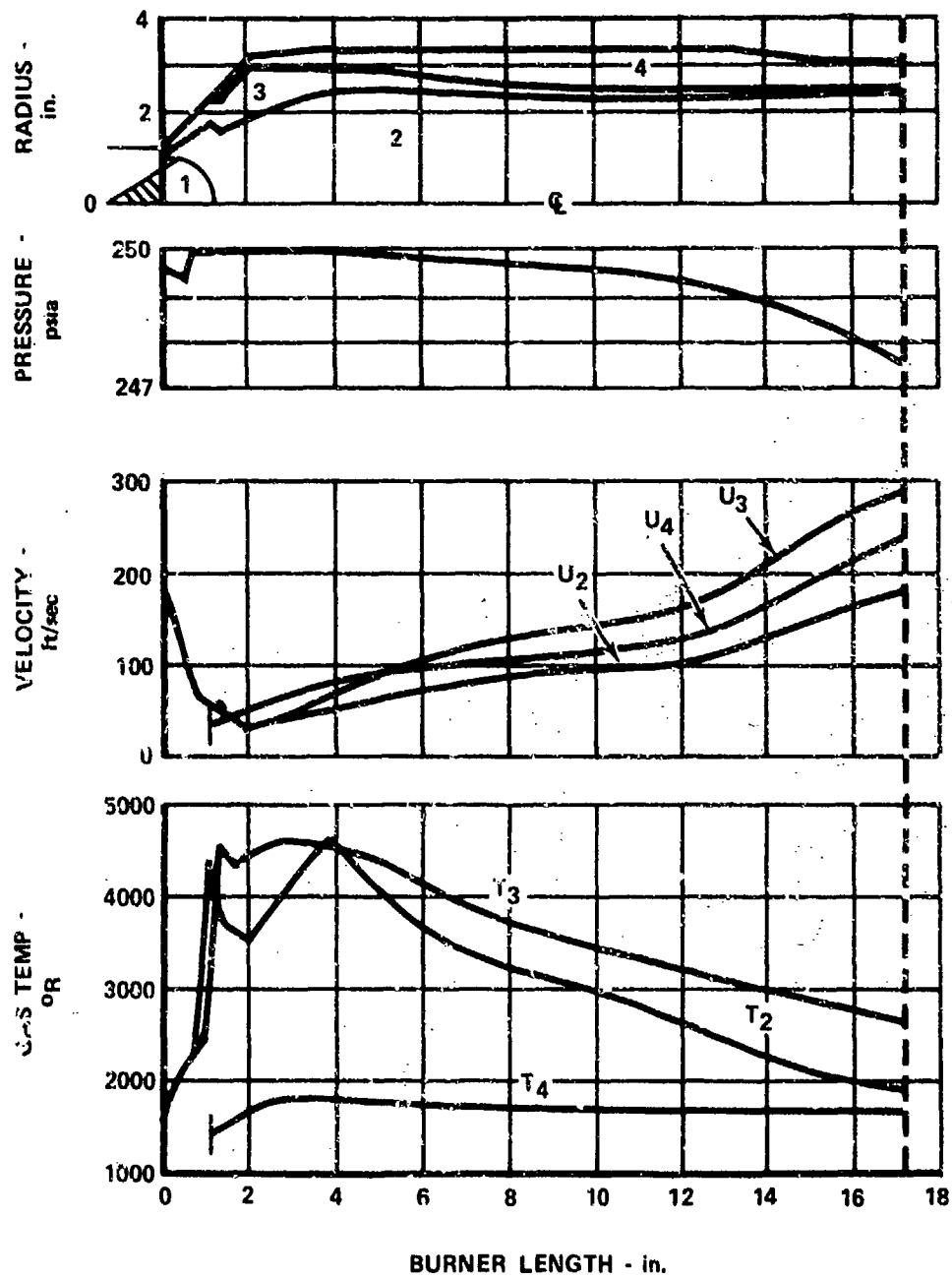


Figure 10. Analysis of a Bluff-Body-Stabilized Can Burner at Idle FD 71968

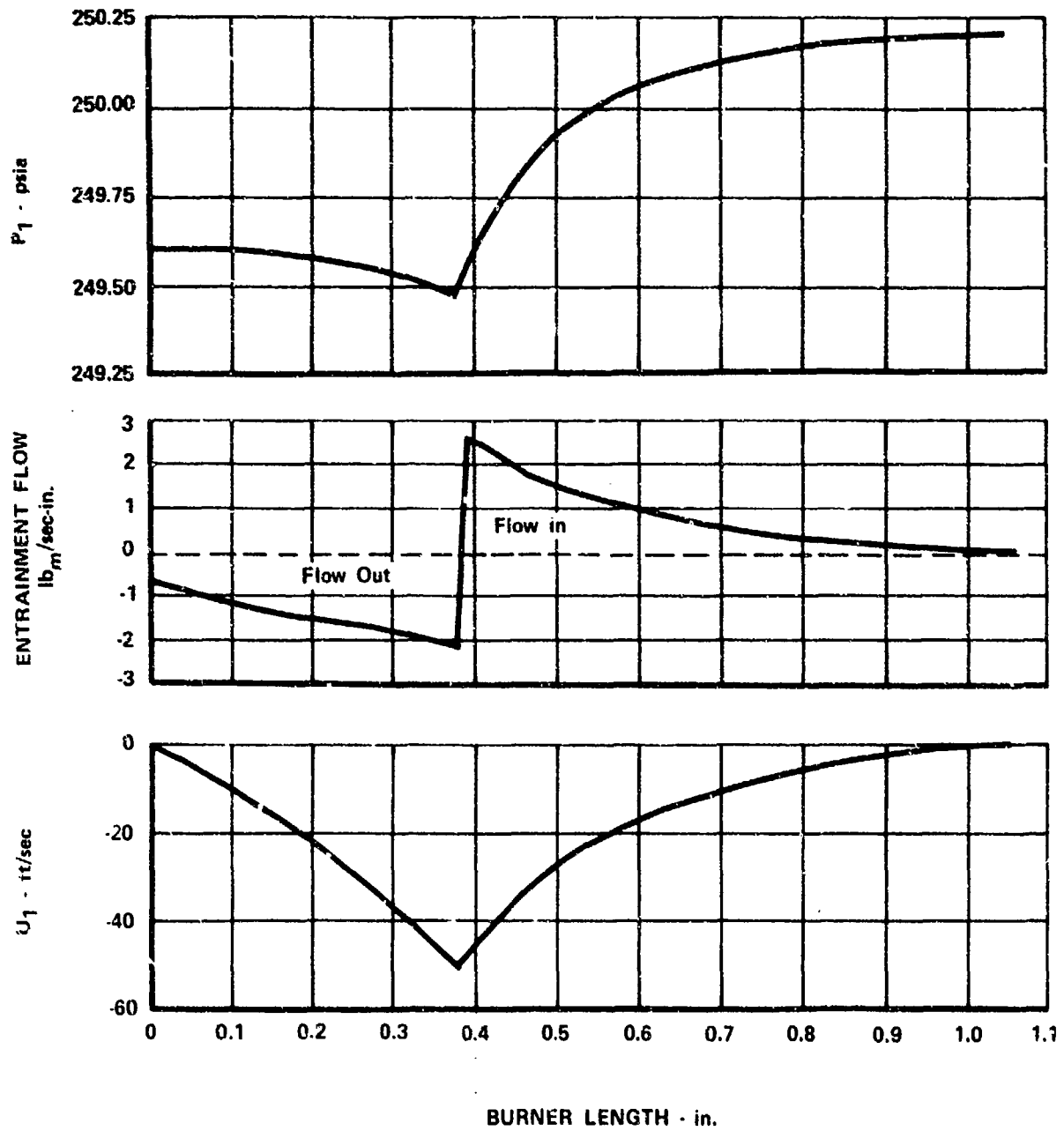


Figure 11. Cold-Flow Analysis of a Bluff-Body-Stabilized Can Burner

FD 71969

2. Discussion

Attempts to gain access to an advanced development engine and combustor rig were not successful owing to priorities within that program. As an alternative, emissions data obtained from current Pratt & Whitney Aircraft commercial engines were substituted. These engines are fitted with conventional swirl-stabilized, liquid-fuel-injection can and annular combustors. A body of such data was accumulated under EPA Contract 68-04-0027, Collection and Assessment of Aircraft Emissions Baseline Data - Turbine Engines and is available in Reference 24.

Emissions survey data for annular premixed and annular piloted swirl combustor configurations became available during the Phase I effort for model evaluation purposes. Funds from Contract F33615-71-C-1870 were not used to obtain these data.

The premixing combustor concept is characterized by one or more pre-mixing passages upstream of the primary combustion zone, wherein fuel is injected and is partially vaporized and mixed with the primary-zone airflow. Burning is stabilized in the wake of a perforated plate flameholder. The objective is to reduce combustion heterogeneity by reducing the impact of the rate-limiting vaporization and fuel-air mixing processes on primary-zone combustion.

The piloted swirl combustor concept makes use of swirl-induced flow instabilities to accelerate mixing between hot pilot exhaust gases and the main combustor fuel and air flows. With this concept, substantially faster mixing rates are provided than those obtainable with conventional turbulent jet mixing, allowing combustion to occur at high velocities with no regions of recirculation. This more rapid mixing results in increased sensitivity of the burning mixture to the addition of dilution air, theoretically permitting controlled quenching for reduction of NO_x emissions.

E. LABORATORY TEST PROGRAMS

1. General

A series of three laboratory research programs were conducted to assist in the development of the theoretical low-power emissions model. These studies, which provided representative data necessary for a practical solution to the low-power emissions problem, consisted of the following:

1. JT8D Burner Probing Tests
2. Turbulent Flame Studies
3. Low-Temperature Hydrocarbon Kinetics Studies.

The burner probing tests provided experimental mappings of UHC, CO, CO₂, O₂, N₂, A, and H₂O concentrations, and temperature distributions within the front end and at the exhaust section of a JT8D burner at simulated idle and approach conditions. This information assisted in the structuring of the main burner analytical model by providing a check on the model predictions. A secondary objective was to provide some assessment of intermediate species concentrations in order to verify the hydrocarbon kinetics scheme. For this pur-

pose, concentrations of low molecular weight hydrocarbons (CH_4 , C_2H_x , C_3H_y), H_2 , and water-soluble aliphatic aldehydes were measured; the latter species were measured only at a limited number of locations.

The turbulent flame studies provided realistic reaction rate data for inclusion into the reacting streamtube analysis of the analytical model. Reaction rates were measured for the rate of disappearance of fuel and for the rate of formation of CO under conditions of temperature, concentration, and turbulence that are typical of gas turbine engine combustors at low-power operation.

The low-temperature kinetics studies provided reaction rate data for vaporized fuel and CO under overall mixture conditions where strong combustion does not occur.

Such mixtures are characterized by high fuel concentrations, low oxygen concentrations, and temperatures ranging from 500 to 1300°F. The objective of this testing was to determine the extent to which chemical reaction under such conditions is responsible for the production of CO, UHC, and aldehydes at low-power operation.

2. JT8D Burner Probing Studies

a. Description of Test Apparatus and Facilities

The burner probing studies were conducted using an existing JT8D single-segment rig. The rig was mounted in a closed duct test facility as shown in figure 12. A JP-5-fired, single-pass heat exchanger was used to supply unvitiated air to the test burner. Remote control valves upstream and downstream of the test section regulated airflow and burner pressure. Existing rig instrumentation was used to set inlet Mach number, temperature, and fuel flow. Burner exit temperatures were also monitored to ensure proper burner operation.

All sampling tests were performed with the same JT8D Bill-of-Material (B/M) smoke reduction burner and fuel nozzle hardware. Sampling probe locations are shown in figure 13. Gas samples were withdrawn 1.54, 2.69 and 5.69 in. downstream of the nozzle face, at two azimuthal positions, and at the center of the exit transition duct. Samples from locations 1 and 2 were obtained with probes shown in figure 14A. Samples from the third front end location and from the burner exhaust were obtained with the probe shown in figure 14B. Both probe designs utilized steam cooling to maintain sample gas temperatures in excess of 300°F. In both designs, the cooling steam was exhausted downstream of the sampling inlet in high velocity jets to prevent dilution of the exhaust gas sample. A remotely controlled traverse mechanism, mounted to the rig sidewall, was used to radially position the sampling probe. A typical installation of the sampling probe and traverse mechanism is shown in figure 15.

The sampling train shown in figure 16 was used to collect gas samples for both batch and on-line analyses. All constituents except NO, NO_2 , and UHC were measured using batch analyses while on-line techniques were used for measuring NO, NO_2 , and UHC concentrations and as a backup technique for determining CO concentrations to verify measurement accuracies at low concentrations (<2500 ppmv). On-line measurements of CO_2 concentration were also made initially to verify compatibility of the batch and on-line techniques. The batch gas sample analysis was

performed on a CEC Model 620-A mass spectrometer and a modified F&M Model 700 gas chromatograph with a Tracor ultrasonic detector. Gas chromatography was required to separate CO and N₂, which appear as a single peak in the gas sample mass spectrum. The on-line analysis of CO and CO₂ was accomplished with a Beckman Model 402 HT hydrocarbon analyzer. A Beckman Model 315 nondispersive infrared analyzer was used to determine the NO concentration. Measurements of NO₂ were made using a Beckman Model 255 nondispersive ultraviolet analyzer. Teflon sample lines were used where possible. All lines were electrically heated to maintain sample gas temperatures in excess of 300°F.

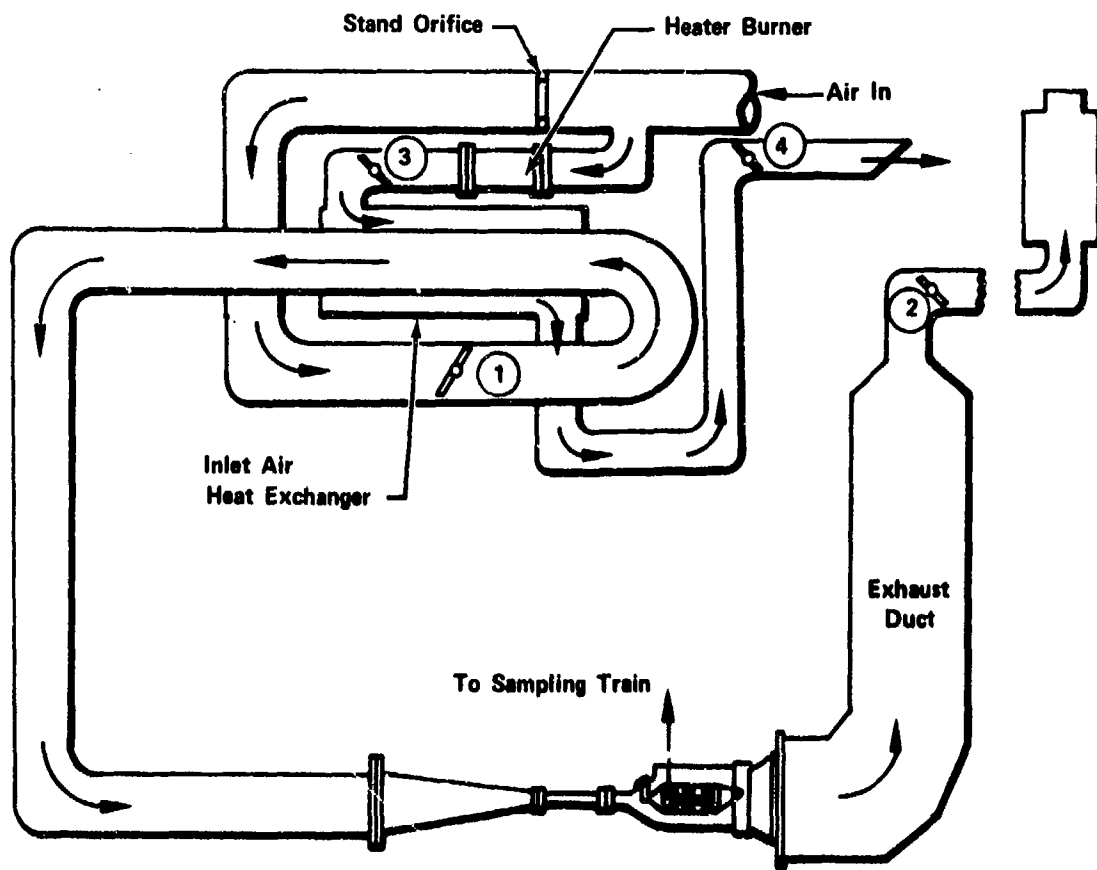
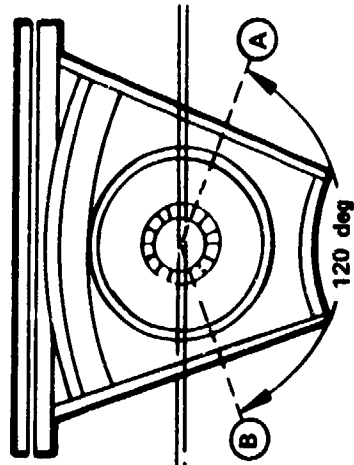


Figure 12. Schematic Diagram of JT8D Burner Probing Rig

FD 56971A

Azimuthal Probe Locations



Axial Probe Locations

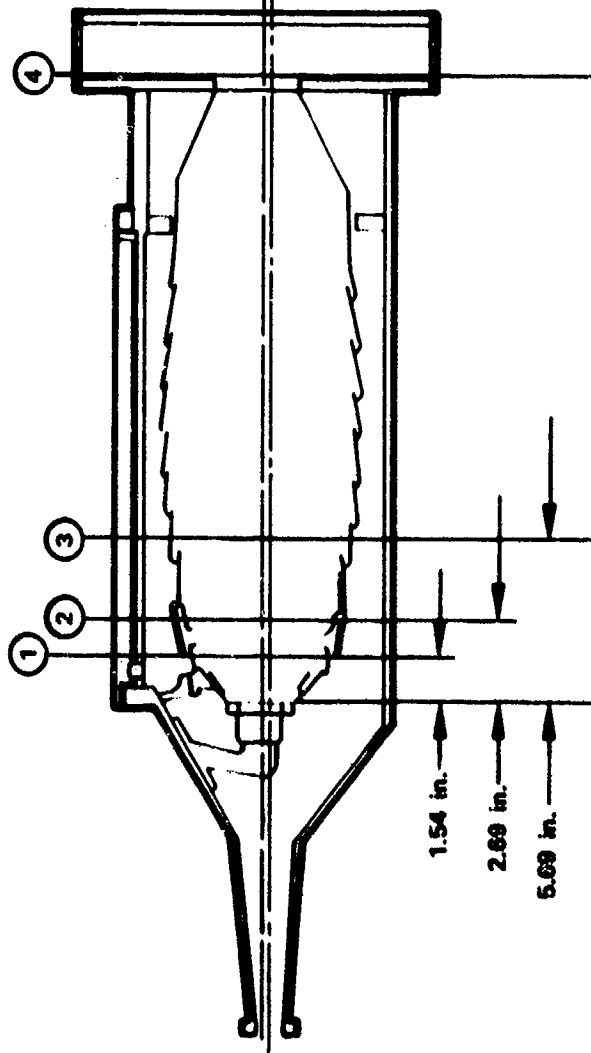


Figure 13. Sampling Probe Locations

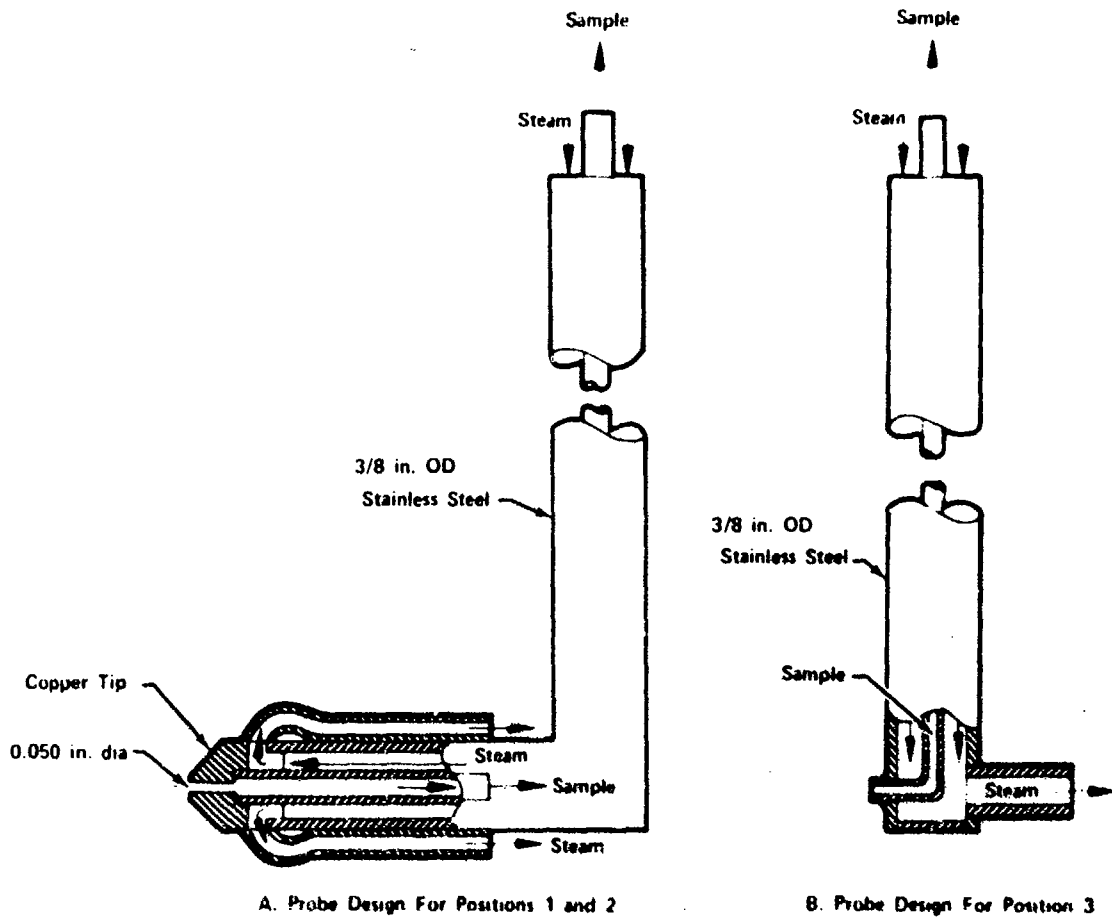


Figure 14. JT8D Sampling Probes

FD 56969A



Figure 15. JT8D Sampling Probe and Traverse Mechanism

FD 71981

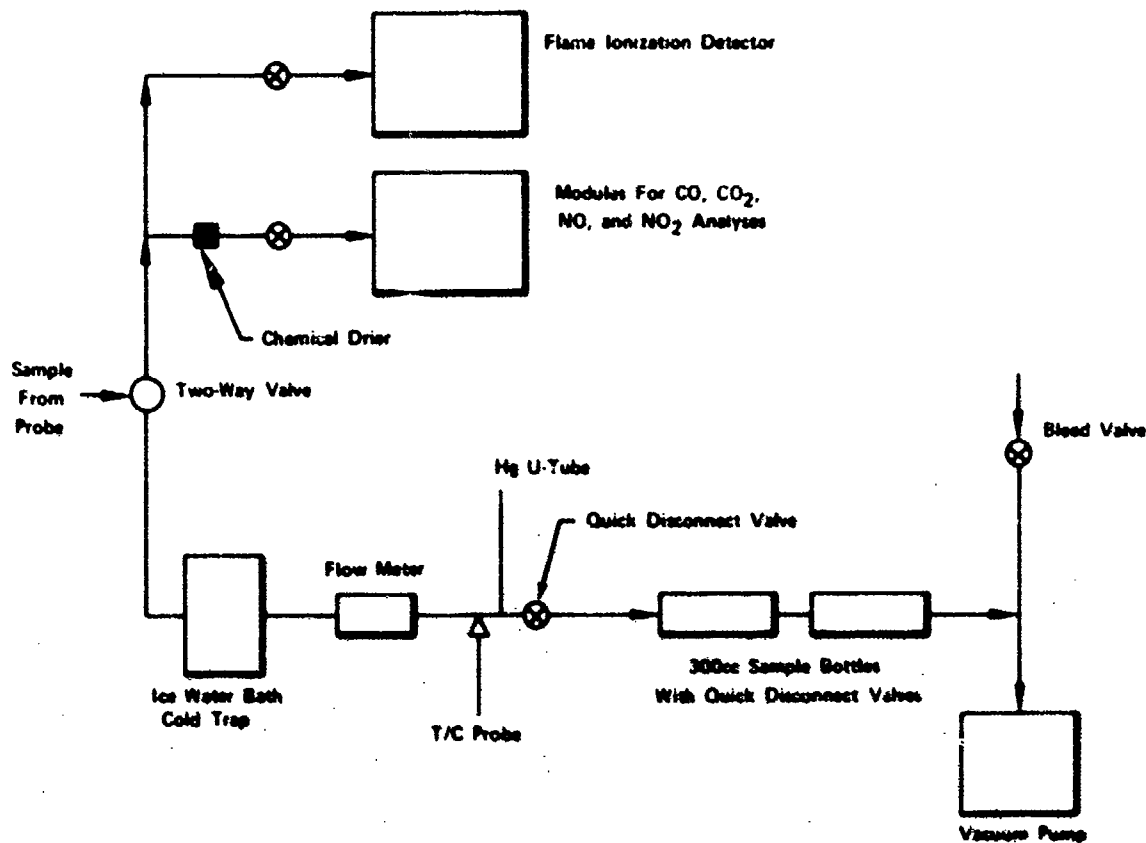


Figure 16. JT8D Burner Probing Sampling Train

FD 71970

In preparing the gas sampling train, both stainless steel and glass sample bottles were available for use. The steel bottles were preferable because sample loss due to leakage occurred less frequently, the bottles could be pressurized without breakage, and handling problems were simplified. However, it was known that at low CO and CO₂ concentration levels (<100 ppmv), error could be introduced by the adsorption of CO and CO₂ on the walls of the steel sample bottle. To investigate this possibility, comparative tests were run with glass and metal bottles using a gas of known composition. The results of these tests indicated that any errors introduced by an adsorption on the metal walls were obscured by the level of experimental uncertainty. Therefore metal bottles were used for the test program.

b. Test Program

Probing of the JT8D burner was accomplished at simulated engine idle and approach conditions. Full sets of gas samples were withdrawn at the locations and conditions shown in tables IV and V. Concentrations of CO, CO₂, O₂, H₂, and UHC were determined at all probe positions, and operating conditions; concentrations of NO and NO₂ were measured at the 2A position during simulated idle operating conditions; and concentrations of aldehydes were measured at the 2B position during simulated idle operating conditions.

Table IV. Test Matrix for JT8D Probing Tests

Axial Probe Location Downstream of Nozzle Face, in.	Operating Condition (See table V.)	Azimuthal Probe Location (See figure 13.)
(1) 1.54	Idle (Half traverse)	B
(2) 2.69	Idle	A, B
(3) 5.69	Idle	A, B
(4) Burner exhaust	Idle	Radial plane of symmetry
(2) 2.69	Approach	B
(3) 5.69	Approach (Half traverse)	B
(4) Burner exhaust	Approach	Radial plane of symmetry

Table V. Operating Conditions for Simulation of Engine Idle and Approach

Condition	Inlet Pressure, in. HgA	Inlet Temperature, °F	Air Flowrate, pph	Fuel Flowrate, pph	Fuel-Air Ratio
Idle	73	240	13,451	101	0.0075
Approach	73	669	9,764	125	0.0131

Concentration-location profiles for most of the aforementioned species obtained during the probing tests and the corresponding calculated fuel-air ratio-location profiles are presented in Appendix I. Concentrations of CO, CO₂, O₂, H₂, and NO measured are reported in ppmv on a dry basis; concentrations of UHC, as equivalent methane, are reported in ppmv on a wet basis. Aldehyde concentrations refer to soluble aliphatic aldehyde concentrations expressed in ppmv as equivalent formaldehyde. Concentrations of NO₂ measured during the probing tests did not exceed 3 ppmv and are, therefore, not included in the data shown in Appendix I. In addition, data on the concentrations of H₂ measured at simulated idle operating conditions and of H₂ and UHC measured in the combustion exhaust gas were also found to be essentially negligible and are not shown in Appendix I.

As indicated in table IV, data at two locations were obtained from half-traverse measurements. This procedure was deemed necessary under some conditions to minimize probe-tip plugging with coke from the decomposition of raw fuel. Plugging of the steam-cooled sampling probes was a persistent problem throughout the test program for all operating conditions. (See figure 17.) However, as a general observation, plugging became more severe during tests in which probing at locations near the nozzle face and at high power settings was involved. On the other hand, probe durability problems were most severe at the end of the primary zone (location 3) where the combustion process was nearing completion, but before significant amounts of dilution air had been added. Experience showed that plugging could be minimized by proper probe design and by arrangement of the test sequence to minimize exposure time.

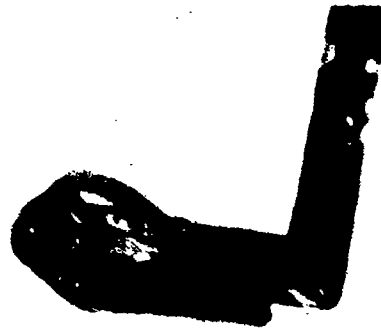


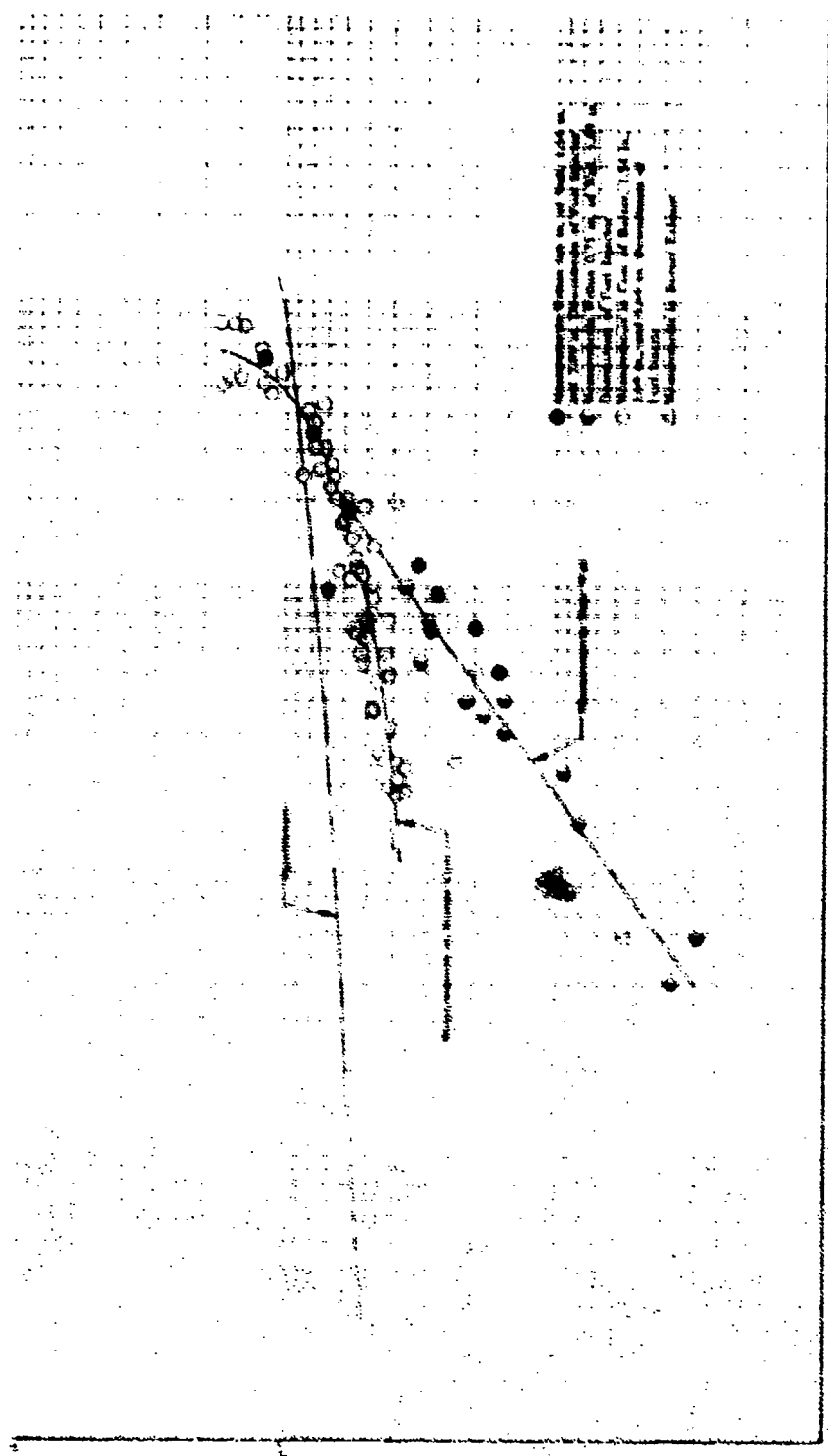
Figure 17. (Upper) View of Gas-Sampling Probe Before Testing; (Lower) View of Gas-Sampling Probe Tip Showing Plugging

FD 71971

c. Discussion of Results

In analyzing the probing data to identify the mechanisms responsible for low-power emissions, local CO concentrations were found to correlate with local fuel-air ratio as shown in figures 18 and 19. Several interesting results emerge from the correlation at simulated idle operating conditions, figure 18:

1. CO concentration is found to be greatly in excess of the equilibrium concentration for lean mixtures and for rich mixtures up to a fuel-air ratio of 0.092
2. CO oxidation is quenched in wall cooling layers, as reflected by the fact the CO concentration is higher near the wall than in the core of the burner
3. CO concentration is a strong function of the local fuel-air ratio.



W. L. HARRIS, JR., M.S.

Figure 14. Variation in Local CO Concentration with Local FA at Simulated Idle Operating Conditions DF 91105

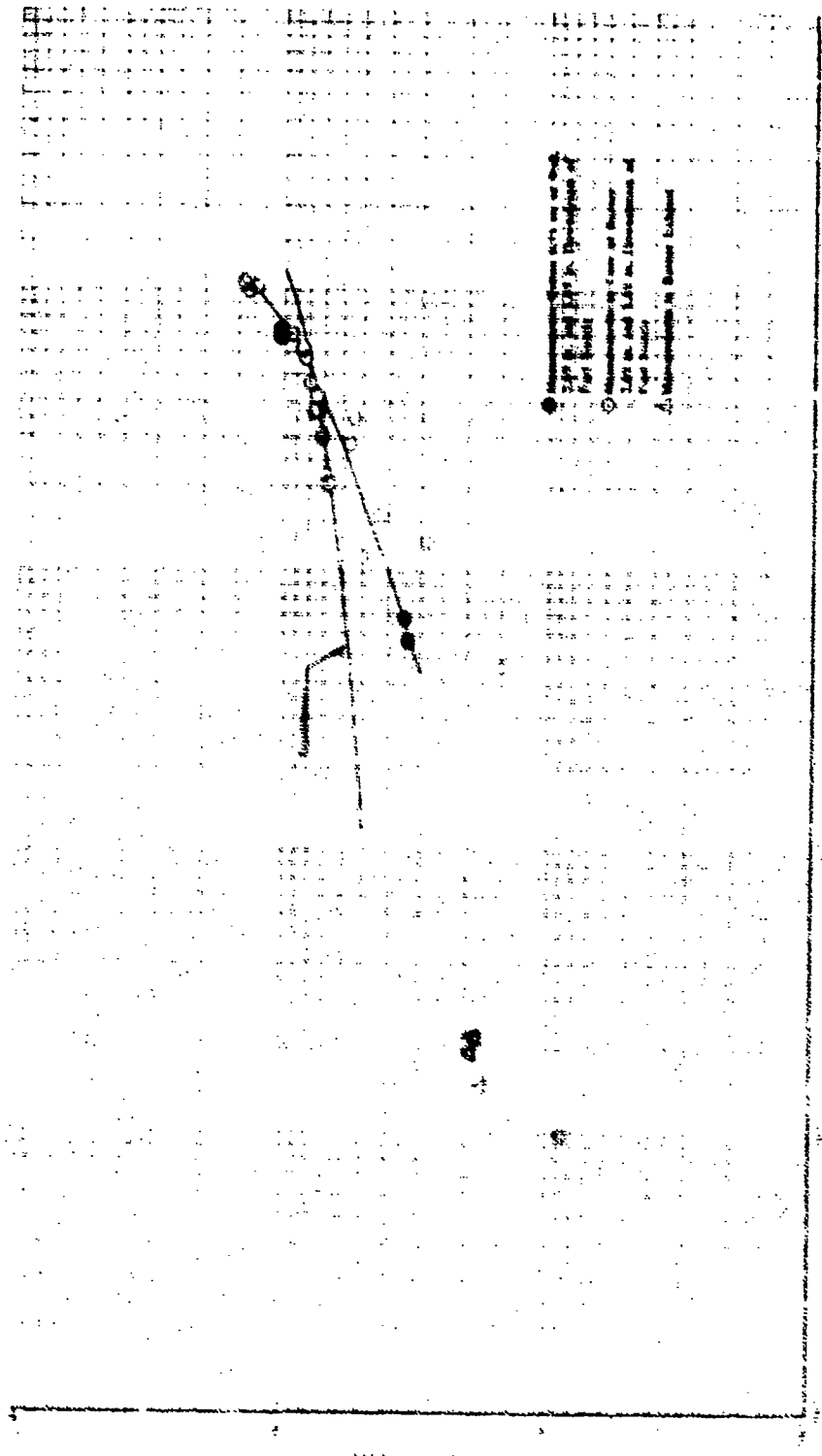


Figure 19. Variation in Local CO Concentration with Local FA at Simulated Approach Conditions DF 91104

The data taken at simulated approach conditions are presented in figure 19. The wall-quenching effect is absent at this operating point, and CO levels within the burner are higher than those at idle conditions at the same fuel-air ratio. However, CO levels within the burner at approach conditions are much closer to the equilibrium values; the exhaust concentration of CO is lower than at idle conditions (i.e., 200 ppmv vs 950 ppmv). In addition, the percentage reduction in UHC concentrations in the combustor exhaust gas is significantly greater than that for CO; UHC concentrations were reduced from 918 ppmv to 7 ppmv equivalent methane.

The reasons for the aforementioned behavior have not been completely explained. However, considering the combustion process as consisting of two successive steps, i.e., the oxidation of fuel to CO followed by the relatively slow conversion of CO to CO₂, the observed behavior suggests that the reduced emissions at approach conditions are primarily the result of the higher burner inlet air temperature. The latter increases the rate of fuel consumption in the primary zone.¹ Near the wall and in the secondary zone, the higher temperature of the combustion products and the cooling and dilution air act to attenuate quenching effects and increase the rate of oxidation of CO to CO₂.

To complete the analysis of the JTSD probing data, local values of combustion temperature and efficiency were computed from the species concentration data that were obtained at simulated idle and approach operating conditions. The local combustion temperature was calculated from an enthalpy balance between the quenched species and the local fuel-air mixture, assuming that the unreacted JP-5 exists in the vapor state and that the dissociation of H₂O to H and OH is equilibrated. Two methods were used to compute the local combustion efficiency:

$$\eta = \frac{\int_{T_c}^{T_{pa}} c_{pa} dT}{\int_{T_c}^{T_{th}} c_{pth} dT} \times 100 \quad (20)$$

$$\eta = \frac{X_{O_2 th} - X_{O_2 in}}{X_{O_2 in} - X_{O_2 th}} \times 100 \quad (21)$$

¹The effect of initial temperature on CO and UHC concentration is readily seen in the results of the turbulent flame study, which are discussed in paragraph E.3, following. In figures 28 and 30, the distribution of CO and UHC is presented for an equivalence ratio of 1.2 and inlet temperatures of 240 and 665°F, corresponding to idle and approach conditions, respectively. It is seen that at 665°F, CO concentrations are greatly in excess of those at 240°F and UHC levels are markedly reduced.

where

T_0 = the initial temperature of the combustible mixture

T_a = actual temperature of combustion products

T_{th} = temperature of combustion products as a result of complete combustion

C_{pa} = heat capacity of quenched combustion products

C_{pth} = heat capacity of products of complete combustion

$X_{O_2 in}$ = $0.2316/(1 + FA)$

X_{O_2m} = mass fraction of oxygen in combustion products

X_{O_2th} = mass fraction of oxygen in products of complete combustion

Equation 20 compares the quantity of energy actually released as a result of combustion to the quantity of energy supplied by the fuel. Equation 21 is an oxygen depletion efficiency based on the ratio of oxygen actually consumed to that consumed at equilibrium.

The resultant temperature and combustion efficiency profiles, corresponding to the probing locations shown in figure 13 are presented in Appendix II. The oxygen depletion efficiency is presented for all probing locations and operating conditions. Corresponding values of the energy efficiency are shown at various locations within the combustor in figures 185, 186, and 188 in that Appendix. It is seen that the agreement between the two methods is poor at the most upstream position in the front end where combustion efficiency is low. The agreement improves with downstream position, the values of combustion efficiency from the two methods becoming virtually identical at the end of the front end. This behavior is attributed primarily to uncertainty as to the chemical and physical state of the unreacted fuel in the low efficiency regions of the combustor.

The CO concentration and combustion temperature profiles were examined to determine the temperature below which CO oxidation is quenched. Using the correlation of CO concentration with fuel-air ratio to identify the quenched state, figure 18, it was found that quenching occurs at approximately 2200° F. A corresponding segregation of UHC concentration into quenched and unquenched states were not observed.

3. Turbulent Flame Studies

a. Description of Test Apparatus and Facility

Turbulent flame tests were conducted in the facility shown schematically in figure 20. Air was supplied to the test section by a remote high-capacity blower and was metered by a calibrated flat-plate orifice. An electrical air heater, 10 kw, supplied the capability for varying air temperatures from 240 to 665°F over the range of airflow rates required. Liquid fuel was supplied from a storage tank, which was pressurized by nitrogen, and was metered by a calibrated rotameter. The fuel was heated by an electrical heater to provide vaporized fuel at the injector inlet. A mixture of 83% isooctane and 17% benzene was selected to simulate JP-5 fuel in both the turbulent flame studies and the low-temperature hydrocarbon kinetic studies; the latter is described in paragraph E.4, following. The isooctane-benzene proportions were selected to represent the principal components of JP-5 fuel. The two-component fuel blend permitted close determination of physical properties, and since it was injected as a vapor, a well defined vaporization temperature was provided.

The test section is shown in figures 21 and 22. Vaporized fuel was injected through a ring injector with six holes directed in the upstream direction to provide the initial fuel dispersion. The fuel-air mixture then passed through a baffled mixing section and was introduced into the test section through a slotted (1.0 by 0.64 in.) flat-plate flameholder. A converging bell mouth was installed to prevent recirculation upstream of the flameholder. The cross-section of the water-cooled rectangular combustion chamber was 1.5 by 3.0 in., and its length was 18.0 in. It was constructed as an assembly of interchangeable sections having various lengths. The probe section allowed probing to be accomplished across either rectangular axis. By selectively interchanging the sections, gas samples could be withdrawn at 1.0-in. increments along the combustion chamber axis.

Gas samples and total pressure measurements were obtained with the probe shown schematically in figure 23. This constant blockage (12%), air cooled, elliptical cross section, stainless steel probe was inserted through the 1.50-in. sidewalls into the gas flowpath. The minor axis of the probe was normal to the flow. Calibration tests were performed on the probe to ensure isokinetic sampling. Samples withdrawn from the test section were collected in stainless steel sample bottles and were subsequently analyzed by the methods described earlier in this report for the JT8D studies.

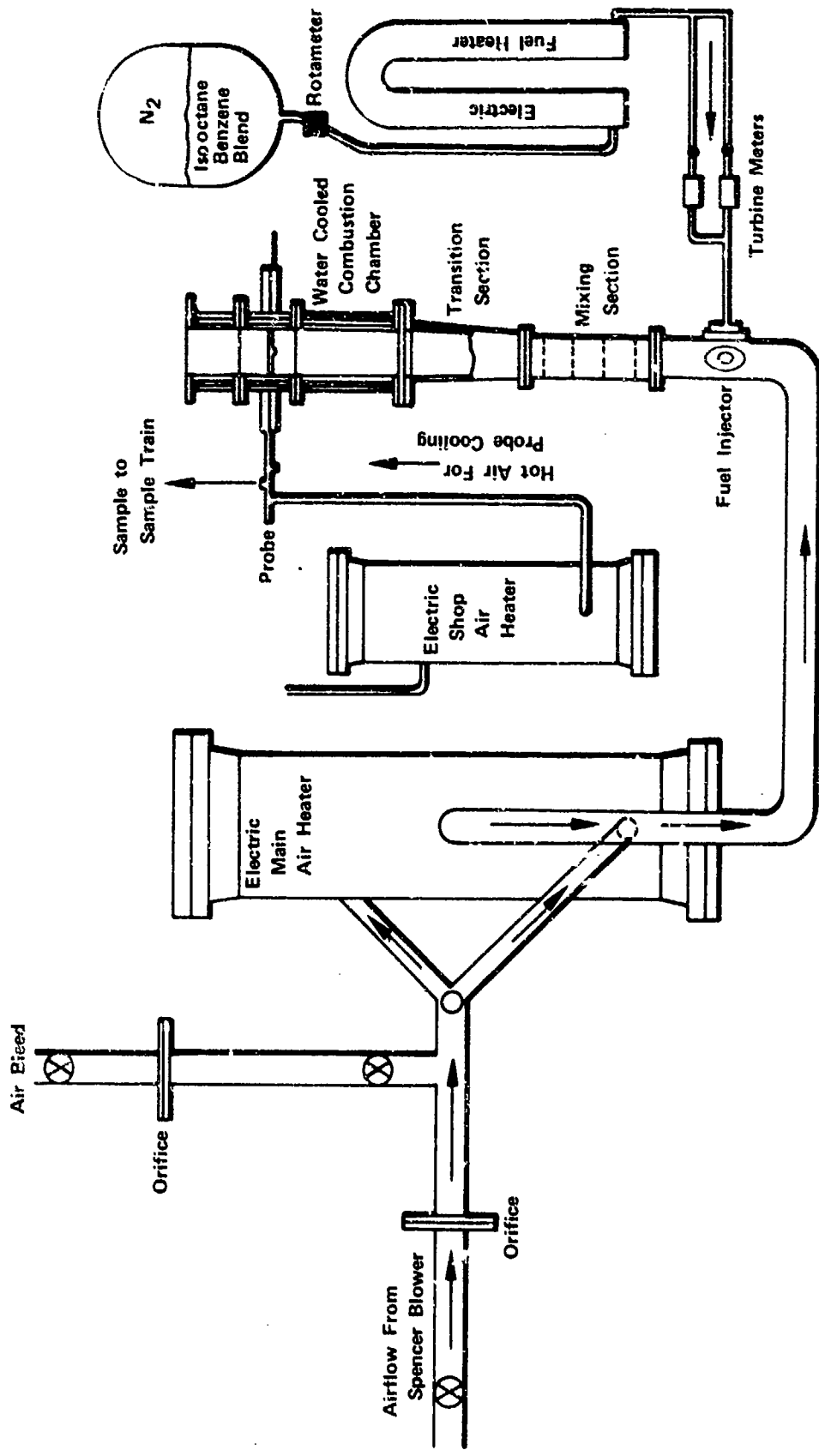
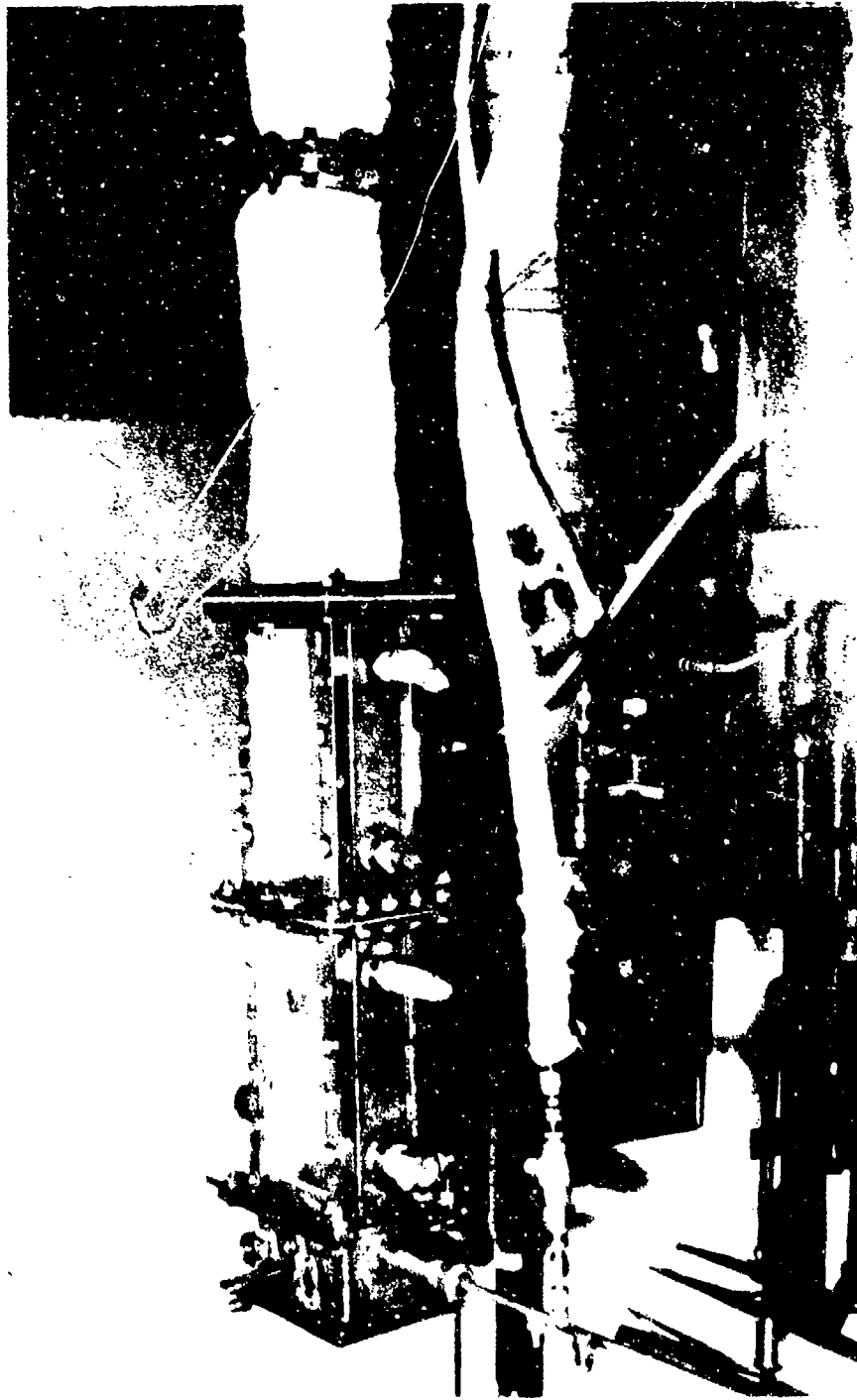


Figure 20. Schematic Diagram of Turbulent Flame Study Rig

FD 56965A



FD 719s2

Figure 21. Test Section for Turbulent Flame Studies

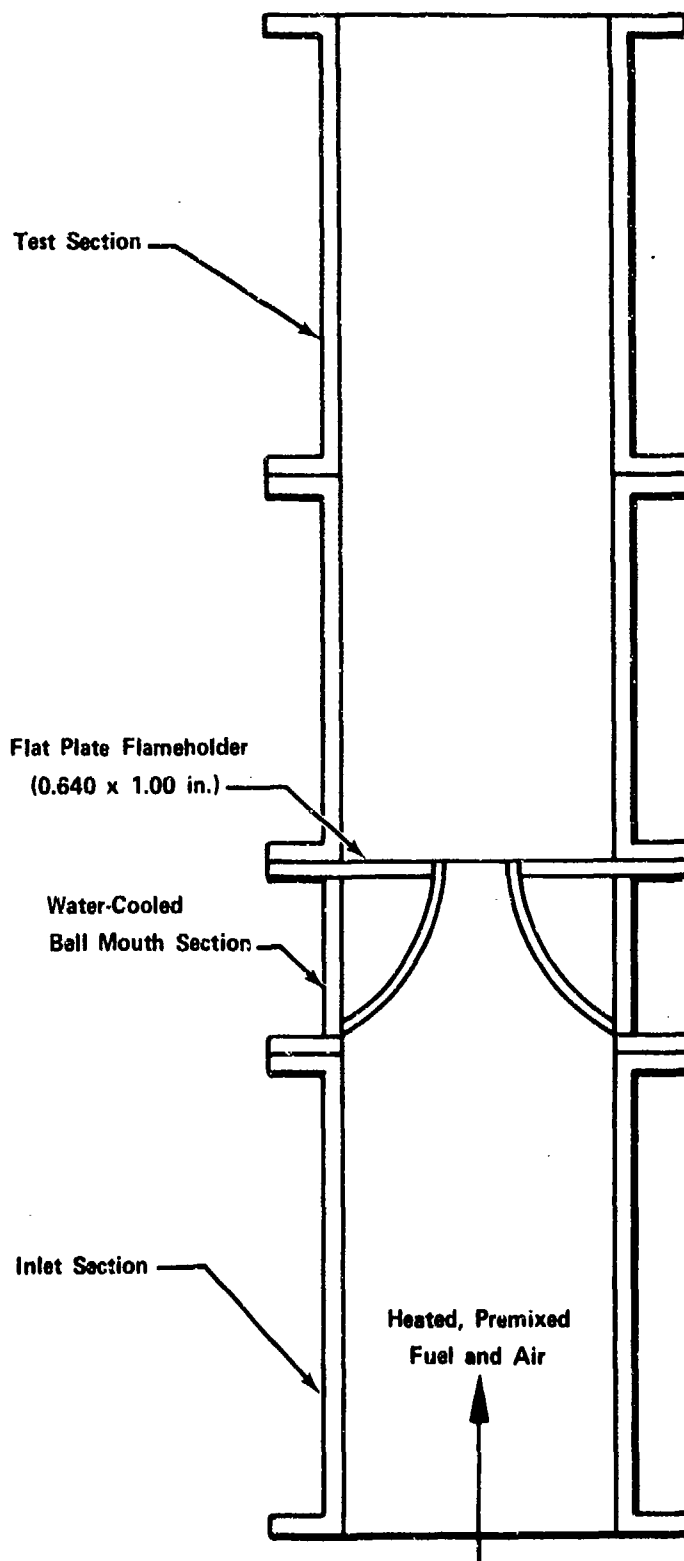


Figure 22. Test Rig for Turbulent Flame Studies

FD 60889A

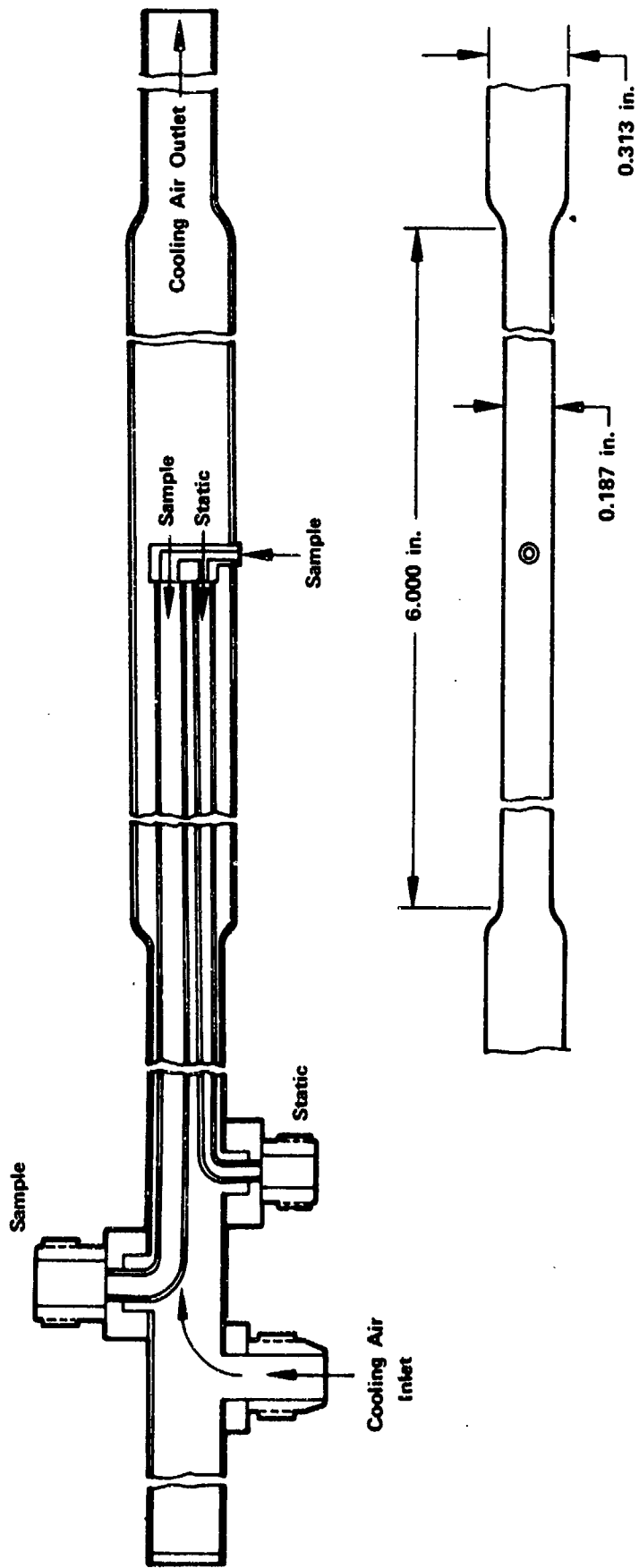


Figure 23. Sampling Probe for the Turbulent Flame Study Test Rig

FD 56976A

b. Test Program

Full sets of gas samples were withdrawn at the locations and conditions shown in table VI. In this table, ϕ is the fuel-air equivalence ratio and T is the inlet temperature. Test conditions were chosen to be representative of the conditions existing within a JT8D burner at low-power operation. The inlet temperature points correspond to the idle and approach conditions in the JT8D burner probing test matrix.

(See paragraph E.2, preceding.) Gas samples were withdrawn along an axis normal to the flow within the chamber and across the 3-in. dimension. Velocity profiles were also measured at each test condition. Typical concentration profiles obtained during these tests are presented in figures 24 through 27. The corresponding centerline concentrations of CO and UHC are shown in figures 28 through 31 as a function of axial distance downstream of the flameholder. Total UHC represents the sum of the individual methane, ethane, propane, and parent fuel (isooctane - benzene blend) values.

c. Discussion of Results

The objective of the turbulent flame studies was to obtain global reaction rate expressions for the rate of disappearance of CO and fuel (total UHC) under conditions of temperature, concentration, and turbulence typical of low power operation. To generate the desired global expressions, local reaction rates for fuel and CO had to be determined from the measured concentration profiles. An analytical procedure was developed for solving the species and momentum conservation equations required to obtain the reaction rates. This calculation procedure is described in Appendix III. Figures 32 and 33 present the resulting reaction rates for fuel and CO at the various locations downstream of the flameholder. For both species, the reaction rates are observed to reach maximum values in the x direction between 4 and 6 in. (from the flameholder) and then fall off as the distance, x, increases. The peak values are much greater for the higher equivalence ratio and temperature conditions.

Table VI. Test Matrix for Turbulent Flame Probing Studies

Axial Probe Location Downstream of Flame- holder, in.	$\phi = 1.0$ T = 240°F	$\phi = 1.2$ T = 240°F	$\phi = 1.2$ T = 665°F
3	*	*	*
4	*	*	*
5	*	*	*
6	*	*	*
7	*	*	
8	*	*	

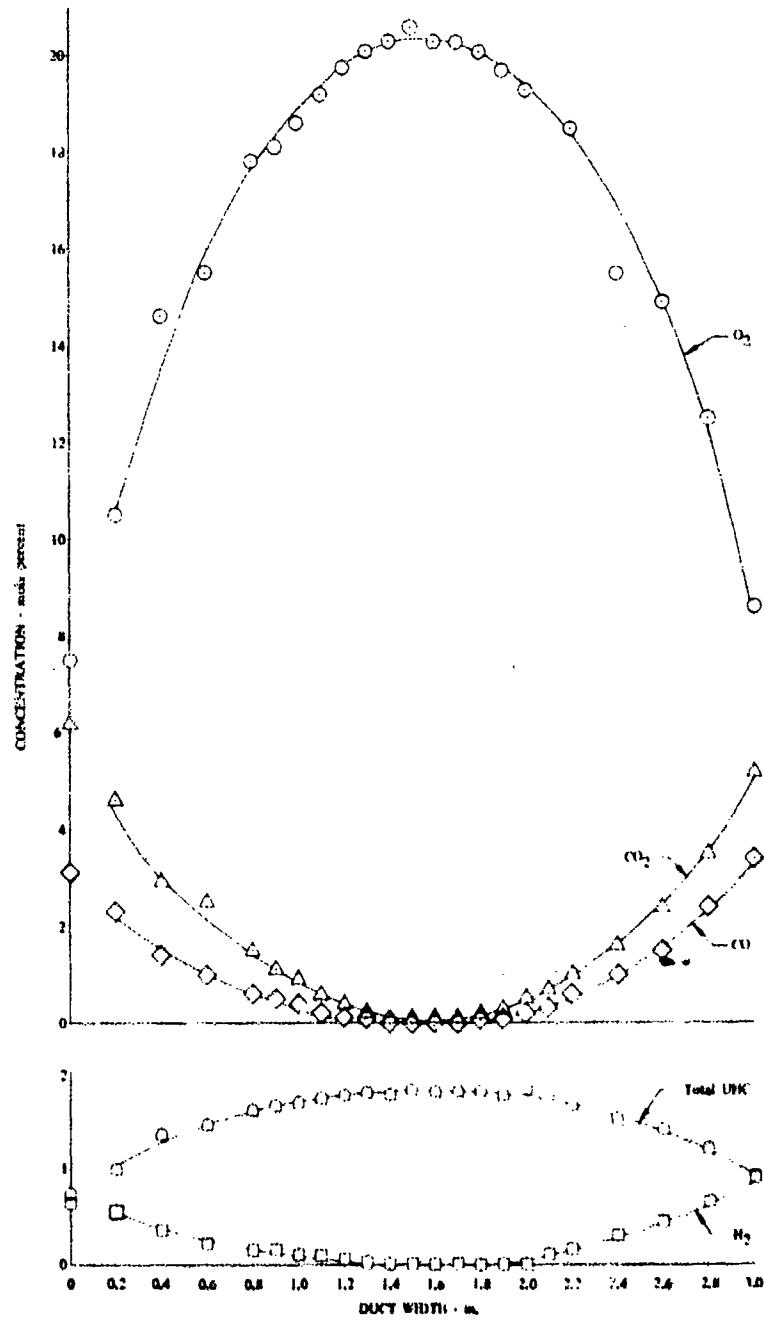


Figure 24. Variation in Combustion Product Concentration with Lateral Position 3 in. Downstream of Flameholder ($\phi = 1.0$, $T = 245^\circ\text{F}$) DF 91103

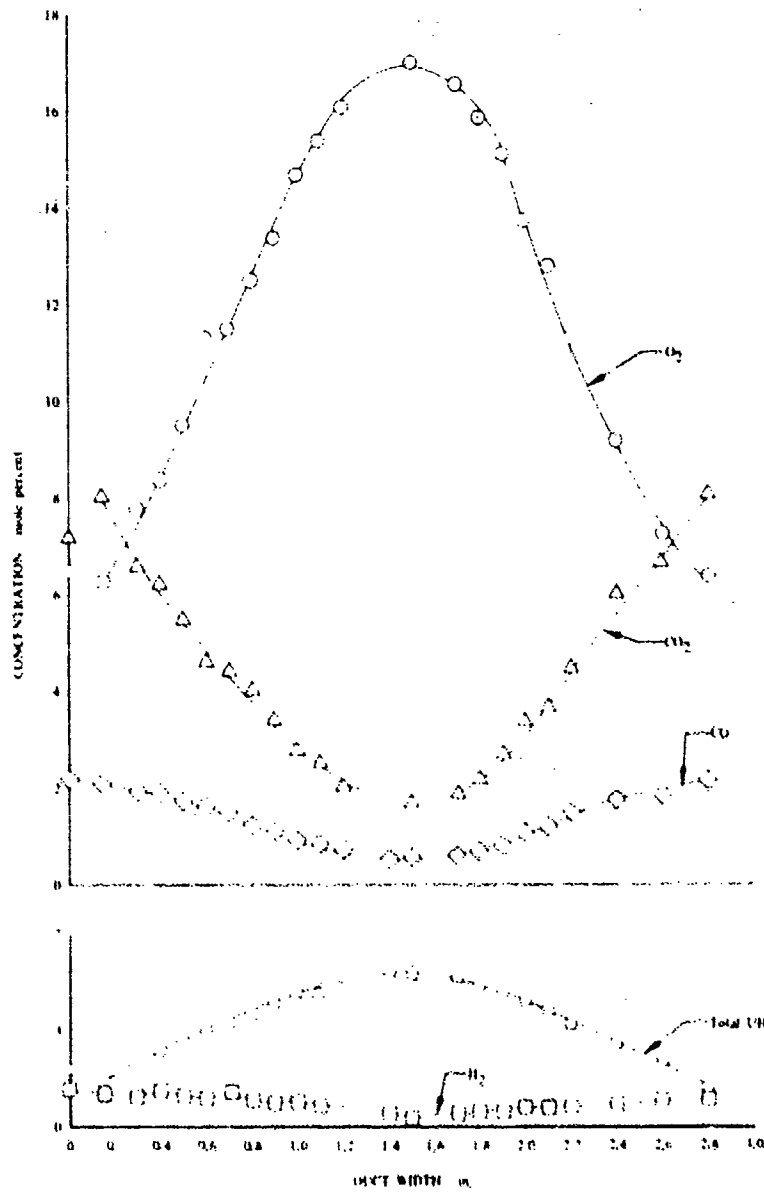


Figure 25. Variation in Combustion Product Concentrations with Lateral Position 5 in. Downstream of Flameholder ($\phi = 1.0$, $T = 240^\circ\text{F}$) DF 91102

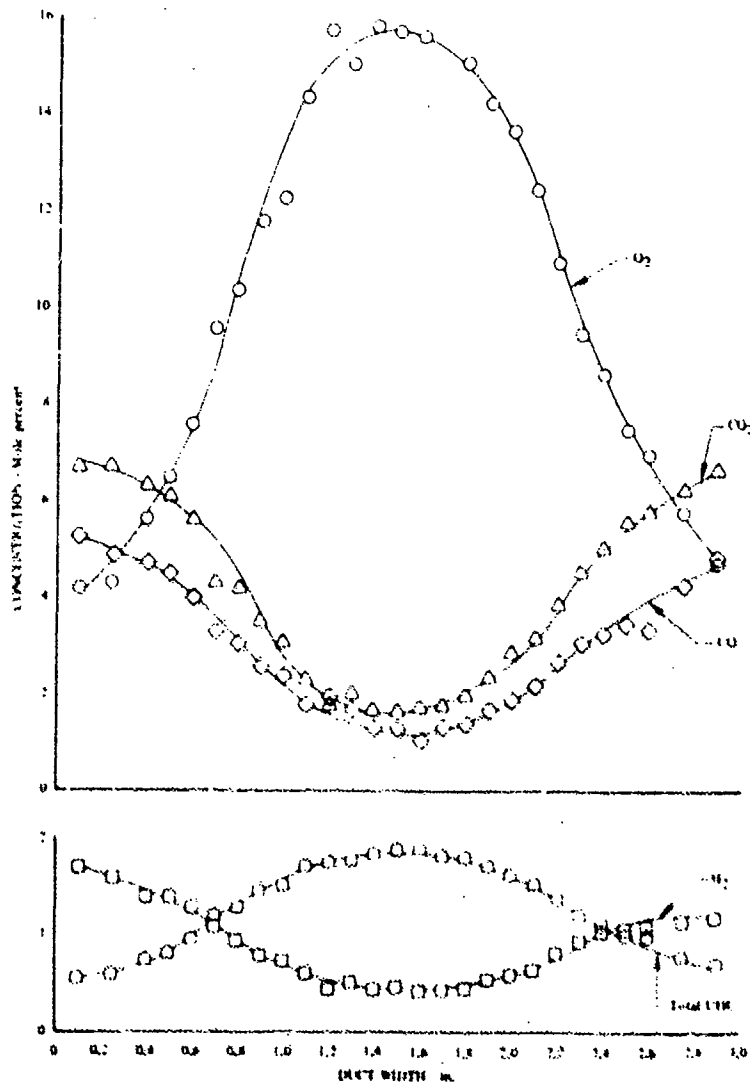


Figure 26. Variation in Combustion Product Concentrations with Lateral Position 5 in. Downstream of Flameholder (ϕ 1.2, T 243°F) DF 91101

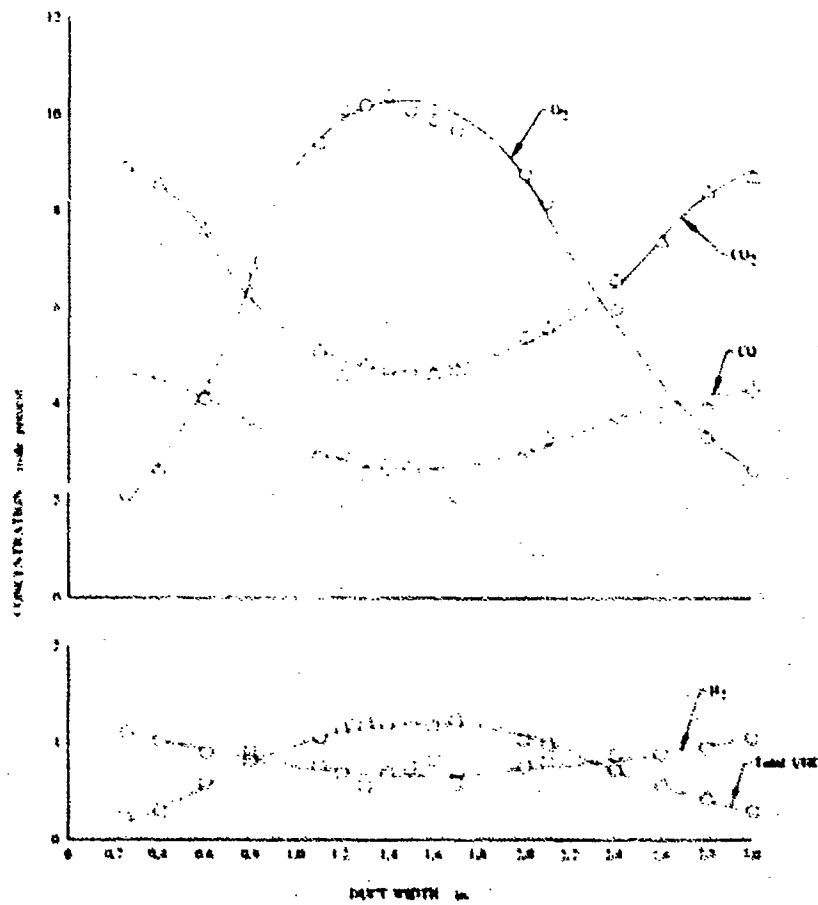


Figure 27. Variation in Combustion Product Concentration with Lateral Position 5 in. Downstream of Flameholder ($\phi = 1.2$, $T = 665^\circ\text{F}$) DF 91100

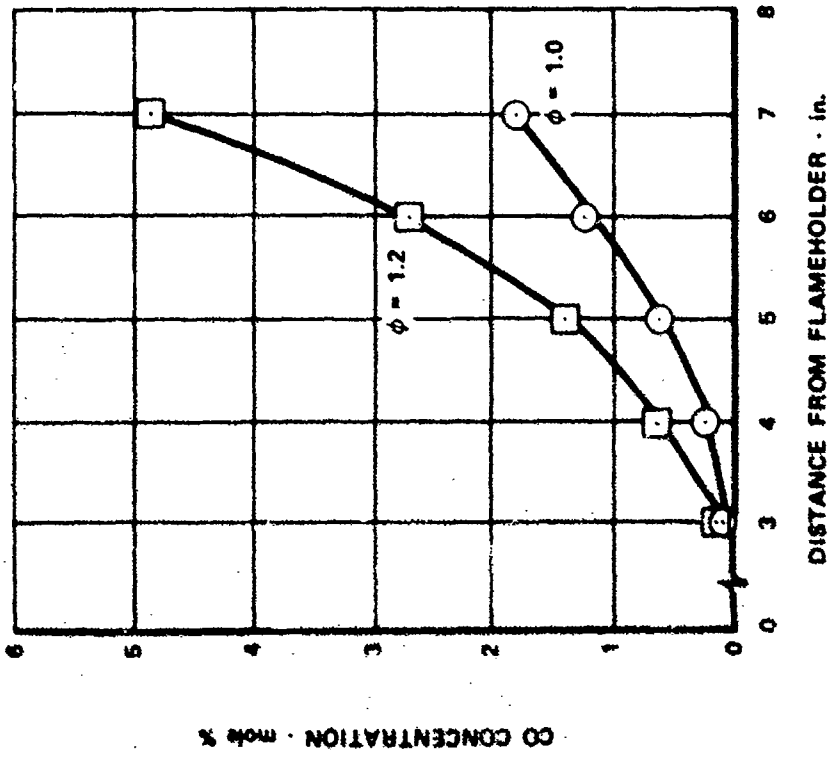


Figure 29. Variation in CO Concentration with Axial Distance from Flameholder and Equivalence Ratio Along Rig Centerline ($T = 240^\circ\text{F}$)

FD 71974

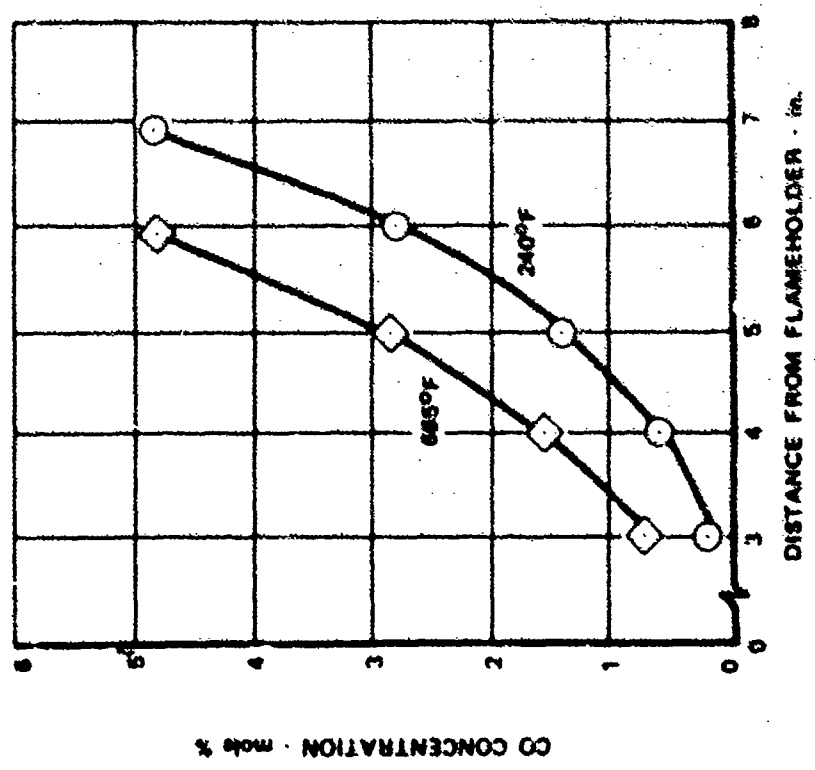


Figure 28. Variation in CO Concentration with Axial Distance from Flameholder and Temperature Along Rig Centerline (Equivalence Ratio = 1.2)

FD 71972

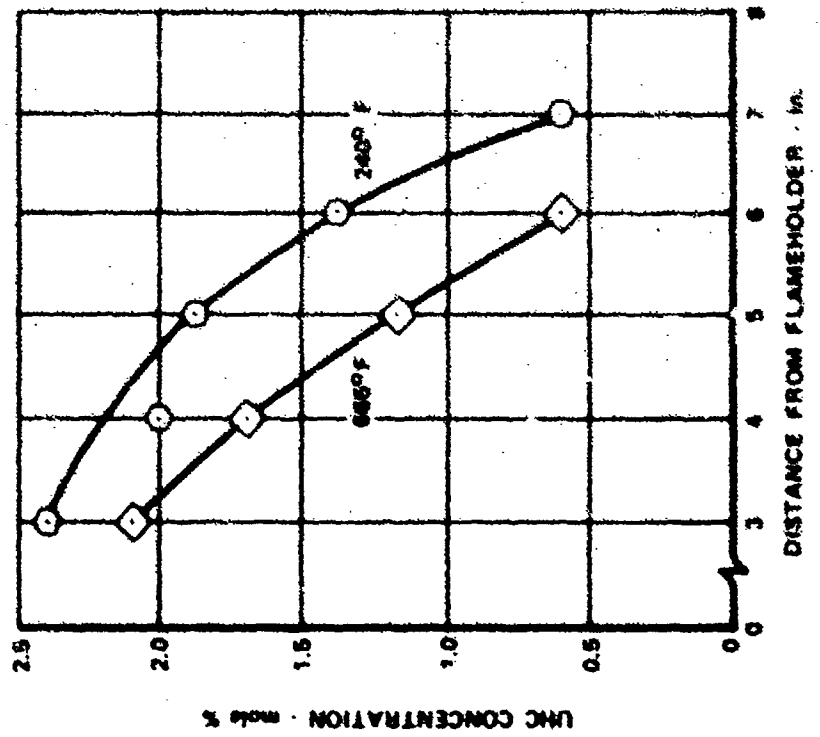


Figure 30. Variation in UHC Concentration with Axial Distance from Flameholder and Temperature Along Rig Centerline (Equivalence Ratio = 1.2)

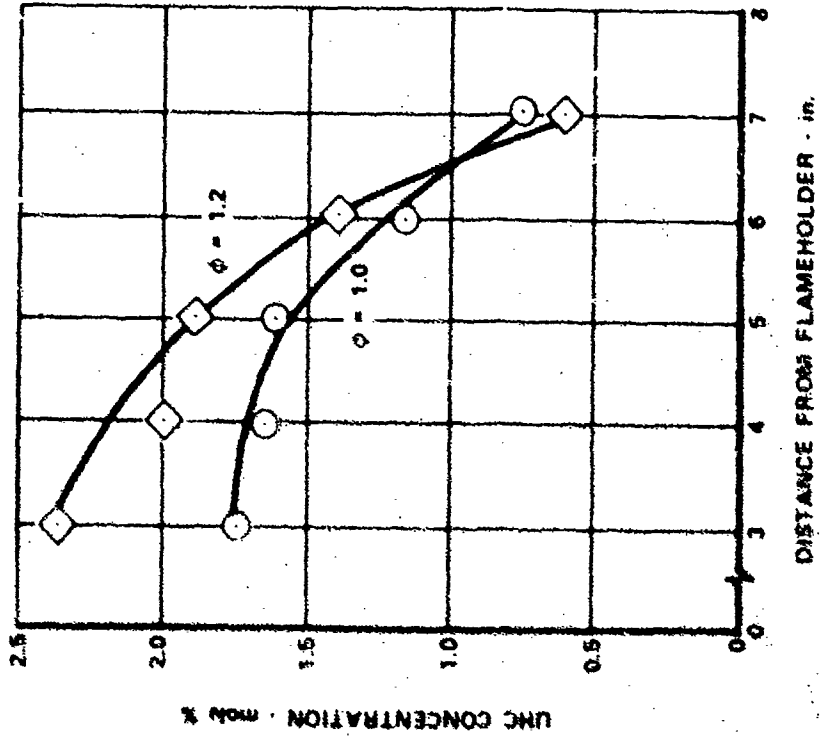


Figure 31. Variation in UHC Concentration with Axial Distance from Flameholder and Equivalence Ratio Along Rig Centerline (T = 240°F)

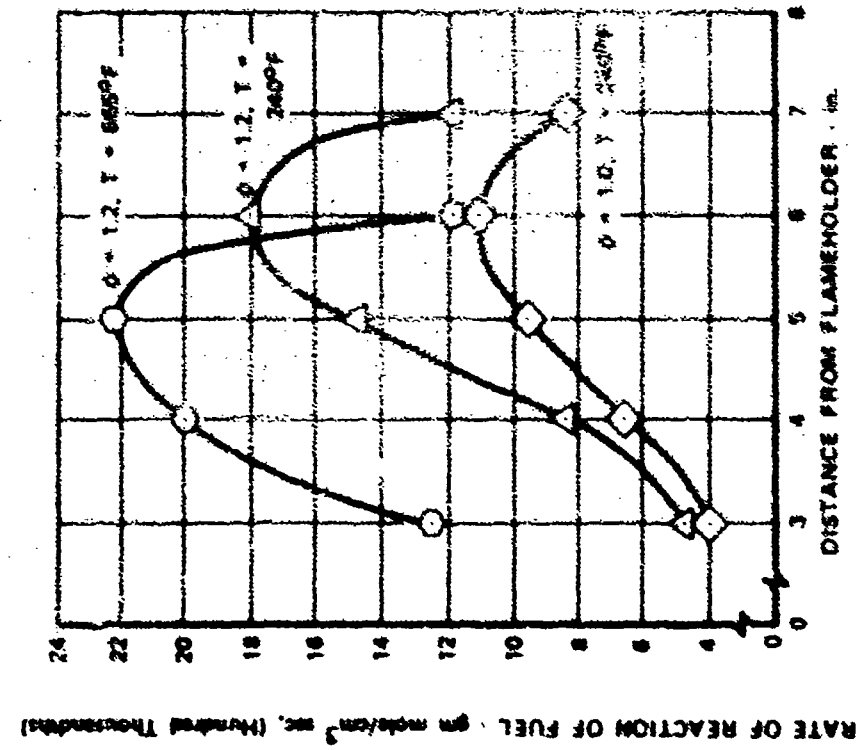


Figure 32. Variation in Fuel Reaction Rate with Axial Distance, Temperature, and Equivalence Ratio

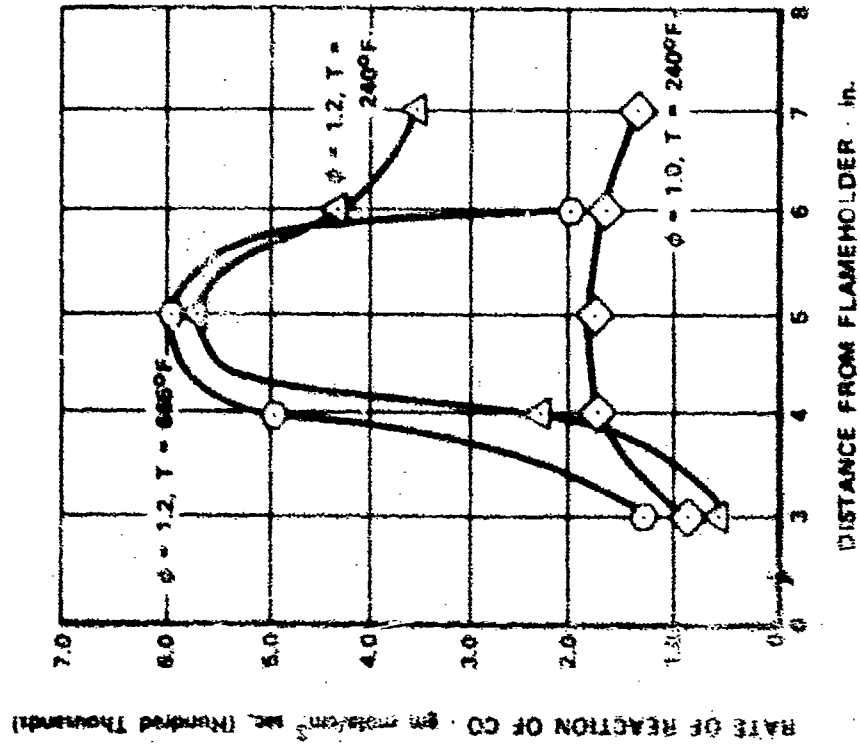


Figure 33. Variation in CO Reaction Rate with Axial Distance, Temperature, and Equivalence Ratio

The fuel reaction rates shown in figure 32 were correlated using the parcel splitting model of Howe and Shipman (Reference 25). This model characterized the turbulent burning zone by spherical parcels of unburned gas dispersed through the burned gas, with reaction occurring at the periphery of the parcels as laminar combustion waves. Measured fuel reaction rate data were fitted to theoretically derived expressions of the form:

$$Q_j \rho_b \bar{r}_o / 2S(X_j - X_{ju}) = b^{abt/3} \quad (22)$$

$$Q_j \bar{r}_o / 2\rho S(X_j - X_{jb}) = b^{abt/3} \quad (23)$$

where

- Q_j rate of fuel consumption, $\text{lb}_m/\text{ft}^3 \text{ sec}$
- ρ_b density of the burned parcels, lb_m/ft^3
- ρ_u density of the unburned parcels, lb_m/ft^3
- ρ combined mixture density of burned and unburned parcels, lb_m/ft^3
- \bar{r}_o initial mean parcel radius, ft
- S normal burning velocity, ft./sec
- X_j initial mass fraction of fuel
- X_{ju} mass fraction of unburned fuel in the mixture of burned and unburned parcels
- X_{jb} mass fraction of burned fuel in the mixture of burned and unburned parcels
- b number of equally sized spherical particles formed when one parcel is split
- a splitting probability, sec^{-1}
- t time, sec

Equation 22 was used where the volume fraction burned was less than 0.2, and equation 23 was used when the fraction was greater than 0.2. In fitting the measured reaction rate data to equations 22 and 23, time was measured from the point where measurable CO was observed. Elapsed time was calculated from the known velocity in the diffusion as follows:

$$t = \frac{X_j - X_{ju}}{V_{CO}}$$

where

x_0 = location where the reaction was deemed to have started as indicated by measurable CO concentration, ft

x_j = location from which sample was withdrawn, ft

\bar{V}_{Oj} = average velocity between x_0 and x_j , ft/sec

The normal burning velocity, S , was determined at each test condition from equation 24, which relates burning velocity to inlet temperature, pressure, equivalence ratio, oxygen content, and fuel composition.

$$S = 3.281 \times 10^{-2} X_I \left\{ (0.381 T^{1.4} (\psi - 0.120) - 100) (2.6 \log A + 0.94) \right. \\ \left. [P^{-0.39}] + 3.281 \times 10^{-2} X_B [(0.00395 T^{1.78} - 100) (2.6 \log B + 0.67)] \right\} \\ [P^{-0.39}] \quad (24)$$

where

$A = \begin{cases} \text{equivalence ratio } (\phi) \text{ for } \phi \text{ less than } 1.03 \\ (2.06 - \phi) \text{ for } \phi \text{ greater than } 1.03 \end{cases}$

$B = \begin{cases} \phi \text{ for } \phi \text{ less than } 1.34 \\ (2.68 - \phi) \text{ for } \phi \text{ greater than } 1.34 \end{cases}$

ψ = oxygen concentration = $O_2 / (O_2 + N_2)$

ϕ = equivalence ratio = $FA / 0.0678$

X_I = mole fraction of isooctane in fuel blend = 0.76

X_B = mole fraction of benzene in fuel blend = 0.24

S = burning velocity, ft/sec

P = pressure atm

T = temperature, °K

Equation 24 was developed by fitting experimental laminar flame speed data presented in Reference 26. Although the pressure dependency was not required in the analysis (all testing was done at 1 atmosphere), pressure terms were included to enhance application to the streamtube combustor model.

Following the practice of Howe and Shipman, the constant b was assumed to be exactly 2, since it could not be independently determined. To determine the constants \bar{r}_0 and a , the logs of the left-hand sides of equations 22 and 23 were plotted against time as shown in figure 34. A straight line was then fitted through the data. The slope of this line defined the average splitting probability, a , and the intercept at $t = 0$ determined the initial mean particle radius, \bar{r}_0 . The tailed point shown in figure 34 was not used in the determination of a and \bar{r}_0 due to difficulties in defining its value when $X_j \sim X_{ju}$, i. e., when burning has just begun. With $\bar{r}_0 = 1/34$ ft and $a = 4660 \text{ sec}^{-1}$, equations 22 and 23 become:

$$Q_j = -68 \frac{\rho_u \rho S}{\rho_b} (X_j - X_{ju})^2 0.31 \times 10^4 t \quad (25)$$

$$Q_j = -68 \rho S (X_j - X_{jb})^2 0.31 \times 10^4 t \quad (26)$$

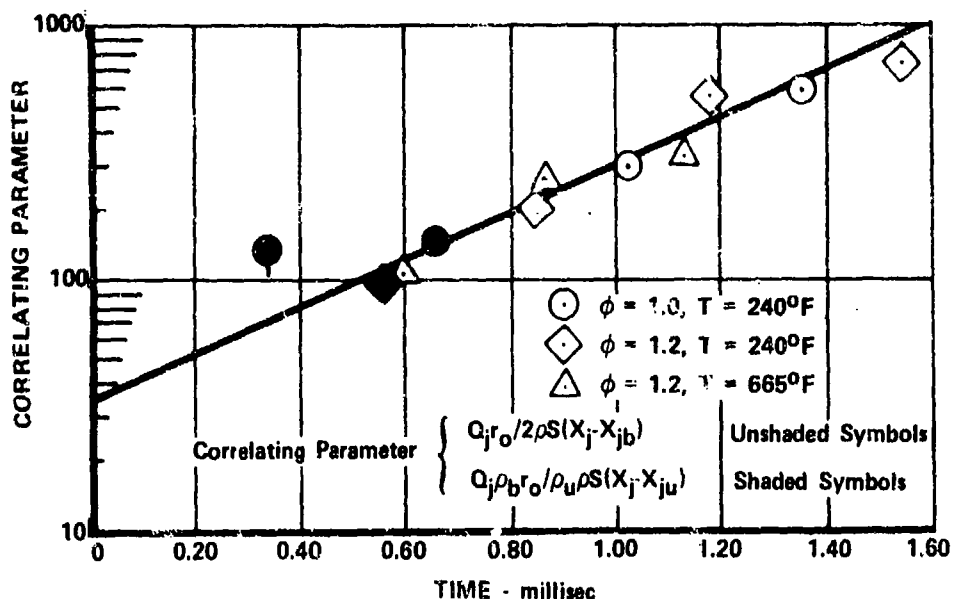


Figure 34. Variation in Correlating Parameter with Time and Test Conditions FD 71979

Corresponding to equations 22 and 23, equation 25 was used when the volume fraction burned was less than 0.5 and equation 26 was used when the fraction was greater than 0.5. As a final check, equations 25 and 26 were used to calculate fuel reaction rates at each test condition. The calculated values are shown plotted against the measured values in figure 35. Agreement was within approximately 20%.

Attempts to correlate the CO reaction rate data with an Arrhenius function or with models similar to the parcel splitting model all failed to yield satisfactory results. This was principally because of uncertainty in determining the split between the competing formation and consumption reactions. The experimental CO reaction rate data obtained in this study are in general agreement with similar data reported by Fenimore and Jones (Reference 27).

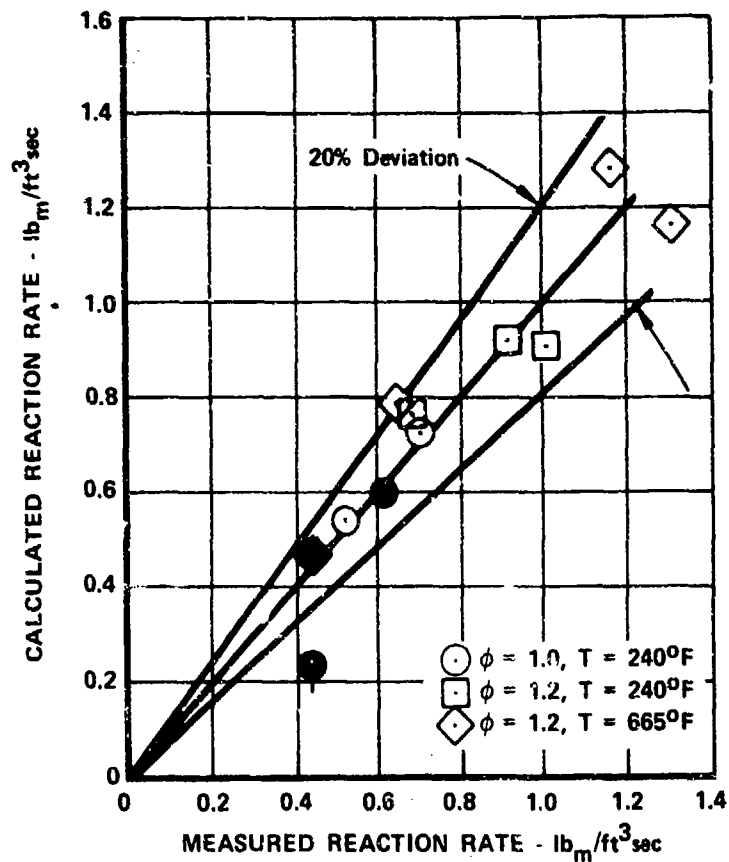
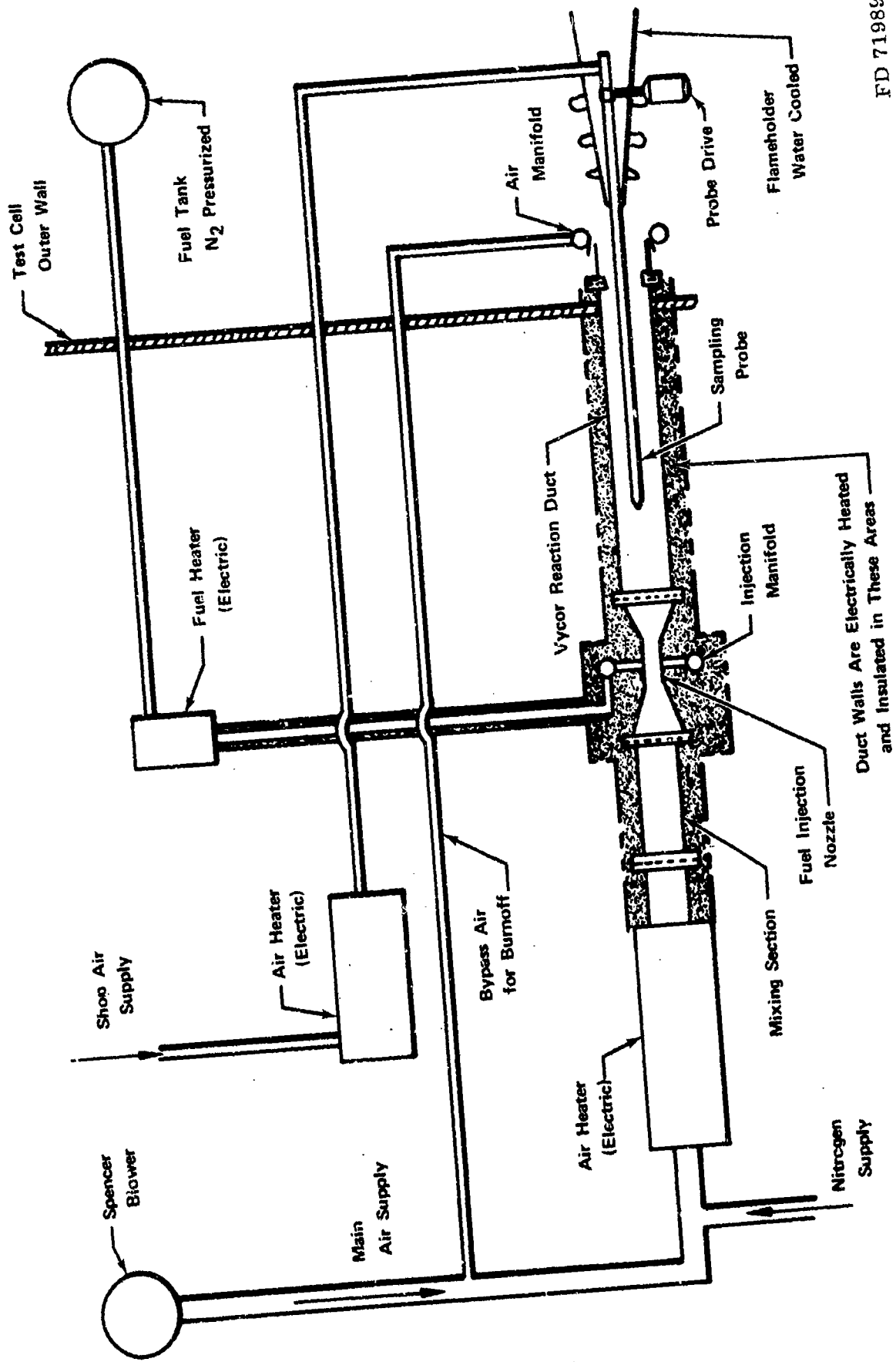


Figure 35. Comparison of the Variation in Actual and Measured Reaction Rates FD 71980

4. Low-Temperature Hydrocarbon Kinetics Studies
 - a. Description of Test Apparatus and Facility

The test apparatus used in the low-temperature kinetics studies is shown schematically in figure 36 and during the early stages of installation in figure 37. Air, supplied from a high-capacity blower, and nitrogen, supplied from a 2000-psig tank, were mixed to provide a source of oxygen-deficient air for use in the tests. The flowrates of air and nitrogen were varied independently to yield the desired total flowrate and concentration of oxygen in the mixture.

After the proper mixture and flowrate were achieved, the oxidizer was passed through a 60 kw electrical heater; this heater was capable of heating the incoming gas to 1800°F. Flow distortions and temperature gradients introduced within the heater were eliminated by passing the nitrogen-diluted air through a series of four baffles. Instrumentation was installed at the exit of the baffle section to confirm the removal of any distortions.



FD 71989

Figure 36. Schematic Diagram of Hydrocarbon Kinetics Rig

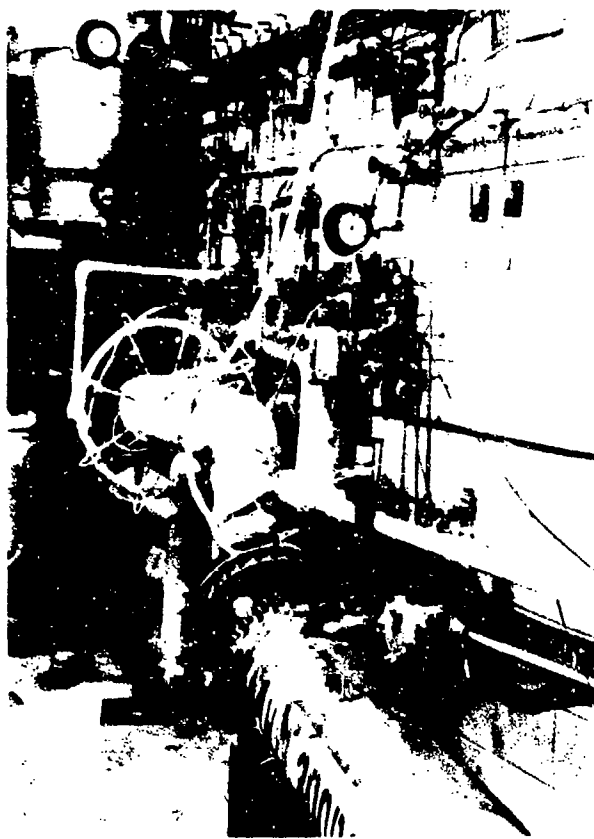


Figure 37. Hydrocarbon Kinetics Rig

FD 71983

Liquid fuel was supplied from two nitrogen-pressurized tanks located outside the test cell. As discussed in paragraph E.3 preceding, a mixture of 83% isooctane and 17% benzene, by weight, was used to simulate JP-5 fuel under laboratory conditions. Before entering the injection section, the fuel was heated and expanded through a throttling valve; the vaporized fuel temperature was approximately 240°F.

The fuel injection section was designed to provide rapid mixing of fuel and air before they entered the test section. To accomplish this, the airflow was first accelerated before it entered the mixing nozzle. In the mixing nozzle the vaporized fuel was injected at high velocities normal to the airflow through eight equally spaced orifices. Subsequent to this, diffusion of the fuel-air mixture produced additional mixing of the two before they entered the test section.

The test section, which was designed to function as an adiabatic reactor, was constructed from a cylindrical vycor tube 6 ft long, with a 2.70 in. inside diameter. Vycor was selected as the duct material to minimize wall catalysis. The duct was heated electrically with beaded nichrome wire wrapped around the duct in a helical fashion to provide constant temperature operation. A 0.5-in. layer of insulation between the wire and duct wall assisted in distributing the heat evenly, while several outer layers of insulation were used to minimize heat loss to the surroundings. Figure 38 shows a photograph of the test section as installed.

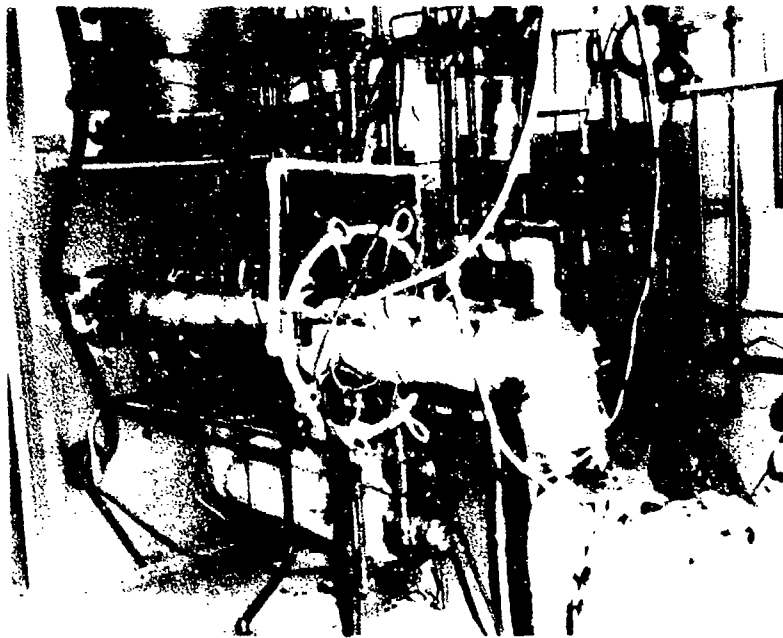


Figure 38. Test Section Installation for the Adiabatic Reactor FD 71984

Since a high-temperature combustible mixture having the potential for autoigniting was being exhausted from the rig, it was necessary to provide a means to control the burnoff of the exhaust product. To accomplish this, the downstream end of the reactor duct was inserted through the outer wall of the test cell, where a flameholder, complete with an ignition source, was located. (See figure 39.) The flameholder, cooled with ethylene glycol, was also designed to serve as a heat shield for the probe, drive mechanism, and associated hardware. As a further precaution, against the possibility of autoignition, the entire burnoff area was shielded by a steel barricade 6 ft high.

The sample probe, shown schematically in figure 40, was used to withdraw exhaust gas samples at selected points along the centerline of the reactor duct. The probe was positioned with a remotely controlled traverse mechanism located in the burnoff area. Sample temperatures in excess of 300° F were maintained within the probe by passing heated air through the probe. The gas samples were transferred through a heated Teflon line for on-line analysis of CO using a Beckman Model 315 NDIR analyzer. The batch analysis system used in the turbulent flame studies was also used for collecting exhaust gas samples at selected points.

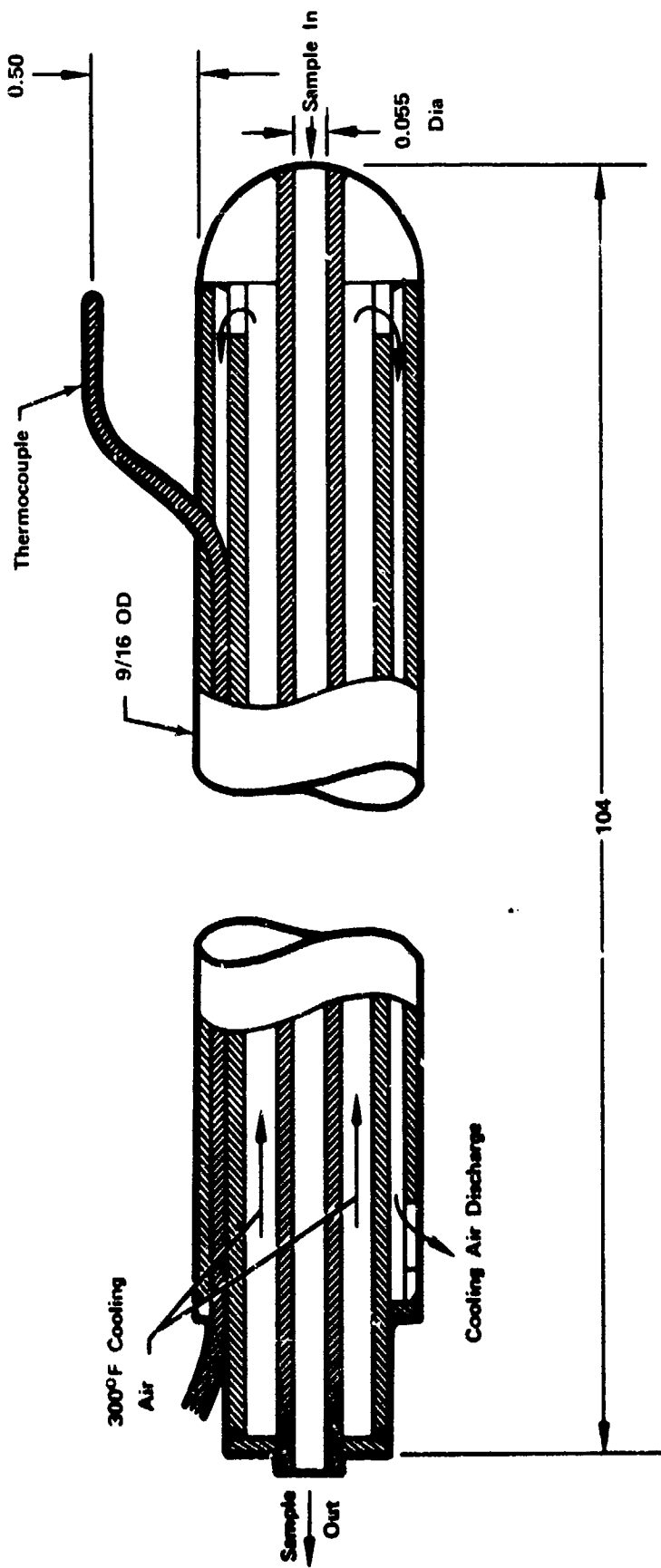


Figure 39. Burn-Off Area

FD 71985

All air and nitrogen flowrates were metered by calibrated orifices. Except for the sample probe cooling air, which was preset with a hand valve located within the test stand, flowrates were controlled by pneumatically operated valves. Fuel flowrates were measured upstream of the fuel heater using a turbine flowmeter and were controlled by remotely operated hand valves. Sampling flowrates were measured with a rotameter and were controlled by a hand valve located within the test stand.

Temperatures were monitored as required for control of all flow measurements. In addition, several skin and ambient temperatures were monitored within the burnoff area and at a number of locations in and around the flow reactor. The exit temperatures of each electrical heater were also monitored to prevent overloading the electrical elements. A chromel-alumel thermocouple, fabricated as an integral part of the sampling probe, was used to monitor reaction temperatures while the entire duct length was being traversed. To correct for radiation errors, the thermocouple was calibrated with and without cooling air to the sampling probe. Without cooling flow, radiation and conduction losses to the sample probe body were eliminated.



FD 71988

Figure 10. Sampling and Temperature Measurement Probe for Adiabatic Reactor Rig

b. Test Program

Initial tests were conducted to establish the range of conditions over which appreciable reaction could be expected. Measurements of CO concentrations were made at the end of the test section at a fuel-air equivalence ratio of 4.9; an oxidizer content of 15.3% oxygen; and at temperatures ranging from 650 to 1025°F. As shown in figure 41, the results indicated that no appreciable reaction occurred below temperatures of approximately 1000°F. For example, for a residence time of 75 msec and a temperature of 1000°F, the CO concentration was 63 ppmv. Subsequent testing was, therefore, limited to fuel-air mixture conditions corresponding to temperatures in excess of 1000°F.

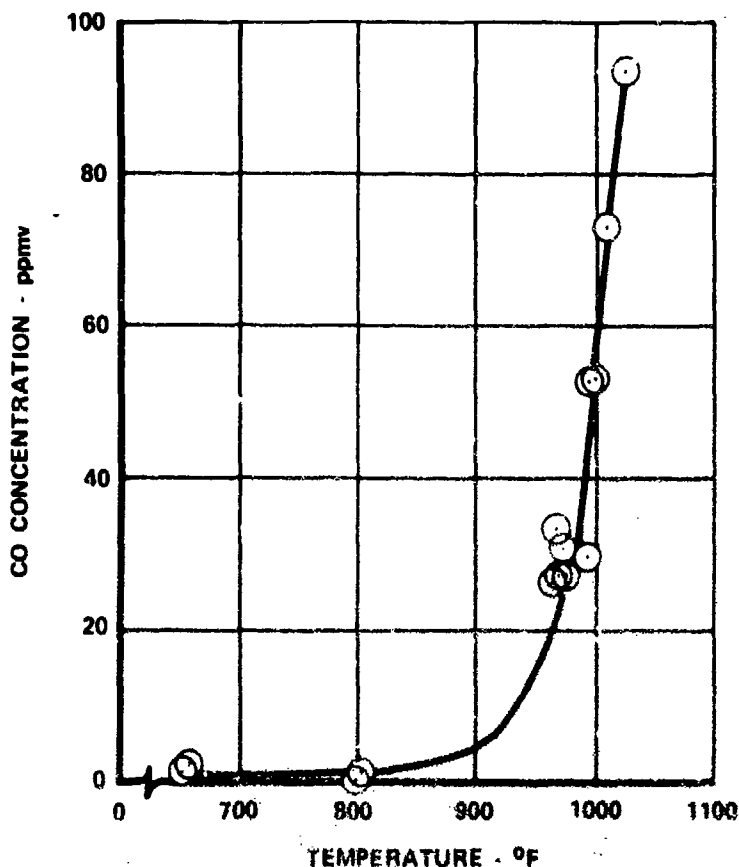


Figure 41. Variation in CO Concentration with Temperature (15.3% O₂, ϕ = 4.9, Residence Time = 75 msec) FD 71986

Measurements of CO concentration were made along the reactor centerline for the range of conditions shown in table VII. The axial distributions of CO obtained with an oxygen concentration of 12.5% are shown in figure 42. Measurements of CO₂ concentration were also obtained during the high temperature run (12.5% oxygen, ϕ = 2.5, and 1257°F) to determine if measurements of this constituent were required at the lower temperature test conditions. Although the

reaction was observed to accelerate toward the end of the test section, as indicated by a measurable temperature rise, no significant concentrations of CO₂ were found.

Table VII. Test Matrix for Adiabatic Reactor Program

O ₂ Concentration, mole %	Equivalence Ratio	Initial Mixture Temperature, °F	Weight Flow of Air + N ₂ , pph
12.5	2.5	1165	226.0
12.5	2.5	1214	220.7
12.5	2.5	1257	212.7
12.5	4.0	1140	225.6
12.5	4.0	1220	214.8
15.3	2.5	1214	262.9
15.3	2.5	1275	254.5
15.3	1.5	1272	256.5

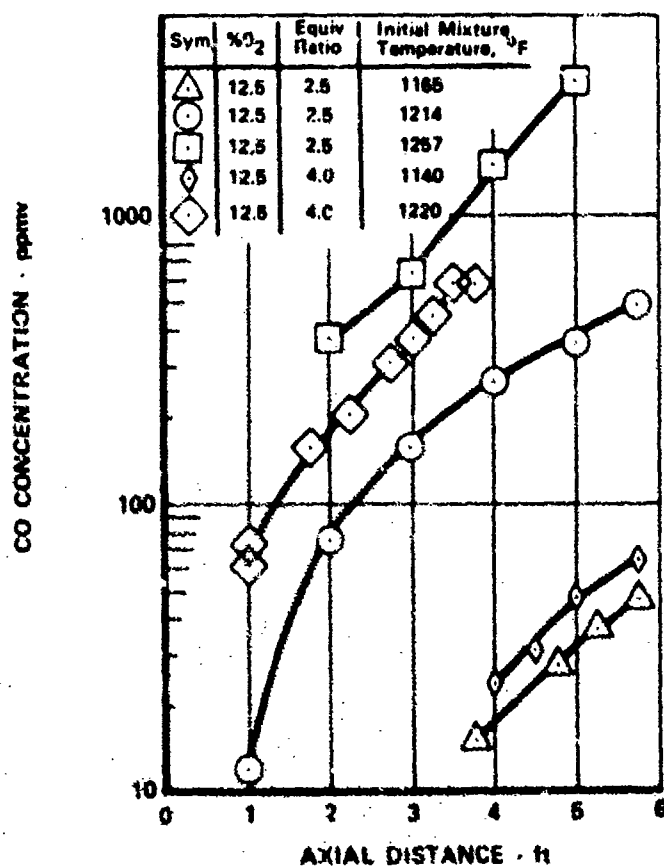


Figure 42. Variation in CO Concentration with Axial Location and Test Conditions FD 71987

c. Discussion of Results

Individual reaction rates for each of the test conditions shown in table VII were required to generate a global reaction rate expression for CO. Since the velocity at each test condition was known, the reaction rates were simply determined by taking the slope of a straight line passed through the individual CO concentration-distance data. As shown in figure 42, most of the data can be correlated with straight lines and, therefore, the error introduced by this graphical approach is minimal. The reaction rates were then subjected to a least squares analysis to fit an Arrhenius' function of the form;

$$Q_{CO} = A N_F^a N_{O_2}^b \rho^{a+b} e^{-E/RT}$$

The analysis yielded values for the exponents a and b, the constant A, and the activation energy E. The resulting rate expression derived for CO is:

$$Q_{CO} = 3.5 \times 10^8 N_F^{0.104} N_{O_2}^{0.431} \rho^{0.535} e^{-52,600/RT} \quad (27)$$

where

Q_{CO} = rate of CO formation, gm-moles/cm³-sec

N_F = mole fraction of fuel

N_{O_2} = mole fraction of oxygen

ρ = density, gm-moles/cm³

R = universal gas constant, 1.987 cal/gm-mole-°K

T = temperature, °K

The accuracy of equation 27 is demonstrated in figure 43, in which the calculated reaction rates are compared with the corresponding measured values. As observed, a satisfactory least squares fit was obtained. However, the small number of data available precluded a statistically accurate determination of the individual correlating coefficients. This is particularly true of the exponents a and b. The use of equation 27 is, therefore, not recommended outside the range of conditions used in the analysis, table VII.

Since the onset of reaction, as indicated by the presence of CO, was found to correlate with an Arrhenius temperature dependence, it is concluded that no significant reaction occurs outside the limits defined by the body of hydrocarbon reaction rate data contained in the literature. A hydrocarbon chemistry model based on rates found in the literature is, therefore, adequate for analytical modeling purposes.

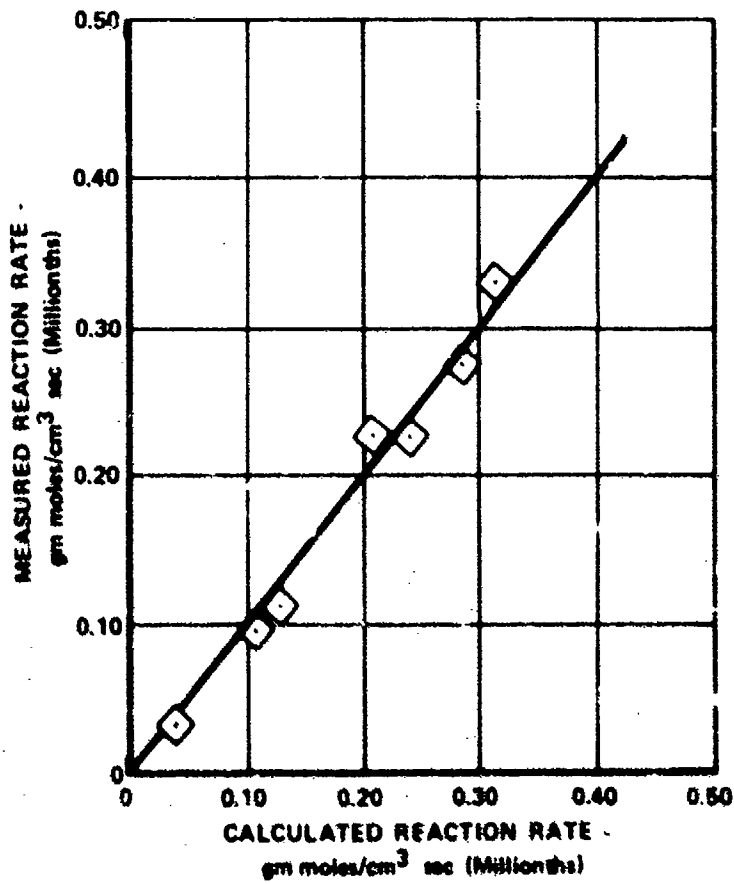


Figure 43. Comparison of Calculated and Actual Reaction Rates for CO FD 72144

SECTION IV

PHASE II - DESIGN ASSESSMENT

A. SUMMARY

Work under Phase II of Contract F33615-71-C-1870 has been completed. In Phase II, component design techniques for reducing low-power emissions by controlling the primary-zone equivalence ratio were evaluated experimentally using a research combustor. Control means included air-staging, fuel-staging, and premixing of fuel and air prior to their being introduced into the combustor.

Four fixed-geometry combustor schemes were used to simulate the operation of a variable-geometry, air-staging combustor. A composite curve of data from the four schemes exhibited high combustion efficiencies over the entire range of fuel-air ratios examined from idle to full power. UHC concentrations were low over this range, but CO concentration levels remained relatively high.

Secondary fuel nozzles mounted immediately downstream of the primary zone of the combustor were used in combination with conventional, dome-mounted fuel nozzles to evaluate axial fuel-staging. Concentrations of objectionable exhaust emissions were high when secondary fuel injectors were used. This has been attributed to inadequate burning length in the secondary fuel zone of the particular research burner used.

Circumferential fuel staging was evaluated using two dome-mounted injector arrangements. In the first, only the fuel nozzles in alternating locations were operated. Both UHC and CO concentration levels remained relatively high. In the second, only half of the fuel nozzles located sequentially were operated. UHC concentrations decreased significantly, but the CO concentration level remained high.

Brief investigations were conducted to evaluate the effects of secondary influences on exhaust emission concentrations and combustion efficiency. Secondary influences included combustor reference velocity, inlet air temperature, fuel atomization, and primary-zone air-film cooling. As reference velocity was increased, CO concentrations increased and UHC concentrations decreased. As inlet temperatures were reduced, both UHC and CO concentrations increased. Poor fuel atomization caused a large increase in concentrations of objectionable emissions, with a corresponding decrease in combustion efficiency. Elimination of primary-zone, air-film cooling had an insignificant effect on reducing emission concentrations.

Very low concentrations of UHC and CO were achieved when fuel-air premixing or carburetion tubes were used to replace the conventional dome-mounted, pressure-atomizing fuel nozzles. Program goal UHC concentrations of 10 ppmw (18 ppmv) at low power were readily achieved. CO goal concentrations of 10 ppmw (ca 10 ppmv) were closely approached. The lowest value of CO concentration achieved in this program at simulated low power operating conditions was 28 ppmw.

B. DISCUSSION

1. Objective and Approach

Phase II was conducted concurrently with the development of the analytical model to evaluate component design techniques for lowering pollutant emission levels at part-power² engine operation and to provide experimental data to assist in refining the theoretical combustor model. Continuous interchange of information between the analytical and experimental programs served to enhance the successful accomplishment of both.

It is virtually impossible to closely control or regulate the environment within current fixed-geometry burners at both high and low-power operating conditions because of the nature in which they operate. Even at full power, the overall fuel-air ratio lies well below the lower flammability limit for mixtures of aircraft fuel and air. Consequently, it is necessary to burn the fuel with but a fraction of the available air at a local fuel-air ratio well within the flammability limits for the fuel-air mixture, and then add the remaining combustor-designated air to the combustion products.

Conventional combustors are typically operated at near-stoichiometric fuel-air ratios in the primary zone at a selected design point such as full power. They are then operated below this design-point fuel-air ratio at all other conditions. At full-power and near-full-power conditions, the reaction temperature in the combustor is high and reaction rates are fast. Consequently, both UHC and CO concentrations in the exhaust gas are very low and combustion efficiencies are typically very high. On the other hand, at low or part-power conditions, these combustors operate at overall and local fuel-air ratios well below those achieved at high power. As a result, combustion temperatures are low and reaction rates are slow; consequently, concentrations of both UHC and CO in the exhaust gas are high, and combustion efficiencies are low.

During low-power operation, the principal combustor-generated exhaust pollutants are UHC and CO. If the concentrations of these species can be decreased, combustion efficiency will be increased directly as shown in the following equation

$$\eta = 100 - 100 \left[\frac{4,343X + 21,500Y}{18.45 \times 10^6} \right] \quad (28)$$

where

- η combustion efficiency, %
- 4,343 heating value of CO, Btu/lb_m
- 21,500 heating value of methane, Btu/lb_m
- X emission index of CO, lb_m CO/1,000 lb_m fuel

² Part-power or low-power combustor operation is defined as that performance associated with the lower one-half of a typical turbine engine power curve; it specifically includes those power points representing idle and taxi operations.

Y = emission index of CH_4 , $\text{lb}_m \text{CH}_4/1,000 \text{ lb}_m \text{ fuel}$

18.45×10^6 = proportionality constant which includes the heating value of the fuel used (18,450 Btu/ lb_m)

This relationship was proposed by Capt. W. S. Blazowski, Fuels Branch, Fuels and Lubrication Division, Wright-Patterson Air Force Base, Ohio.

Three promising means of reducing pollutant emissions levels during low-power operation were evaluated during the experimental program: air staging, fuel staging, and premixing. The principal objective of each was to closely control the environment within the combustor to effect a more complete reaction between fuel and air, thereby minimizing the formation of the products of incomplete combustion, viz., UHC and CO .

With the air-staging concept, combustion chamber environmental control was achieved by changing the distribution of air entering the combustor as the rate of fuel flow was changed so that the local fuel-air ratio in the primary zone was kept at a predetermined, constant value. Hence, although the overall fuel-air ratio increases as the rate of fuel flow is increased and decreases as the rate of fuel flow is decreased, the desired primary-zone fuel-air ratio does not change.

With the axial fuel staging concept, control of the environment within the combustor was achieved by changing the distribution of fuel entering the combustor as the rate of fuel flow was changed. As a result, a preestablished local fuel-air ratio was achieved but not exceeded in the vicinity of each injection station. Although the overall fuel-air ratio increases as the rate of fuel flow is increased, local desired fuel-air ratios in the vicinity of the axial fuel injection stations do not exceed the predetermined value.

With the premixing concept, control of the combustion environment was accomplished by intimately mixing fuel and air in a predetermined ratio prior to their being introduced into the burner. A homogeneous combustible mixture, in a controlled range of fuel-air ratios, was thereby presented to the reaction front. Undesirable reaction products that are formed as a result of nonuniform fuel concentration and temperature profiles in the primary zone are reduced or eliminated. Premixing in combination with air staging affords an ideal means for reducing objectionable emissions at both low and high-power conditions.

2. Constraints and Qualifications

This comprehensive experimental component investigation was conducted to define and assess promising combustor design techniques for increasing low-power combustion efficiency and, consequently, improving low-power exhaust emission characteristics. However, of the design features offering potential, only those of a practical design having reasonable maintainability and reliability were considered for evaluation. The intended risk level of this program was considered to be such, nevertheless, that at least one novel or unique design approach for improving part-power performance would be considered. However, regardless of the approach taken, it was essential that combustor performance be maintained at all power settings with no appreciable increase in emissions at operating points other than low power. Means for providing performance improvements during low-power operation at the expense or compromise of performance at high-power operation were not considered to be acceptable approaches for accomplishing the objectives of Phase II.

During low-power operation, the principal combustor-generated exhaust pollutants are UHC and CO; a third pollutant, NO_x , is generally produced only in small quantities under these conditions. However, as combustion efficiency is improved, the reaction temperature is increased and although concentrations of UHC and CO are reduced, the concentration of NO_x is often increased. Though the oxides of nitrogen have little or no effect on overall combustion system performance, they are, nevertheless, undesirable byproducts of airbreathing combustion. In sufficient concentration they are by themselves toxic, and in combination with hydrocarbons in the presence of sunlight they react to produce smog. Therefore, continuous attention was to be given to the presence of this pollutant since potential compromises to improve overall exhaust emission performance by decreasing UHC and CO concentrations at the expense of increasing NO_x concentration have already been observed and are not necessarily desirable.

Calculations of combustion efficiency using both a rigorous thermodynamic approach that considers all measured products of combustion and the simplified approach of equation 28 yielded results that were essentially the same. Therefore, unless otherwise noted, combustion efficiencies derived from exhaust gas analyses in this program were obtained through the use of equation 28.

Of equal importance to the successful development of design techniques for enhancing low-power combustor performance was the accurate analysis of exhaust products sampled during the test program. Not only was it necessary to measure combustion efficiency accurately, but verification of low emission levels was also required to determine trace quantities of the exhaust gas constituents resulting from low combustion efficiency. Therefore, a number of guidelines were established relating to the experimental portion of this phase of work, including:

1. Concentrations of UHC, CO, CO_2 , NO_x , and water vapor were to be measured during each test.
2. To accommodate variations in exhaust constituent levels existing at the exit plane of the combustor, means for multi-point sampling at the exit plane were to be incorporated.
3. On-line measurement techniques were to be employed extensively. If batch sampling should be used, care was to be taken to ensure that no further reaction of the constituents occurred between the time the samples were taken and the time they were analyzed.
4. Sampling techniques used were to be such that further reactions of constituents within the sampling line were prevented.
5. Initially, measurement methods responsive to both NO and NO_2 were to be used to determine the concentrations of NO_x . The measurement of NO_2 was to be discontinued if sufficient empirical evidence indicated that the concentration of NO constituted more than 95% of the NO_x concentration.

6. The method for measuring water vapor was to include the determination of the pH level in the exhaust sample.
7. Methods for measuring CO, NO, NO₂, and UHC were to be sensitive to concentrations to 10 ppmw and accurate to within ± 5 ppmw. For CO₂ and water vapor, the measurement accuracies were to be within $\pm 0.05\%$ by weight.
8. All exhaust constituents were to be measured at the same time under steady-state operating conditions, and local sampling point temperature and pressure conditions were also to be recorded. In addition, absolute humidity (weight of water per unit weight of dry air) of the combustor inlet air was to be noted periodically during a test run.
9. All tests were to be conducted using JP-5 fuels.

3. Experimental Combustors

a. General

Tests conducted to evaluate design concepts in Phase II were accomplished using derivatives of an annular research burner that had the basic arrangement shown in figure 44. This hardware was designed to be generally representative of conventional static-fed combustors. Diameters of the outer and inner liners of the flametube were 18 and 10 in., respectively. The length of the burner from the primary fuel nozzle injection station at the dome to the exit plane of the discharge transition duct was 16 in. The combustor was fabricated from heavy-gage (0.0625 in.) Hastelloy-X sheet stock. This unusually thick material was selected for the research burner to provide physical resistance to overcome both geometrical distortions associated with thermal stresses developed during testing and mechanical forces generated during programmed modifications. The walls and dome were film-cooled by air entering the combustor through judiciously placed louvers along the inner and outer liners.

The first arrangement of the basic research burner is referred to as combustor A. This hardware and its modifications were used to evaluate the air and fuel staging concepts. The second arrangement is referred to as combustor B. This burner and its modifications were used to evaluate the fuel-air premixing concept. Detailed descriptions of combustors A and B are presented in the following paragraphs.

Combustors A and B both had the same nominal design point: a reference velocity of 100 ft/sec, and a temperature rise commensurate with an overall fuel air ratio of 0.022.

To simplify the test matrix, all tests were conducted at one inlet pressure (approximately 15.5 psia), and for most tests, the inlet temperature was held constant at 400°F. This temperature corresponds approximately to idle conditions for an advanced high pressure ratio engine.

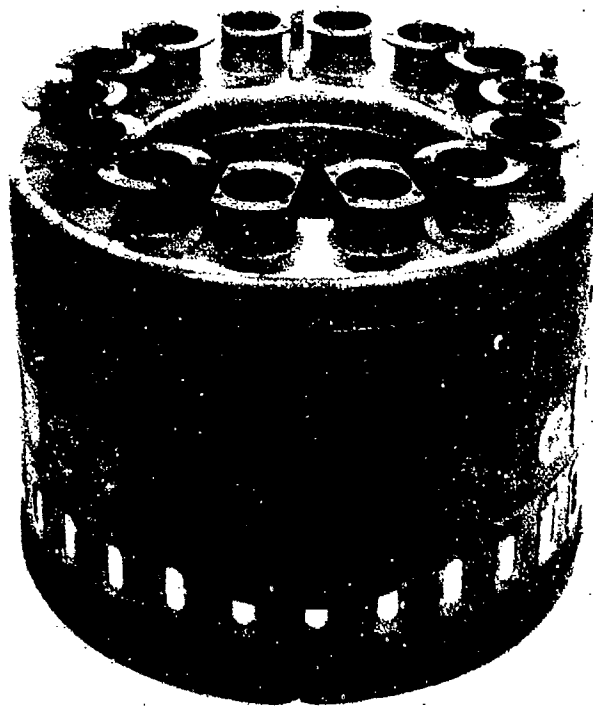


Figure 44. Combustor A Prior to Installation in Rig Case

FE 112131

For the purpose of calculating airflow distributions within the combustors, actual hole areas were multiplied by discharge coefficients of 0.62 for penetrator holes and 0.80 for cooling holes. In combustor A, a discharge coefficient of 0.85 was used for the primary air swirlers. In combustor B, the premixing tube flowrates were determined experimentally as a function of total pressure drop prior to the combustor test program. In combustor A, the total pressure drop of the liner was 1.8%; in combustor B, a pressure drop of 3.5% was used to enhance operation of the premixing tubes.

b. Combustor A

Combustor A was arranged to easily accommodate modifications required for the evaluation of air and fuel staging concepts. It was provided with two fuel injection stations, as shown in figure 45. The first station was located in the dome and served the primary zone in both air and fuel staging tests. The other station, located halfway between the dome and the exhaust plane, served the secondary zone in the fuel-staging tests. The primary zone fuel system consisted of 14 fuel nozzles evenly spaced along the mean circumference of the dome. The fuel nozzles used in both primary and secondary zones were pressure atomizing, simplex type, producing a 90-deg dispersion angle hollow cone spray. The secondary zone fuel system consisted of 14 fuel nozzles mounted on the outer liner of the combustor so that the spray axis of each nozzle was normal to the horizontal axis of the combustor. The nozzles were centered within holes in the outer liner through which secondary combustion air entered. Circumferential locations for the secondary nozzles were staggered with respect to those for the primary zone nozzles. In figure 46, combustor A is shown with secondary nozzles mounted for fuel-staging tests; the primary zone fuel nozzles are not mounted.

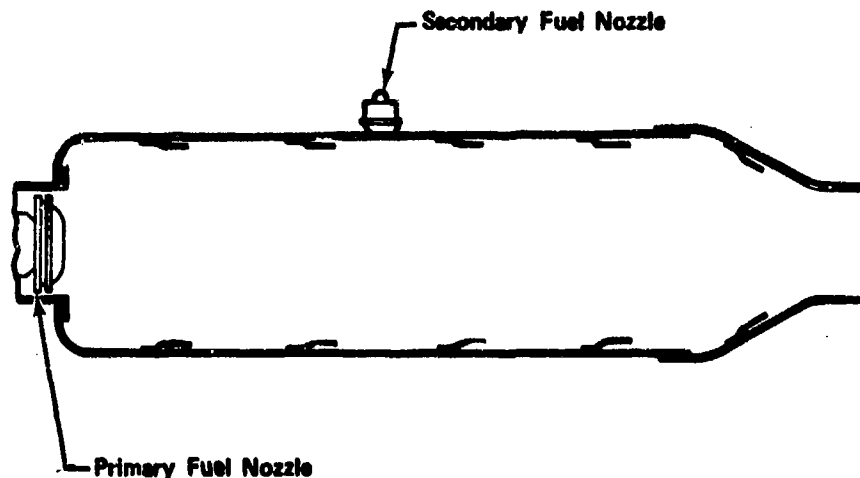


Figure 45. Research Combustor Arrangement

FD 71991

The combustor A penetration air hole pattern consisted, first of all, of 28 primary holes in each of the inner and outer liners; these holes were staggered circumferentially with respect to both the primary and secondary nozzles. Next, 28 dilution slots in each liner were located in-line circumferentially with either primary or secondary zone fuel nozzles. Finally, 28 intermediate zone holes were located in the outer liner only, with alternate holes serving as injection ports for the secondary nozzles. All penetration holes were equally spaced around the circumference of the combustor, and directly opposed to corresponding holes in the opposite liner.

Rows of film cooling air holes were located at four axial stations on each of the inner and outer combustor liners, at one station on each of the outer and inner transition liners, and in a circular pattern around each primary zone nozzle boss. Cooling airflow passing through these holes impinged on louvers attached to the inside surfaces of the walls and was directed along those surfaces as a convective cooling film.

Flame stabilization in the primary zone was accomplished by 14 axial flow air swirlers mounted around the primary nozzles; and by recirculation flow from the primary penetration air jets. The axial-flow air swirler around each fuel nozzle had an outer diameter of 1.68 in., an inner diameter of 1.20 in., and incorporated 16 vanes. In alternating locations, swirlers contained vanes arranged at an angle of 45 deg to the horizontal axis; in the remaining seven locations, swirlers contained vanes arranged at an angle of 135 deg to the horizontal axis.

In accomplishing the air staging tests, changes in combustor airflow distribution were achieved by varying the areas of the penetration and cooling holes, and the primary swirler passages. This was done by affixing temporary sheet metal patches containing the required hole areas atop existing air-entry holes. Each airflow distribution, therefore, involved only simple modifications to the combustor hardware; to change from one air distribution to another, all that was involved was to remove existing patches and replace them with a new set. This method was also used to set up the required airflow distributions for the fuel-staging tests and for all other tests conducted with combustor A. Figure 46 shows combustor A as it was modified for Scheme 4-1A.



Figure 46. Combustor A Modified for Scheme 4-1A Arrangement FE 119108

c. Combustor B

The principal differences between combustors A and B were that combustor B was provided with premixing tube fuel injectors to replace the primary zone fuel nozzles and primary air swirlers used in combustor A, and that the secondary fuel injection station used in combustor A was eliminated. A schematic diagram of combustor B is presented in figure 47.

The tubes were mounted in the bosses used for the primary nozzle/swirler assemblies in combustor A. Changes in combustor airflow distribution, as required for the various tests performed with combustor B, were accomplished by means of the temporary sheet metal patches described earlier. Each of the premixing tube fuel injector assemblies, shown in detail in figures 48 and 49, consisted of a 1-inch diameter premixing tube with a pressure-atomizing fuel nozzle mounted in one end and a primary air swirler mounted in the other. Air was forced through the tube by the differential pressure acting across the combustor. An inlet venturi minimized total pressure loss at the entrance to the premixing tube and a centerbody mounted in the swirler provided a low loss transition to the annular swirler passage at the exit. The fuel nozzle used was a pressure atomizing, simplex type having a 90-deg dispersion angle hollow spray cone. Initial atomization and distribution of the fuel in the air entering the tube

was provided by the fuel nozzle. Subsequent atomization occurred in the pre-mixing tube as the result of droplet shattering in the high velocity airstream. Dispersion of droplets in the airstream also occurs, along with initial vaporization and mixing of fuel vapor and air. At the swirler discharge plane, an airflow deflector ring was mounted at the end of the outer wall. This ring served as a final means for atomizing fuel that might have collected on the wall of the tube. High velocity air passing over the lip of the deflector broke up any film of liquid fuel on the wall, shearing it into small droplets.

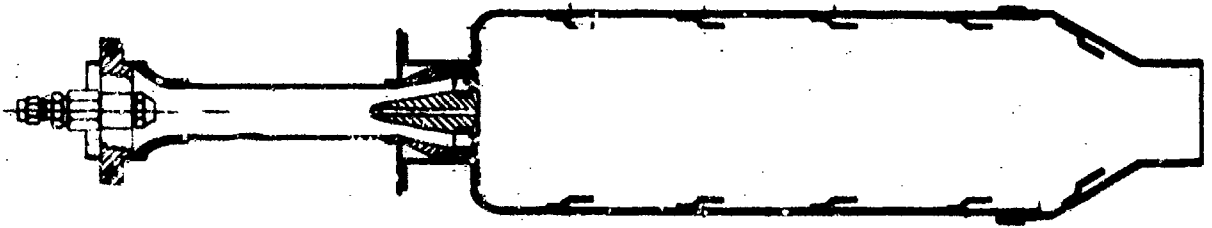


Figure 47. Schematic Diagram of Combustor B

FD 71992

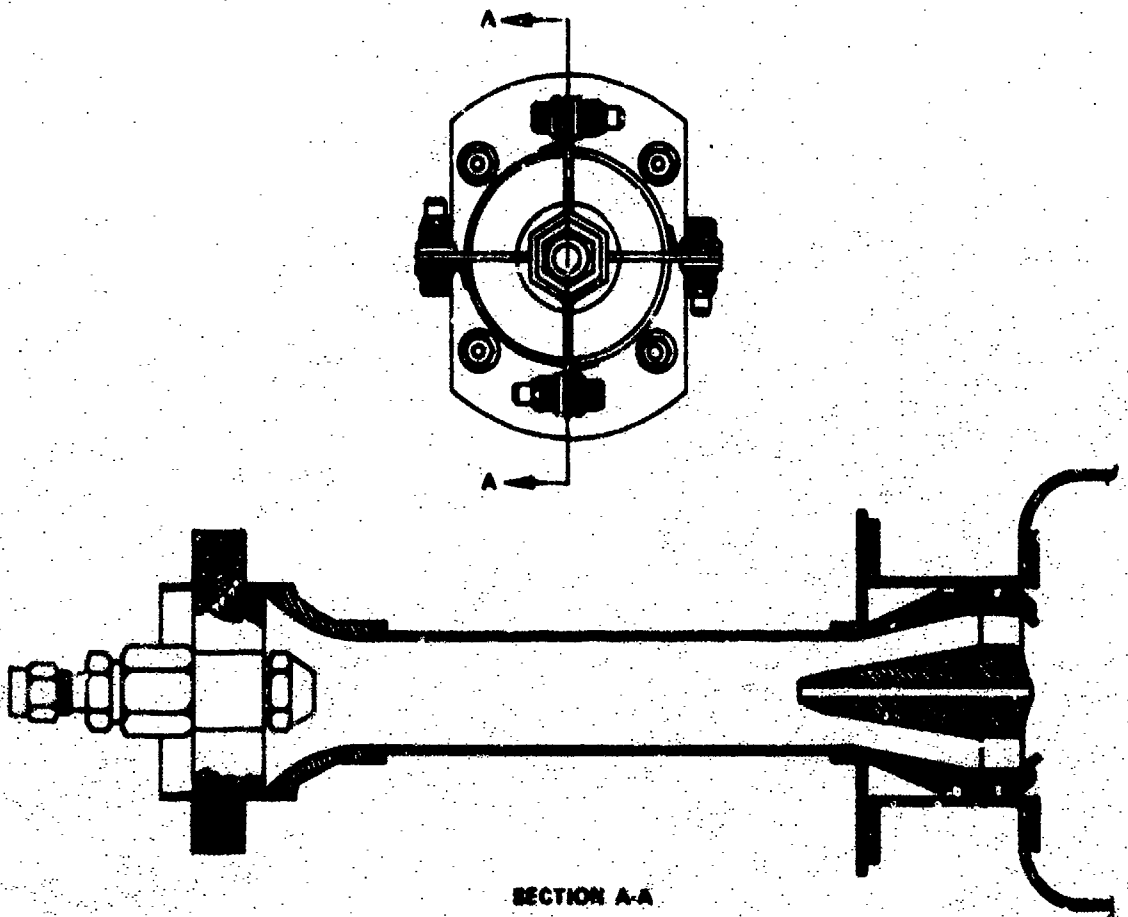


Figure 48. Carburetion Tube Assembly

FD 71993

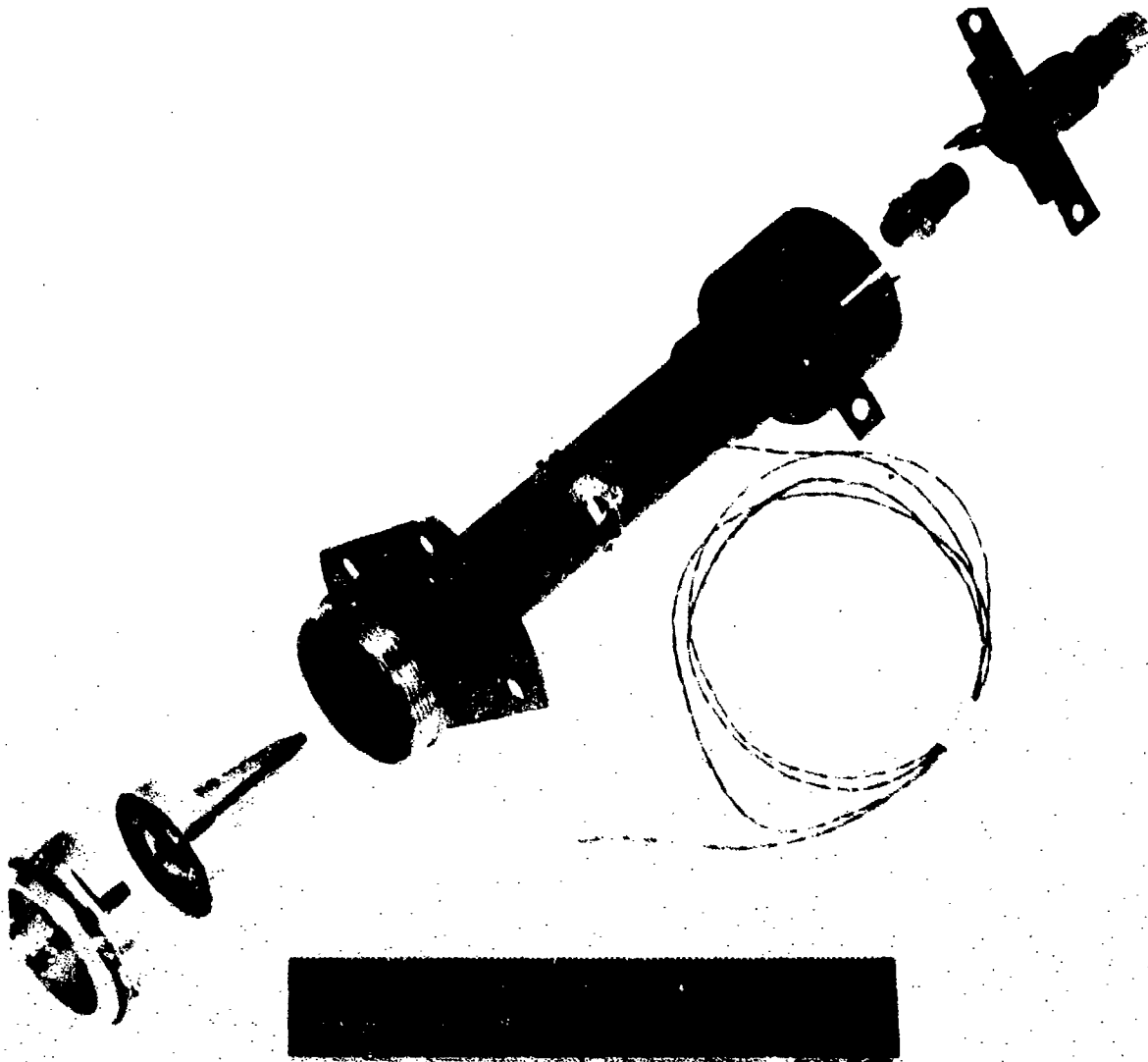


Figure 49. Carburetion Tube Assembly Prior
to Test

FE 123804

The premixing tubes used in combustor B were 6 in. long. This length was determined from preliminary flow tests to be adequate for good intermixing of fuel and air. Although it is believed that shorter tube lengths may also suffice, no attempt was made in Phase II to determine the minimum length required. Instead, a margin of premixing capability was sought, so that the test program could be directed toward determining the effects of premixing on emissions rather than methods for implementing it. The tubes were designed to prevent flameholding and autoignition within the premixing passages by providing mixture residence times much shorter than those needed for a sustained reaction. This approach allowed fuel-air equivalence ratios near the stoichiometric value to be maintained in the tube: providing the capability for premixing all the primary zone fuel and air (cooling airflow excluded). At a typical operating point, the mixture velocity within the tube was approximately 200 ft/sec at an equivalence ratio of 0.8 for a combustor overall fuel-air ratio of 0.008. Flameholding within combustor B was provided primarily by the premixing tube swirlers; in some tests, it was also provided by recirculating flow from primary penetration air jets.

4. Test Rig and Stand

The test rig used in the experimental program is shown schematically in figure 50. It consisted of a large upstream plenum chamber, a test section in which the combustor was mounted, and a traverse case containing temperature, pressure, and gas-sampling probes. The traverse case was also used to collect exhaust gas from the test section and to direct this gas into the exhaust system of the test facility. The upstream plenum chamber was designed to diffuse the combustor inlet airflow to very low velocities to minimize the possibility of obtaining nonuniform flow distributions around the combustor. External aerodynamic influences were not considered in this research program.

Unvitiated air was supplied to the combustor from the bleed ports of a J75 turbojet slave engine. An indirect heat exchanger was provided in the airflow system to maintain combustor inlet air temperature at the desired level. In most of the tests conducted in this program, the rate of airflow to the combustor was approximately 6 lb_m/sec and the air temperature was maintained at approximately 400°F. All tests were conducted at combustion chamber pressures slightly above atmospheric.

5. Traverse and Sample-Gas Transfer Systems

Temperature, pressure, and exhaust gas composition distributions for the entire exhaust gas flowfield at the exit plane of combustors A and B were determined during each experimental test. A four-arm, rotating traverse probe assembly, shown schematically in figure 51, and during assembly in figure 52, was used in the accomplishment of these measurements. Two of the probe arms, located 180 deg apart, had five equally spaced, radially positioned platinum/platinum-10% rhodium, aspirated thermocouples alternating with four comparably spaced total-pressure probes. The remaining two probe arms, also located 180 deg apart, but positioned circumferentially halfway between the first pair of arms, contained inlet ports at five equally spaced radial positions through which a small quantity of exhaust gas from the combustor was continuously abstracted. The inlet ports for one arm are shown in figure 53. Gas entering the inlet ports discharged into a common line in each arm. The gas samples from each line then discharged into a single manifold. This consolidated sample was directed through a heated transfer line to a set of on-line gas analysis instruments (described in the paragraph B.6, following) from which the average composition of the exhaust gas at a fixed circumferential location was obtained. Up to the Teflon, electrically heated transfer line shown in figure 54, the gas sample line was fabricated from stainless steel.

As the traversing probe was rotated through an angle of 180 deg around the centerline of the burner, each pair of arms surveyed half of the combustor discharge annulus. An entire 360-deg survey was thereby accomplished by rotating the traversing probe system through only 180 deg. For the tests conducted in this program, exit plane measurements for a full traverse were taken at 12-deg intervals during the 180-deg survey. A total of 150 discrete temperature measurements, 120 discrete pressure measurements, and 15 ten-point average exhaust gas composition measurements were obtained in each survey.

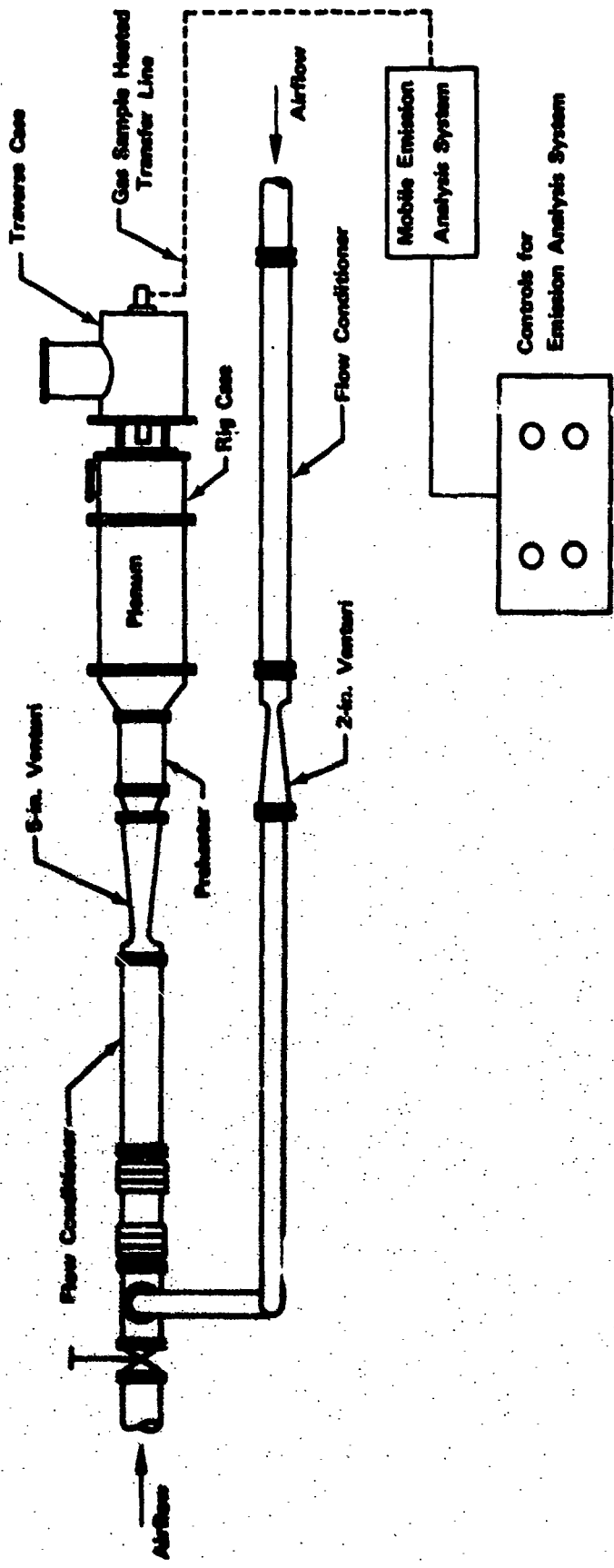


Figure 50. Schematic Diagram of Test Stand and Rig

FD 71994

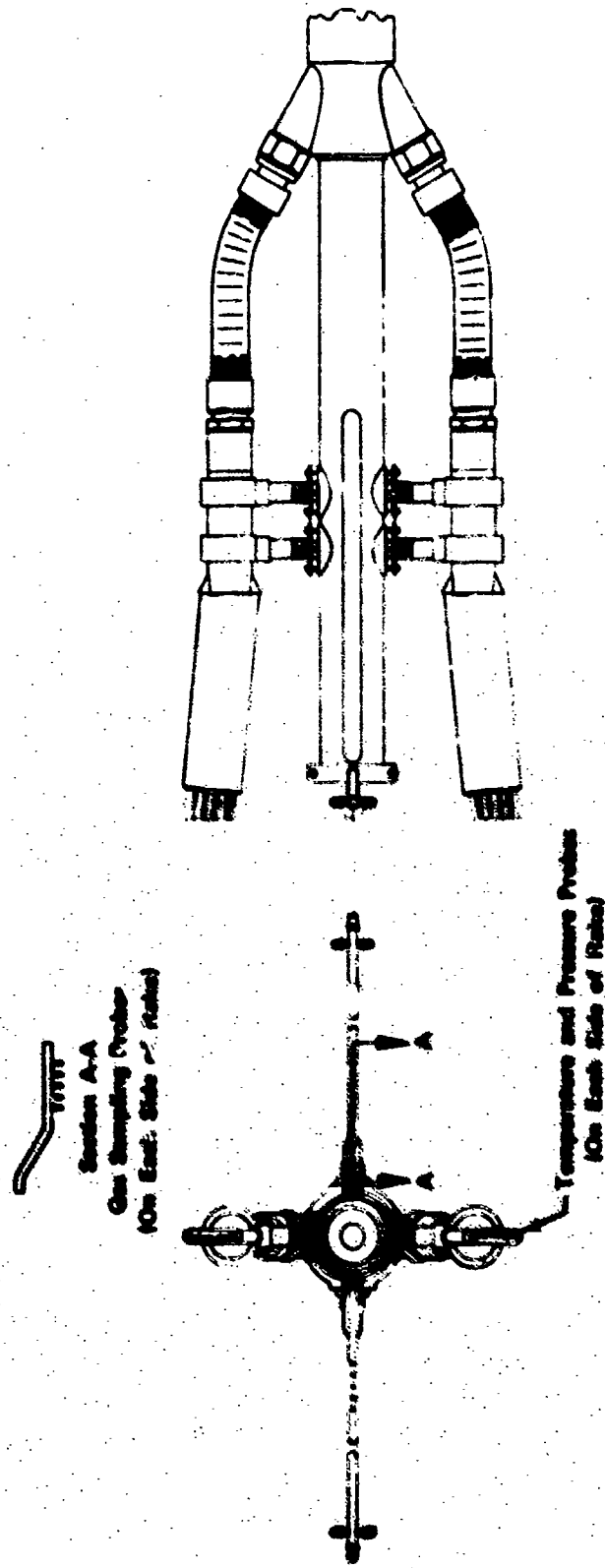


Figure 51. Schematic Diagram of Traverse Probe Configuration

FD 71995



Figure 52. Traverse Probe System During Assembly FD 71995



Figure 53. Sample Gas Inlet Ports on Rake Arm FD 71996

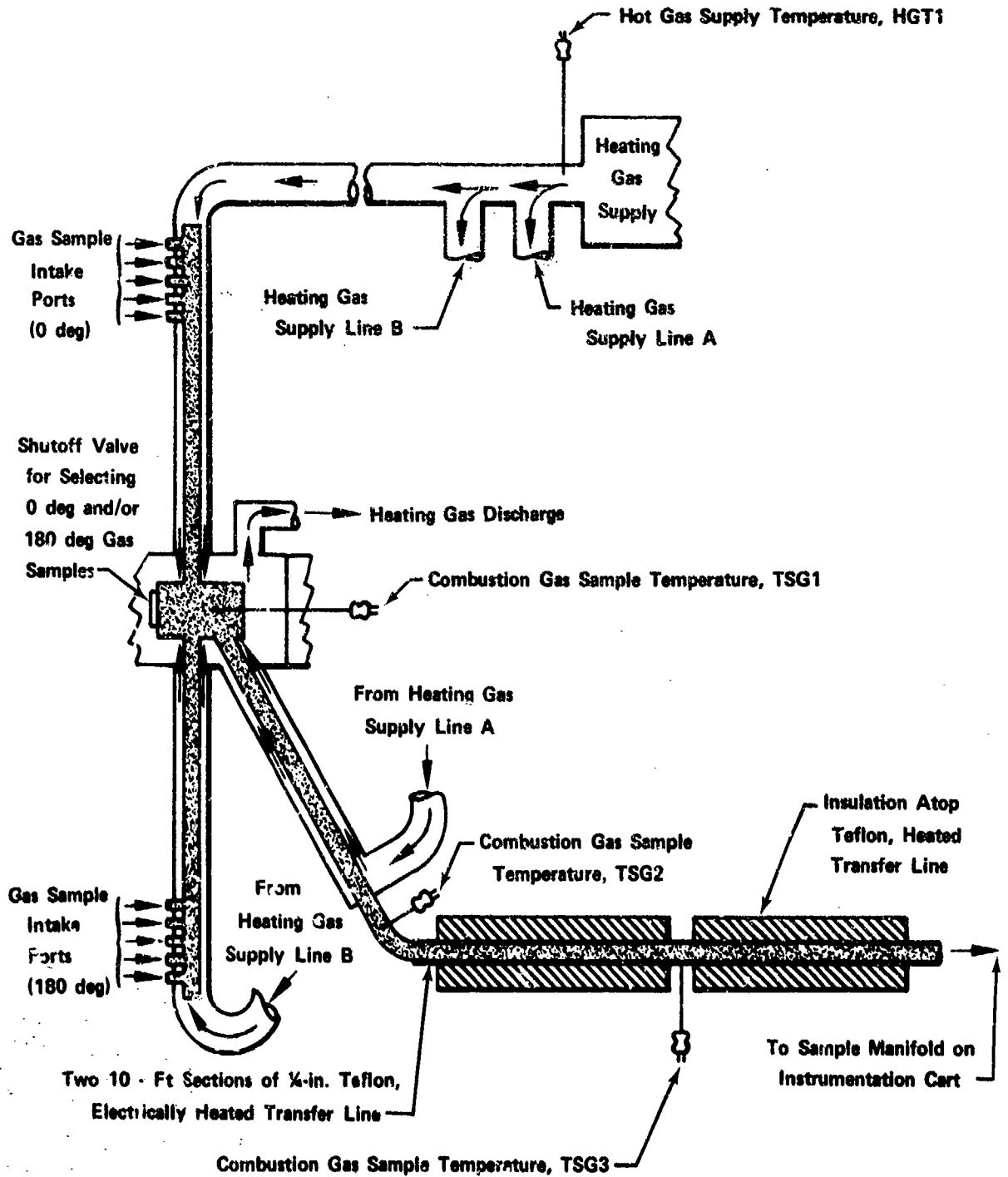


Figure 54. Schematic Diagram of Original Sample - Gas Transfer System - FD 56955B

In the initial gas sampling and analysis system, combustor exhaust gas was transferred from the ex't traverse probe to the mobile gas analysis cart through two 10-ft sections of well-insulated, electrically heated Teflon tubing having a wall thickness of 0.035 in. After a number of tests had been conducted, analysis of the data indicated the presence of a leak in the Beckman Instruments-supplied Teflon tubing. Subsequent physical examination of the line, after the insulation had been removed, revealed a large crack in the tube wall approximately 4 ft from the beginning of the second section of transfer line; a location where the line was subjected only to the load resulting from its own weight.

Generally, if the gas-sample pressure in the transfer line is greater than ambient, leakage of the gas sample to the environment does not present a problem; the leakage is always from inside to outside. However, if the gas sample pressure is subatmospheric, no leaks whatsoever can be tolerated, because a flow of ambient air into the sample gas will occur, which will dilute the sample an indeterminate amount. In the rig arrangement used in Phase II, the sample gas pressure was subatmospheric; consequently no leaks could be allowed. This necessitated development and use of procedures to ensure that there were no leaks in the sampling and measurement system.

An investigation of the line failure was conducted. It was determined that the transfer line supplied by the vendor was faulty, and that this was a problem that had been reported by a number of their customers. The vendor stated that the quality of Teflon that they had received from their supplier was inferior to the grade stipulated by Beckman and that, as a consequence, the heated lines showed a propensity to explode during use.

The remaining 10-ft section of transfer line was then scrupulously inspected. After it was certain that there were no visible flaws, the line was reinsulated and connected to the sampling probe discharge line and to the UHC analyzer inlet line. (The cart and related equipment were moved closer to the combustor rig to accommodate the decreased length of transfer line.)

Figure 54 is a schematic diagram of the sample-gas transfer system as it was originally arranged for tests No. 1-1A-1 through No. 1-1A-20; figure 55 is a schematic diagram of the system as it was arranged for tests commencing with No. 1-1B-1. The single section of transfer line, shown in figure 55, was used throughout the rest of the program without incident.

In this experimental program the temperature of the gas sample was maintained at an elevated level from the probe tip to the UHC analyzer. Keeping the sample hot should prevent FID-detectable species from condensing in the transfer line. (See Reference 28.) The Teflon portion of the transfer line was electrically heated; the remaining stainless steel sections of the line were convectively heated using hot air from an external source.

Sample gas temperatures were closely monitored along the transfer circuit from the probe tip to FID analyzer. As shown in figure 56, four thermocouple stations were in the gas transfer circuit for tests up to No. 1-1A-20. Three thermocouple stations were incorporated during tests commencing with No. 1-1B-1. The variations in sample gas temperature with flowpath location for tests conducted in Phase II are shown in figures 57 and 58. As observed, sample gas temperatures were quickly reduced to values below those that would encourage continuing reactions among the exhaust species, but above those levels at which condensation of UHC species could be a problem.

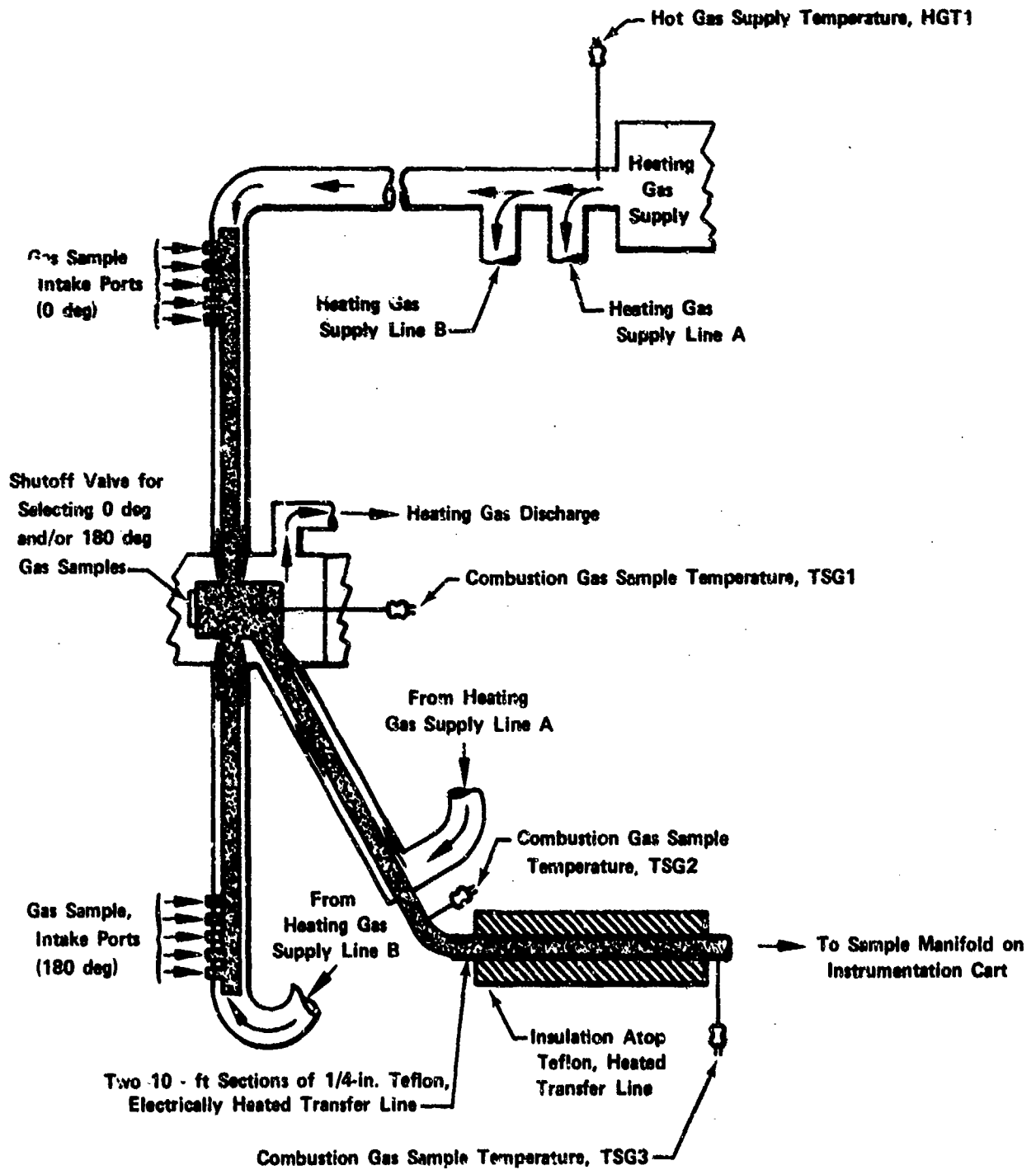
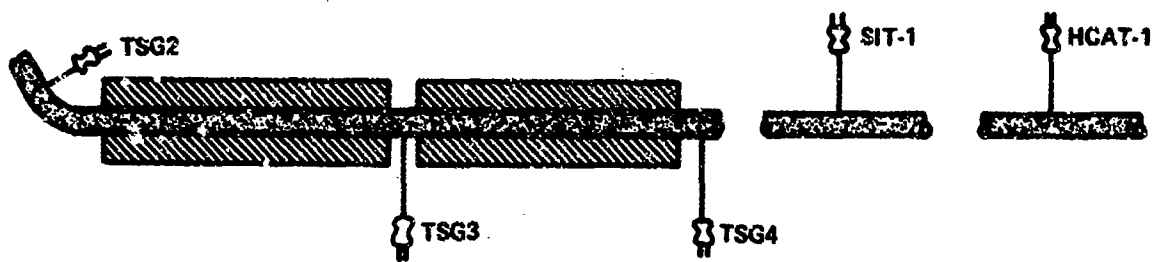
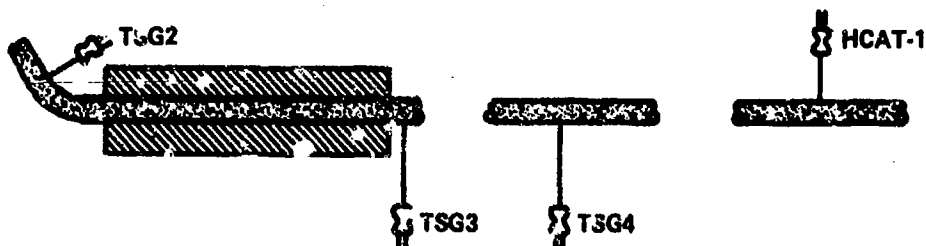


Figure 55. Schematic Diagram of Modified Gas - Transfer System

FD 56955A



For Tests Through 1-1A-20



For Tests Commencing With 1-1R-1

Figure 56. Combustor Gas Sample Transfer System Arrangement FD 71997

6. Exhaust Gas Analysis System

The composition of exhaust gas abstracted at the exit plane of combustors A and B was determined using an on-line, mobile instrumentation system, which was developed independently of this exploratory development program. The instrumentation system is shown schematically in figure 59 and on location at the test stand in figure 60. It consisted of the appropriate circuits, controls, and quantitative analytical instrumentation to determine the concentrations of UHC, CO, CO₂, NO, NO₂, water vapor, and O₂. UHC concentrations were determined using a modified Beckman 402 flame ionization detector (FID); concentrations of CO, CO₂ and water vapor were determined using modified MSA Lira Model Series 300 nondispersive infrared (NDIR) analyzers; NO concentrations were determined using a modified Beckman Model Series 315 NDIR analyzer; concentrations of NO₂ were determined using a modified Beckman Model Series 255 nondispersive ultraviolet (NDUV) analyzer; and concentrations of O₂ were determined using a Beckman Model Series 742 polarographic analyzer. Prior to our modifying the Beckman equipment, serious delays in accomplishing the program objectives were encountered because of design, development, and field support problems with the analyzers as received from the vendor.

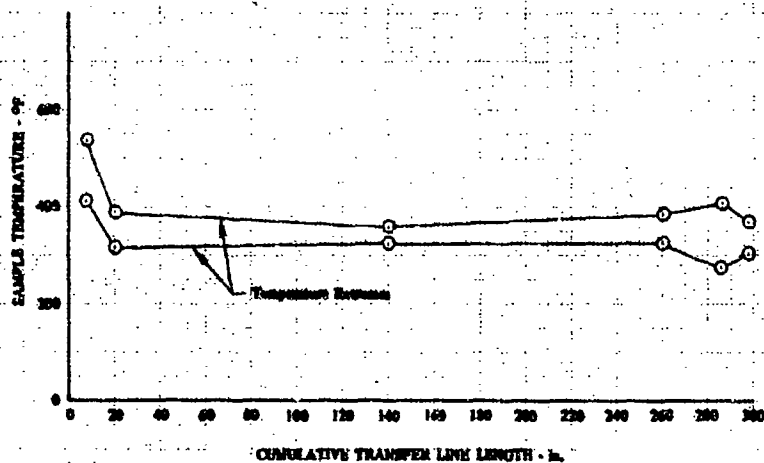


Figure 57. Variation in Sample Gas Temperature with DF 96046 Length for Original System

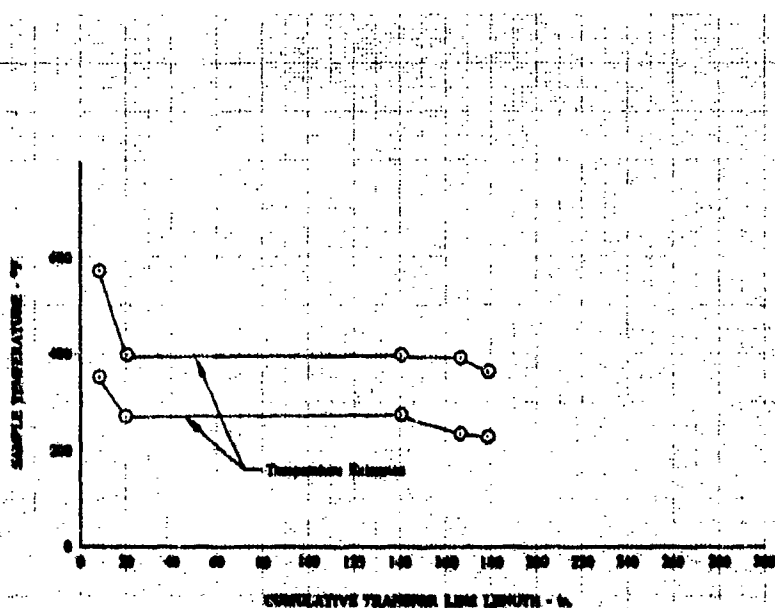
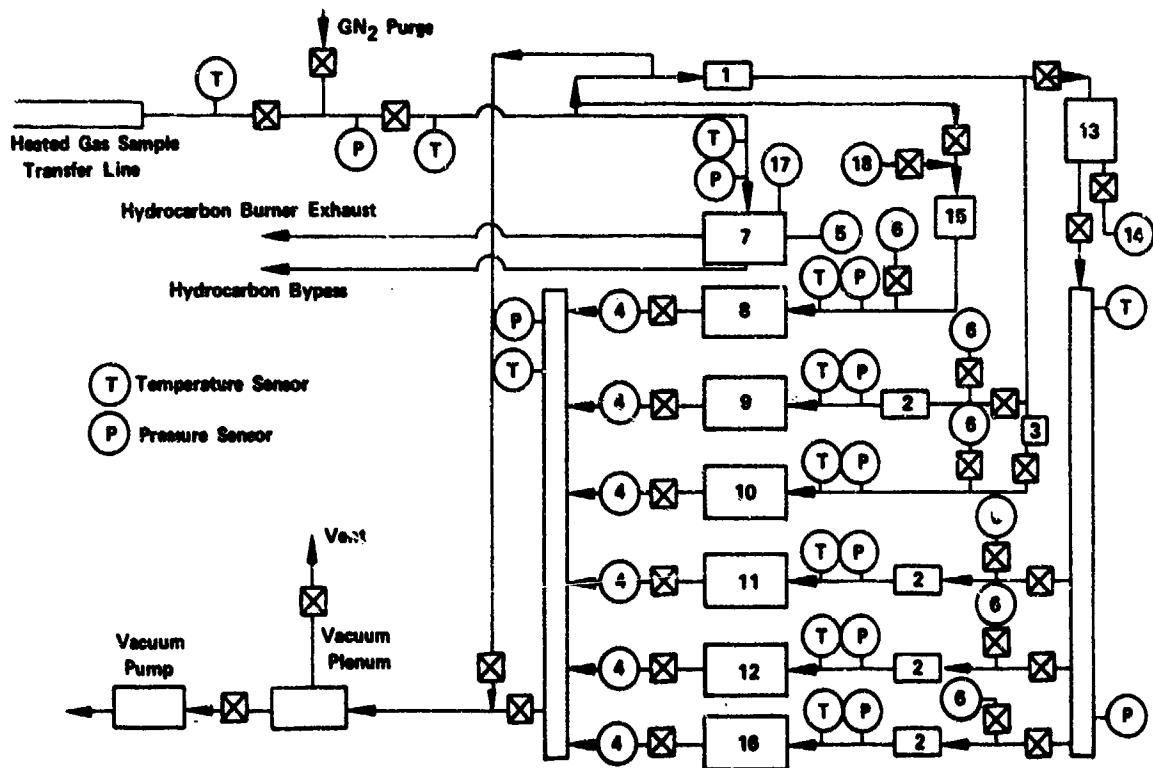


Figure 58. Variation in Sample Gas Temperature with DF 96047 Length for Modified System



- | | | |
|------------------------|-------------------------------|-------------------------------|
| 1. 10-Micron Filter | 7. Hydrocarbon Analyzer | 13. Cooling Coil and Ice Bath |
| 2. Drierite Cylinder | 8. Water Vapor Analyzer | 14. Water Sample Tap |
| 3. Particulate Trap | 9. Nitric Oxide Analyzer | 15. 50-Micron Filter |
| 4. Calibrated Orifices | 10. Nitrogen Dioxide Analyzer | 16. Oxygen Analyzer |
| 5. Oven Temperature | 11. Carbon Monoxide Analyzer | 17. Burner Temperature |
| 6. Calibration Gas | 12. Carbon Dioxide Analyzer | 18. Rig Air Sample Inlet |

Figure 59. Schematic Diagram of Instrumentation Measurement System FD 71998

The instruments were calibrated using vendor-certified span gases. Typical certifications obtained for the calibration gases are shown in figures 61 and 62. The gases were supplied in desired concentrations of the species of interest in carrier or dilution gases. Standard high-pressure cylinders were used for shipment of the gases from the vendor and for their subsequent storage. The shelf life for the majority of the calibration gases containing the species of interest was unlimited; however, the operating shelf life for the NO and NO₂ gases was finite. The vendor recommended that these gases be replaced after 3 months. Nitrogen was used as the carrier gas for all of the calibration fluids except NO₂; in this case air had been recommended and used by the vendor.

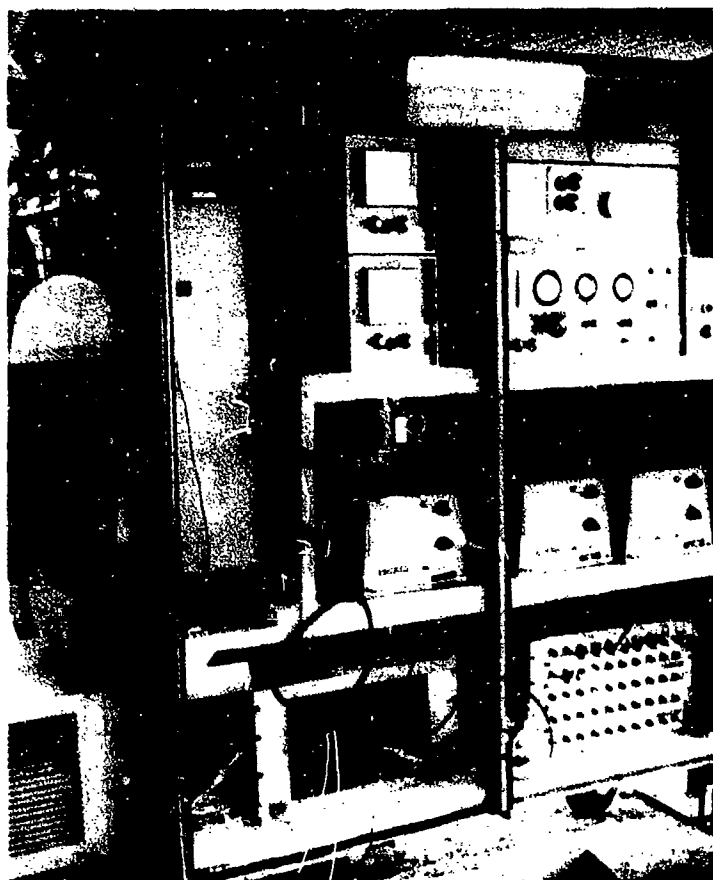


Figure 60. Instrumentation Measurement System FE 124483

The analyzers in the exhaust gas analysis system had the following characteristics. The possible full-scale error for each of the multiple ranges of the UHC analyzer was $\pm 1\%$; the maximum full-scale sensitivity for this instrument was 0-1 ppmv. The CO analyzer had a maximum full-scale sensitivity of 0.1% CO (by volume) with a possible full-scale error of $\pm 0.2\%$. The NO and NO₂ analyzers had maximum full-scale sensitivities of 0-500 ppmv and 0-200 ppmv, respectively; their possible full-scale errors were 1.5 ppmv and 1 ppmv, respectively. The water vapor analyzer had a maximum full-scale sensitivity of 0-1% H₂O (by volume) with a possible full-scale error of $\pm 0.2\%$. Finally, the full-scale sensitivity of the O₂ analyzer in the range used during the Phase II tests (0-25% O₂, by volume) was $\pm 1\%$.

The instrumentation system shown in figure 59 incorporated two independent gas-sample transfer circuits. These circuits emanated from the single, heated, exhaust gas supply line that delivered exhaust gas from the traverse probe to the instrumentation system. (See paragraph B.5.) One circuit was externally heated; sample gas flowing along this path was directed to the FID for UHC analysis. The second circuit was insulated but not heated externally; sample gas flowing into this path was directed through three parallel lines. One line was directed to the NDIR water vapor analyzer; one line was directed to the NO and NO₂ analyzers (which were arranged in parallel); and one line was directed to the distribution manifold. The gas sample was not physically or chemically conditioned (other than being directed through filter screens) prior to its entering the water vapor and NO₂ analyzers. The gas sample was conditioned, however, prior to its entering the remaining analyzer. A drying or absorbing agent contained in a cylinder was incorporated at the inlet to the NO NDIR analyzer to eliminate water vapor from the sample gas and prevent its interfering with the NO analysis.



UNION CARBIDE CORPORATION

LINDE DIVISION

2365 EAST LINDEN AVENUE, LINDEN, NEW JERSEY 07036

SPECIALTY GAS PLANT

PHONE: 201 - 925-0822

TO **United Aircraft Corp
Pratt & Whitney
Fla. Res. & Dev Center
W. Palm Beach, Fla.**

DATE **8-2-72**
NOTE BOOK NO. **46-011**
SHIPPING ORDER **15973**
TEST REPORT

PURCHASE ORDER NO. 063756

ANALYTICAL DATA

CYLINDER NO. LK74486

<u>Contents</u>	<u>Reported</u>
Nitric Oxide	185ppm
Nitrogen Dioxide	1.1ppm
Carbon Monoxide	4.1ppm
Total Hydrocarbons	4.1ppm
Nitrogen	Balance

T. Schirripa
ANALYST

A. E. Holmer
QUALITY CONTROL SUPERVISOR

CC

Figure 61. Typical Vendor Certification for NO Calibration Gas



MATHESON GAS PRODUCTS

POST OFFICE BOX 88
EAST RUTHERFORD, NEW JERSEY 07073
TELEPHONE: (201) 933-2400

A DIVISION OF WILL ROSS, INC.

Pratt & Whitney Aircraft
Division of United Aircraft Corporation
United, Florida

Date April 24, 1972

Attention: Purchasing Department

Our Invoice # 75685

Your P.O. # F051062

Lot No. 042172-2
042172-1

Gentlemen:

Below are the results of the analysis you requested, as reported by our laboratory. Results are in volume percent, unless otherwise indicated.

LABORATORY REPORT ON GAS ANALYSIS

Cyl #6-3613		Cyl # 6-3843	
Mixture Req.	Analysis	Mixture Req.	Analysis
Nitrogen Dioxide	50 PPM	50 PPM	144 PPM
Nitrogen	78.0%	Nitrogen	78.0%
Oxygen	20.8%	Oxygen	20.8%
Argon	0.94%	Argon	0.94%
Carbon Dioxide	less than 0.005%	Carbon Dioxide	less than 0.005%

Analyst John Oliveri JO:jb

The only liability of this Company for gas which fails to comply with this analysis shall be replacement thereof by the Company without extra cost.

MANUFACTURERS AND DISTRIBUTORS OF LABORATORY COMPRESSED GASES AND ASSOCIATED EQUIPMENT

Figure 62. Typical Vendor Certification for NO₂ Calibration Gas

The sample gas flowing to the distribution manifold was directed through a line contained within an ice-water bath upstream of the manifold to condense the major part of the water contained therein. The partially dried gas sample leaving the condenser and the manifold to enter the CO, CO₂, and O₂ analyzers was further dried by passing through cylinders containing drying agents immediately upstream of the analyzers.

The condensed water from the sample gas was removed from the ice-water bath after each full-traverse test and the pH of the condensate was measured using calibrated pH paper and a Beckman Model Series SS-1 pH meter. No pH measurements were made after partial-traverse tests because the quantity of condensate was essentially negligible. Full and partial-traverse tests are defined later. (See paragraph B.8, Test Classification.)

7. Concept Evaluation

a. Air and Fuel Staging

With reference to figure 63, the air staging and fuel staging concepts evaluated in the experimental program can be described by four primary parameters. The first, PSAR, is the ratio of the air flowrate in the primary zone to the air flowrate in the secondary zone. The second, PSFR, is the ratio of the fuel flowrate in the primary zone to the fuel flowrate in the secondary zone. The next, PHIP, is the fuel-air equivalence ratio in the primary zone. The fuel-air equivalence ratio is defined as the ratio of the local and stoichiometric fuel-air ratios for the fuel-air mixture of interest. The last, FA, is the overall fuel-air ratio for the combustor.

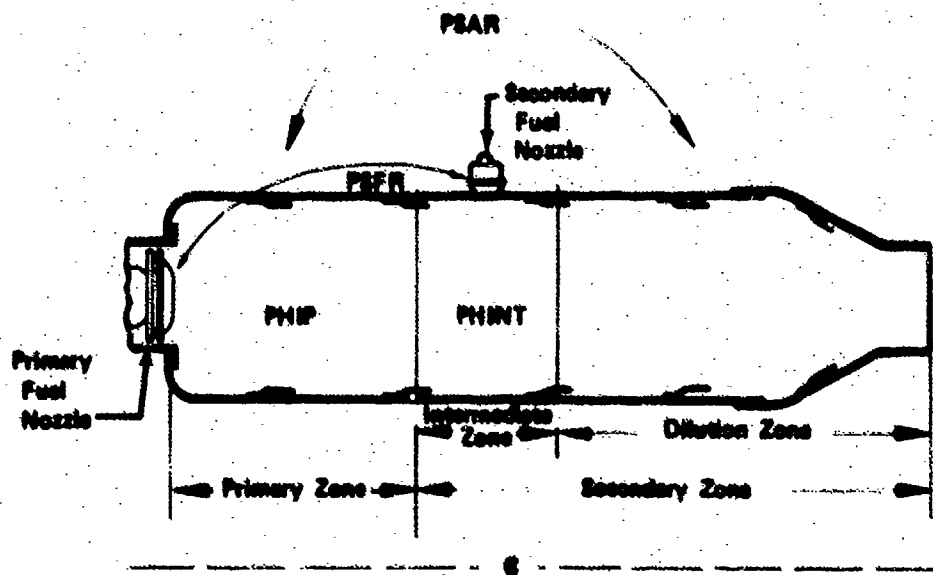


Figure 63. Research Combustor Nomenclature

FD 65741A

Three of the preceding four variables are independent. If any three are specified, the fourth can be readily derived from the combustor geometry shown in figure 63.

$$PSAR = \frac{1}{[(PHIP)(0.068)/FA] [(PSFR + 1)/PSFR] - 1} \quad (29)$$

$$PSFR = \frac{[(PHIP)(0.068)/FA] [PSAR/(PSAR + 1)]}{1 - [(PHIP)(0.068)/FA] [PSAR/(PSAR + 1)]} \quad (30)$$

$$PHIP = (FA/0.068) [PSFR/(PSFR + 1)] [(PSAR + 1)/PSAR] \quad (31)$$

$$FA = \frac{(PHIP)(0.068)}{[PSFR/(PSFR + 1)] [(PSAR + 1)/PSAR]} \quad (32)$$

Evaluation of the air-staging concept involved determining the variation in distribution and concentration of exhaust pollutants with the air distribution parameters PSAR and PHIP, and the overall fuel-air ratio, FA, at specific values of combustor inlet air temperature, pressure, and flowrate. A practical combustor design based upon the air-staging concept would require means to continuously vary the air distribution as FA was varied. No attempt was made to synthesize such a configuration in this program, however. Instead, as discussed earlier, a research combustor was modified to have sufficient flexibility to facilitate the predetermined variation of airflow distribution into the burner. For discrete values of PSAR, the variation in emission concentration and distribution at the exit plane of the research burner was determined over a range of overall fuel-air ratios. Results from tests involving the systematic variation of PSAR were then combined to describe results that should be obtainable from a combustor having a continuously modulating air distribution system.

Evaluation of the axial fuel-staging concept involved determining the variation in distribution and concentration of exhaust pollutants with the air distribution parameters PSAR and PHIP, the fuel-distribution parameters PSFR and PHINT, and the overall fuel-air ratio, FA, at specific values of combustor air inlet temperature, pressure, and flowrate. PHINT has been defined as the intermediate-zone equivalence ratio. (See figure 63.) Each test series consisted of selecting a discrete value of the air distribution parameter PSAR, which established the primary-zone equivalence ratio PHIP, and increasing the overall fuel-air ratio by introducing additional fuel into the combustor through the secondary fuel nozzles located downstream of the primary zone. As FA was increased, then, PSFR decreased and PHINT increased.

b. Premixing

Whereas the air and fuel staging concepts described in the preceding section could be readily evaluated with respect to four derived parameters, this was not found to be the case with the fuel-air premixing concept. Although some parameters peculiar to the premixing concept were derived, and are described later in this report, it was felt that the operational characteristics and performance of the premixing tubes could be better determined by examining them as a function of general variables. The general variables investigated included liner total

pressure drop, primary airflow distribution, and primary fuel flow distribution. Evaluation of the premixing concept, then, involved determining the variation in distribution of exhaust pollutants with variations in these general factors.

8. Test Classification

Two types of tests were conducted during this experimental program. The first was a full-traverse test in which a detailed examination of the temperature, pressure, and composition field was made at the discharge plane of the combustor. Measurements taken during a full-traverse test were described earlier. (See paragraph B.5, Traverse and Sample Gas Transfer System.)

The second was a partial traverse test in which the traversing probe was not rotated through a full 360 deg to acquire data at 15 circumferential locations. Instead, the probe was rotated through less than 360 deg and data at less than 15 circumferential locations were obtained. In some cases, the traverse probe was held stationary at a single location that was essentially representative of an average species concentration, and combustor operating conditions were varied to examine the resulting trends. Partial-traverse tests were also used when, during the conduct of a full-traverse test, it became apparent that the design concept being investigated did not show sufficient promise to justify a full-traverse test. The partial-traverse test provided a means to acquire a great deal of information expeditiously regarding the identification and development of improved component design techniques.

In the graphical presentation of data shown in the following sections, full-traverse data are represented by open symbols; partial-traverse data are represented by closed or darkened symbols.

9. Combustor A Test Program

a. General

Combustor A was used to investigate the general concept of controlling primary-zone equivalence ratio over a wide range of fuel-air ratios. Two principal means of accomplishing this control were considered: axial air staging, or variable airflow, in which the rate of airflow to the primary zone was varied with a concomitant variation in secondary and dilution airflow rate to maintain a constant total pressure drop across the burner as the primary-zone fuel flow-rate was changed; and fuel staging, or variable fuel flow, in which the airflow distribution throughout the burner remained fixed, and one fuel injection zone was used for low-power (low fuel-air ratio) operation and another zone was used, in combination with the first, for augmentation to high-power (high fuel-air ratio) operation. (See figure 63 for the regions in the burner defined as the primary, secondary, and dilution zones.) Although one type of air-staging was evaluated, axial, in which the amount of air allowed into each of the three principal zones was controlled (paragraph B.7, Concept Evaluation), two types of fuel staging were examined. The first was axial fuel staging in which the secondary fuel injection zone was significantly separated in the axial direction from the primary fuel injection zone (as shown in figures 48 and 63). The second was circumferential fuel staging in which the primary zone of the combustor was supplied with fuel from only seven of the fourteen normal, dome-mounted fuel nozzles. In some of these fuel-staging tests, seven sequentially located fuel nozzles were used (the

remaining seven sequentially located fuel nozzles were disconnected from the fuel supply manifold). In the remaining circumferential fuel-staging tests, seven alternately located fuel nozzles were used (the remaining seven alternately located fuel nozzles were disconnected from the fuel supply manifold).

In the following paragraphs, the results of the combustor A test program are presented. Observations and conclusions offered are those derived from an experimental, phenomenological viewpoint. A comparison of the experimental data obtained during the evaluation of combustor A with predictions generated using the general analytical model described in Section III is presented in Section V. The paragraphs are arranged in the general sequence in which the experimental program was accomplished, commencing with the determination of baseline emission characteristics for the research combustor used, and concluding with the results obtained from the circumferential fuel staging tests. In general, the data presented and discussed include combustion efficiency, determined from both exhaust gas temperature and species concentration measurements; and pollutant species concentrations and distributions as functions of fuel-air ratio for specific design configurations. Although the text is replete with graphical presentations to quantify discussion of the data, no extensive tables of data are interspersed. Instead, capacious tables of data are offered in the appendixes.

b. Baseline Emissions Characteristics

The intent of this initial series of tests was to establish baseline emissions characteristics for combustor A over a range of fuel-air ratios that encompassed both low-power and high-power conditions. Results from these tests were intended to serve as a datum for a representative full-scale, static-fed, annular combustor that had been designed without provision for reducing or eliminating undesirable exhaust emissions. The results were to serve as a basis of comparison for test results that were to be obtained later in the experimental program. The baseline configuration of combustor A, designated Scheme 1-1A, was designed to operate at an overall fuel-air ratio of 0.022. A summary showing the airflow distribution schedule for Scheme 1-1A is presented in figure 64. At the overall design fuel-air ratio of 0.022, the primary-zone equivalence ratio (PHIP) for this configuration was 0.7, and the primary-to-secondary airflow rate ratio (PSAR) was 0.86 (this was the highest value of PSAR evaluated during the combustor A test program). The total amount of air used for cooling of the Scheme 1-1A burner (COOLP) was approximately 30% of the combustor total airflow. This was a conservative amount that had provided ample cooling of the liners in previous tests using this combustor. Approximately 30% of this total was used for cooling the liners and dome in the primary zone (CAP). The amount of air entering the primary zone through the dome-mounted fuel nozzle swirlers (SWAP) was approximately one-third of the total air entering the primary zone. The remaining air entering the primary zone to achieve a PHIP of 0.7 at a fuel-air ratio of 0.022 was defined as primary penetration air (PAP). Dilution-zone penetration air was supplied equally from the ID and OD liners. As described earlier, there were two air penetration holes for each primary fuel injector; this was considered to be consistent with conventional practice, providing an acceptable scale of turbulence for mixing. The exact arrangement and location of air supply holes is shown in figure 44.

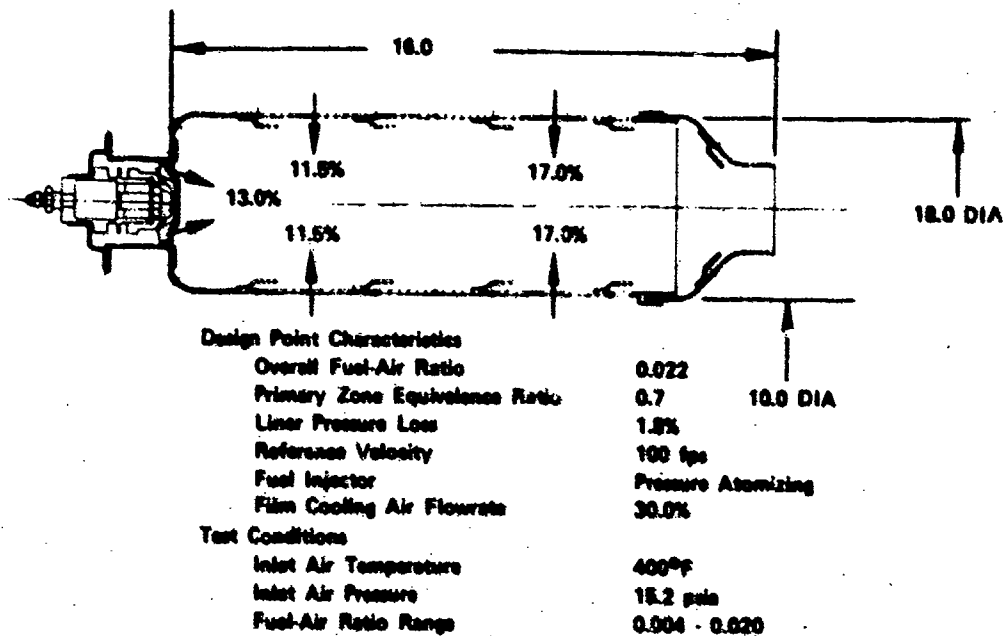


Figure 64. Summary Sheet for Combustor A
Schemes 1-1A and 1-1B

FD 71999

In the course of the initial baseline tests with Combustor Scheme 1-1A, it became apparent that the combustion efficiencies being obtained in the low fuel-air ratio range were higher than those that were usually experienced in practice with conventional combustors. In general, combustion efficiency would be expected to peak-out at its design-point value (in this case 0.022) and then gradually drop off as the fuel-air ratio was reduced to that corresponding to idle operation.

An ostensible reason for the results obtained was that the fuel injectors being used provided a greater degree of fuel atomization at the low flowrates associated with idle operation than fuel nozzles typically used in practice. The fuel injectors used in the initial baseline tests were common, simplex, oil-burner nozzles that provided a 90-deg, hollow-cone dispersion of JP-5 fuel at a design-point flowrate of 4 gph at a differential pressure of 125 psi.

Accordingly then, a second series of baseline tests was conducted using the same combustor arrangement, but a different set of fuel nozzles. The overall combustor scheme used for these tests was referred to as 1-1B. The replacement nozzles were also common, simplex, oil-burner injectors that provided a 90-deg, hollow-cone dispersion of JP-5 fuel; however, their design-point flowrate was 2 gph at a differential pressure of 125 psi. The fuel flowrate-pressure drop characteristics for the two sets of fuel nozzles are shown in Figure 65. Although no experimental determination was made of the spray characteristics of either set of nozzles, estimates of the Sauter mean diameter (SMD) of the spray from each type as a function of pressure drop were made using the method of Reference 29. (See table VIII.) Lower combustion efficiencies, more in keeping with conventional practice, were thus obtained in the idle range using the 2-gph fuel nozzles. As a result of the use of two different fuel injectors, a more comprehensive set of baseline test results was obtained.

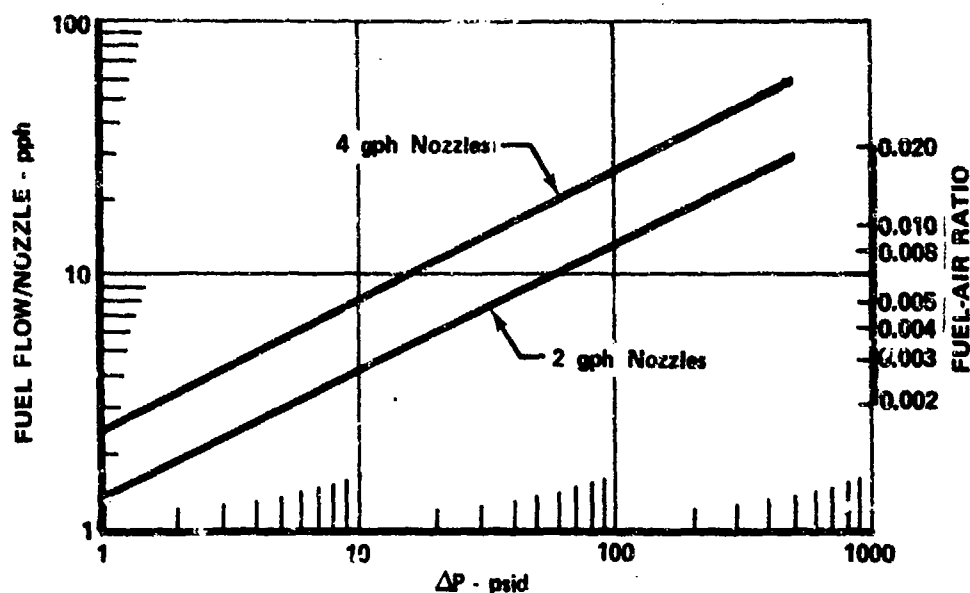


Figure 65. Variation in Fuel Flowrate and FA with Pressure Drop

FD 72145

Table VIII. Predicted Droplet Diameters

FA	Fuel Flowrate, pph	2 gph Nozzles		4 gph Nozzles	
		ΔP , psid	SMD, microns	ΔP , psid	SMD, microns
0.002	3.09	5.3	109	1.5	180
0.004	6.17	21.2	74	6.0	124
0.008	12.34	86.0	50	23.8	85
0.012	18.51	190.0	41	50.0	69
0.016	24.70	340.0	34	88.0	60
0.018	27.80	430.0	32	112.0	56
0.022	33.90	625.0	29	163.0	50

Figure 66 shows the variations in combustion efficiency, using both temperature and exhaust gas analysis measurements, with fuel-air ratio for both sets of baseline tests. Throughout this report values of combustion efficiency determined using temperature measurements will be referred to as EFFMB; values of combustion efficiency determined using gas analysis measurements will be referred to as EFFGA. For Combustor Scheme 1-1A, values of EFFMB ranged from 92% at a fuel-air ratio of 0.0027 to 97% at fuel-air ratios above 0.006. On the other hand, EFFGA was higher over this range of fuel-air ratios, from approximately 4 percentage points at the low-power end to approximately 2 percentage points at the higher. This trend was not nearly as pronounced for the tests conducted using the 1-1B configuration even though generally high levels of combustor efficiency were obtained. In fact, the number of tests in which EFFMB was greater than EFFGA were nearly the same as those for which the opposite was observed.

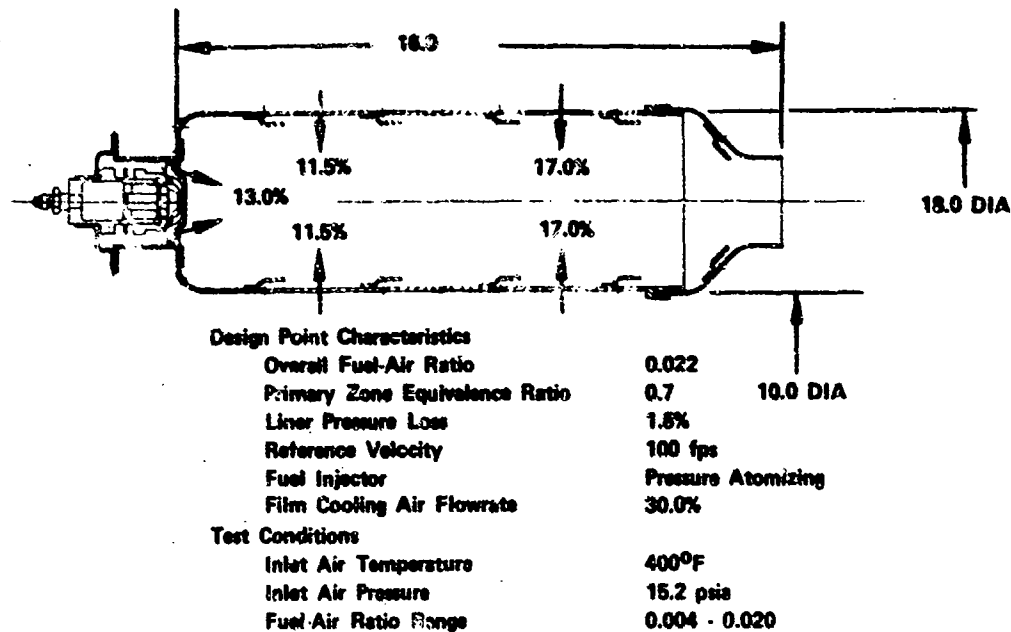


Figure 64. Summary Sheet for Combustor A
Schemes 1-1A and 1-1B

FD 71999

In the course of the initial baseline tests with Combustor Scheme 1-1A, it became apparent that the combustion efficiencies being obtained in the low fuel-air ratio range were higher than those that were usually experienced in practice with conventional combustors. In general, combustion efficiency would be expected to peak-out at its design-point value (in this case 0.022) and then gradually drop off as the fuel-air ratio was reduced to that corresponding to idle operation.

An ostensible reason for the results obtained was that the fuel injectors being used provided a greater degree of fuel atomization at the low flowrates associated with idle operation than fuel nozzles typically used in practice. The fuel injectors used in the initial baseline tests were common, simplex, oil-burner nozzles that provided a 90-deg, hollow-cone dispersion of JP-5 fuel at a design-point flowrate of 4 gph at a differential pressure of 125 psi.

Accordingly then, a second series of baseline tests was conducted using the same combustor arrangement, but a different set of fuel nozzles. The overall combustor scheme used for these tests was referred to as 1-1B. The replacement nozzles were also common, simplex, oil-burner injectors that provided a 90-deg, hollow-cone dispersion of JP-5 fuel; however, their design-point flowrate was 2 gph at a differential pressure of 125 psi. The fuel flowrate-pressure drop characteristics for the two sets of fuel nozzles are shown in figure 65. Although no experimental determination was made of the spray characteristics of either set of nozzles, estimates of the Sauter mean diameter (SMD) of the spray from each type as a function of pressure drop were made using the method of Reference 29. (See table VIII.) Lower combustion efficiencies, more in keeping with conventional practice, were thus obtained in the idle range using the 2-gph fuel nozzles. As a result of the use of two different fuel injectors, a more comprehensive set of baseline test results was obtained.

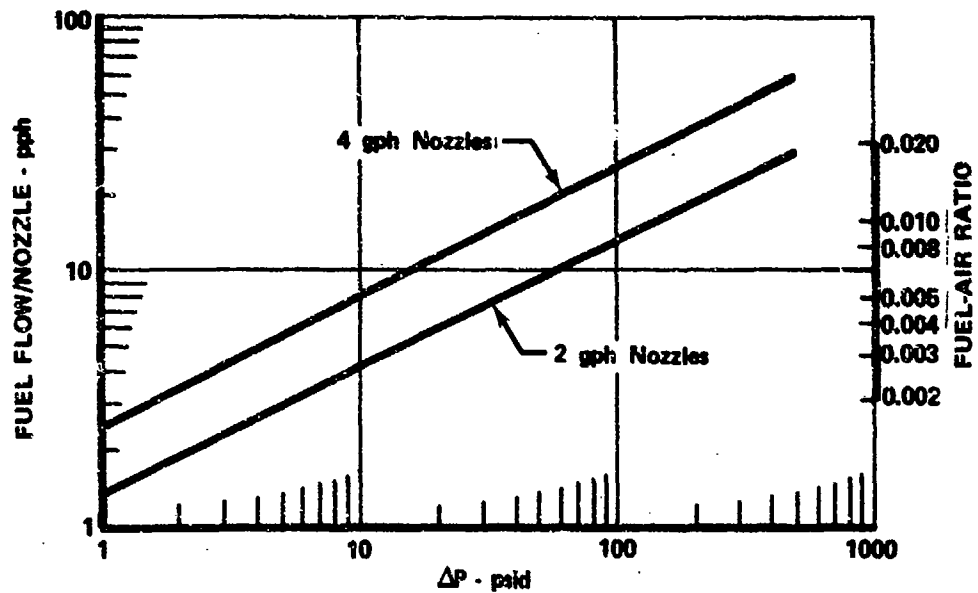


Figure 65. Variation in Fuel Flowrate and FA with Pressure Drop

FD 72145

Table VIII. Predicted Droplet Diameters

FA	Fuel Flowrate, pph	2 gph Nozzles		4 gph Nozzles	
		ΔP , psid	SMD, microns	ΔP , psid	SMD, microns
0.002	3.09	5.3	109	1.5	180
0.004	6.17	21.2	74	6.0	124
0.008	12.34	86.0	50	23.8	85
0.012	18.51	190.0	41	50.0	69
0.016	24.70	340.0	34	88.0	60
0.018	27.80	430.0	32	112.0	56
0.022	33.90	625.0	29	163.0	50

Figure 66 shows the variations in combustion efficiency, using both temperature and exhaust gas analysis measurements, with fuel-air ratio for both sets of baseline tests. Throughout this report values of combustion efficiency determined using temperature measurements will be referred to as EFFMB; values of combustion efficiency determined using gas analysis measurements will be referred to as EFFGA. For Combustor Scheme 1-1A, values of EFFMB ranged from 92% at a fuel-air ratio of 0.0027 to 97% at fuel-air ratios above 0.006. On the other hand, EFFGA was higher over this range of fuel-air ratios, from approximately 4 percentage points at the low-power end to approximately 2 percentage points at the higher. This trend was not nearly as pronounced for the tests conducted using the 1-1B configuration even though generally high levels of combustion efficiency were obtained. In fact, the number of tests in which EFFMB was greater than EFFGA were nearly the same as those for which the opposite was observed.

The reasons for the differences between EFFMB and EFFGA in the Scheme 1-1A series have not been completely ascertained. One might be tempted to accept EFFMB as correct if precedence or past experience were the predominant influence. However, an error of only 2% in EFFMB is needed to achieve the EFFGA values. To encounter such an error in temperature measurements used to determine EFFMB is not inconceivable. On the other hand, an error of over 100% in measured concentrations of UHC and CO would be needed to have EFFGA match EFFMB. It is highly improbable that such concentration measurement errors could be obtained at low values of fuel-air ratio where UHC and CO concentrations are relatively high. It would appear that EFFGA at low fuel-air ratios should be more correct than EFFMB. Unfortunately, others who have conducted tests to compare temperature and concentration determined combustion efficiencies have also observed EFFMB to be lower, and significantly lower in some cases, than EFFGA, see Reference 30. Of the 27 tests reported in Reference 30, only four showed EFFGA lower than EFFMB, however, the values of fuel-air ratio for these four tests were all greater than 0.008. Under these circumstances, it is not inconceivable that EFFMB was higher than EFFGA because the measured temperatures were higher due to catalytic reactions occurring at the tips of the thermocouples. Additional work needs to be done in this area of efficiency measurement using thermocouples before any conclusions can be drawn.

Figure 67 shows the variation in UHC concentration with fuel-air ratio for tests conducted using Combustor Schemes 1-1A and 1-1B. In the initial series using 2-gph fuel nozzles, UHC concentrations less than 10 ppmv were measured above a fuel-air ratio of approximately 0.007; this level is not characteristic of operating engines. The UHC level was not elevated that dramatically, on an absolute level, when the 4-gph fuel nozzles were substituted. On a relative basis, however, the UHC concentration did increase ten-fold at a fuel-air ratio of 0.006: demonstrating the strong influence of fuel droplet size on completeness of combustion (for a system in which the residence time is fixed).

In general, for Combustor Schemes 1-1A and 1-1B, as the overall fuel-air ratio was reduced below its design-point value of 0.022, which corresponded to a PHIP of 0.7, UHC emission concentration increased. Although the absolute levels were relatively low, the trends were similar and significant. They indicated that as the fuel-air ratio was decreased, PHIP was further removed from its design-point value, the primary zone became leaner, the local combustion temperature decreased, and the concentration of UHC in the combustor exhaust gas increased. This increase in UHC concentration resulted in the decrease in combustion efficiency. (As shown in equation 28, the influence of UHC in the exhaust gas is the predominant variable influencing combustion efficiency, contributing four times as much to inefficiency, for each emission index unit, as CO.)

Figure 68 shows the variation in CO concentration with fuel-air ratio for tests conducted using Combustor Schemes 1-1A and 1-1B. For the tests of Scheme 1-1A, CO concentration initially decreased, passed through a minimum at a fuel-air ratio of approximately 0.007 and then commenced to increase. In tests of the 1-1B combustor arrangement, CO concentration increased continuously with fuel-air ratio.

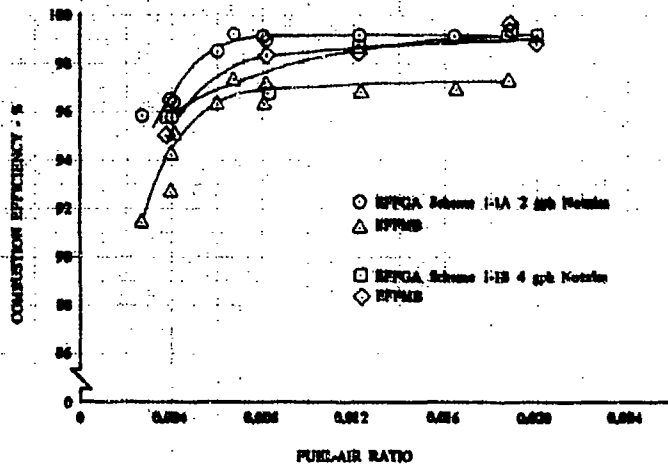


Figure 66. Variation in Combustion Efficiency with Fuel-Air Ratio for Tests with Combustor Schemes 1-1A and 1-1B DF 96048

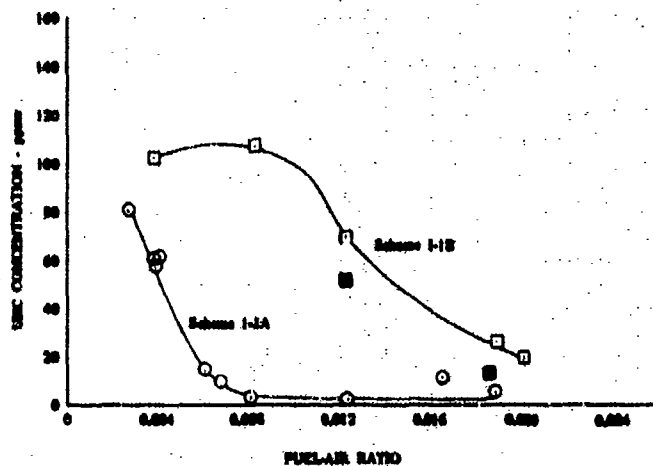


Figure 67. Variation in UHC Concentration with Fuel-Air Ratio for Tests with Combustor Schemes 1-1A and 1-1B DF 96049

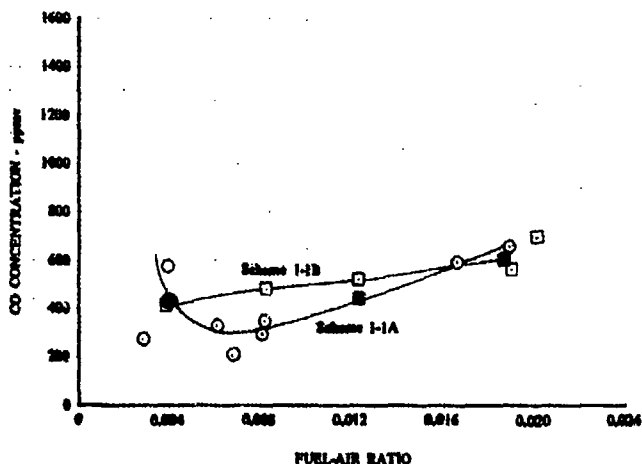


Figure 68. Variation in CO Concentration with Fuel-Air Ratio for Tests with Combustor Schemes 1-1A and 1-1B DF 96050

The differences in the shape of the CO concentration-fuel-air ratio curves for the two schemes at very low fuel-air ratios can be attributed to differences in the effective local equivalence ratios within the primary zones of the combustors which are caused by different degrees of fuel atomization produced by the two types of fuel nozzles. At higher fuel-air ratios, the trends were generally similar, and in terms of combustor operating characteristics, can be attributed to the fact that as the fuel-air ratio was increased, combustion loading was increased and the reaction front was moved downstream out of the primary zone. At the higher fuel-air ratios, the reacting gases were quenched by dilution air in the secondary zone. In general, CO concentration would be expected to decrease with increasing fuel-air ratio as long as the reaction front remained upstream of the dilution zone, as might be the case if the fuel droplets were small, but would increase if the reacting mixture contacted the dilution air and was quenched. If large droplets are present, this quenching occurs at very low fuel-air ratios because these droplets require a longer length to burn to completion and, therefore, come into contact with cold penetration air sooner. This proposition was supported by visual observations of the combustion process during the tests. At a fuel-air ratio of approximately 0.004, a visible, luminous flame front was observed that extended from the primary zone approximately half way to the dilution zone. However, at a fuel-air ratio of approximately 0.012, the flame front extended the entire length of the combustor to the exit plane. These observations were only qualitative, but they do provide a plausible explanation for the trend observed. The overall levels of CO concentration obtained with baseline Schemes 1-1A and 1-1B, however, were substantially above, acceptable low-emission limits throughout the entire range of fuel-air ratios examined.

The variations in the concentrations of NO, NO₂, and NO_x (NO + NO₂) with fuel-air ratio for Schemes 1-1A and 1-1B are shown in figures 69 through 71. NO concentrations generally increased with increasing fuel-air ratio in the tests of both schemes; however, the levels were noticeably lower for those in which 4-gph fuel nozzles were used. NO₂ concentrations, on the other hand, were nearly the same for both schemes over most of the range of fuel-air ratios examined. However, at the highest values of fuel-air ratio, NO₂ concentrations measured during tests of the 1-1B scheme were markedly lower. Concentrations of NO and NO₂ in combination are shown in figure 71. NO_x levels obtained during tests of the 1-1A scheme were approximately twice those obtained during tests of Combustor Scheme 1-1B. These concentration levels were generally representative of those observed in exhaust gas from operational engines having combustor inlet air temperatures in the 400°F range. (See Reference 31.)

c. Evaluation of Air Staging

The concept of air staging was evaluated by systematically varying the combustor airflow distribution to achieve a near-constant value of PHIP over the range of FAs corresponding to those from idle to full-power operation. In conventional burner design practice, a fixed airflow distribution is used that provides near-stoichiometric values of PHIP only at full-power conditions. Therefore, at lower values of FA, as discussed earlier, PHIP is much lower, ranging to values of 0.3 and less at idle. With the air-staging concept, primary-zone airflow is controlled and is reduced during idle operation to achieve a value of PHIP near the stoichiometric value.

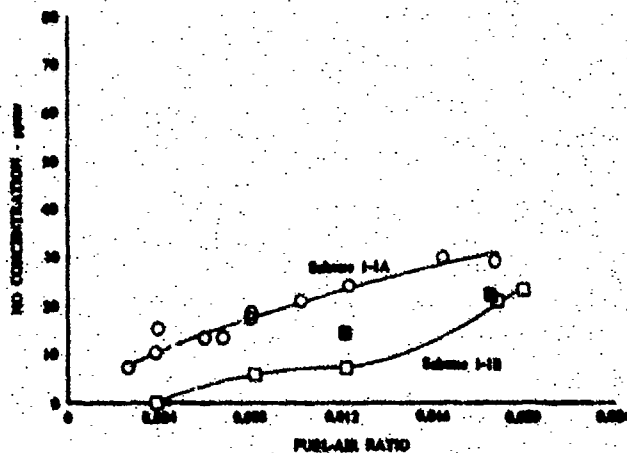


Figure 69. Variation in NO Concentration with Fuel-Air Ratio for Tests with Combustor Schemes 1-1A and 1-1B DF 96051

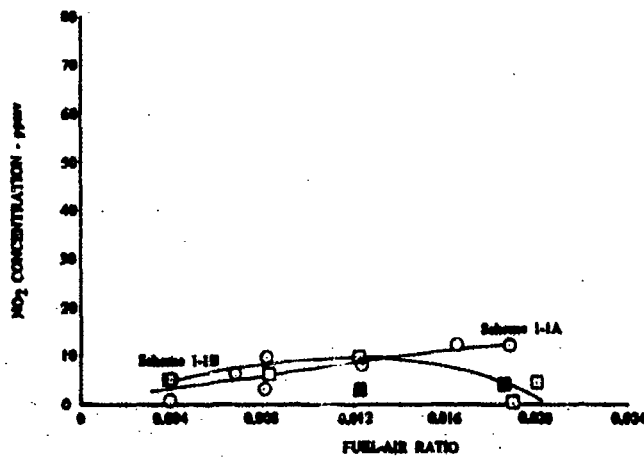


Figure 70. Variation in NO₂ Concentration with Fuel- DF 96052 Air Ratio for Tests with Combustor Schemes 1-1A and 1-1B

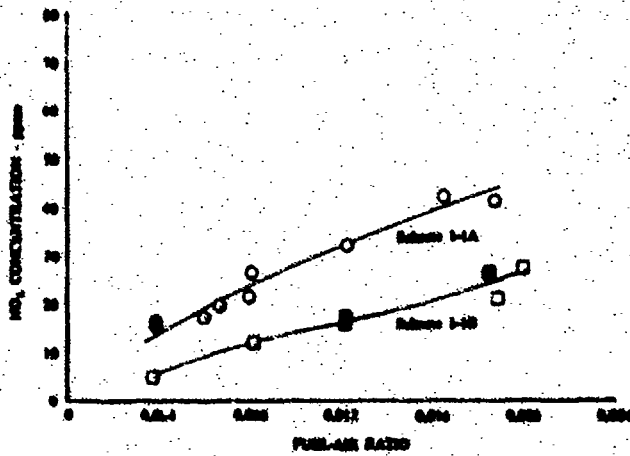


Figure 71. Variation in NO_x Concentration with Fuel- DF 96053 Air Ratio for Test with Combustor Schemes 1-1A and 1-1B

PSAR was designated as the defining parameter in the air-staging tests. As discussed in the preceding section, this parameter defines the combustor airflow distribution required to achieve a desired value of PHIP at a particular value of the overall FA. The interrelationships between these derived parameters were presented in an earlier section.

To vary the combustor airflow distribution in actual practice would, of necessity, require some mechanical or aerodynamic means for continuously adjusting combustor air-inlet hole area to provide the optimum airflow distribution in the primary zone for a given value of FA. In the tests conducted under Phase II the adjustment feature was achieved not in a continuous mode but by using four fixed airflow distribution schemes, each designed for a different value of FA. The important design-point parameters for these four schemes are shown in table IX. Summaries of the airflow distribution for the four schemes are shown in figures 64, and 72 through 74.

Table IX. Air-Staging Design-Point Parameters

Scheme	PSAR	Design-Point FA	PHIP at Design-Point FA
1-1A	0.86	0.022	0.7
1-1B			
2-1A	0.31	0.016	1.0
3-1A	0.21	0.012	1.0
4-1A	0.13	0.008	1.0

With reference to table IX, each scheme was tested over a range of FAs centered about the design-point value. It was expected that combustion efficiency would be high in the vicinity of the design point for each scheme, with a decline occurring at both extremes of the FA range evaluated. Therefore, by combining the results from the evaluation of four different airflow distribution schemes having four different design-point FAs, the good performance (high combustion efficiency and low UHC and CO concentrations) achievable with a continuously variable air distribution system could be estimated.

To isolate the influence of PSAR as completely as possible, care was taken with the experimental hardware to retain the same combustor hole pattern and the same values of the swirler-to-penetration airflow ratio in the primary zone of each of the four schemes. Variations in combustor airflow distribution were accomplished by changing individual air-entry hole areas within the fixed distribution pattern. Thus, the parameter PSAR could be altered without introducing the additional influences that might have resulted had changes been made in the air-entry distribution pattern.

Of the two types of fuel nozzle used in the baseline tests, the 4-gph coarser atomizing injectors were selected for use in all of the air-staging tests because they were more representative of conventional practice.

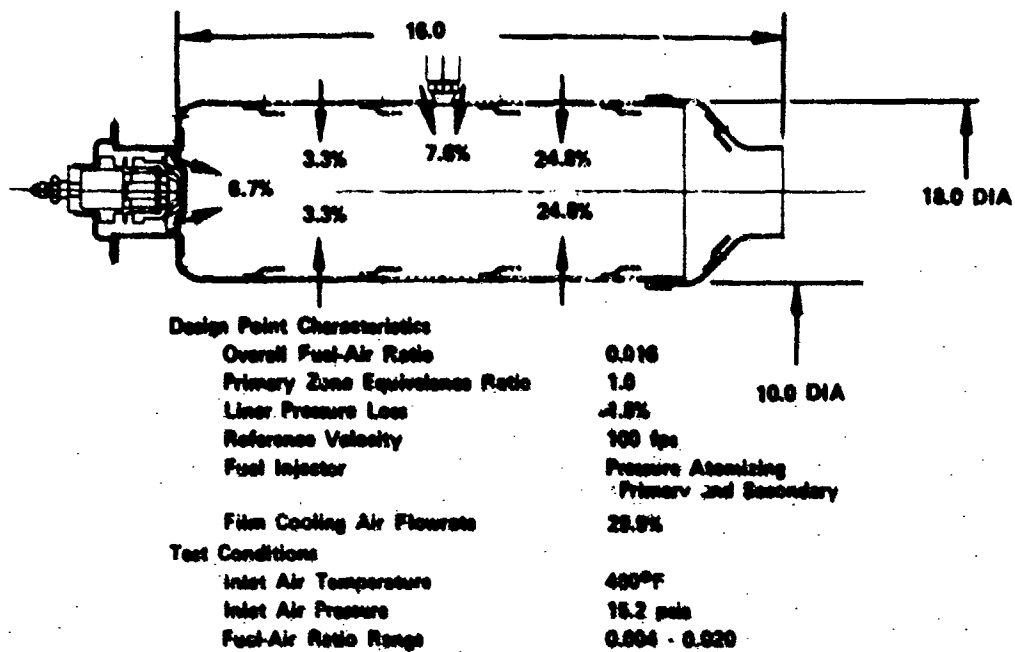


Figure 72. Summary Sheet for Combustor A
Scheme 2-1A

FD 72100

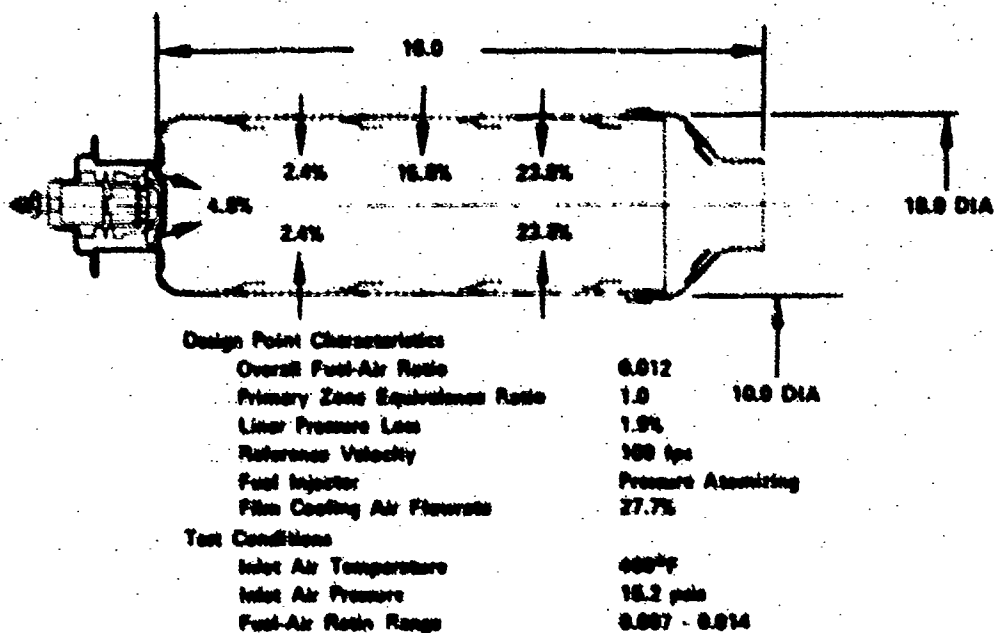


Figure 73. Summary Sheet for Combustor A
Scheme 3-1A

FD 72101

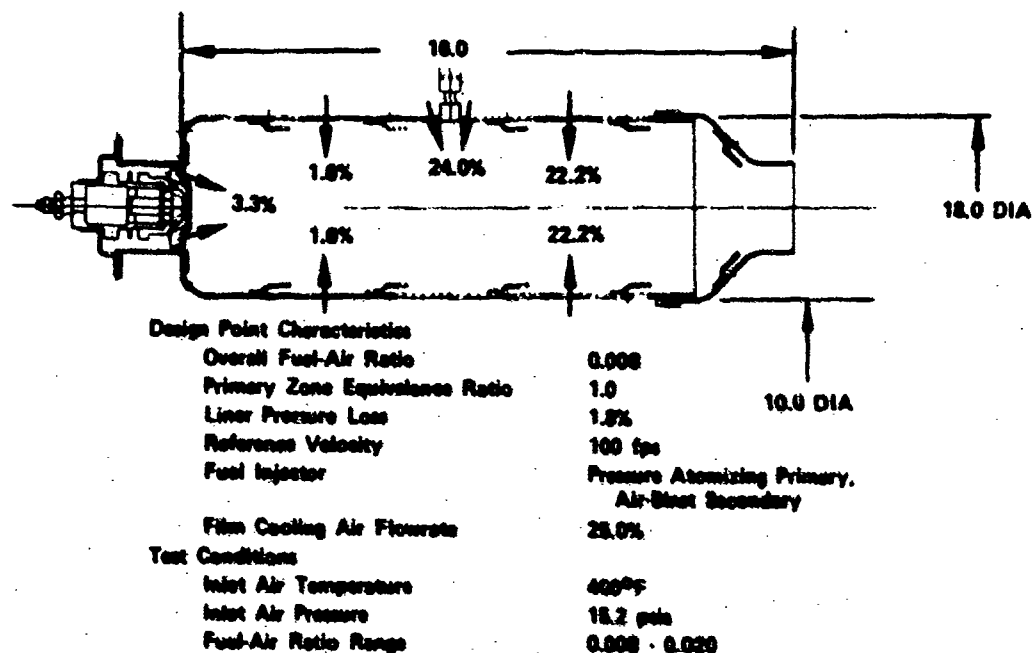


Figure 74. Summary Sheet for Combustor A
Scheme 4-1A

FD 72103

Test results obtained with the four schemes verified the expected improvements in combustion efficiency at low-power as PSAR was decreased. The variation in both EFFMB and EFFGA with FA and PSAR is shown in figure 75. The curve showing the data for Scheme 1-1B, in which PSAR was 0.86, is a reproduction of the baseline results that were shown in figure 66 for tests conducted with 4-gph nozzles. This scheme, which had a design-point FA of 0.022, exhibited combustion efficiencies in excess of 99% in its design-point range and above 98% to an FA of 0.008. At values of FA lower than 0.008, a decline in efficiency to 95% was observed. Scheme 4-1A, in which the PSAR was 0.13 and the design-point FA was 0.008, demonstrated higher efficiencies at low-power operation as anticipated; efficiency levels were maintained in excess of 98% to an FA of 0.0045. At values of FA above 0.010, the level dropped below 98%, indicating that the useful range of operation for Scheme 4-1A was in the range of FAs from 0.0045 to 0.010. With Scheme 3-1A, in which the PSAR was 0.21 and the design-point FA was 0.012, efficiencies above 98% were maintained over a range of FAs from 0.007 to 0.014. Scheme 2-1A, with a PSAR of 0.31 and a design-point FA of 0.016, demonstrated high efficiencies over the broadest range of FAs; levels near 99% were achieved over an FA range of 0.006 to 0.014, and levels in excess of 98% were attained up to an FA of 0.019. By combining the best portions of each curve, combustion efficiencies can be maintained above 98% down to an FA of 0.0045. Figure 75 shows, therefore, that air staging can be used to extend the same high values of combustion efficiency obtained at full-power operation to the low-power range.

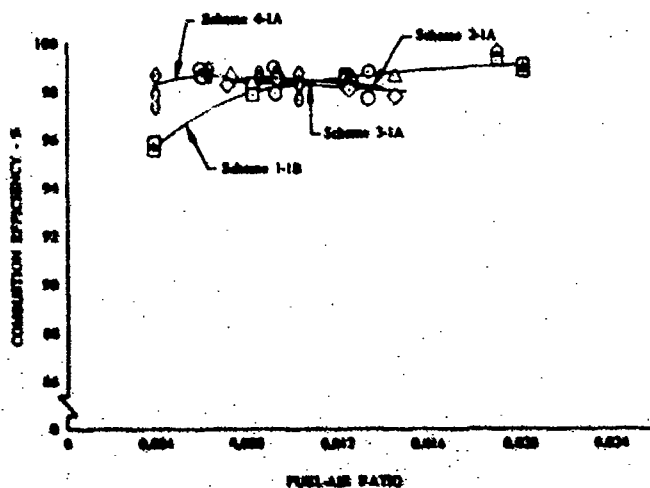


Figure 75. Comparison of Variations in Combustion Efficiency with Fuel-Air Ratio for Tests Conducted with Combustor Schemes 1-1B, 2-1A, 3-1A, and 4-1A DF 96054

The variation in UHC concentration with FA and PSAR for the four combustor schemes evaluated is shown in figure 76. Scheme 1-1B, the baseline, configuration exhibited relatively low levels of UHC concentration only in the vicinity of the design-point FA. Scheme 4-1A achieved the greatest reduction in UHC concentrations at very low values of FA. Schemes 2-1A and 3-1A exhibited UHC concentration levels below baseline values over the FA range from 0.008 to 0.019. By combining the best portions of each of the preceding curves, UHC concentration levels below 45 ppmv can be maintained over the FA range from 0.004 to 0.020.

Scheme 4-1A, which had been expected to produce the lowest concentration of UHC during idle operation, exhibited an increasing trend in UHC concentration above an FA of 0.006. This curve crossed and exceeded the UHC curve for Scheme 2-1A at an FA of approximately 0.0092. This trend is believed to have been caused by an over-rich condition in the primary zone, which might be the result of an assumption used in establishing the design point, viz., that all primary penetration airflow recirculates in the combustor and is fully utilized in the reaction process. It would appear that this assumption is not entirely correct; only part of the penetration air is effectively recirculated and that the actual, experimentally determined, design-point FA is closer to 0.005. In this case, the original design-point FA of 0.008 corresponds to a PHIP of 1.6, which is well beyond stoichiometric and sufficiently high to cause a decline in combustion efficiency and an increase in UHC concentration. No explanation is readily apparent for the behavior of UHC concentration with FA for Scheme 3-1A; it had been expected that Scheme 3-1A would have produced lower UHC emission levels than Scheme 2-1A.

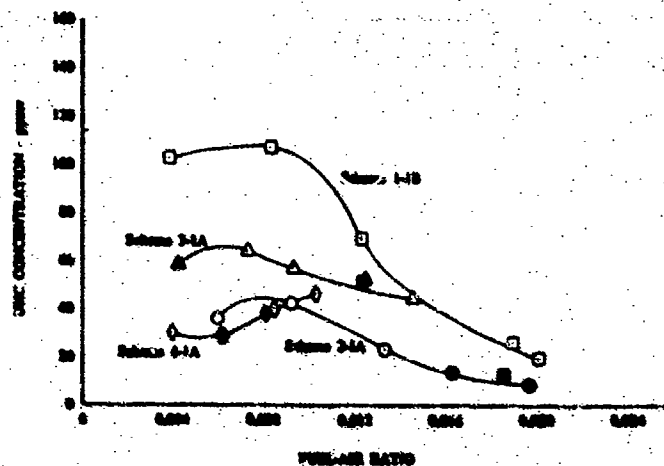


Figure 76. Comparison of Variations in UHC Concentration with Fuel-Air Ratio for Tests Conducted with Combustor Schemes 1-1B, 2-1A, 3-1A, and 4-1A DF 96055

The variation in CO concentration with FA and PSAR is shown in figure 77. The baseline configuration produced CO concentration levels in excess of 400 ppmv over the FA range from 0.004 to 0.020. Reductions in these levels were achieved in Schemes 2-1A, 3-1A, and 4-1A in the lower-power range. By combining the best portions of the CO concentration - FA curves for each scheme a composite curve can be synthesized that has CO concentration levels increasing from a low value of approximately 140 ppmv at an FA of 0.004 to a high value of 600 ppmv at an FA of 0.0185. This composite curve would be composed of the Scheme 4-1A results in the FA range less than 0.006; of Scheme 2-1A results in the FA range between 0.006 and 0.012; and of Scheme 1-1B results at values of FA above 0.012. Again, as in the case of UHC, no explanation is readily apparent for the fact that Scheme 3-1A, with a design-point FA of 0.012, produced higher concentration levels of CO than Scheme 2-1A with a design-point FA of 0.016 in the low power range.

The CO concentrations obtained with all four schemes evaluated were high, representing decrements in combustion efficiency from 0.7 to 1%. However, the general capability of reducing CO emission levels at low-power conditions by incorporating the air staging concept was demonstrated. The inability to achieve lower CO concentration levels may be due to a limitation of the fuel delivery means (pressure-atomizing fuel nozzles) that were employed, or to detailed considerations relating to the admission of air into the four research burner configurations.

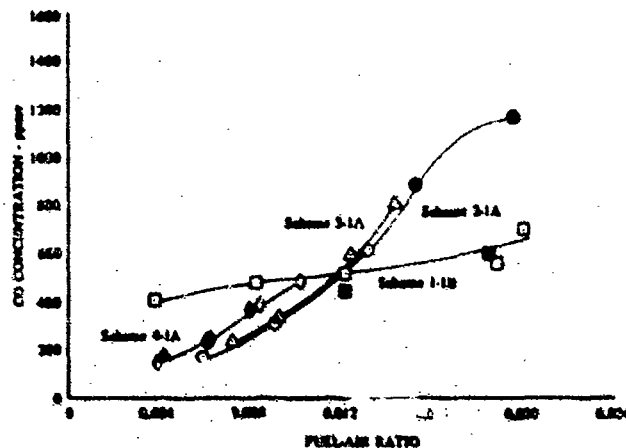


Figure 77. Comparison of Variations in CO Concentration with Fuel-Air Ratio for Tests Conducted with Combustor Schemes 1-1B, 2-1A, 3-1A, and 4-1A

DF 95056

The variations in NO , NO_2 , and NO_x ($\text{NO} + \text{NO}_2$) concentrations are shown in figures 78 through 80, respectively. The trends shown conform generally to those expected. Both NO and NO_2 concentrations increased with increasing values of FA, and with decreasing values of PSAR. These results indicate simply that higher concentrations of NO and NO_2 were formed as the primary zone became richer and reaction temperatures increased. In the case of Combustor Scheme 4-1A, however, there was a decrease in concentrations of both NO and NO_2 with FA in the FA range from 0.008 to 0.010. In this range, values of PHIP were above stoichiometric, and it is believed that the declines in concentrations correspond to decreased reaction temperatures commensurate with equivalence ratios greater than stoichiometric.

An exception to the general trend of nitrogen oxide concentrations increasing with FA is seen in figure 80 where the NO_x concentration for Scheme 3-1A is higher at an FA of 0.004 than at 0.008. No explanation is readily apparent for this trend.

Data contained in figures 78 through 80 for UHC, CO, and NO_x concentrations, respectively, have been cross-plotted in figures 81 through 83 in terms of variations in pollutant concentrations with PSAR for various values of FA. For both UHC and CO, the lowest concentration levels attained for a nominal idle FA of 0.008 were achieved at a PSAR of 0.31 using Scheme 2-1A. As discussed in a preceding section on UHC results, it is believed that the effective design-point FA was actually different than the original calculated value, i.e., 0.016 for Scheme 2-1A, and was, in fact, approximately 60% lower. Under these circumstances, Scheme 2-1A would have been operating at a PHIP of 0.8 at an FA of 0.008, which is ideal for producing low concentrations of UHC and CO.

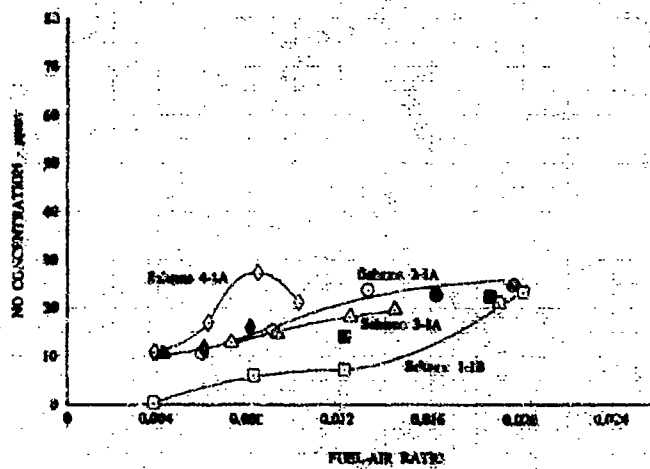


Figure 78. Comparison of Variations in NO Concentration with Fuel-Air Ratio for Tests Conducted with Combustor Schemes 1-1B, 2-1A, 3-1A, and 4-1A

DF 96057

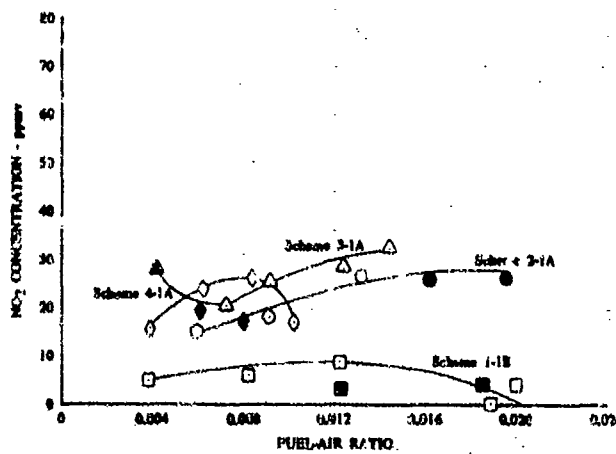


Figure 79. Comparison of Variations in NO₂ Concentration with Fuel-Air Ratio for Tests Conducted with Combustor Schemes 1-1B, 2-1A, 3-1A, and 4-1A

DF 96058

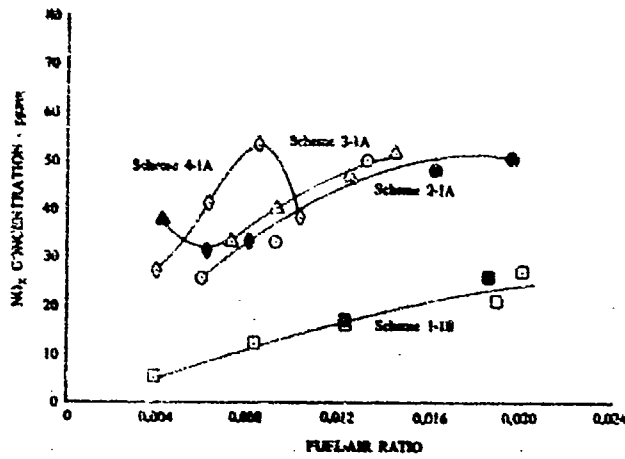


Figure 80. Comparison of Variations in NO_x Concentration with Fuel-Air Ratio for Tests Conducted with Combustor Schemes 1-1B, 2-1A, 3-1A, and 4-1A

DF 96059

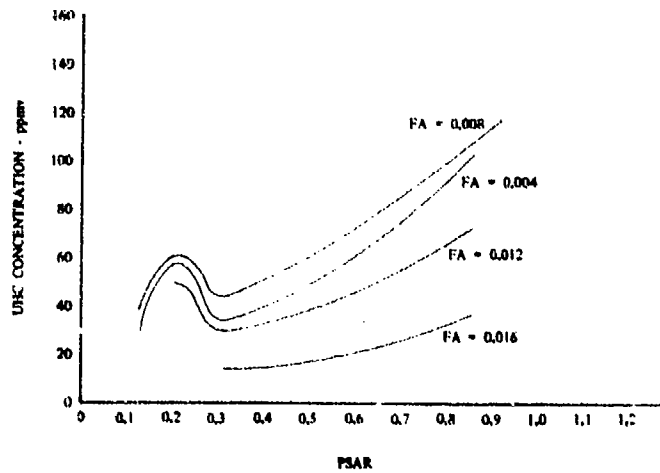


Figure 81. Variation in UHC Concentration with PSAR and FA for Tests with Combustor Schemes 1-1B, 2-1A, 3-1A, and 4-1A

DF 96060

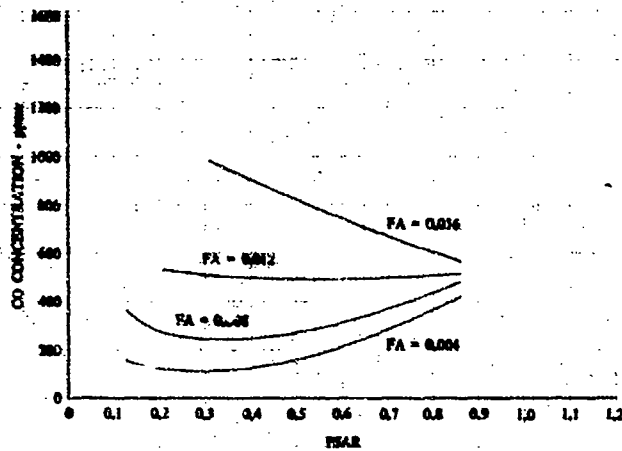


Figure 82. Variation in CO Concentration with PSAR and FA for Tests with Combustor Schemes 1-1B, 2-1A, 3-1A, and 4-1A

DF 96061

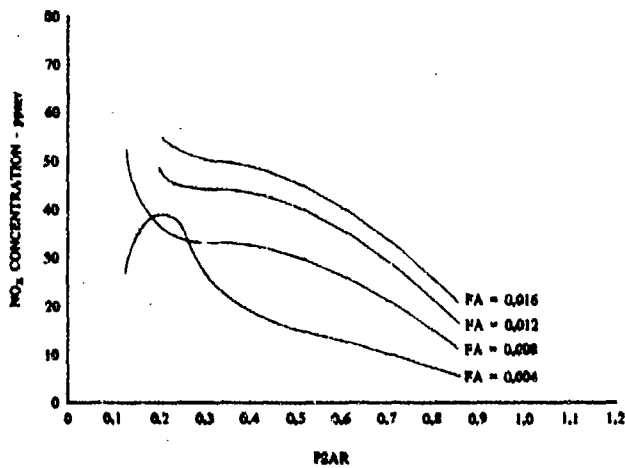


Figure 83. Variation in NO_x Concentration with PSAR and FA for Tests with Combustor Schemes 1-1B, 2-1A, 3-1A, and 4-1A

DF 96062

The variation in NO_x concentration with PSAR is shown in figure 83. Except for the hump in the curve at an FA of 0.004 for a PSAR of 0.21, a reasonably consistent family of curves was obtained. Figure 83 shows clearly that NO_x concentration increases both with decreasing PSAR and increasing FA; the direction of both trends leads to increases in reaction temperature.

d. Evaluation of Axial Fuel Staging

The concept of axial fuel staging has been generally described in preceding paragraphs. In brief, with axial fuel staging, both primary and secondary fuel injection zones are used. The primary fuel injection zone, located in the forward part of the combustor served to provide a flowrate of fuel into the combustor commensurate with low-power engine operation. PHIP was maintained at a limiting value for idle-operation by incorporating a fixed, low-power, combustor airflow distribution schedule and limiting the primary injection zone fuel flowrate. The secondary fuel injection zone, located further downstream near the axial midpoint of the burner, was used to provide flowrates of fuel into the combustor to achieve values of FA greater than those corresponding to idle conditions. Fuel from the secondary zone was used to augment that from the primary zone to achieve values of FA up to those corresponding to full-power operation. The experimental hardware used in the evaluation tests has been described earlier. (See paragraph B.3, Experimental Combustors.) Specifically, however, the hardware was arranged to accommodate two different fixed airflow distributions and two types of secondary fuel nozzles.

The two airflow distributions represented values of PSAR of 0.15 and 0.31, corresponding to Combustor Schemes 4-1A and 2-1A, respectively. (These schemes were described earlier.)

The two types of fuel nozzles used in the secondary injection zone were air-blast and pressure-atomizing. Air-blast fuel nozzles were used initially because of their demonstrated capability in previous experimental programs to provide extremely good fuel atomization at low flowrates. Unfortunately, it was not discovered until later in this test program that these air-blast fuel injectors provided very poor atomization under the conditions of fuel flow and burner pressure drop at which they were being operated. Atomization characteristics for the air-blast nozzles are shown in figure 84. The good physical characteristics that had been observed with these nozzles in previous programs were largely caused by the available air pressure being much higher than it was in the fuel-staging test series. This information was not obtained, however, until after the series had been completed. Accordingly, then, an additional test series was conducted using pressure-atomizing fuel nozzles in the secondary injection zone. These pressure atomizing nozzles were the same as those used in the 1-1A test series, viz., those having design-point flowrates of 2 gph JP-5 at a differential pressure of 125 psi; their flow characteristics were shown earlier in figure 65.

The potential for the axial fuel-staging concept to serve as hypothesized with the specific combustor configurations was somewhat questionable from the onset of the experimental program. Analytical predictions made using the preliminary combustor model, indicated that secondary-zone performance would be poor; concentrations of UHC and CO in the combustor exhaust gas would be high. This conclusion was predicated on the fuel and air arrangement in the vicinity of the secondary injection zone. Physical limitations of the research combustor

configuration were such that only a very short mixing and burning length, approximately 2 in., was available from the axial location at which secondary fuel entered the burner to the location at which air entered through dilution jets. Despite the anticipated poor performance predicted by the preliminary analytical model, the axial fuel-staging tests were conducted as planned not only to evaluate axial fuel-staging as a design concept, but also to provide experimental data to verify or negate the model predictions. The use of data from closely controlled experiments is invaluable in guiding, qualifying, and refining analytical prediction methods. In the case of the fuel-staging concept, analytical predictions were verified by experiments.

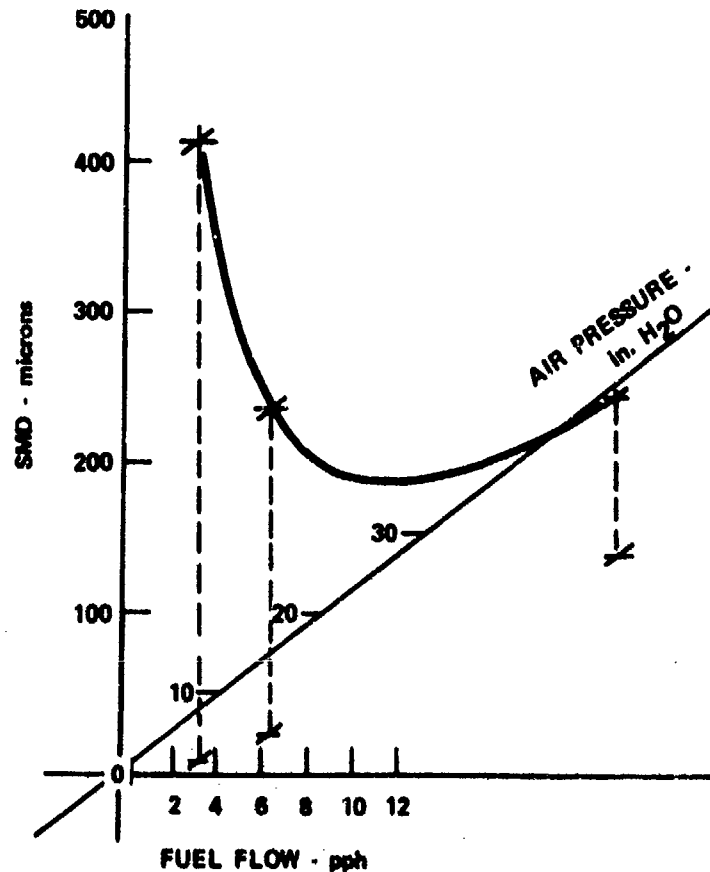


Figure 84. Variation in Sauter Mean Diameter with Air Differential Pressure and Fuel Flow FD 72103

The variation in UHC concentration with FA and PHIP, for the initial series of fuel-staging tests is shown in figure 85. Additional curves, superimposed on this figure for comparison include the variation in UHC concentration with FA from tests of Combustor Scheme 4-1A without secondary fuel injection, and from tests of baseline Scheme 1-1B. The UHC concentration levels obtained using secondary fuel injection were two orders of magnitude higher than those obtained using the baseline 1-1B configuration or the 4-1A nonstaged arrangement. UHC concentration increased with increasing values of FA and with decreasing values of PHIP. (For a given value of FA, PHIP was decreased by transferring fuel

from the primary zone to the secondary zone fuel injectors.) The general conclusion from these tests regarding UHC emission levels obtained during fuel-staging tests is that very high concentrations of UHC were observed whenever fuel was supplied through the secondary injectors, and that the concentrations increased in proportion to the amount of secondary fuel added.

Figure 86 shows the variation in CO concentration with FA and PHIP for the initial series of fuel-staging tests. Superimposed on this figure are results from baseline test series 1-1B and from tests of Combustor Scheme 4-1A without secondary fuel injection. As in the case of UHC emissions, CO concentration levels increased only one order of magnitude. It would appear that UHC was being quenched at a more rapid rate than the rate at which fuel was being converted to CO.

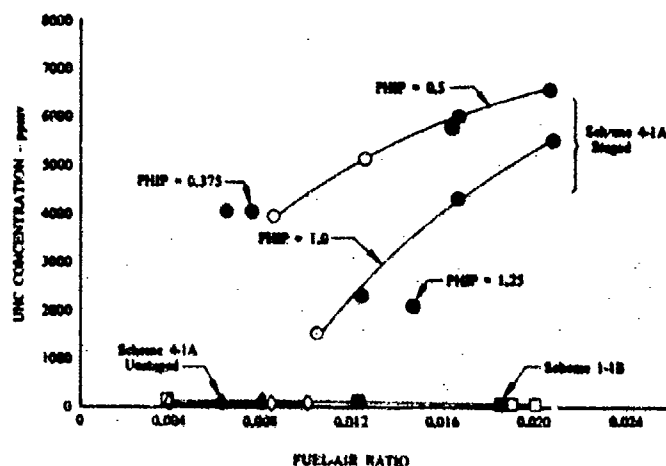


Figure 85. Comparison of Variations in UHC Concentration with FA and PHIP for Tests Conducted with Combustor Schemes 4-1A and 1-1B

DF 96063

The variation in NO_x concentration with FA and PHIP is shown in figure 87, with reference curves for data obtained from tests of Schemes 1-1B and 4-1A (without secondary fuel injection). The NO_x concentration levels observed when secondary fuel injection was incorporated were higher than those obtained from either the baseline tests or tests of Scheme 4-1A without secondary fuel injection. NO_x concentration levels generally increased with both FA and PHIP. At values of FA less than 0.0166, NO_x concentrations increased directly with increasing values of PHIP; however, at values of FA greater than 0.0166, NO_x concentration levels increased more rapidly with decreasing values of PHIP. It is suspected that at an FA near 0.0166, a transition occurs in the mechanism(s) responsible for the formation of nitrogen oxides. For values of PHIP in the range from 0.5 to 1.25 up to an FA of 0.0166, NO_x was most likely formed primarily by

a thermally induced mechanism, i.e., as FA was increased, the reaction temperature was also increased, the rate of reaction for NO_x formation was greater, and more NO_x was formed. However, at values of FA greater than 0.0166 for a PHIP of 0.5, the thermal mechanism appears to be supplanted or hyperactivated by another mechanism and NO_x concentration levels increased significantly. With due reservation, because of a lack of detailed substantiation, it is conjectured that the other mechanism responsible for increasing NO_x concentrations is catalytic in nature. When high NO_x concentrations have been observed in this experimental program, primarily in the fuel-staging and atomization evaluation tests, high concentrations of UHC have also been observed. It is not inconceivable that homogeneous catalytic reactions involving partially oxygenated hydrocarbon species could be responsible for the high NO_x levels. Additional work should be undertaken in this area to better understand mechanisms contributing to the formation of oxides of nitrogen in gas turbine engine combustion chambers.

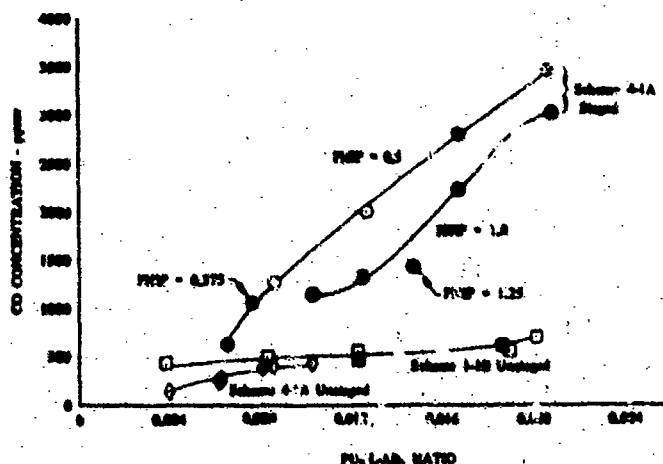


Figure 86. Comparison of Variations in CO Concentration with FA and PHIP for Tests Conducted with Combustor Schemes 4-1A and 1-1B

DF 98064

The variation in combustion efficiency, both EFFMB and EFFGA, with FA is shown in figure 28. Inasmuch as only two full-traverse tests were conducted, only two data points are shown for EFFMB. Full temperature traverses were necessary to calculate meaningful values of EFFMB. The decision to eliminate most of the full-traverse tests that had been originally planned for evaluating axial fuel-staging, in deference to partial traverse tests, was predicated on the high levels of objectionable emissions observed while testing. Values of EFFGA shown in figure 88 were calculated from partial-traverse concentration data. Concentration-based values of combustion efficiency calculated from small population samples have inherently greater accuracy than thermocouple-based calculations. Consequently, values of EFFGA for both full and partial-traverse tests are presented in figure 88.

In general, it can be seen that efficiency increases with FA despite the fact that both UHC and CO concentrations also increase. This behavior indicates that even though the absolute concentrations of UHC and CO increased with FA, the fuel-flow normalized concentrations, i. e., emission indexes, decreased. As shown in equation 28, combustion efficiency increases as UHC and CO emission indexes decrease.

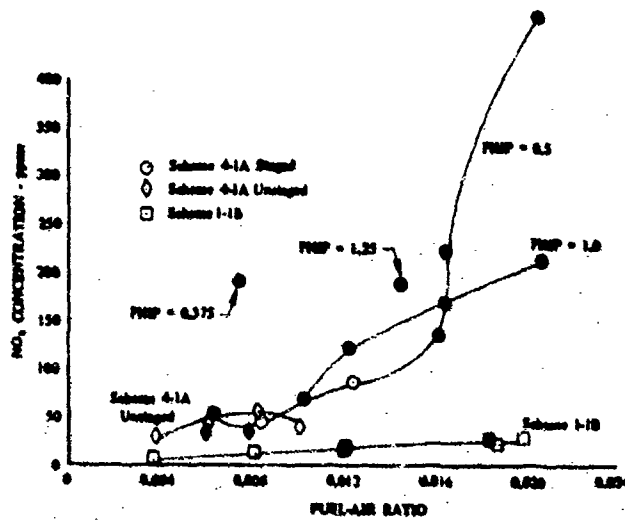


Figure 87. Comparison of Variations in NO_x Concentration with FA and PHIP for Tests Conducted with Combustor Schemes 4-1A and 1-1B

DF 96065

The reason for the discrepancy between EFFMB and EFFGA is believed to be due to catalytic reactions of combustor exhaust products such as UHC and air on the platinum/platinum-10% rhodium thermocouples and thermocouple sheaths in the exit traverse probe. If this does, in fact, occur in the immediate vicinity of thermocouples, erroneously high exit traverse temperatures would be recorded, resulting in higher values of combustion efficiency than those calculated from exhaust emission concentrations.

A second series of axial fuel staging tests was conducted to ascertain whether the poor results obtained with the axial fuel-staging concept were due to the air distribution scheme (4-1A) and secondary fuel nozzles (air-blast) used or to the concept itself. A leaner front end air-distribution scheme was selected to decrease the quantity of quenching air aft. The fuel nozzles selected for use in the secondary injection zone were the 2-gph pressure-atomizing type that had performed so well in the 1-1A baseline test series. This nozzle-combustor configuration was referred to as Scheme 2-1B.

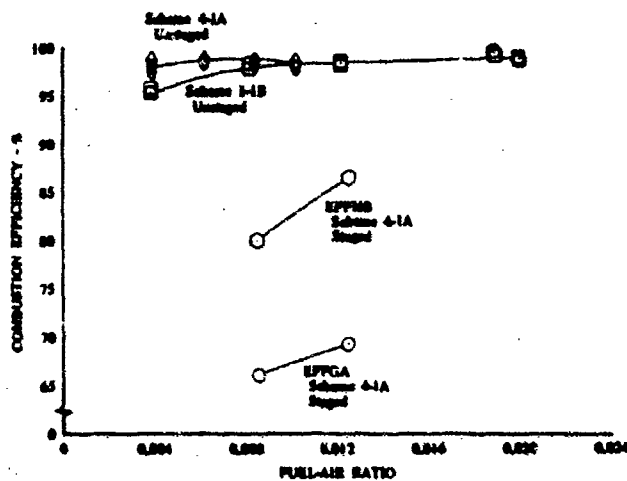


Figure 88. Comparison of Variations in Combustion Efficiency with FA and PHIP for Tests Conducted with Combustor Schemes 4-1A and 1-1B DF 96066

Experimental evaluation of Scheme 2-1B demonstrated that the trends in UHC and CO concentrations with FA and PHIP were similar to those observed in the first series; the concentration levels, however, were somewhat less in the second series. These results are shown in figures 89, and 90 for UHC and CO, respectively, with results obtained from the Scheme 4-1A series shown superimposed for reference. The slightly lower UHC and CO concentration levels are attributed to both the air distribution and fuel injection modifications incorporated in Scheme 2-1B.

Strangely enough, as shown in figure 91, significantly lower concentrations of NO_x were obtained in the tests of Scheme 2-1B than were obtained in the first axial fuel-staging series using Scheme 4-1A. The reason for this trend is still unclear. Conditions throughout the combustors in the 4-1A and 2-1B series should have been quite similar.

The variation in combustion efficiency with FA and PHIP is shown in figure 92. As with Scheme 4-1A, combustion efficiency increased as PHIP was increased; the efficiency levels for Scheme 2-1B, however, were higher than those for Scheme 4-1A. This trend follows because UHC and CO concentrations in the exhaust gas from the Scheme 2-1B combustor were less than they were from the 4-1A. The discrepancies between concentration-determined and temperature-determined combustion efficiencies were also observed in the tests of Scheme 2-1B for the same reasons described earlier.

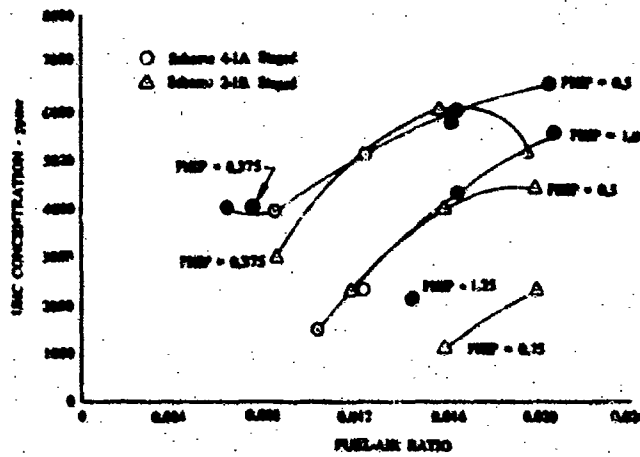


Figure 89. Comparison of Variations in UHC Concentration with FA and PHIP for Tests Conducted with Combustor Schemes 4-1A and 2-1B.

DF 96067

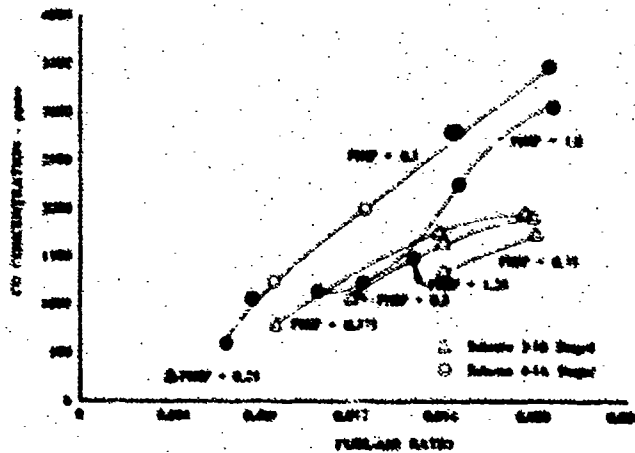


Figure 90. Comparison of Variations in CO Concentration with FA and PHIP for Tests Conducted with Combustor Schemes 4-1A and 2-1B.

DF 96068

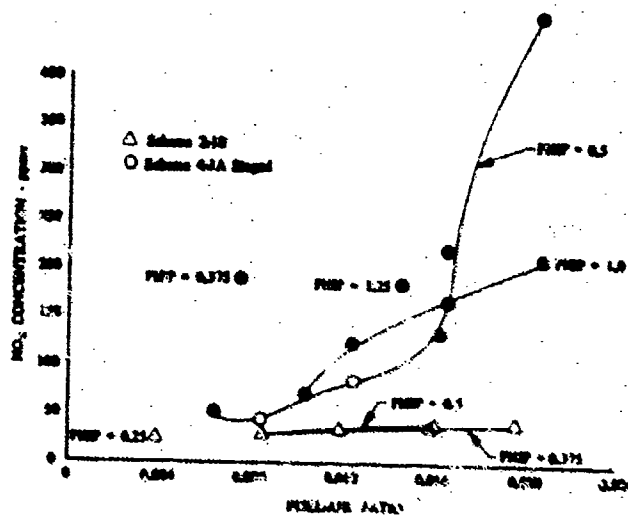


Figure 91. Comparison of Variations in NO_x Concentration with FA and PHIP for Tests Conducted with Combustor Schemes 4-1A and 2-1B

DF 96069

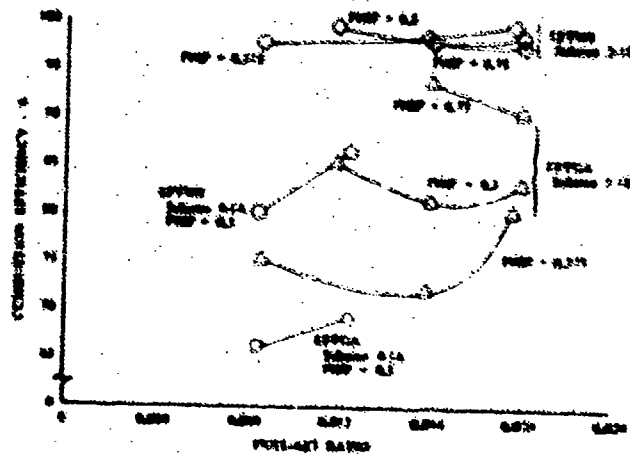


Figure 92. Comparison of Variations in Combustion Efficiency with FA and PHIP for Tests Conducted with Combustor Schemes 4-1A and 2-1B

DF 96070

In the fuel-staging tests conducted using combustor Schemes 4-1A and 2-1B, very high concentrations of objectionable emissions were produced. The emission levels were generally proportional to the amount of secondary fuel injected into the burner, at a given value of PHIP. The results described might be due simply to the method of secondary fuel injection and to the physical constraints of the research burner used. If so, the axial fuel-staging concept might not have received a completely fair appraisal. However, the extended combustion zone that results when two fuel injection zones are widely separated can promote the formation of NO_x by increasing the residence time of combustion gases at elevated temperatures. Also, the low equivalence ratios that were eliminated in the primary zone during low-power operation by providing a fixed low-power airflow distribution tend to reappear in the secondary zone, downstream, under conditions in which secondary fuel flowrates are low. This is the result of the large quantity of secondary combustion air required for operation at values of FA corresponding to full-power that, at intermediate values of FA, cause low-secondary-zone equivalence ratios and contribute to the high concentrations of UHC and CO observed.

e. Evaluation of Reference Velocity and Ancillary Effects

A limited number of full and partial traverse tests were conducted in an attempt to examine the influence of combustor reference velocity on UHC, CO, and NO_x emission levels. These tests were accomplished to support development of the streamtube combustor model. Unfortunately, with the experimental arrangement used, it was not possible to readily vary reference velocity at fixed values of FA without also varying the air and fuel flowrates. For example, to set a higher reference velocity at a fixed value of FA, it was necessary to increase both air and fuel flowrates. As a result, the liner and fuel nozzle pressure drops were increased.

The increase in fuel vaporization and reactant mixing rates within the combustor, afforded by higher fuel nozzle and liner pressure drops, respectively, appeared to be a significant factor in lowering UHC emission concentrations. This is readily apparent from the data shown in table X and figure 93. If reference velocity, which is essentially a measure of residence time, were the primary influence, then, as reference velocity was increased, the UHC concentration would also be expected to increase because of the reduced residence time for the reactants within the combustor. However, as shown in figure 93, the UHC concentration decreased instead, indicating that the effects of increased fuel atomization and reactant mixing strongly counteracted and overwhelmed the effect of reduced residence time.

On the other hand, for CO oxidation, as shown by the lower curve in figure 54, it would appear that as reference velocity was increased, the reaction front was displaced toward the aft end of the burner (combustor loading was increased) and was brought into contact with jets of primary and secondary air. These jets of 405° F air reduced local temperatures below the quenching level for CO oxidation. (See Section III.E.2, JT8D Burner Probing Studies.) With reference to figure 54, as reference velocity was increased from approximately 75 to 100 fps, the influence of 11.5% air jets on local quenching was significant. However, as the reference velocity was increased from approximately 100 to 150 fps, the reaction front was simply displaced aft without being acted upon by any intermediate zone air jets (figure 64). However, when the reference velocity was increased to approximately 170 fps, the reaction front contacted the 17.0% dilution air jets, and local quenching of the CO oxidation reaction was again observed, as shown by the measured increase in CO concentration in the exhaust gas (figure 94).

Table X. Summary of Selected Data for Tests Conducted Using Combustor Schemes 1-1A, 1-1B, and 4-1A

Test No.	Fuel-Air Ratio	Total Fuel Flow, pph	Fuel Nozzle Pressure Drop, psid	Reference Velocity, fps	Air Inlet Temperature, °F	Burner Pressure Drop, %
1-1A-10	0.0040	87.50	22	102	403	1.73
1-1A-11	0.0039	87.50	22	102	400	1.78
1-1A-12	0.0027	60.80	9	102	395	1.70
1-1A-13	0.0067	148.00	63	102	390	1.72
1-1A-14	0.0080	173.00	86	101	400	1.74
1-1A-15	0.0060	130.10	49	102	407	1.74
1-1A-16	0.0039	85.40	21	102	405	1.73
1-1A-17	0.0123	265.00	205	102	400	1.79
1-1A-18	0.0165	356.10	375	101	400	1.83
1-1A-19	0.0186	405.60	481	101	407	1.84
1-1A-20	0.0081	177.40	90	102	400	1.78
1-1B-1	0.0082	179.08	24	104	400	1.79
1-1B-2	0.0038	84.65	6	107	400	1.82
1-1B-3	0.0122	267.37	53	105	395	1.83
1-1B-4	0.0041	134.96	14	148	395	3.43
1-1B-5	0.0083	265.81	53	146	395	3.40
1-1B-6	0.0125	402.83	120	146	395	3.50
1-1B-7	0.0189	403.35	120	101	400	1.82
1-1B-8	0.0200	433.70	136	103	400	1.88
1-1B-9	0.0122	267.63	54	105	401	1.80
1-1B-10	0.0185	401.37	120	103	400	1.89
1-1B-11	0.0084	324.14	78	171	405	4.51
1-1B-12	0.0082	159.92	19	79	250	1.26
1-1B-13	0.0083	131.22	13	77	395	1.01
1-1B-14	0.0084	211.75	34	99	246	1.92
1-1B-15	0.0082	282.47	59	131	245	3.34
1-1B-16	0.0081	177.52	24	104	400	1.74
1-1B-17	0.0081	132.87	14	104	410	1.72
1-1B-18	0.0102	221.93	37	104	400	1.74
1-1B-19	0.0082	177.40	24	104	400	1.77
1-1B-20	0.0082	133.57	14	104	400	1.76
4-1A-1	0.0082	133.88	14	103	399	1.60
4-1A-2	0.0084	179.53	24	104	400	1.62
4-1A-3	0.0039	85.94	6	106	394	1.63
4-1A-4	0.0102	221.91	37	104	396	1.65
4-1A-5	0.0080	175.34	20	105	405	1.63
4-1A-6	0.0039	85.36	6	106	405	1.63
4-1A-7	0.0102	221.48	37	105	405	1.68
4-1A-8	0.0081	134.33	14	106	400	1.65

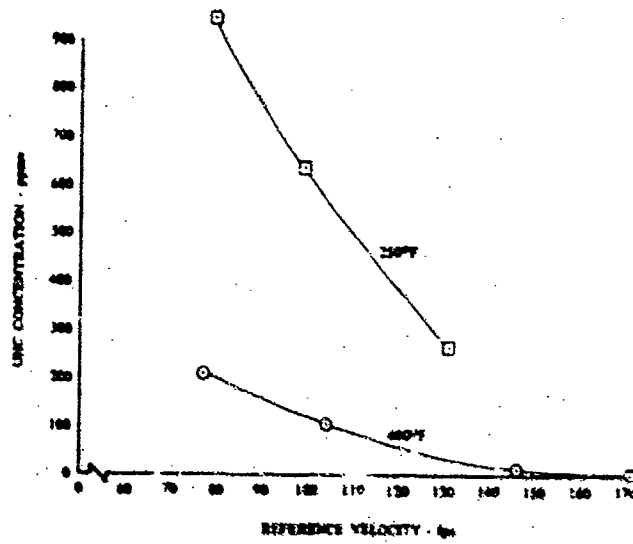


Figure 83. Variation in UHC Concentration with Reference Velocity and Inlet Temperature for Tests Conducted with Combustor Scheme 1-1B

DF 96071

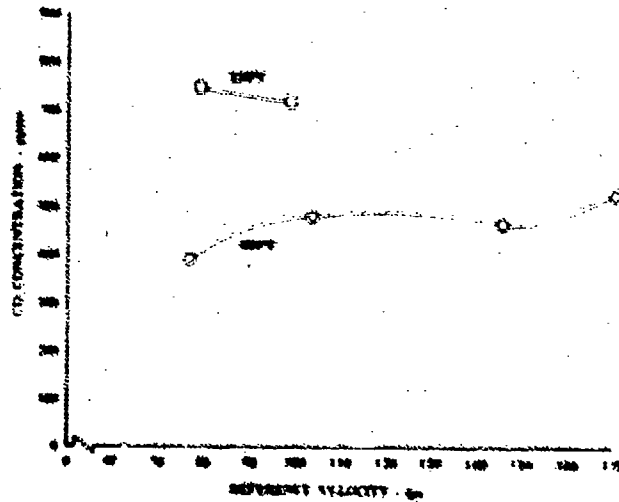


Figure 94. Variation in CO Concentration with Reference Velocity and Inlet Temperature for Tests Conducted with Combustor Scheme 1-1B

DF 96072

The variation in NO_x concentration with reference velocity and FA is shown in figure 95. It appears from this curve that residence time had a significant influence on the NO_x concentration levels observed. As reference velocity was increased (residence time was decreased), the NO_x levels decreased. This is understandable inasmuch as NO_x is formed by the prolonged residence of reactants at elevated temperatures.

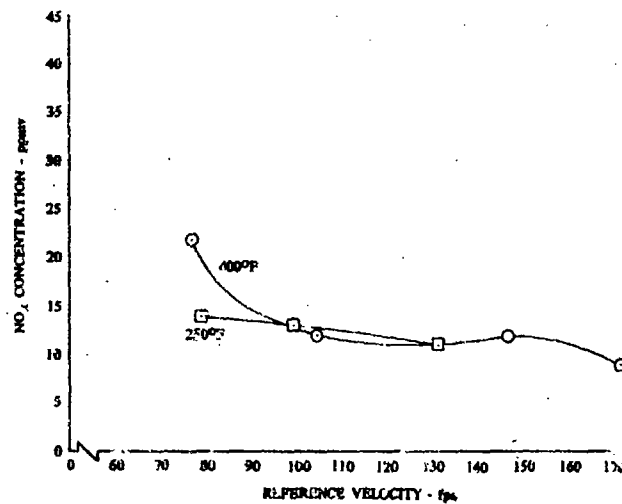


Figure 95. Variation in NO_x Concentration with Reference Velocity and Inlet Temperature for Tests Conducted with Combustor Scheme 1-1B DF 96073

f. Evaluation of Inlet Air Temperature Effects

A limited number of full- and partial-traverse tests were conducted to examine the influence of inlet air temperature on UHC, CO, and NO_x emission levels.

Figure 93 and table X show the variation in UHC concentration with reference velocity and fuel nozzle pressure drop at an FA of 0.008 and inlet air temperatures of 250 and 400°F for the 1-1B combustor. Reference velocity was used as the principal independent variable because the majority of tests involved were conducted at a fixed value of FA and only inlet air temperature and those quantities affecting reference velocity were varied.

As discussed in paragraph B.9.e, combustor pressure drop and fuel nozzle pressure drop appear to be much more influential in reducing UHC emission levels than reference velocity. However, it is readily apparent that regardless of whether reference velocity, burner pressure drop, or fuel nozzle pressure drop is used as the independent variable, the influence of inlet air temperature is significant. For example, at a reference velocity of 100 fps, the UHC concentration was increased by a factor in excess of 6 when the inlet air temperature was reduced from 400°F to 250°F; at a reference velocity of 75 fps, the factor was approximately 5; and at a reference velocity of 130 fps, the factor was approximately 7.

These increases are the direct result of decreasing the inlet air temperature and are not the result of burner pressure drop or fuel nozzle pressure drop variations. In fact, in the tests conducted at 250°F, both of these variables were larger than their 400°F counterparts at comparable values of reference velocity.

The effect of inlet air temperature on CO concentration is shown in figure 94. Although only two data points were obtained at 250°F, these are adequate to establish that CO levels were significantly higher at reduced inlet temperatures. This trend is attributed to more effective quenching of the CO to CO₂ reaction caused by colder penetration air.

The effect of inlet air temperature on NO_x concentration is shown in figure 95. Concentration levels at 250° and 400° F were nearly the same at reference velocities greater than 100 fps. However, at lower reference velocities the NO_x concentration levels varied inversely with temperature. At given values of reference velocity and FA, the NO_x levels observed at an inlet temperature of 400° F were higher than they were at 250° F. This reflects the general temperature trend observed in other tests that NO_x formation is enhanced as reaction temperature is increased.

g. Evaluation of Air-Blast Fuel Nozzle Effects

A single series of tests was conducted in which the air-blast fuel nozzles that had been used in the secondary injection zone of Combustor Scheme 4-1A during the first series of fuel-staging tests were used in the primary zone of one of the research burner configurations. The objective of the series was to determine if the poor emission levels obtained during the fuel-staging tests were largely the result of the air-blast fuel nozzles that had been used.

To accomplish these tests, Combustor Scheme 2-3A was used. This combustor had the same general features as Scheme 2-1A; i. e., a primary-zone equivalence ratio of 1.0 at an FA of 0.016, resulting from a PSAR of 0.31. However, for Scheme 2-3A the OD liner, which had been modified to accommodate staged fuel injectors, was returned to its former, nonstaged condition. Directly opposed, intermediate-zone air penetration holes were added to both the OD and ID liners, replacing the OD-only penetration holes that had been used in Scheme 2-1A in conjunction with secondary fuel injectors. The total hole area and distribution were kept the same as they had been in the basic 2-1A arrangement to maintain the same liner total pressure loss.

The variation in UHC concentration with FA is shown in figure 96. Included in this figure, for reference, are data obtained from tests of baseline Combustor Scheme 2-1A in which 4-gph, pressure-atomizing fuel nozzles were used. UHC concentration levels obtained using air-blast fuel nozzles were two orders of magnitude greater than those obtained using the pressure-atomizing fuel nozzles. In addition, UHC concentrations for Combustor Scheme 2-3A increased with increasing values of FA, instead of decreasing as observed for Scheme 2-1A. These results indicate that the air-blast fuel nozzles were directly responsible for the trends shown and that their spray quality rapidly deteriorated as fuel flow was increased. These results were verified when the air-blast fuel nozzle characteristics, shown in figure 84, were obtained. Under the conditions of fuel flow and air pressure drop used in the experimental program, values of fuel droplet SMD were very high. Consequently, the fuel was not being properly prepared to readily vaporize and react with air to form CO.

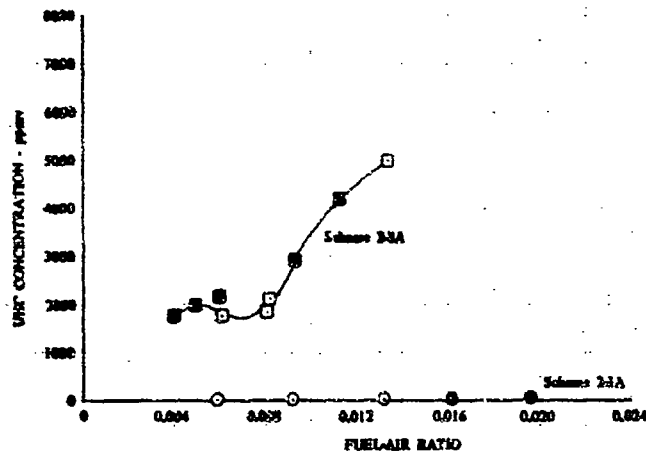


Figure 96. Comparison of Variations in UHC Concentration with Fuel-Air Ratio for Tests Conducted with Combustor Schemes 2-3A and 2-1A DF 96074

The variation in CO concentration with FA is shown in figure 97 for tests conducted using Combustor Schemes 2-3A and 2-1A, for reference. Both the shape of the curve and the CO concentration levels from the Scheme 2-3A tests were different than those obtained from the 2-1A tests. The peculiar reversal was double-checked on the test stand to be certain that an instrumentation problem had not developed. CO concentrations were measured for tests commencing at low values of FA and progressing to the higher, and for tests commencing at high values and progressing to the lower; the double reversal in CO concentration with FA was well defined. It is suggested that this trend is simply peculiar to the air-blast fuel nozzles used.

The variation in combustion efficiency with FA is presented in figure 98 for Combustor Schemes 2-3A and 2-1A. The generally low levels obtained for Scheme 2-3A are due to the high concentrations of UHC and CO that were observed in the exhaust gas. Although EFFMB and EFFGA showed the same general trends over the FA range investigated, their absolute values differed significantly. This situation is very similar to that obtained in fuel-staging tests of Combustor Scheme 4-1A. The hypothesis suggested earlier to explain the Scheme 4-1A results is also suggested to explain the Scheme 2-3A results. The platinum/platinum-10% rhodium thermocouples and sheaths served as catalytic surfaces on which UHC could react to completion; thereby causing the thermocouple to indicate a higher value of emf than it would have had no catalytic reaction been involved.

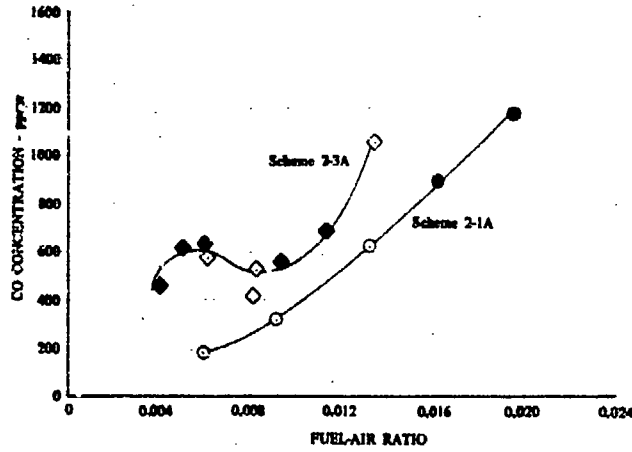


Figure 97. Comparison of Variations in CO Concentration with Fuel-Air Ratio for Tests Conducted with Combustor Schemes 2-3A and 2-1A

DF 96075

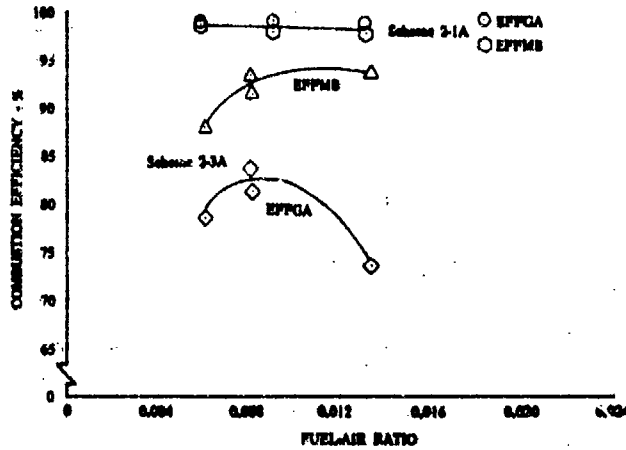


Figure 98. Comparison of Variations in Combustion Efficiency with Fuel-Air Ratio for Tests Conducted with Combustor Schemes 2-3A and 2-1A

DF 96076

The variation in NO_x concentration with FA is shown in figure 99 for Combustor Schemes 2-3A and 2-1A. Below an FA of 0.0087, the NO_x concentration levels for the pressure-atomizing fuel nozzles were higher than those obtained with the air-blast. This trend reflects the fact that higher mean reaction temperatures were achieved in tests of the pressure-atomizing fuel nozzles (higher values of combustion efficiency) than in those of the air-blast. At values of FA above 0.0087, NO_x concentrations obtained with the air-blast nozzles were higher. A possible explanation for observations of this type was suggested earlier in paragraph 7.e.

h. Evaluation of Circumferential Fuel Staging Effects

Circumferential fuel staging offers another means for controlling PHIP. It requires no change in conventional combustor hardware other than providing a vehicle for shutting off the flow to some of the primary-zone fuel nozzles during low-power operating conditions.

Two types of circumferential fuel staging arrangements were investigated. The first was alternate fuel nozzle staging in which fuel was supplied to seven of 14 fuel nozzles in an alternate "on-off" pattern in the baseline 1-1B combustor configuration. The second was sequential fuel nozzle staging in which fuel was supplied to seven fuel nozzles in sequence, and the burner was operated with the remaining seven fuel nozzles "off" in a half-lit condition. The latter arrangement was much more effective in reducing UHC and CO concentration emission levels than the alternate fuel nozzle staging arrangement. Both schemes, however, yielded high NO_x concentrations.

The exhaust gas temperature and concentration profiles from the circumferential fuel-staging tests were anticipated to be quite different from those obtained in the more conventional tests. In the case of alternate fuel nozzle staging, these profiles were expected to be cyclic because only those fuel nozzles in alternating locations were to be in operation. In the case of sequential fuel nozzle staging, these profiles were expected to be extremely warped because seven nozzles in sequence serving half of the burner were to be in operation and the other seven in sequence were not.

Consequently, if the gas sampling means used in previous tests of this program were also used in the circumferential fuel staging tests, it would not be possible to acquire a representative gas sample. As discussed earlier the sample probe was initially arranged to acquire exhaust gas samples through inlet ports in each of two arms located 180 deg apart. Gas entering the ports in each arm were then directed to a common manifold from which a consolidated sample was then transferred to the analytical instrumentation system. If such an arrangement were used to obtain exhaust gas samples from a combustor in which a cyclic concentration and temperature profile were anticipated, then one of the probe arms would be acquiring exhaust gas directly in line with operating fuel nozzles and the other arm would be acquiring exhaust gas in line with an inoperative fuel nozzle. The net result of mixing sample gases from the two probe arms then would be a gas sample providing mean emissions concentrations at each circumferential location rather than one providing the real, nonnormalized value. Therefore, to acquire real, nonnormalized exhaust gas samples at the exhaust plane of the combustor the gas path through one of the probe arms was closed. This was accomplished using a valve located at the inlet to the mixture manifold immediately aft of the probe locating ball. Traverses of 180 deg were then made using the

single sample probe arm, instead of 360 deg traverses using two arms. Employing this technique, detailed descriptions of the emissions concentration signatures resulting from circumferential fuel staging were achieved.

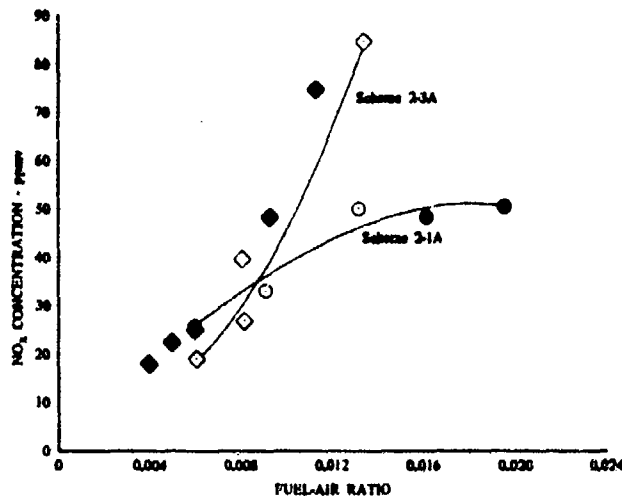


Figure 99. Comparison of Variations in NO_x Concentration with Fuel-Air Ratio for Tests Conducted with Combustor Schemes 2-3A and 2-1A DF 96077

The variation in UHC concentration with FA is shown in figure 100 for both sequential and alternate fuel staging. Included in this figure, for reference, are data from baseline Combustor Scheme 1-1B.

In the sequential tests, half of the burner was operated at an effective value of FA that was twice the overall value, and the other half was operated (or not operated) at an effective FA of zero. It might be expected, then, that the average concentration of UHC at the exhaust plane would be that corresponding to the average of zero and the value of UHC concentration in the exhaust gas corresponding to the concentration measured in the baseline tests in which the value of FA was twice the overall value of FA in the staging test. As may be seen in figure 100, this was indeed the case. At an overall value of FA of 0.008 in the sequential fuel-staging test, the measured UHC concentration was approximately 20 ppmv; this value was half that obtained at an FA of 0.016 in the baseline tests. This result implies that the two halves of the burner function essentially independently, each having its own FA and producing UHC concentration levels corresponding to those obtained at the same half-burner value of FA in the baseline tests.

In tests of the circumferential alternate fuel-staging concept, UHC concentrations were significantly higher than those obtained in the baseline tests. This result is attributed to the interaction between adjacent reacting and nonreacting regions in the primary zone. Hot gases from the reacting regions downstream of

operating fuel nozzles expand into colder nonreacting regions where a sharp decrease in temperature and equivalence ratio occurs. Consequently, local UHC concentrations increase sharply within the chamber and at the exhaust plane.

Figure 101 shows the variation in UHC concentration with circumferential location. The data shown for sequential fuel staging encompasses a 180 deg sector centered at the interface between the hot (lit) and cold (unlit) sections of the burner. Some spillage of UHC is evident from the hot sector into the cold. UHC concentration levels in the hot region are on the order of 40 ppmv, whereas those in the cold region approach zero, for an overall average UHC concentration of approximately 20 ppmv. The data for alternate fuel nozzle staging show that peaks of UHC concentration occur downstream of the nonoperating fuel nozzles. This reflects the low reaction temperatures and low equivalence ratios at these locations.

The variation in CO concentration with FA is shown in figure 102. Levels for both the sequential and alternate staging concepts were higher than those obtained in the baseline Scheme 1-1B (unstaged) tests. As in the case of UHC concentrations, these results are believed to reflect the interaction of hot reacting gases with the cold air in the nonoperating sections of the combustor. Below approximately 2200°F, the conversion of CO to CO₂ is terminated with high concentrations of CO observed in the exhaust gas. In the alternate staging tests, the reaction zones downstream of each operating fuel nozzle were surrounded by cold air from swirlers around nonoperating fuel nozzles. This promoted cooling of the reactants and produced very high exit concentrations of CO. In the sequential staging tests, contact between the hot reacting gases and cold air was limited to the interface between the operating and nonoperating halves of the burner. While this arrangement was less effective in cooling the combustion reaction, the sensitivity of the CO to CO₂ reaction, plus the tendency of the hot gases to diffuse into the cold half of the burner, resulted in a net increase in CO concentration in the exhaust gas relative to levels obtained in the baseline (unstaged) tests.

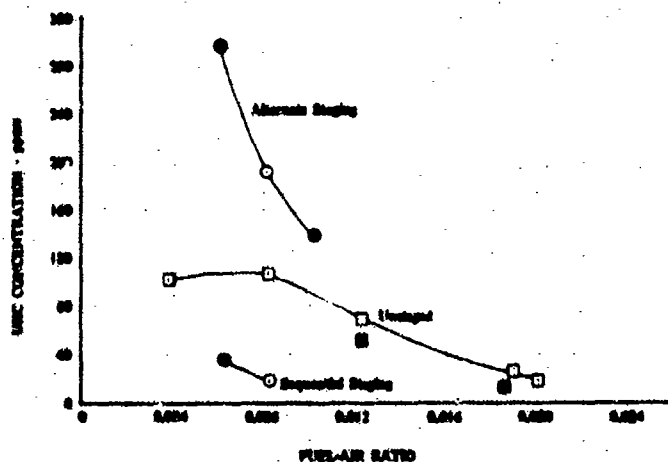


Figure 100. Variation in UHC Concentration with Fuel-Air Ratio for the Circumferential Fuel-Staging Tests Conducted with Combustor Scheme 1-1B

DF 96078

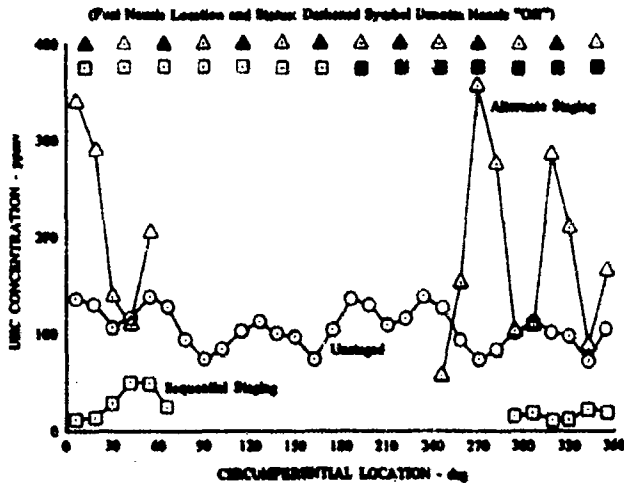


Figure 101. Variation in UHC Concentration with Circumferential Location for the Circumferential Fuel-Staging Tests Conducted with Combustor Scheme 1-1B at a Nominal Fuel-Air Ratio of 0.008 (Fuel Nozzle Status and Location Shown) DF 96079

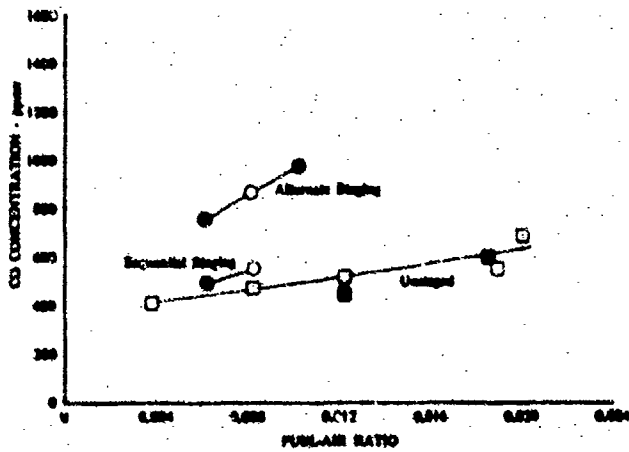


Figure 102. Variation in CO Concentration with Fuel Air Ratio for the Circumferential Fuel-Staging Tests Conducted with Combustor Scheme 1-1B DF 96080

In figure 103, the variation in CO concentration with circumferential location is presented. The curve for sequential staging exhibits considerable spillage of CO from the hot sector into the cold sector, with levels of 100 ppmv measured in the middle of the nonoperating half of the combustor (i. e., the data point at 257 deg). The curve for alternate staging exhibits the same periodic variation as that found with UHC in figure 101. Although the CO levels are considerably higher than the UHC levels, the periodic variation is less pronounced. This is believed to reflect the greater sensitivity of CO to cold air temperatures and the ability of CO to diffuse into the surrounding regions of the combustor.

The variation in NO_x concentration with FA is shown in figure 104. In both the sequential and alternate staging tests, higher levels of NO_x were obtained than in the baseline Scheme 1-1B (unstaged) tests. This can be partially explained by the fact that higher peak reaction temperatures (caused by higher local equivalence ratios) were produced by using only seven of the 14 primary fuel nozzles. However, the levels obtained are higher than those associated with increased equivalence ratios alone. For example, at an FA of 0.008 levels of 18 ppmv were obtained in both the sequential staging and alternate staging tests. If half the burner had been operating at an FA of 0.016 (twice the overall FA of 0.008) the baseline curve indicates that a level of about 20 ppmv would have been produced in half of the burner. In the remaining half, however, a level of zero ppmv would have been obtained (corresponding to an FA of zero), with a resulting overall average of 10 ppmv. This hypothetical case represents the maximum reaction temperatures and therefore the highest NO_x concentrations attainable at an overall FA of 0.008. The 18 ppmv level actually obtained was nearly twice as high. In other tests, a correlation has been noted between high NO_x concentrations and high concentrations of UHC. While this might account for the unusually high NO_x concentrations in the case of alternate staging at very low values of FA (where UHC levels as high as 295 ppmv were measured), it does not account for the fact that high NO_x levels were measured in the sequential staging tests where relatively low UHC concentrations (less than 40 ppmv) were observed. Thus, no apparent satisfactory explanation is available currently for the high NO_x levels obtained.

The data obtained in these tests, with the hardware described, indicate that simply staging the fuel flow to the primary zone nozzles in a conventional annular combustor does not significantly reduce both UHC and CO at low power conditions. Alternate staging was observed to be severely limited by interactions between adjacent regions of reacting and nonreacting flow. Sequential staging was observed to produce a reduction in UHC concentrations at low power, but cause a slight increase in CO and NO_x concentrations because of the aforementioned interactions. Unless both air and fuel are staged in the primary zone, eliminating the presence of cold, nonreacting flow, these approaches appear to offer little promise.

1. Evaluation of Primary-Zone Film-Cooling Effects

Film-cooling air on the walls of a combustor contributes to a more heterogeneous combustion process. In particular, the layer of relatively cold air along the flameside boundary of the primary zone is exposed to burning fuel droplets that penetrate into the cooling film where they are totally or partially extinguished by a sudden drop in temperature. In this way, high concentrations of partially reacted species can be formed in layers along the walls. Unless these species are subsequently entrained into the main flow stream and are reacted to completion, they contribute to the overall levels of UHC and CO concentrations measured at the exit of the combustor.

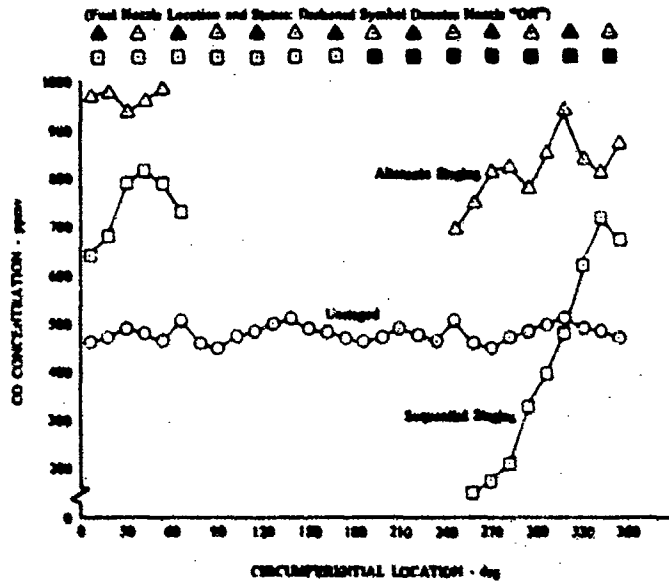


Figure 103. Variation in CO Concentration with Circumferential Location for the Circumferential Fuel-Staging Tests Conducted with Combustor Scheme 1-1B at a Nominal Fuel-Air Ratio of 0.008 (Fuel Nozzle Status and Location Shown)

DF 96081

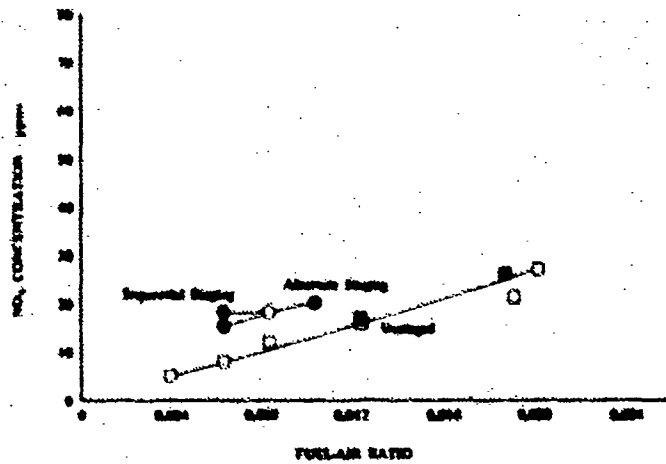


Figure 104. Variation in NO_x Concentration with Fuel Air Ratio for the Circumferential Fuel-Staging Tests Conducted with Combustor Scheme 1-1B

DF 96082

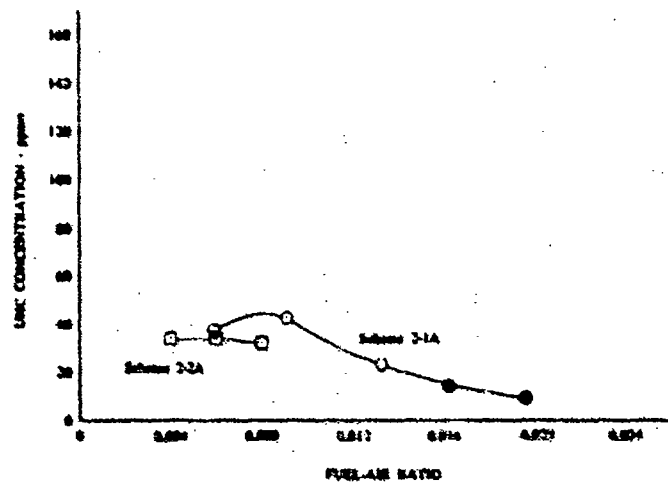
A limited series of tests was conducted to determine the portion of the exit-plane emissions that were derived from the quenching of reactants in the film-cooling layer of the primary zone. Combustor Scheme 2-1A (PSAR of 0.31) was chosen for these tests as that arrangement having the best airflow distribution for low-power operation (based on the air-staging test results). Film-cooling air was prevented from entering the primary zone by means of temporary sheet metal patches. To maintain constant combustor total pressure drop, the reduction in total open hole area resulting from closing the primary cooling holes was compensated for by an equal increase in the area of the primary penetration holes. The combustor was then operated at values of FA in the low-power range. Comparison of test results from this series with those obtained using Combustor Scheme 2-1A in the air-staging tests (with the full complement of cooling) made it possible to determine the influence of primary zone film cooling on emissions levels.

In the tests with no primary-zone film cooling, a slight decrease in the concentrations of UHC and NO_x , and a slight increase in the concentration of CO were observed. The variations in UHC, CO, and NO_x concentrations with FA are shown in figures 105 through 107 respectively. For reference, data are included in these figures for the tests conducted previously with the full complement of cooling. The data obtained for Combustor Scheme 2-1A without film cooling is confined to values of FA below 0.008 because of the desire to avoid excessive metal temperatures in the uncooled sections of the combustor.

As may be seen in figure 105, the elimination of primary-zone cooling caused a slight downward shift in UHC concentrations but did not change the general trend of its variation with FA. This result is consistent with the hypothesis that UHC is formed in part by the extinguishing of burning fuel in the film cooling layer of the primary zone. When this layer was eliminated in these tests, a slight decline in UHC concentrations resulted.

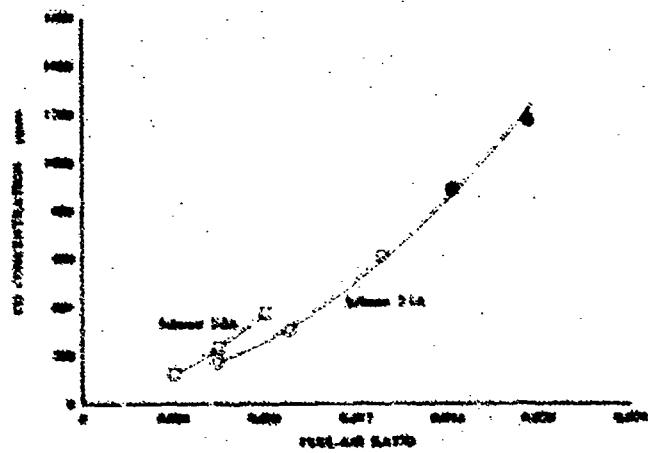
In figure 106, it may be seen that an opposite shift occurred in CO concentrations when film-cooling air was removed. This result is not unexpected because of the manner in which CO is produced. CO is an intermediate combustion product formed when an otherwise efficient reaction is cooled too rapidly. This process occurs more in the free-stream regions of the combustor, where relatively cold penetration air mixes with the products of combustion, than along the flameside boundaries where only limited surface contact occurs between hot combustion gases and the layer of cold film-cooling air. Thus, the elimination of the film-cooling layer would not be expected to reduce CO concentrations significantly. In fact, if the air that has been used for film cooling is added to the free stream, as was done in this case, it might be expected that CO concentrations would increase, as they did in these results.

The variation in NO_x concentration with FA is shown in figure 107. Lower concentration levels were obtained in the tests with no primary film cooling. Results of this type ordinarily indicate either that peak reaction temperatures have been lowered or that the residence time of reactants at elevated temperatures has been diminished. Because nothing was done to affect residence times, the former change must have occurred. This would be the case if the hypothesis set forth in the discussion of CO concentrations is true. The primary zone film-cooling air, when readmitted as penetration air would have lowered the effective equivalence ratio, thereby reducing peak reaction temperatures and causing a decline in NO_x concentrations. Thus, the results obtained for oxides of nitrogen also tend to support the hypothesis for the increase in CO levels.



DF 96083

Figure 105. Comparison of Variations in UHC Concentration with Fuel-Air Ratio for Tests Conducted with Combustor Schemes 2-2A and 2-1A



DF 96084

Figure 106. Comparison of Variations in CO Concentration with Fuel-Air Ratio for Tests Conducted with Combustor Schemes 2-2A and 2-1A

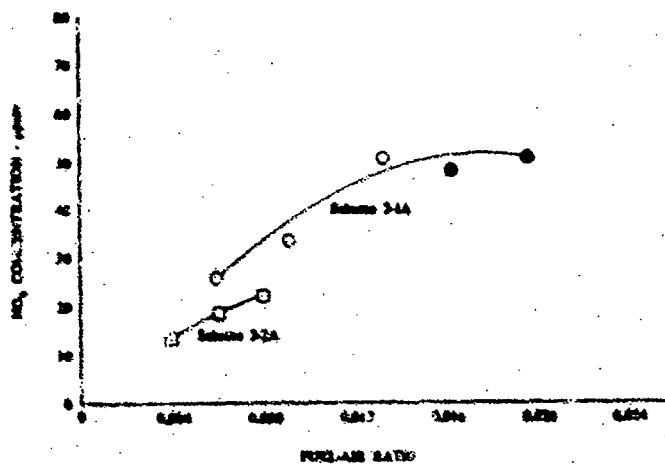


Figure 107. Comparison of Variations in NO_x Concentration with Fuel-Air Ratio for Tests Conducted with Combustor Schemes 2-2A and 2-1A

DF 96085

The variation in combustion efficiency with FA is presented in figure 108. Elimination of primary-zone film cooling produced only a slight change in EFFGA. However, a decline of about 3.5% was registered in EFFMB. One hypothesis that accounts for this result is that significantly more heat was transferred from the dome and upstream liners of the combustor in the tests without primary film cooling because of increased radiation from the generally hotter metal surfaces to the rig case. This heat loss was reflected in generally lower exit traverse temperatures and resulted in erroneously low thermocouple efficiency readings. Values of EFFGA are accepted as correct.

The results obtained in these tests indicate that slight reductions in NO_x and UHC concentrations can be achieved by the elimination of primary-zone film cooling. In the combustor configuration tested, these reductions were made at the expense of a slight increase in CO concentrations. Several implications of these results merit additional comment. The relatively small effect of primary-zone film cooling on emissions may not apply in other cases. Different front-end configurations and different amounts of cooling may affect the interaction between the cooling film and the reacting mixture. In combustors with very high concentration levels of UHC and CO at low-power operation, the influence of film cooling may be relatively more important. The slight reduction in NO_x obtained in these tests may have been due to increased radiation cooling of the reaction in the primary zone. If this is the case then the various schemes which might be implemented to remove the cooling film from the metal surface of the primary zone (such as convective cooling of the outside surface) could eliminate this radiative cooling and restore NO_x concentrations to their original levels.

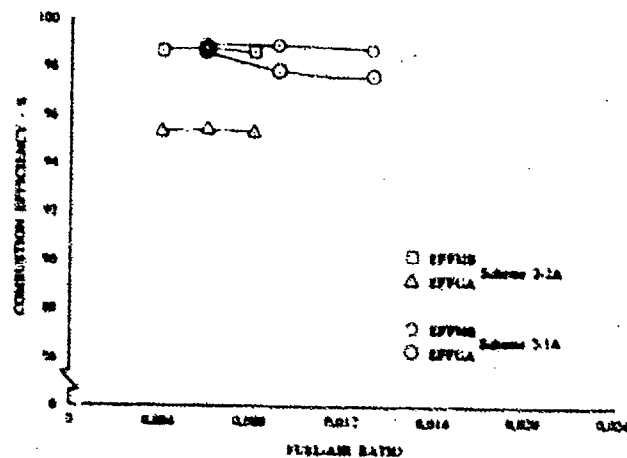


Figure 108. Comparison of Variations in Combustion Efficiency with Fuel-Air Ratio for Tests Conducted with Combustor Schemes 2-2A and 2-1A DF 96086

10. Combustor B Test Program

a. General

Combustor B was used to investigate another means for controlling P. IP, and thereby regulating the formation and concentration of objectionable exhaust emissions during low-power operating conditions. In this concept, fuel and air in controlled proportions were mixed prior to their being injected into the primary zone of the combustion chamber.

The primary motive for the design, fabrication, and testing of a second combustor, combustor B, was to evaluate pertinent areas not covered by combustor A testing. The design of combustor B was to be based principally on the results from the analytical model of Phase I, the results from combustor A testing, and an evaluation of material obtained from research literature and in-house studies.

Combustor B embodied features resulting from consideration of the aforementioned criteria to achieve reduced emissions at low power. These features included means for providing good fuel and air management with resulting controlled burning within desired fuel-air ratio limits over the range of combustor operation.

Throughout the course of the program, as the results of Phase I and Phase II testing and the Phase I modeling effort have become known, a concept of what was required to achieve emission-free operation in a gas turbine combustor was evolved. The main points of this concept may be summarized as follows; fuel must be mixed with air and prepared for burning before injection into the combustor; and combustion must take place within a narrow range of primary zone equivalence ratios. These two points were chosen as the foundation for the design for combustor B.

Good fuel preparation was accomplished by mixing fuel and air in premixing or carburetion tubes, which replaced the conventional fuel injectors used in combustor A. Control of primary-zone FA was provided by two methods, fuel and air staging. These drew upon the experience already gained with combustor A.

Except for those features related to premixing and the staging of fuel or air, combustor B was identical to combustor A. This close similarity in design made it possible to relate the results obtained with combustor B to those already obtained with combustor A. Table XI shows a summary of the design features of combustor B. Details of the designs of the carburetion tube fuel injectors, were presented in an earlier section.

The design of combustor B was based on good fuel preparation and closely controlled burning at desired values of FA. Good fuel preparation involves presenting fuel and air to the combustion zone in as homogeneous a condition as possible. Ideally, fuel preparation occurs before the onset of combustion; if it does not, the final stages of fuel dispersion, atomization, and vaporization, and the mixing of fuel with air occur simultaneously in the midst of the combustion process. Burning then occurs at a variety of different local equivalence ratios as fuel, in various stages of preparation, ignites. Only when proper preparation of all of the fuel precedes ignition can it be ensured that combustion will occur at a known or predictable value of equivalence ratio. Combustor B incorporated fuel preparation means that provided a near-homogeneous mixture of fuel and air to the combustor over a range of design-point equivalence ratios to establish the most desirable value for reducing harmful exhaust emissions.

Conventional fuel injectors generally fall short of ideal fuel preparation in several respects. First, liquid fuel is dispersed in the air as a spray of fine droplets. Vaporization occurs as the droplets move through the air. At some point, ignition of the very rich fuel-air mixture around the droplet occurs, and combustion takes place at high values of equivalence ratio. Although adequate amounts of air may be available in the primary zone at large for lower equivalence ratios, combustion occurs mainly at local equivalence ratios outside the ideal range.

Second, the mixing of burning fuel and air continues on a nonuniform basis as the reaction progresses. In some regions, excessive amounts of air may be mixed with the reacting constituents, lowering the temperature and quenching the reaction. In other regions, inadequate amounts of air may be added, resulting in oxygen-starved mixtures that cannot burn to completion before they pass out of the primary zone.

Third, the quality of fuel preparation varies with engine operating conditions. At full power, both fuel atomization and the distribution of droplets over the volume of the primary zone are excellent. The droplets burn rapidly and mix effectively with the available air. If sufficient primary-zone air has been admitted to achieve an average equivalence ratio just under stoichiometric, reaction products, including NO_x , can be low. At low power operating conditions, on the other hand, fuel injector pressure drop is reduced, resulting in relatively large droplets and poor distribution over the primary-zone volume. Even with air-assist-type fuel injectors, which utilize inlet air pressure drop for better atomization, large droplet burning can still occur at equivalence ratios outside the ideal range, resulting in incomplete combustion and large amounts of undesirable exhaust emissions.

Table XI. Combustor B Basic Design Features

Type Combustor	Annular, Static Fed, Film Cooling, Carburetion Tubes With Swirler Discharge
Length, in.	16.0
Height, in.	4.0
Outer Diameter, in.	18.0
Inner Diameter, in.	10.0
Combustor Ref Area, sq in.	176.0
Type Fuel Injectors	Carburetion Tubes
Number of Fuel Injectors	14
Combustor Material	Hastelloy X
Wall Thickness, in.	0.0625
Design Point Conditions	
Fuel-Air Ratio	0.022
Volumetric Heat Release, Btu/hr-atm-ft ³	5.2 x 10 ⁶
Based on	
Inlet Pressure, psia	330
Combustor Airflow, lb _m /sec	120
Combustor Ref Velocity, ft/sec	100
Combustor Total Pressure Drop, % (Inlet Total)	3.5

Good fuel preparation of the quality required for combustor B involves the atomization and dispersion of liquid fuel in air, subsequent evaporation of the droplets, and thorough mixing of fuel vapor and air prior to introduction into the combustor. The premixing or carburetion tubes were designed to satisfy all these requirements. Six series of tests were conducted using combustor B to evaluate and refine the selected premixing concept, and to investigate methods of combining this concept with both air and fuel staging. The initial tests were conducted over a low-power FA range, 0.004 to 0.010, to determine the effects of primary-zone airflow distribution and combustor air pressure drop on emissions reduction. In the remaining tests, methods of extending combustor operation into the intermediate and full-power ranges were investigated. These means included the use of air staging, circumferential fuel staging, and carburetion tubes in a fixed combustor geometry.

b. Evaluation of Liner Total Pressure Drop Effects

To provide fuel-air mixture velocities in the premixing tubes sufficiently high to prevent flameholding and autoignition, an increase in liner total pressure drop to 3.5%, from the 1.8% used in the combustor A tests, was required.

Therefore, to relate the results obtained using combustor B to those obtained using combustor A, the effect of increasing the liner total pressure drop for combustor A from 1.8 to 3.5% had to be determined.

Accordingly, the first series of tests conducted with combustor B was accomplished with a configuration (including the 4 gph pressure-atomizing fuel nozzles) almost identical to Scheme 4-1A. The two notable differences were the increased pressure drop feature, and a decrease in design-point PHIP from 1.0 to 0.8. This latter modification was made in order to establish some commonality with the remaining combustor B configurations that were designed with a PHIP of 0.8. The new burner configuration, designated Scheme 5-1B, was achieved by decreasing the size of all air-entry holes to effect the desired twofold increase in pressure drop. The scheme sheet for the 5-1B configuration is shown in figure 109. Test results obtained using this combustor were then compared with those previously obtained using combustor A Scheme 4-1A. Combustor Scheme 5-1B produced lower concentrations of UHC, higher concentrations of CO, and approximately the same concentrations of NO_x as those generated by Scheme 4-1A.

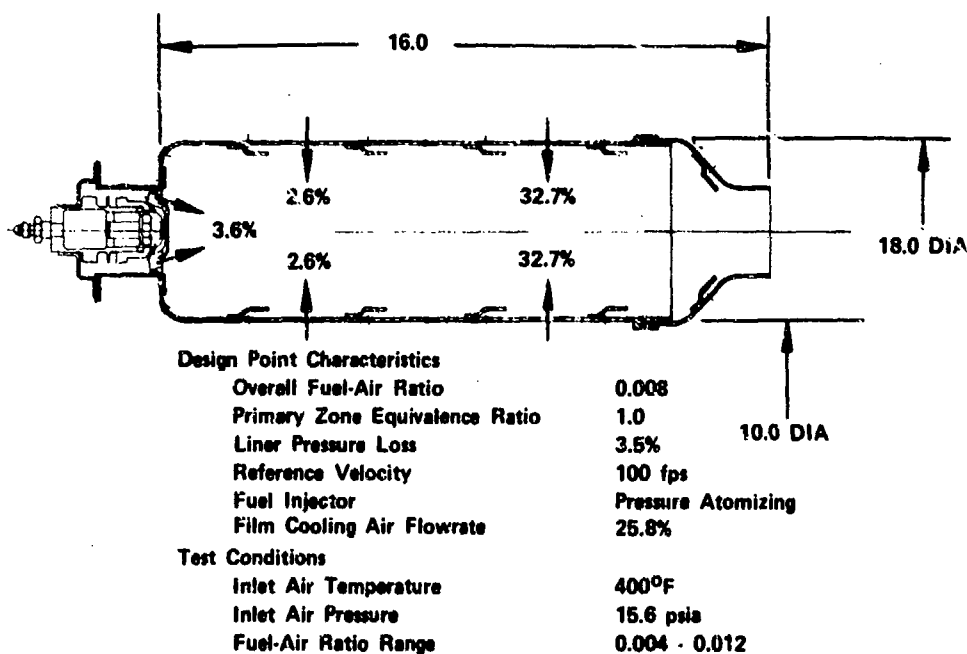


Figure 109. Summary Sheet for Combustor B Scheme 5-1B

FD 72104

The variation in UHC concentration with FA for combustor Schemes 5-1B and 4-1A (for reference) are shown in figure 110. Scheme 5-1B demonstrated significantly lower concentrations than those obtained with the 4-1A configuration. At values of FA greater than 0.005, UHC concentrations were less than 10 ppmv. This trend is attributed to an increased turbulence level in the primary zone caused by the increased liner total pressure loss.

The trends in UHC concentration with FA for Schemes 4-1A and 5-1B are quite different above an FA of 0.006. The upward trend exhibited by Scheme 4-1A, and not by 5-1B, is attributed to the 4-1A primary zone being over-rich.

Scheme 4-1A was designed to have a PHIP of 1.0; Scheme 5-1B was designed to have a PHIP of 0.8. The greater amount of air in the primary zone of the latter scheme is believed to have prevented the primary zone from becoming over-rich and contributing to high concentrations of UHC in the exhaust gas.

The variation in CO concentrations with FA for combustor Schemes 4-1A and 5-1B are shown in figure 111. Above an FA of 0.004, the rate of change of CO concentration with FA was much greater for Scheme 5-1B than for Scheme 4-1A, and at an FA of 0.010 the absolute value of CO concentration was also significantly greater. These generally higher values are believed to be the result of two events. First, the decrease in PHIP increased the amount of air in the primary zone that was available to effect a greater conversion of fuel into CO (the low UHC concentrations attest to this). Second, a higher quenching effectiveness was achieved in the secondary zone as a result of the greater liner total pressure loss.

The variation in NO_x concentration with FA is presented in figure 112 for Schemes 5-1B and 4-1A. The curves are similar in shape and magnitude, with Scheme 5-1B exhibiting higher concentration levels at values of FA of 0.008 and 0.010, and Scheme 4-1A exhibiting higher levels at 0.004 and 0.006. Both schemes produced an increase in NO_x as FA was increased (peak reaction temperatures increased) and a subsequent decrease as values of PHIP exceeded unity and reaction temperatures began to drop. The curve for Scheme 5-1B is somewhat shifted to the right (higher values of FA) with respect to the curve for Scheme 4-1A. This is believed to be a result of the increase in the quantity of air added to the primary zone of Scheme 5-1B, which caused a corresponding shift in PHIP. If both combustor schemes had been designed with the same value of PHIP, little difference in the NO_x concentrations would most likely have been observed despite the difference in liner total pressure drops.

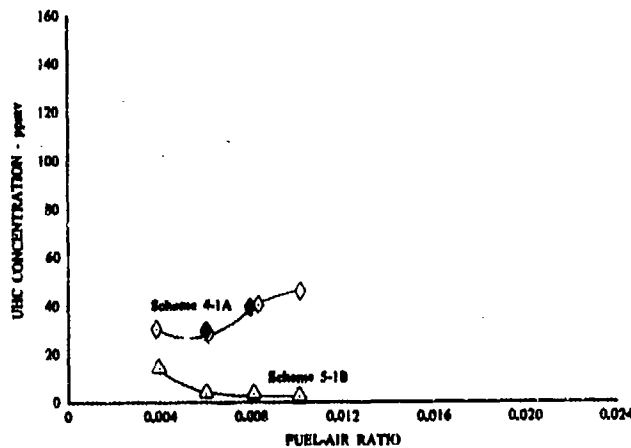


Figure 110. Comparison of Variations in UHC Concentration with Fuel-Air Ratio for Tests Conducted with Combustor Schemes 5-1B and 4-1A

DF 96087

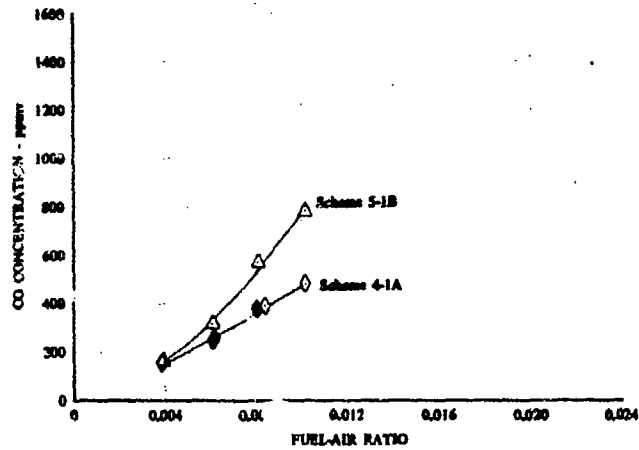


Figure 111. Comparison of Variations in CO Concentration with Fuel-Air Ratio for Tests Conducted with Combustor Schemes 5-1B and 4-1A DF 96088

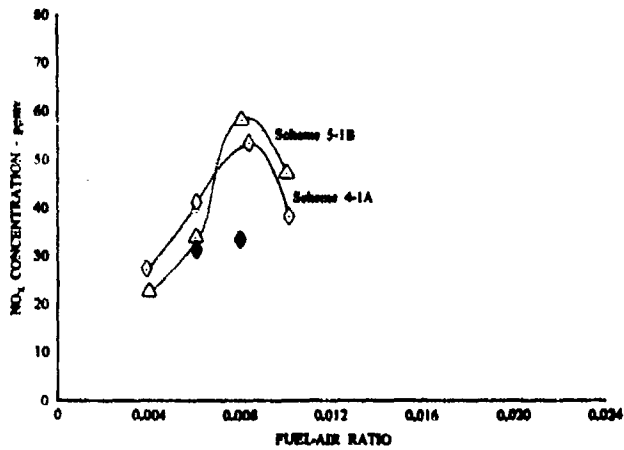


Figure 112. Comparison of Variations in NO_x Concentration with Fuel-Air Ratio for Tests Conducted with Combustor Schemes 5-1B and 4-1A DF 96089

The variation in combustion efficiency with FA is presented in figure 113 for Schemes 5-1B and 4-1A. The results obtained for the two schemes are in close agreement, reflecting the fact that differences in the combined (weighted) totals of UHC and CO concentrations were small.

Results obtained in these initial tests have established that increasing combustor liner pressure drop from 1.8% to 3.5% does not yield an across-the-board reduction in objectionable emissions concentration at low power. On the basis of these results, reductions in emission concentrations achieved in subsequent tests with carburetion tube fuel injectors can be attributed exclusively to the premixing concept rather than to increased liner pressure drop.

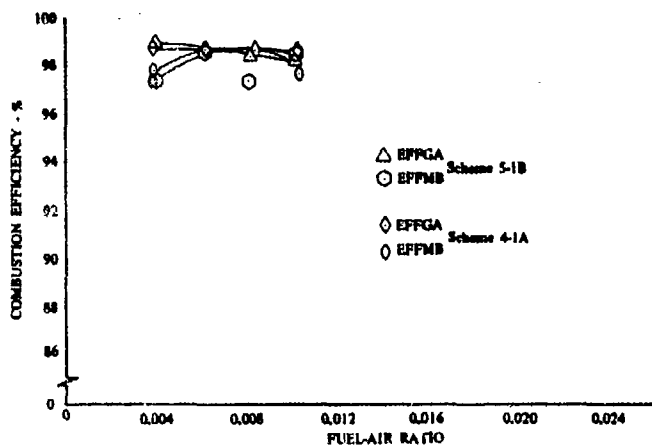


Figure 113. Comparison of Variations in Combustion Efficiency with Fuel-Air Ratio for Tests Conducted with Combustor Schemes 5-1B and 4-1A DF 96090

c. Evaluation of the Basic Premixing Combustor

The basic fuel-air premixing concept was evaluated using combustor Scheme 5-1A. A schematic diagram showing the salient features of this configuration is shown in figure 114 and a photograph of the physical hardware prior to testing is shown in figure 115. The combustor airflow distribution was arranged to provide a PSAR of 0.18, with the entire primary-zone airflow entering through the premixing tubes. The design-point PHIP with this arrangement was 1.0 at an overall FA of 0.008.

The first test series was conducted at values of FA in the low-power operating range from 0.004 to 0.012, both above and below the design-point FA of 0.008. Results obtained showed that the concentrations of CO and NO_x were significantly lower than the values obtained during tests of the 5-1B configuration; and the UHC concentrations, above the lean blowout FA limit (LBO), were as good as they were in the 5-1B series.

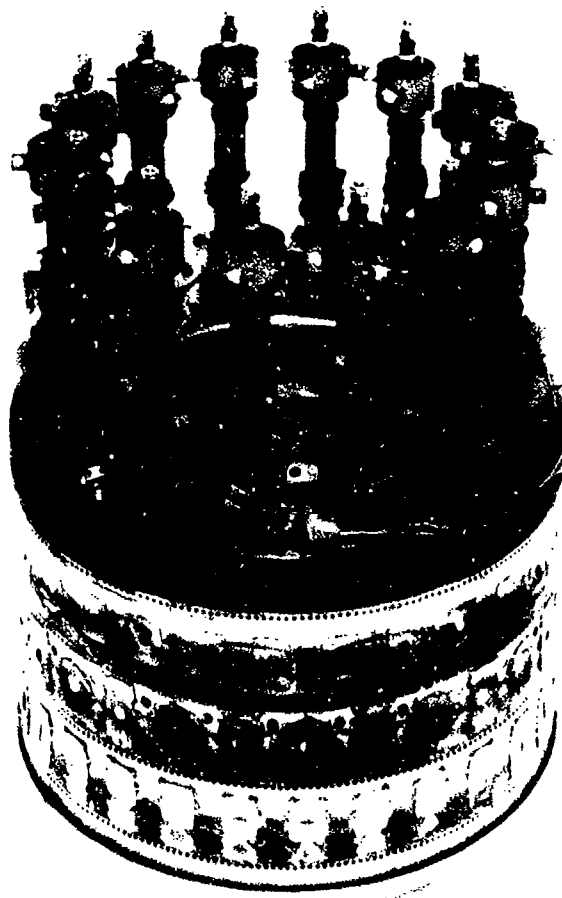


Figure 114. Combustor Scheme 5-1A

FE 125486

The improvements in low-power emissions obtained with the 5-1A arrangement were made at the expense of increasing the LBO. The LBO observed in the 5-1A series was approximately 0.0049 and in the 5-1B series it was approximately 0.002. For comparison, the LBO observed in the baseline 1-1B series was 0.0014.

After the test series had been completed, an obstruction in the inlet to the burner was discovered. A thermocouple junction box used in the flashback monitoring system for the carburetion tubes had been mounted in close proximity to the combustor, impeding the flow of air into one of the carburetion tubes. This obstruction resulted in a lower airflow rate through the tube, which yielded a locally high equivalence ratio in that section of the primary combustor zone being fed by the partially air-starved tube. Emission concentrations at the exhaust plane in line with the affected tube were noticeably different from those in line with the other carburetion tubes. Consequently, the obstruction was removed and the test series was repeated. A discussion of this first test series and the effect of combustor inlet airflow distortion on emission concentrations and distribution is presented later in this report.

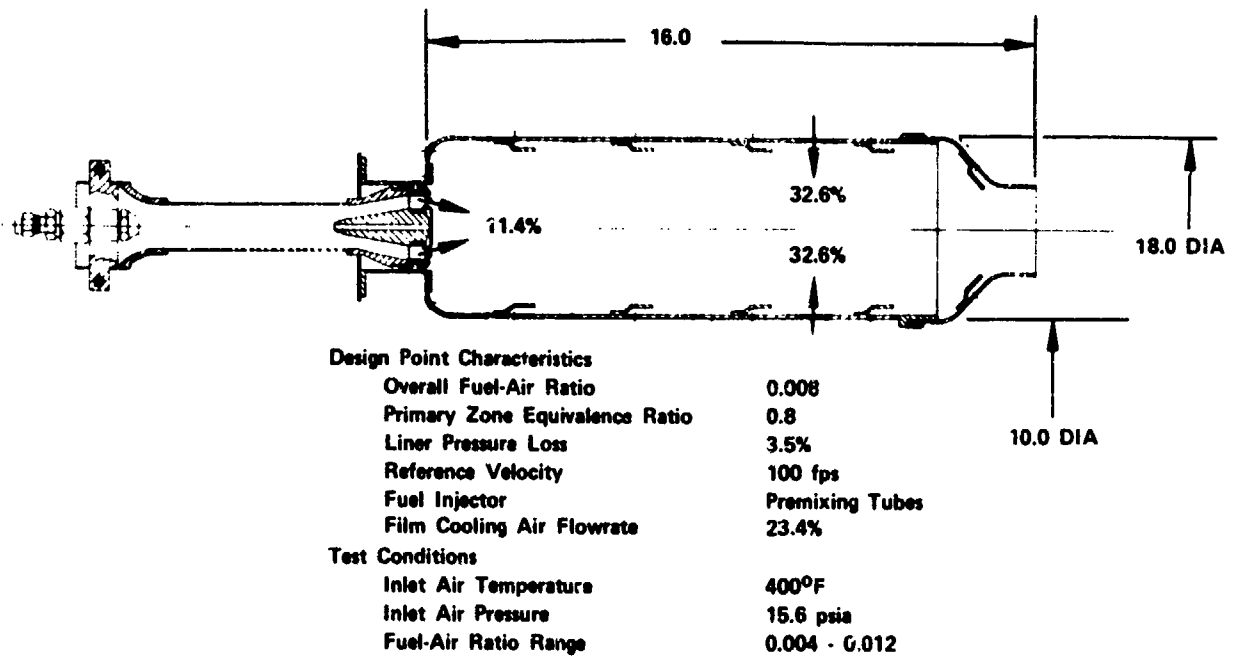


Figure 115. Summary Sheet for Combustor B
Scheme 5-1A

FD 72105

Tests accomplished with combustor Scheme 5-1A were accomplished at reference velocities of approximately 120 fps instead of at the nominal design-point value of 100 fps. This change was necessary to compensate for a problem that had been encountered when modifying the combustor hardware to the 5-1A configuration. The combustor total hole area after modification was approximately 20% greater than that needed to provide a liner pressure drop of 3.5%. To compensate for this, combustor airflow rate was increased until the desired 3.5% liner total pressure drop was achieved. The effect of the resulting increased reference velocity on emissions concentration was considered to be essentially negligible, however. In the combustor A test program, it had been found that higher values of reference velocity, as produced by increased airflow rates, generally resulted in higher concentrations of CO and lower concentrations of NO_x. Inasmuch as the tests with combustor B Scheme 5-1A produced the lowest CO levels observed in any test up to this point in the Phase II experimental program, the effect of the 20% increase in reference velocity can probably be discounted. The lower NO_x levels that were observed, however, could be due in part to the higher reference velocities. The observed effect of reference velocity on NO_x concentration was discussed earlier.

The variation in UHC concentration with FA is shown in figure 116 for Schemes 5-1A and 5-1B. Both schemes produced very low levels of UHC at low-power operating conditions; at values of FA greater than 0.008, the UHC concentrations produced by combustor Scheme 5-1A were slightly lower. The differences, however, are on the order of but 1 ppmv. At values of FA below 0.008, however, Scheme 5-1A exhibited a sharper increase in UHC concentrations as FA was decreased. This trend was a consequence of the higher LBO experienced with Scheme 5-1A. A concentration of 38 ppmv at an FA of 0.0049 marked the beginning of an exponential rise in UHC at the onset of LBO for Scheme 5-1A.

In comparison, the UHC concentration obtained with combustor Scheme 5-1B was 15 ppmv at an FA of 0.004; this value of FA, however, was well above its lean limit, and the value of UHC concentration observed was simply the result of a low value of PHIP.

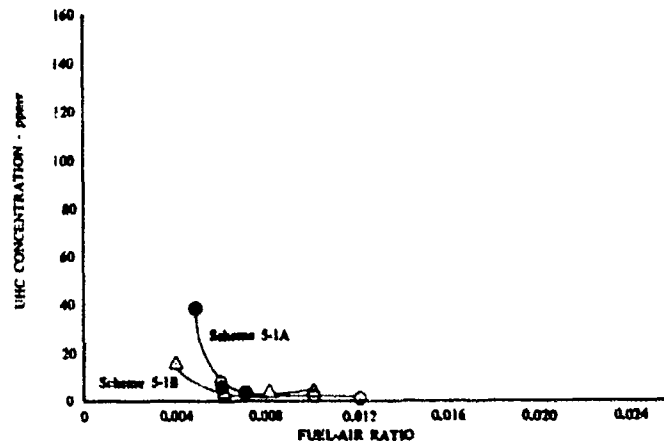


Figure 116. Comparison of Variations in UHC Concentration with Fuel-Air Ratio for Tests Conducted with Combustor Schemes 5-1A and 5-1B DF 96091

The variation in CO concentration with FA is shown in figure 117 for combustor Schemes 5-1A and 5-1B. The curve for the Scheme 5-1A data passes through a minimum value of 58 ppmv at an FA of 0.006. This concentration was the lowest obtained for CO up to this point in the experimental program. Conditions appeared to be nearly ideal in the primary zone in order for these low concentrations of CO to have been achieved. At the FA of 0.006, the fuel-air mixture discharged through the carburetion tube had an equivalence ratio of 0.8; this value was sufficiently high for efficient reaction, but lean enough to provide the necessary air for initiating the conversion of CO to CO₂. In addition, quenching air was added to the primary-zone reaction products sufficiently far downstream to preclude dilution air from terminating the CO-to-CO₂ reaction. At values of FA above 0.006 the primary zone became fuel-rich, resulting in a shortage of air for the oxidation of CO. However, the concentration levels and the rate of change of CO concentration with FA at values of FA above 0.006 are somewhat deceiving. In nearly all tests conducted in this experimental program burner inlet temperature was maintained at a value of approximately 400° F. Consequently, all emission concentrations above those corresponding to low-power, or idle, must be tempered in light of this normalization. In an actual engine situation, burner inlet temperature is not a fixed value, but increases as the power demand (increased values of FA) is increased. From both kinetic studies and direct observation, as discussed in Section III, CO concentration decreases as burner inlet temperature increases. Therefore, values of CO concentration above an FA of 0.006 would, in a real engine situation, be lower than those shown in figure 117. However, to ascertain

relative effects and trends, comparing emission concentrations for a given configuration with those of a baseline system has been shown in this program to be a good, reasonable, comparative experimental technique. Detailed evaluation of a final combustor configuration should be accomplished in an experimental arrangement that more closely simulates actual engine conditions. Now, at values of FA less than 0.006, the combustor inlet temperature used in the experimental program was approximately the same as it would have been in practice; however, the primary zone became lean, resulting in lower flame temperatures and a less efficient reaction. Higher values of CO concentrations were achieved because the rate of conversion of fuel to CO was slower at the lower equivalence ratios and the CO-to-CO₂ reaction was delayed. This delay resulted in relatively large concentrations of CO being in the reaction products entering the dilution zone from the primary. Consequently, the jets of dilution air quenched the CO before it could be oxidized. In comparison, Scheme 5-1A exhibited a relative overall decrease in CO concentrations in the low-power FA range, which was primarily due to better preparation of the reactants by the carburetion tube fuel injectors.

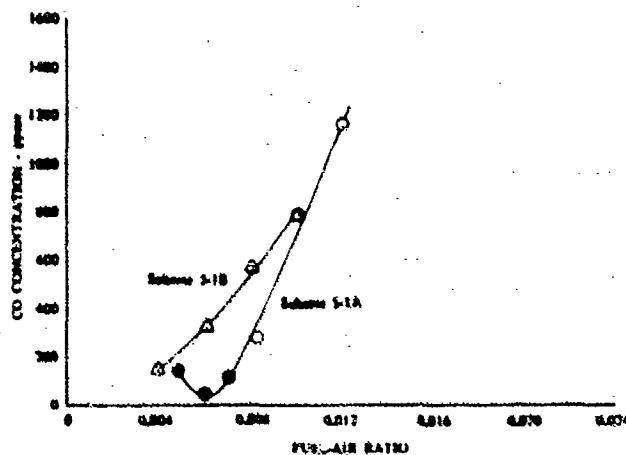


Figure 117. Comparison of Variations in CO Concentration with Fuel-Air Ratio for Tests Conducted with Combustor Schemes 5-1A and 5-1B DF 96002

The variation in NO_x concentration with FA is shown in figure 118 for combustor B, Schemes 5-1A and 5-1B. Both curves are similar; they each initially increase with FA and then decrease. In the case of Scheme 5-1B, NO_x concentration increases with FA to a value of 0.008, reflecting the increase in reaction temperature with FA; and then decreases above an FA of 0.008, reflecting the nonincrease in temperature beyond this value of FA, for the reasons presented in the preceding discussion on CO emissions. The curve for Scheme 5-1A is shifted somewhat to the right of that for 5-1B. This is attributed to PHIP being lower for the 5-1A arrangement. NO_x concentration levels observed for Scheme 5-1A were lower than for 5-1B because of the increased design-point reference velocity for Scheme 5-1A. As discussed earlier, increased reference velocity results in

a decreased residence time. The lower the residence time in the primary zone for a reacting fuel-air mixture, the lower will be the resulting NO_x concentration.

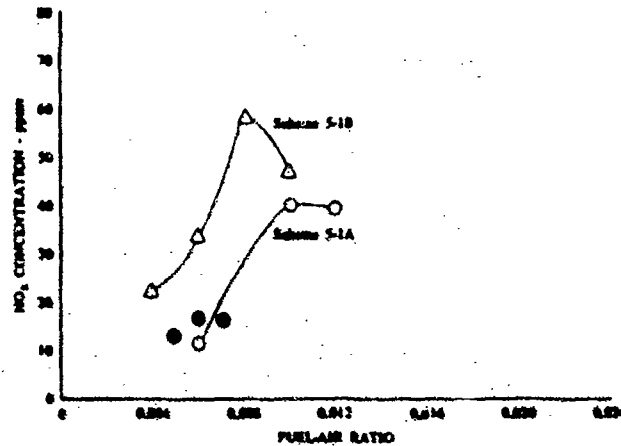


Figure 118. Comparison of Variations in NO_x Concentration with Fuel-Air Ratio for Tests Conducted with Combustor Schemes 5-1A and 5-1B DF 96093

The variation in combustion efficiency with FA for combustor Schemes 5-1A and 5-1B are shown in figure 119. Higher efficiencies were obtained with Scheme 5-1A than with 5-1B, primarily as a result of the much lower concentrations measured at the low-power condition. Over the entire FA range evaluated, EFFGA obtained for Scheme 5-1A was greater than 99%. Close agreement was also obtained between EFFGA and EFFMB in this series.

d. Evaluation of Primary Zone Airflow Distribution

Although the carburetion tubes were designed to admit all the primary-zone air required for complete combustion at an overall FA of 0.008, it was conjectured that better performance could be obtained (better flame stabilization, lower values of LBO, and lower emissions) if part of the combustion air were admitted to the combustor through primary penetration holes.

A series of tests was conducted, therefore, in which the primary zone airflow distribution (the relative proportions of carburetion tube and penetration airflow) was systematically varied. The defining parameter used in these tests was PXPAR, the premixing-to-penetration airflow rate ratio. In the basic premixing combustor arrangement (Scheme 5-1A) described in the previous section, PXPAR was infinite; all primary-zone combustion air was introduced into the burner through the carburetion tubes and the quantity of primary-zone penetration airflow supplied was zero. In the current test series, additional values of PXPAR (1.8, 1.0, 0.6) were investigated. A separate combustor configuration with appropriate penetration hole and carburetion tube deflector areas for the desired

flowsplit was used to evaluate each value of PXPARG. The three new configurations were designated Schemes 5-2A, 5-3A, and 5-4A. Their salient features are presented schematically in figures 120 through 122. Data were obtained for each scheme at several values of FA for concentrations in the low-power range. Comparisons of the emission concentrations and the combustor operating characteristics at these values of PXPARG and FA made it possible to determine, within the limitations of the hardware, the best split between carburetion tube and primary penetration airflows to achieve the greatest reduction possible.

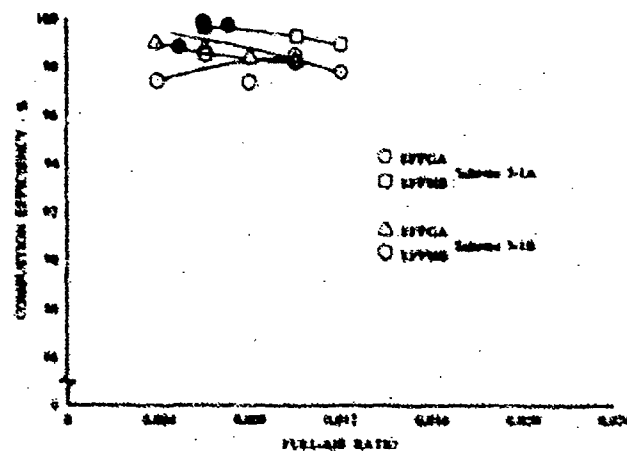


Figure 119. Comparison of Variations in Combustion Efficiency with Fuel-Air Ratio for Tests Conducted with Combustor Schemes 5-1A and 5-1B

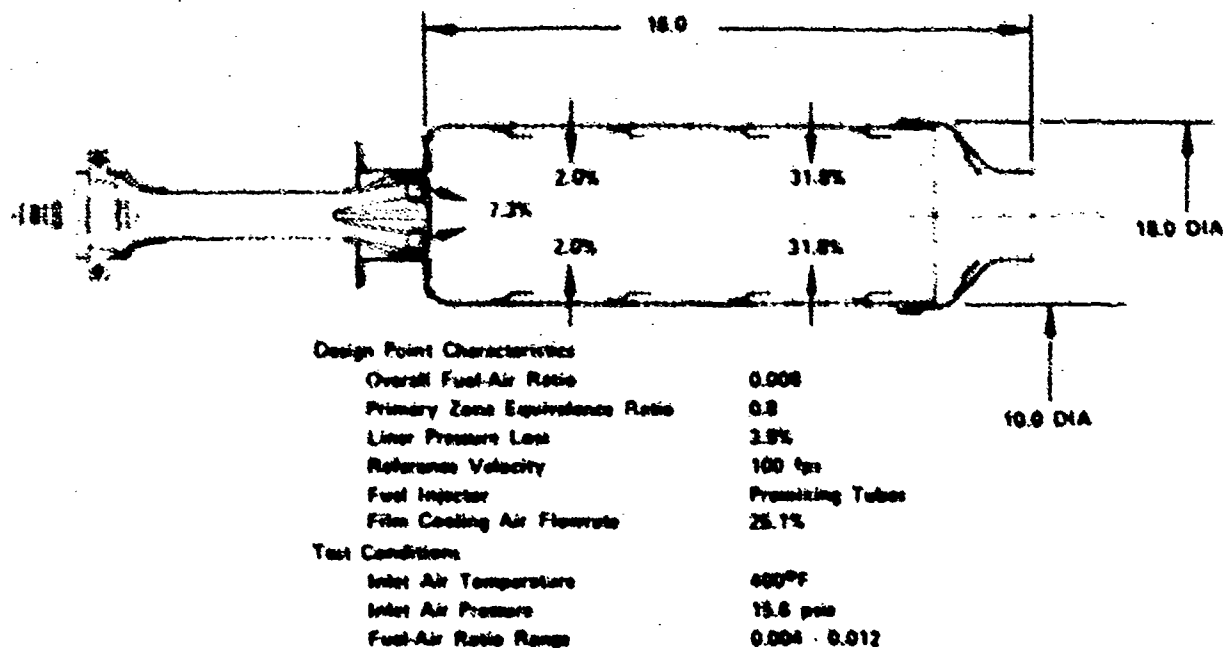
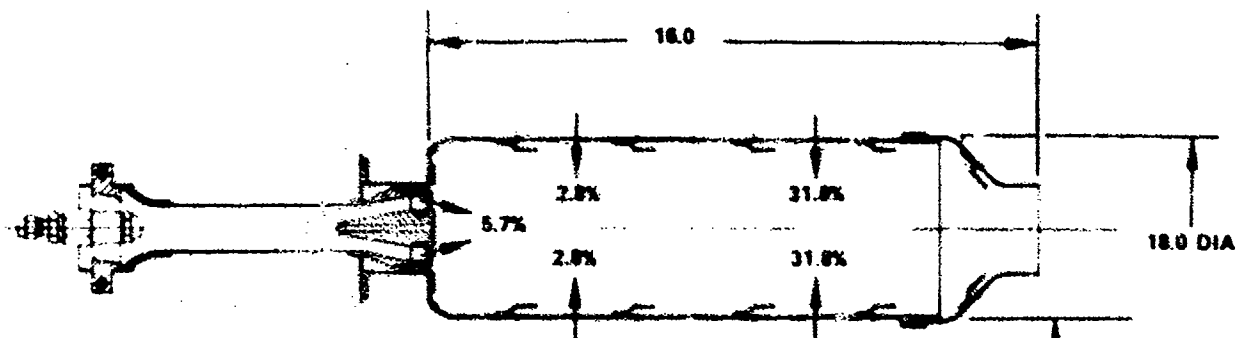


Figure 120. Summary Sheet for Combustor B Scheme 5-2A

FD 72106



Design Point Characteristics

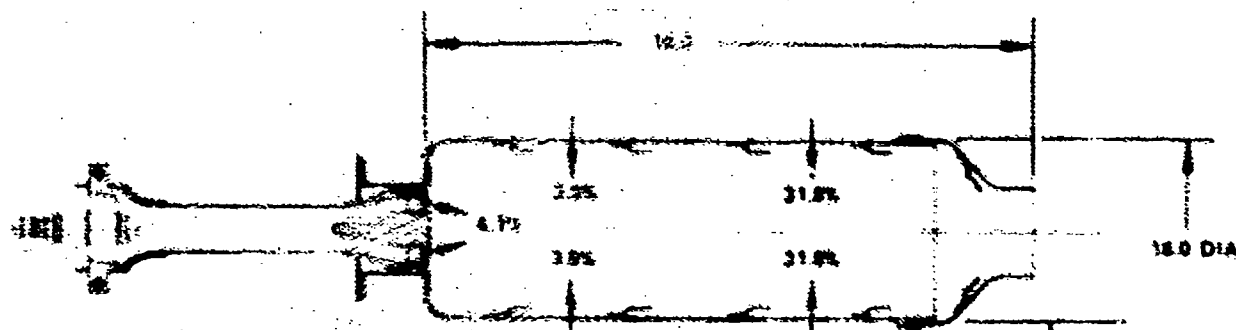
Overall Fuel-Air Ratio	0.008
Primary Zone Equivalence Ratio	0.8
Loss Pressure Loss	3.5%
Reference Velocity	100 fps
Fuel Injector	Premixing Tubing
Film Cooling Air Flowrate	25.1%

Test Conditions

Inlet Air Temperature	400°F
Inlet Air Pressure	15.6 psia
Fuel-Air Ratio Range	0.004 - 0.012

Figure 121. Summary Sheet for Combustor B
Scheme 5-3A

FD 72107



Design Point Characteristics

Overall Fuel-Air Ratio	0.008
Primary Zone Equivalence Ratio	0.8
Loss Pressure Loss	3.5%
Reference Velocity	100 fps
Fuel Injector	Premixing Tubing
Film Cooling Air Flowrate	25.2%

Test Conditions

Inlet Air Temperature	400°F
Inlet Air Pressure	15.6 psia
Fuel-Air Ratio Range	0.004 - 0.012

Figure 122. Summary Sheet for Combustor B
Scheme 5-4A

FD 76108

The test results obtained revealed that emissions concentrations, LBO, and general performance were affected by variations in PXP. In particular, adjustments in PXP brought about a reduction in CO (by a factor of 2) with respect to the very low levels obtained with the basic premixing configuration (Scheme 5-1A), discussed earlier. Generally, it was found to be more advantageous to inject some of the primary-zone airflow through penetration holes in the liner than to supply all of the air through the carburetion tubes.

The variation in UHC concentration with FA is shown in figure 123 for Schemes 5-1A, 5-2A, 5-3A, and 5-4A: these schemes represent values of PXP of ∞ , 1.8, 1.0, and 0.6, respectively. The generally low UHC concentrations observed with Scheme 5-1A were again observed with the three new schemes; UHC concentrations less than 10 ppmv were obtained with each at values of FA greater than 0.006. These levels are well below the program goal of 10 ppmw (13 ppmv). At values of FA above 0.007 there was no significant difference in concentration levels for the four schemes. This result reflected the basic importance of premixing fuel and air to promote an efficient reaction. By comparison, the influence of primary airflow distribution appeared, as far as UHC was concerned, to be of secondary importance. At values of FA less than 0.007, differences can be noted in the rates at which UHC concentration levels increased as FA was decreased and LBO was approached. These differences reflect the influence of primary airflow distribution (PXP) on LBO, which is discussed later in this section.

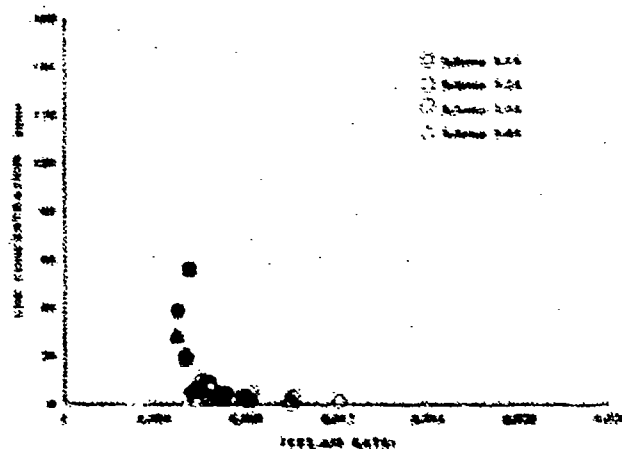


Figure 123. Comparison of Variations in UHC Concentration with Fuel-Air Ratio for Tests Conducted with Combustor Schemes 5-1A, 5-2A, 5-3A, and 5-4A. DF 96036

The variation in CO concentration with FA is shown in figure 124. All four schemes exhibited very low concentrations of CO near an FA of 0.006. The bucket-shaped concentration - FA curve obtained with Scheme 5-1A was also obtained for Schemes 5-2A, 5-3A, and 5-4A. However, the low CO concentration exhibited by Scheme 5-1A was improved upon by two of the three new combustor schemes, in inverse proportion to PXPAR. With combustor Scheme 5-1A, the value of PXPAR was ∞ and the CO concentration was 58 ppmv; with Scheme 5-2A, PXPAR was 1.8 and the concentration of CO was 32 ppmv; and with Scheme 5-3A, PXPAR was 1.0 and the CO concentration observed was 28 ppmv. With Scheme 5-4A in which the PXPAR was 0.6, however, the CO concentration increased to 51 ppmv. These results showed that PXPAR had a decidedly influential effect on CO concentration levels and that for a given general combustor configuration PXPAR could be optimized to reduce CO concentration.

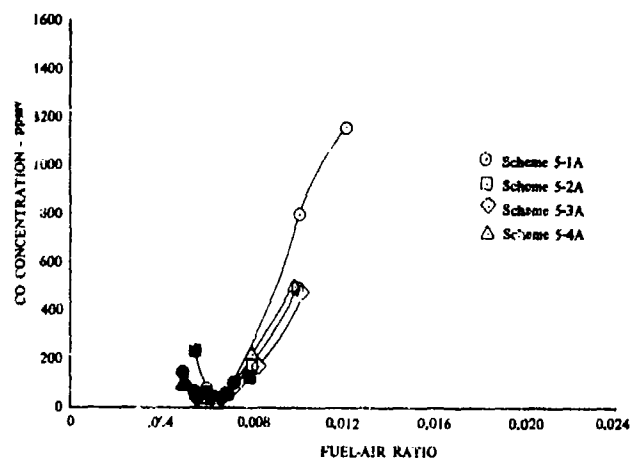


Figure 124. Comparison of Variations in CO Concentration with Fuel-Air Ratio for Tests Conducted with Combustor Schemes 5-1A, 5-2A, 5-3A, and 5-4A DF 96096

The reason suggested for the trends observed, at least in part, is that the primary penetration air in Schemes 5-2A and 5-3A promoted better mixing, and resulted in more CO being converted to CO_2 in the favorable environment in which the PHIP was 0.8. In poorer mixing environments (such as in Scheme 5-1A), more CO passed from the primary zone unreacted and was quenched by dilution air. Although the shifting of combustion air from the carburetion tubes to the primary penetration holes made less air available for premixing, any resultant deterioration in quality of fuel preparation that might have occurred was outweighed by the benefits of better primary-zone mixing: down to the PXPAR of 0.6 (Scheme 5-4A).

The variation in NO_x concentration with FA is shown in figure 125. The family of curves for the four schemes is confined to a relatively narrow band.

At values of FA greater than 0.008, nearly identical results were obtained; however, below an FA of 0.008, some variation was experienced. The trend shown simply indicates that NO_x concentration increased as peak reaction temperatures were increased by increasing FA. Above an FA of 0.010 the tendency for NO_x concentration to increase with FA for Scheme 5-1A decreases. This trend is due to an over-rich condition in the primary zone. At values of FA less than 0.008, Schemes 5-1A and 5-2A exhibited somewhat lower NO_x concentration levels than the other two schemes. This trend may be a result of more thorough premixing of fuel and air. In Scheme 5-1A, all combustion air was admitted into the primary zone through the carburetion tubes. This resulted in good premixing of fuel and air, faster reaction rates, and short residence times at elevated temperatures. As a result, this scheme produced the lowest NO_x concentration levels. In Scheme 5-2A, which utilized a modest amount of primary penetration air, the NO_x concentration levels produced were higher than those in Scheme 5-1A, but lower than those in Schemes 5-3A and 5-4A. This implies that an intermediate degree of premixing results in intermediate concentration levels of NO_x . It thus appears that NO_x levels in the low-power range are directly related to the degree of premixing. It is also evident that with the premixing concept NO_x levels were reduced below those achieved using conventional pressure-atomizing fuel injection. This may be seen by comparing the levels obtained here with those obtained for Scheme 5-1B in which 4-gph fuel nozzles were used (figure 118); NO_x concentrations observed with the pressure-atomizing system are higher by 5 to 20 ppmv.

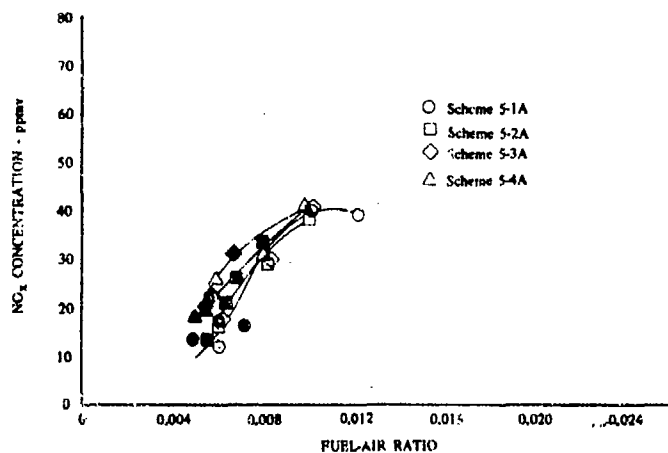


Figure 125. Comparison of Variations in NO_x Concentration with Fuel-Air Ratio for Tests Conducted with Combustor Schemes 5-1A, 5-2A, 5-3A, and 5-4A DF 93097

Combustion efficiencies obtained using Schemes 5-2A, 5-3A, and 5-4A were very close to those obtained using Scheme 5-1A. The data for these schemes have not been presented graphically because of their close similarity to the curves presented for Scheme 5-1A in figure 119. Instead, values for both EFFGA and EFFMB are presented in tabular form in Appendix VI. High efficiencies were obtained

throughout, in keeping with the low levels of UHC and CO concentrations measured. Generally close agreement between values of EFFMB and EFFGA was also obtained.

In the initial tests of the premixing concept using Scheme 5-1A, a value of LBO was measured that was considerably in excess of that obtained with the pressure-atomizing nozzles using Scheme 5-1B. With Schemes 5-2A, 5-3A, and 5-4A, high values of LBO were also measured. In the discussion of the basic premixing combustor, presented earlier, an LBO of 0.0049 was quoted for Scheme 5-1A. This value corresponded to the point at which the energy level of the exothermic process was so low that the reaction would not propagate when the fuel flow was increased. The determination of this point is difficult and subject to error. For the purpose of comparing values of LBO in this discussion, an alternative definition was chosen. LBO was defined as the point at which the concentration of UHC exceeded 10 ppmv as FA was decreased. Although this point does not truly represent blowout, it does identify the sharp increase in emissions that appears immediately before LBO occurs. With reference to figure 123, values of LBO of 0.0058, 0.0063, 0.0056, and 0.0056, according to the aforementioned definition were obtained using Schemes 5-1A, 5-2A, 5-3A, and 5-4A, respectively. These results indicate that for all but one of the schemes, as the amount of carburetion tube airflow was decreased (PXPARG decreased), LBO decreased slightly. The exception was Scheme 5-2A (PXPARG = 1.8), in which the highest value of LBO was measured. The decline in LBO with decreasing PXPARG appears to reflect the inherently narrow flammability limits of a premixed reaction. These limits occur because of the homogeneity of the mixture, which eliminates locally rich pockets of fuel and air that can sustain the combustion process at very low values of FA. The high value of LBO observed with Scheme 5-2A is not readily understood.

During accomplishment of the tests in this program, visual observations of the combustion process within the research burners were periodically made. As shown in figure 50, the rig case and traverse case were separated by a finite distance. By standing aft of the rig case at an angle approximately 30 deg to the axis of flow, it was possible to see within the burner up to the dome and injectors. Information on items such as flame structure, flame-front location, and quantity of luminous flame were obtained. In the premixing tests the quantity of luminous flame observed near the injectors was very revealing. In general, at values of FA corresponding to a low-power design point (0.006 - 0.008), a predominately blue flame was observed. At greater values of FA, as the tubes became more heavily loaded with fuel, large droplets of fuel began to be emitted in the discharge flow from the carburetion tubes. This resulted in a luminous flame indicative of droplet burning and elevated emissions levels. In tests of this series, the amount of luminous flame decreased as FA was decreased, and disappeared entirely, leaving only blue flame, prior to LBO.

PXPARG also had an influence on the quantity of luminous flame present. At an FA of 0.008, the flame within combustor Scheme 5-1A (PXPARG = ∞) was approximately 10% luminous; with Scheme 5-2A (PXPARG = 1.8), zero; with Scheme 5-3A (PXPARG = 1.0), 5%; and with Scheme 5-4A (PXPARG = 0.6), 50%. It appeared that the increased degree of mixing promoted by primary penetration air jets in Scheme 5-2A helped to further atomize and vaporize the small quantity of large droplets in the discharge flow of the carburetion tubes and, as a result, served to eliminate the luminous flame. In the other three schemes, luminous flame was encountered either because of the absence of primary penetration air (in Scheme 5-1A) or because of excessive amounts of penetration air (in Schemes 5-3A or 5-4A) that resulted in less carburetion tube air available for premixing

fuel and air. Thus, if the quantity of luminous flame is used as an indicator of premixing and mixing effectiveness, Scheme 5-2A can be cited as the best configuration, representing a well-balanced combination of carburetion tube and primary penetration hole airflows.

e. Evaluation of Fuel-Air Premixing in Combination with Air Staging

Tests conducted using combustor B up to this point in the program were accomplished at values of FA in the low-power range. These tests were designed to determine the basic operating characteristics of a premixing-type burner and to optimize PXPAP at low-power for an injector-burner combination. Improvements in low-power emission concentrations attainable with good fuel preparation, as provided by carburetion tubes, were ascertained.

Emission-free operation over the FA range from low to high power requires that the proper proportions of fuel and air be maintained in the combustion zone at all operating conditions. In the combustor A test program it was demonstrated that FA could be controlled by using the air-staging concept. The method of air distribution employed involved varying primary and secondary airflow distributions simultaneously in order to conserve the overall total effective hole area of the burner and maintain liner total pressure loss at a constant value. As the primary-air hole area was reduced at low power, for example, the secondary-air hole area was increased. Consequently, liner pressure drop was eliminated as a variable in the air-staging evaluation tests.

A major difficulty in implementing the type of air-staging described above is in devising a means for varying both primary and secondary hole areas using practical combustor hardware. The problem can be simplified, however, if only the primary-air hole area were varied, allowing liner total pressure drop to vary within allowable limits. This approach was evaluated in the test series described in the following paragraphs.

A variable airflow distribution burner was simulated using two fixed-geometry configurations of combustor B. Scheme 5-5A, described in figure 126, represented the low-power configuration; Scheme 5-7A, described in figure 127, represented the full-power configuration. The overall operation of the simulated combustor was evaluated by combining the results of the tests conducted using the two burner schemes. During high-power combustor operation, simulated by using Scheme 5-7A, the primary-air penetration holes were fully open, admitting the amount of air required to achieve complete combustion at a design-point FA of 0.022. The liner total pressure drop at this value of FA was 3.5%. Now, as FA was decreased, the primary-air penetration hole area was decreased to maintain a constant value of PHIP. Accordingly, burner pressure drop increased because the secondary-air hole area was not opened to compensate for the decrease in primary zone air hole area. At a low-power FA of 0.008, using combustor Scheme 5-7A, the primary-air penetration holes were completely closed; all of the air required for combustion was admitted into the burner through the carburetion tubes. Liner total pressure drop for Scheme 5-7A at this FA had increased to approximately 7%.

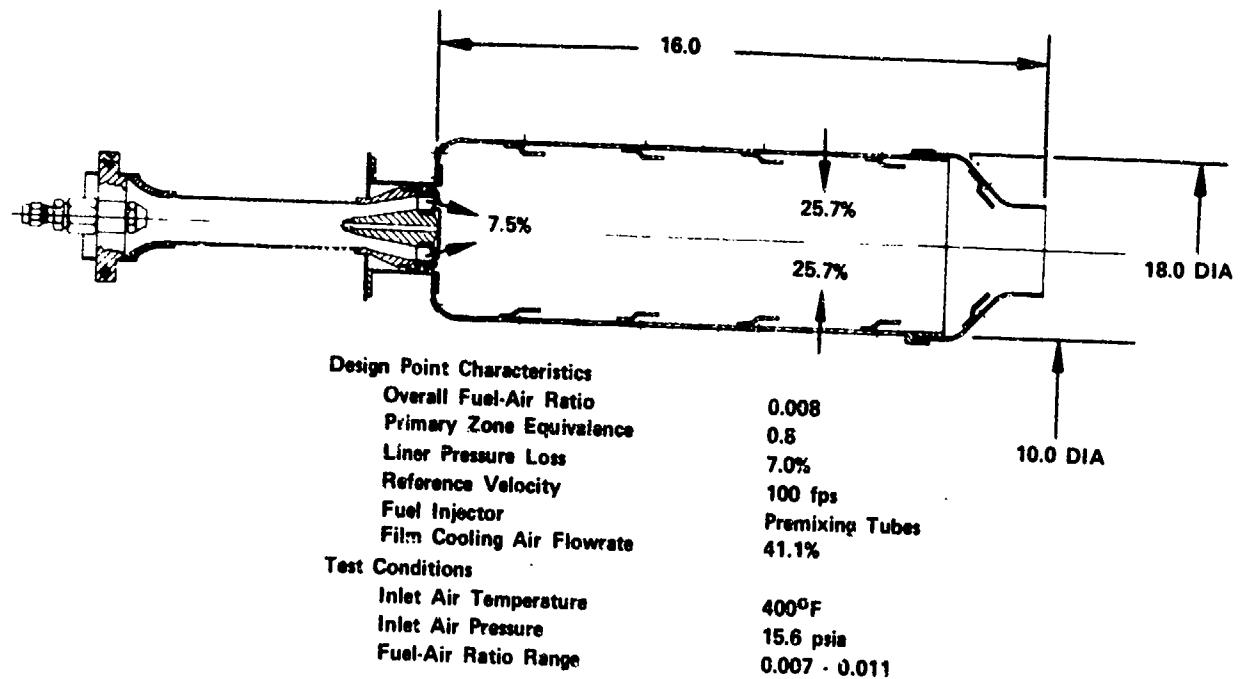


Figure 126. Summary Sheet for Combustor B Scheme 5-5A FD 76109

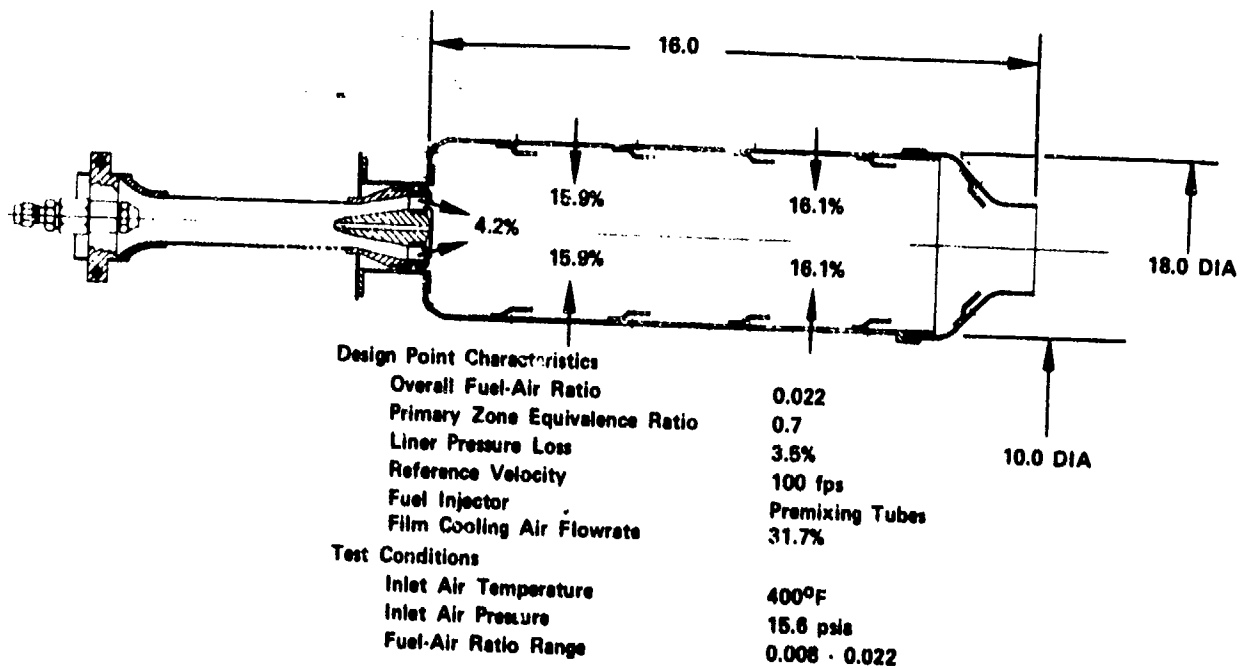


Figure 127. Summary Sheet for Combustor B Scheme 5-7A FD 76110

Although it was expected that this simulation of a variable airflow distribution combustor would produce lower emissions at idle (because of the increased liner total pressure drop), and generally good performance at full power (because of premixed fuel injection), the test results were generally disappointing in both respects. At low power, simulated by using Scheme 5-5A, LBO increased significantly to the highest value observed to date in the experimental program: 0.007. At high power, simulated by using Scheme 5-7A, extremely high concentrations of UHC and CO were obtained; the values were higher than those observed in the tests of the baseline combustor A Scheme 1-1B, which also had a design-point of 0.022, but which also used pressure-atomizing fuel nozzles.

The variation in UHC concentration with FA is presented in figure 128 for Schemes 5-5A and 5-7A. Scheme 5-5A displayed very low UHC levels at values of FA greater than 0.008. These compared to the levels obtained in previous tests using combustor B. Below an FA of 0.008, UHC concentration levels increased sharply because of the very high LBO. Scheme 5-7A exhibited very high concentrations of UHC at full-power values of FA. These levels are believed to be the result of poor fuel preparation at high values of FA; the fuel flows were extremely high, the airflows were extremely low, and premixing of the two was poor. Consequently, the distribution of the fuel and air discharging from the carburetion tubes into the primary zone of the combustor was inadequate.

The variation in CO concentration with FA is shown in figure 129. Included with the data for Schemes 5-5A and 5-7A are the data for Scheme 5-3A (also shown in figure 124), in which test series the lowest concentrations of CO were observed, prior to the series of Schemes 5-5A and 5-7A. In the FA range between 0.008 and 0.010 Scheme 5-5A produced even lower concentrations of CO than Scheme 5-3A. These lower values of CO concentration observed with Scheme 5-5A are believed to be the result of the increased liner total pressure loss.

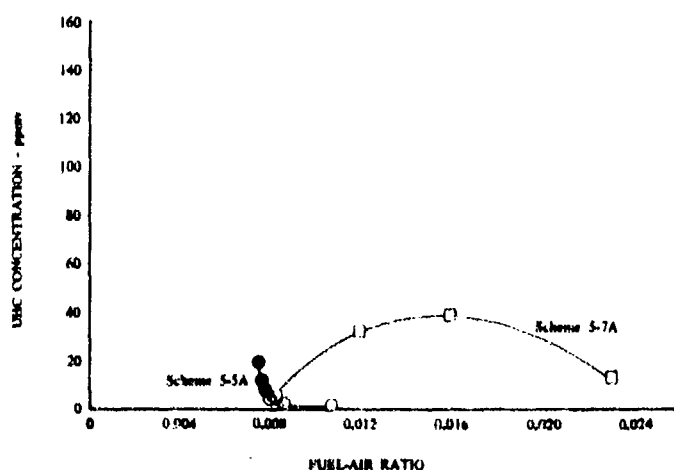


Figure 128. Variation in UHC Concentration with Fuel-Air Ratio for Tests Conducted with Combustor Schemes 5-5A and 5-7A

DF 96098

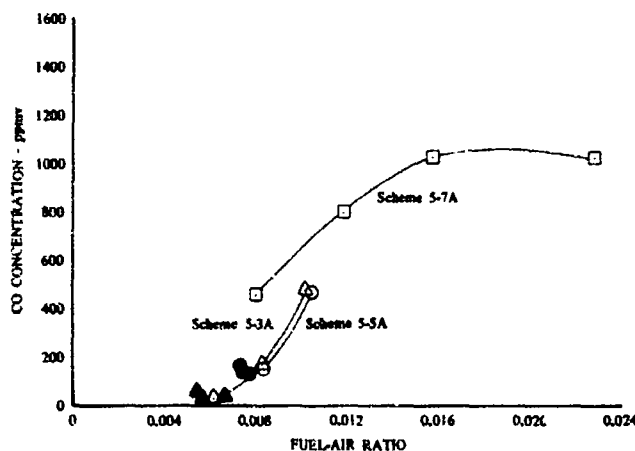


Figure 129. Variation in CO Concentration with Fuel-Air Ratio for Tests Conducted with Combustor Schemes 5-3A, 5-5A, and 5-7A

DF 96099

The very high CO concentrations obtained with Scheme 5-7A are believed to reflect overloading of the carburetion tubes with fuel at high values of FA, as discussed earlier, and quenching of reaction products by primary penetration air at intermediate values of FA.

The variation in NO_x concentrations with FA is presented in figure 130 for Scheme 5-5A only. Data for NO concentrations were not obtained with Scheme 5-7A because of an instrumentation malfunction; consequently, no data for NO_x with Scheme 5-7A are presented. In the curve for Scheme 5-5A, the NO_x concentration observed at an FA of 0.0084 (28 ppmv) was the lowest value obtained at that fuel-air ratio in the full-traverse tests accomplished using combustor B. However, a very high concentration of NO_x (55 ppmv) was observed with the same combustor configuration at an FA of 0.0105. The sharp increase in concentrations between these two values of FA is believed to reflect the sharp increase in reaction temperatures as FA was increased from 0.008 to 0.010 (PHIP increased from approximately 0.8 to 1.0). The slope of the curve is steeper than that obtained for Scheme 5-1A (in which all combustion air entered through the carburetion tubes, as it did in Scheme 5-5A) because of the differences in liner total pressure drop. The 7% pressure drop in Scheme 5-5A promoted better mixing and fuller realization of the maximum reaction temperatures at a given value of FA, than the 3.5% value in Scheme 5-1A.

The variation in combustion efficiency with FA is presented in figure 131. The high levels obtained with Scheme 5-5A reflect the very low concentrations of UHC and CO measured at values of FA above LBO. In Scheme 5-7A, relatively high levels were obtained in the intermediate and full-power ranges. The differences between EFFMB and EFFGA observed in the test series of Schemes 5-5A and 5-7A are attributed to the same causes discussed earlier for series exhibiting similar trends. No explanation is readily apparent for the values of EFFMB above 100%.

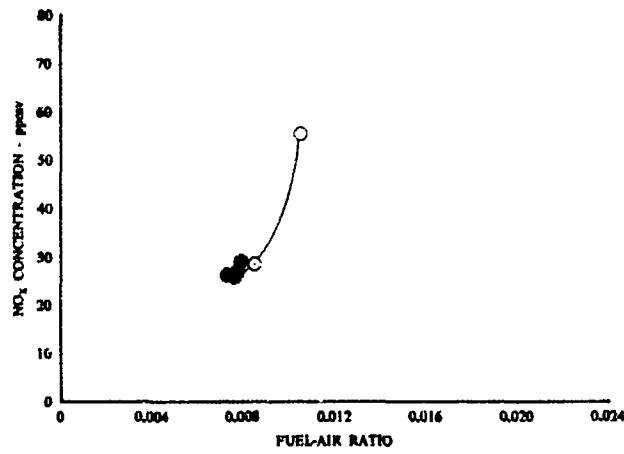


Figure 130. Variation in NO_x Concentration with Fuel-Air Ratio for Tests Conducted with Combustor Schemes 5-5A

DF 96100

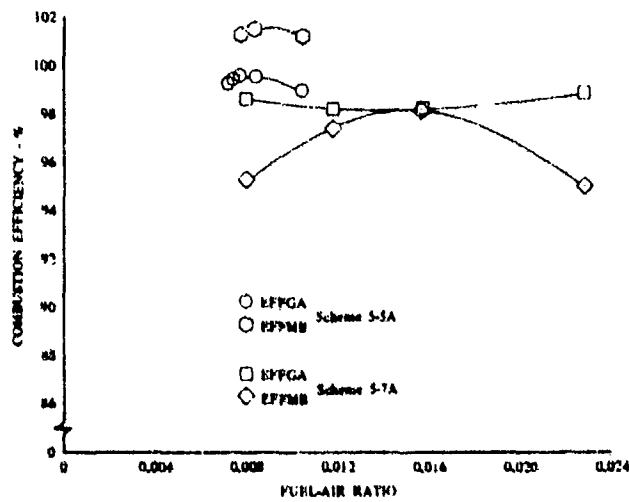


Figure 131. Variation in Combustion Efficiency with Fuel-Air Ratio for Tests Conducted with Combustor Schemes 5-5A and 5-7A

DF 96101

Tests conducted of the air staging concept with combustor B have indicated that several features of the simulated variable-airflow-distribution burner must be changed. First, the restriction of not varying carburetion tube airflow must be lifted to prevent overloading of the tubes at high fuel flowrates. Second, the flameholding capability of the carburetion tubes must be improved to lower the lean blowout limit at high values of liner pressure drop. Third, the primary penetration air must be introduced more gradually to ease the quenching of CO. If these changes are accomplished, the concept of air staging investigated in these tests shows great promise for producing low emissions over the entire FA range from idle to full power.

f. Evaluation of Circumferential Fuel Staging with Combustor B

With combustor A, it was determined that simply staging the fuel flow to the primary-zone pressure atomizing fuel nozzles in a conventional annular combustor did not yield significant reductions in low-power emission concentrations. The two types of circumferential staging evaluated, alternate and sequential, were found to be severely limited because of interactions between adjacent regions of reacting and nonreacting flow in the combustor, as discussed earlier. It was concluded that unless both the fuel and air were staged in the primary zone, circumferential staging holds little promise as a method for reducing low-power emissions.

Despite the poor results obtained with circumferential fuel staging using combustor A, it was conjectured that better results might be obtained if carburetion tube fuel injectors were used. The premixed fuel-air emanating from the carburetion tubes might react nearly to completion before appreciable interference occurred from adjacent streams of cold air. Accordingly, a brief series of tests was conducted using Scheme 5-7A, described in the preceding section, to evaluate both the sequential and alternate modes of the circumferential fuel-staging concept. As in the tests conducted using combustor A Scheme 1-1B, fuel flow to seven of the 14 carburetion tubes was stopped; but the airflow was not blocked in the fuel-inoperative tubes.

Results obtained using combustor B were not significantly different from those obtained using combustor A with pressure-atomizing fuel nozzles. No significant reductions in UHC or CO concentrations were obtained with either mode of fuel staging with combustor B.

The variation in UHC concentration with FA is shown in figure 132 for both alternate and sequential circumferential staging. Included for reference are data for Scheme 5-7A in the unstaged mode. The concentration levels obtained with the sequential staging arrangement are higher than those obtained using the unstaged configuration. In the FA range evaluated, a given UHC concentration was achieved with the sequential-staged burner at half the FA at which this concentration was achieved with the nonstaged configuration. This is unusual because even though only half the combustor is operating at twice the overall FA with the staged burner, the overall average UHC concentration observed corresponded to the entire combustor operating at twice the overall FA. The reason for this result may be seen by referring to figure 133, where the variation in UHC concentrations with circumferential location at an FA of 0.008 are presented. In the curve describing the sequential staging data it is noted that a sharp peak in UHC concentration occurs just within the nonoperating half of the burner. The concentration peak observed indicated that a strong interaction occurred between the two halves of the

burner. It is conjectured that part of the reacting mixture near the interface of the two halves moved into the nonoperating side of the burner where a sharp decrease in equivalence ratio and temperature occurred. Locally high levels of UHC concentration resulted, which accounted for the aforementioned peak. The UHC concentration levels obtained for the alternate circumferential staging configuration are much higher than those obtained in the unstaged case, as shown in figure 132. It is suggested that the interaction described for the sequential staging system was responsible for the high UHC concentrations observed with the alternate system as well. In figure 133, it may be seen that concentration peaks in the alternate staging data curve tend to occur at nonoperating nozzle locations. This is ascribed to interactions between adjacent regions of reacting and nonreacting flow, in which reactants were cooled and diluted by their contact with the surrounding cold air; consequently, high local concentrations of UHC were formed.

The variation in CO concentration with FA is presented in figure 134. The curve describing the sequential staging data is virtually an extension of the unstaged curve. The CO concentration levels obtained with sequential staging at a given value of FA were approximately half those obtained in the unstaged tests at twice the value of FA. As discussed earlier in the section on circumferential fuel staging using combustor A, this result implies that the two halves of the burner function essentially independently, with the overall average exit concentration being the average of zero (the concentration corresponding to an FA of zero), and the value corresponding to twice the overall FA in the unstaged tests. Verification of this is shown in the curve describing the sequential staging data, figure 135, wherein there appeared to be a clear separation in concentration levels between the operating and nonoperating halves of the burner. The curve describing the data obtained for the alternate staging arrangement, in figure 134 shows that CO concentrations were higher than those for sequential staging, and higher than those projected for the unstaged combustor in the low-power range. The reason suggested for this trend can be seen by referring to figure 135, where the curve describing the data for the alternate staging arrangement shows very high concentrations of CO in line with both operating and nonoperating carburetion tubes. CO produced in the reacting regions of flow appeared to diffuse readily into the nonoperating regions, with the result that appreciable quenching occurred in both regions, and that the overall average exit concentrations were high.

Data for NO concentrations were not obtained in the circumferential staging tests using Scheme 5-7A because of an instrumentation malfunction. Consequently, information relating to the variation in NO_x concentration with FA was not determined.

The variation in combustion efficiency with FA is shown in figure 136. The levels obtained during both sequential and alternate staging tests reflect the UHC and CO concentrations levels discussed earlier in this section. In the case of alternate staging, good agreement was obtained between EFFMB and EFFGA. In the case of sequential staging, however, the values of EFFMB were above 100%. These efficiency levels might be the result of the method used to determine EFFMB. In calculating EFFMB in this test program an area-weighted technique was used. Generally, the area-weighted average is very nearly equal to the mass-weighted average. However, in situations wherein strong temperature and mass differences occur over large distinct areas of the exit flow field, area weighting the average exit temperature could yield results

different from mass weighting. This point was not pursued further because of the generally poor emission concentration levels obtained with the circumferential fuel staging concepts.

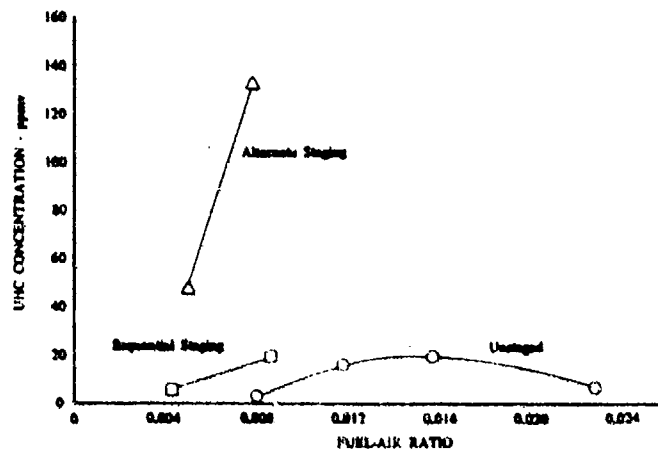


Figure 132. Variation in UHC Concentration with Fuel-Air Ratio for the Circumferential Fuel-Staging Tests Conducted with Combustor Scheme 5-7A

DF 96102

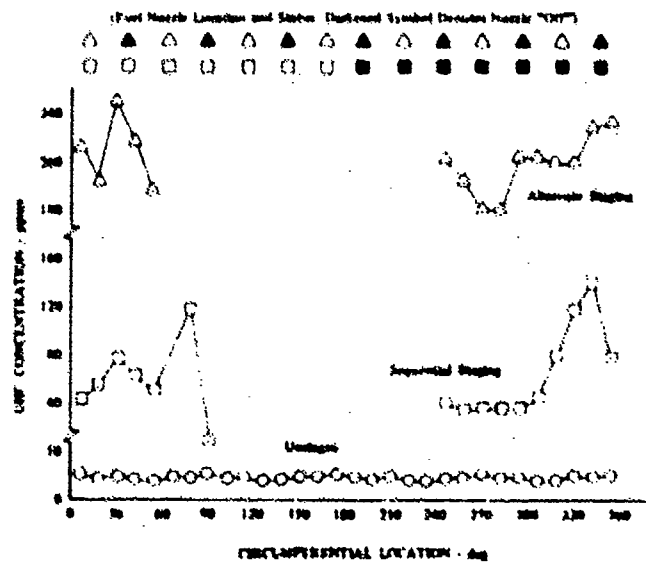


Figure 133. Variation in UHC Concentration with Circumferential Location for the Circumferential Fuel-Staging Tests Conducted with Combustor Scheme 5-7A at a Nominal Fuel-Air Ratio of 0.008 (Fuel Nozzle Status and Location Shown)

DF 96103

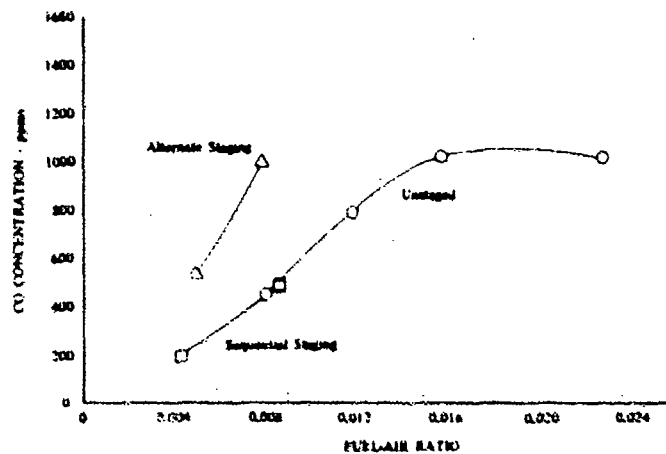


Figure 134. Variation in CO Concentration with Fuel-Air Ratio for the Circumferential Fuel-Staging Tests Conducted with Combustor Scheme 5-7A

DF 96104

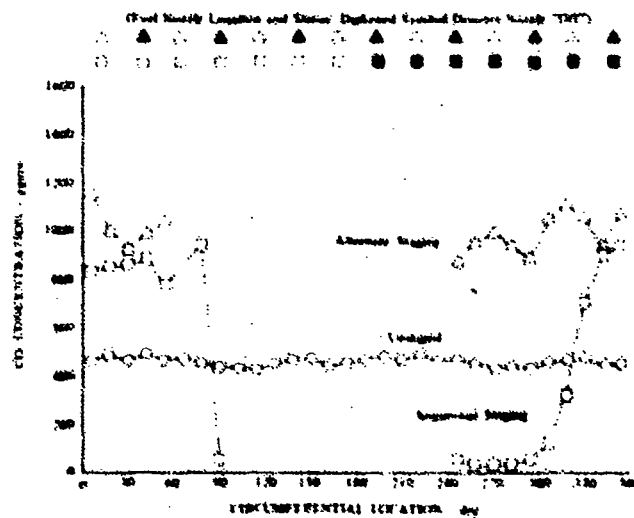


Figure 135. Variation in CO Concentration with Circumferential Location for the Circumferential Fuel-Staging Tests Conducted with Combustor Scheme 5-7A at a Nominal Fuel-Air Ratio of 0.008 (Fuel Nozzle Status and Location Shown)

DF 96105

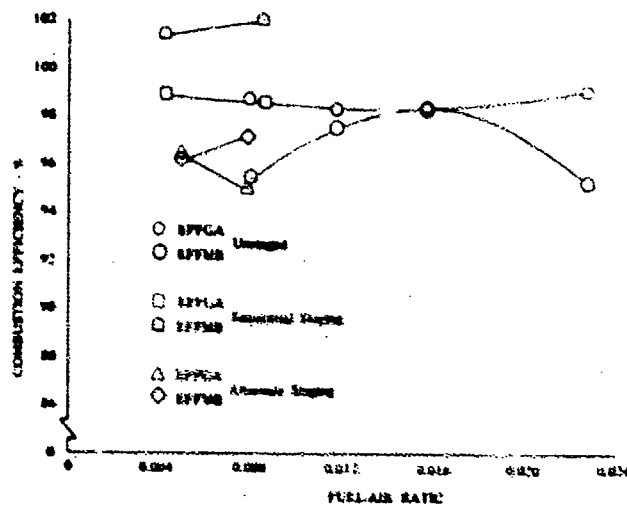


Figure 136. Variation in Combustion Efficiency with DF 96106 Fuel-Air Ratio for the Circumferential Fuel-Staging Tests Conducted with Combustor Scheme 5-7A

g. Evaluation of Carburetion Tubes with a Fixed-Geometry Combustor

Although some form of air or fuel staging will probably be necessary to achieve low concentrations of objectionable exhaust emissions over a wide range of fuel-air ratios, a significant reduction might be achieved if the premixing concept were used in combination with a fixed-geometry combustor that had a conventional, full-power FA design point. The final test series of Phase II was conducted using a modification of combustor B to evaluate the potential of such a configuration.

Combustor B Scheme 5-7A had been designed previously for full-power operation. In the air-staging tests, this configuration was operated over the FA range from 0.008 to 0.022. However, as discussed earlier, high concentrations of UHC and CO were produced at intermediate and full-power values of FA. Two features of this scheme contributed largely to the high concentrations. First, the small carburetion-tube discharge area that was required to simulate air-staging restricted the airflow and caused poor fuel atomization at high fuel flowrates. Second, the rather large primary-air penetration holes quenched the CO oxidation reaction and caused high concentrations of CO in the combustor exhaust gas. In this final series of tests, the features contributing to poor performance in Scheme 5-7A were corrected; the carburetion-tube discharge area was increased, and the large primary-air penetration holes used in Scheme 5-7A were replaced by a combination of smaller holes in the primary and intermediate zones. The resultant configuration, designated Scheme 5-8A, is described in figure 137.

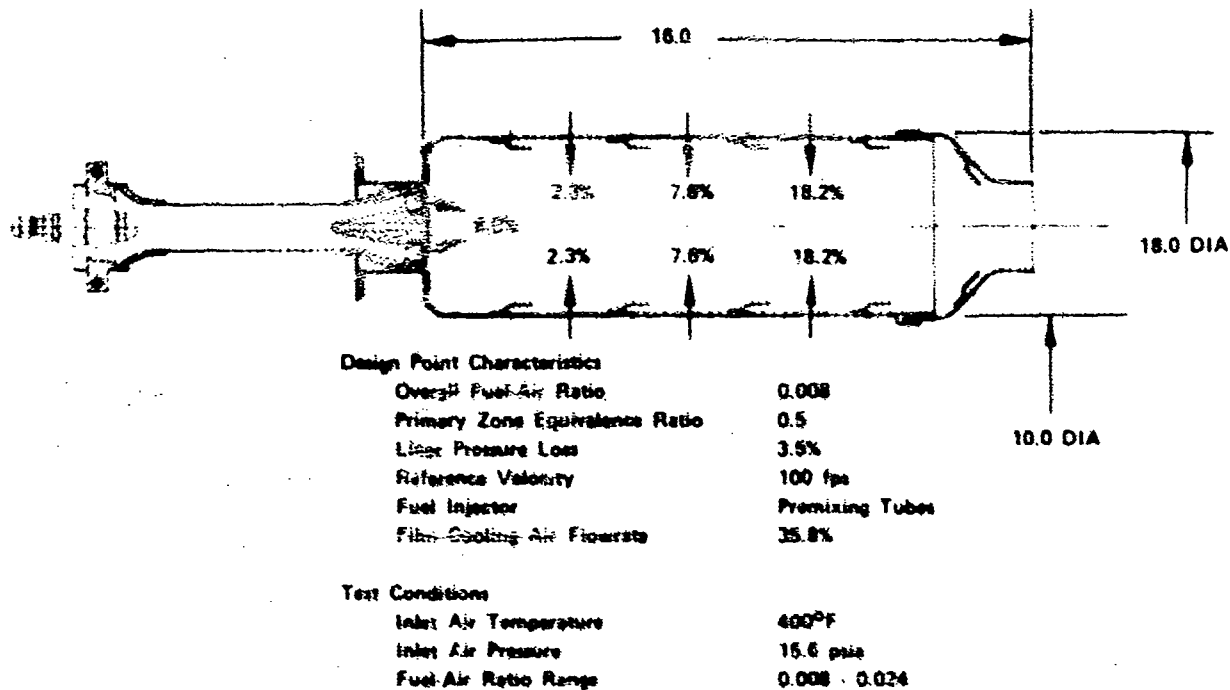


Figure 137. Summary Sheet for Combustor B
Scheme 5-8A

FD 72111

In the design of Scheme 5-8A, use was made of information generated in previous tests of the experimental program. First, results of the primary-zone airflow distribution tests indicated that Scheme 5-2A was the best overall configuration at low power. The primary-zone configuration from this scheme was incorporated into Scheme 5-8A. Next, in several series of tests, the combustion process was viewed and it was observed that the reaction zone at high combustor loadings elongated and extended to the plane of the downstream dilution holes at high values of FA. Based on this, an elongated primary zone was defined for Scheme 5-8A that included both the primary and intermediate penetration holes. It was anticipated that during low-power operation, the reaction would be confined to the vicinity of the carburetion-tube and primary penetration air injection sites, and that the intermediate holes would provide gradual dilution of the products of combustion. At full-power operation, combustor loading would be very high and the reaction zone would have elongated to include the intermediate holes as a source of combustion air. Thus, a fixed combustor geometry was provided that appeared to be capable of satisfying many of the requirements for providing low emissions concentrations over the entire FA range from idle to full power.

Scheme 5-8A was operated over the FA range from 0.0066 to 0.0241. Very good test results were obtained, with significant improvements achieved in CO and UHC concentrations, combustion efficiency, and visual flame quality over the entire FA range tested. The steep rise in CO encountered in previous carburetion tube schemes on the high FA side of the CO concentration - FA curve was flattened. UHC concentration levels were less than the program goal of 10 ppmw over the entire range tested. Values of combustion efficiency were above 99.5% over the entire range. Visual flame quality was the best obtained in the entire experimental program, ranging from a completely blue flame at idle to a predominantly transparent hot gas at intermediate and full power. These improvements were obtained at the expense of an increase in LBO to an FA of 0.0063.

The variation in UHC concentration with FA is shown in figure 138. Very low concentrations were obtained, with the maximum level of 12 ppmv observed an FA of 0.0241. These results surpassed the program goal of 10 ppmw (18 ppmv) UHC at low power. The curve describing the data passes through a minimum point of 5 ppmv at an FA of 0.0072. The gradual slope between that point and the maximum point at an FA of 0.0241 has been attributed to a slight deterioration in the quality of fuel preparation as the carburetion tubes became more heavily loaded with fuel.

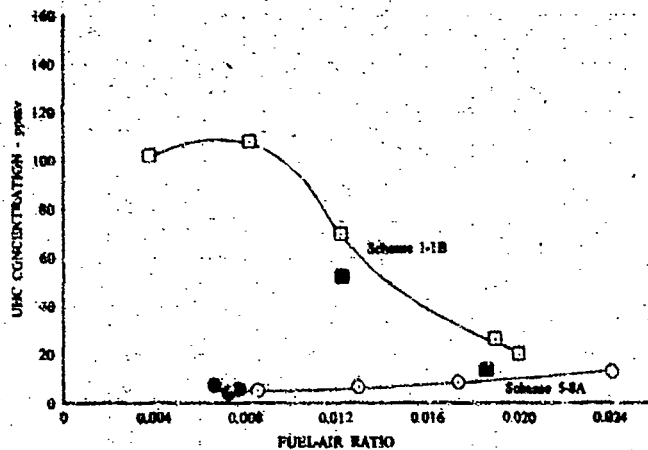


Figure 138. Comparison of Variations in UHC Concentration with Fuel-Air Ratio for Tests Conducted with Combustor Schemes 5-8A and 1-1B DF 96107

The variation in CO concentration with FA is shown in figure 139. A minimum concentration of 69 ppmv was measured at an FA of 0.0072. From that point, CO levels increased gradually to a maximum of 725 ppmv at an FA of 0.0241. At values of FA greater than 0.007, the concentrations measured were lower than those obtained in any other tests with combustor A or with combustor B. These results reflect the successful combination of the primary-zone airflow distribution used in Scheme 5-2A (which produced very low CO concentrations at low power), and the gradual introduction of air in the intermediate zone in the amount required for complete combustion at full power, without excessive quenching of CO at low power. Although further reductions will be required to achieve the program goal of 10 ppmw CO at idle, the results obtained in Scheme 5-8A represent a substantial improvement with respect to previous results and provide a strong endorsement for the methods employed. It is suggested that the desired reductions can be effected by further tailoring the hole pattern for the gradual addition of intermediate-zone air, and by providing better premixing through refinements in carburetion tube design.

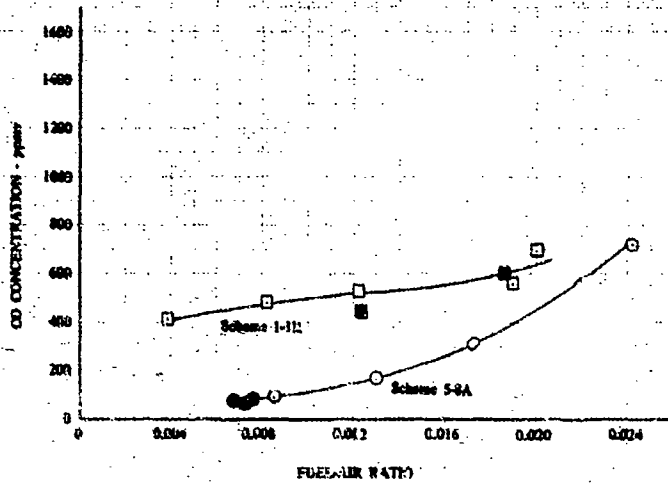


Figure 139. Comparison of Variations in CO Concentration with Fuel-Air Ratio for Tests Conducted with Combustor Schemes 5-8A and 1-1B

DF 96108

The variation in NO_x concentration with FA is shown in figure 140. Included for reference is the curve describing the data for the baseline combustor A configuration with 4 gph fuel nozzles. The curve for Scheme 5-8A is higher than the one describing the baseline scheme. It is suggested that this result is due to the better fuel preparation achieved in Scheme 5-8A, which produces a more intense reaction with higher peak temperatures.

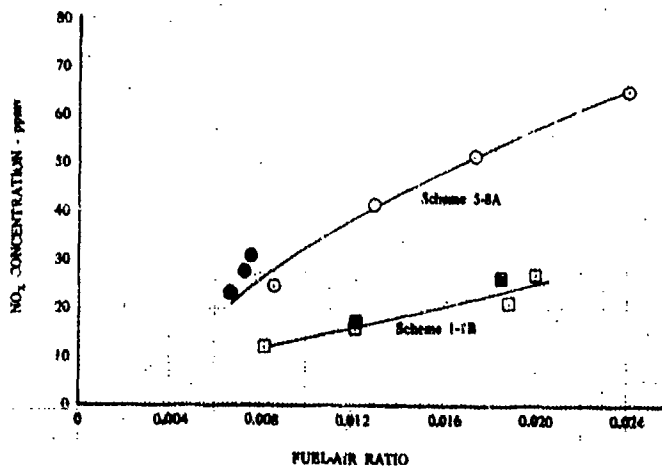


Figure 140. Comparison of Variations in NO_x Concentration with Fuel-Air Ratio for Tests Conducted with Combustor Schemes 5-8A and 1-1B

DF 96109

The variation in combustion efficiency with FA is presented in figure 141. The curve for Scheme 5-8A represents fulfillment of one of the original program goals: an entirely flat efficiency curve at near-100% levels over the entire FA range from idle to full power. The values for both EFFMB and EFFGA are in close agreement and, except for one point, are above 99.5% over the entire range.

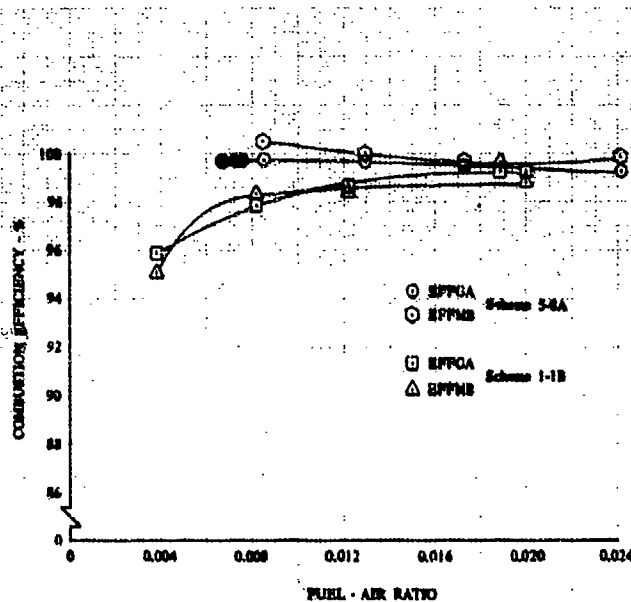


Figure 141. Comparison of Variations in Combustion Efficiency with Fuel-Air Ratio for Tests Conducted with Combustor Schemes 5-8A and 1-1B DF 96110

In general, very good performance was obtained using the carburetion-tube fuel injectors in a fixed geometry combustor designed for operation at full power. By utilizing the concept of an extended primary zone with the gradual addition of combustion air, reduced emissions were obtained over the entire FA range from idle to full power. The approach taken in these tests shows great promise and confirms the possibility of an ultimate solution to the general emissions problem that avoids the use of variable geometry hardware.

h. Evaluation of Airflow Blockage Effects

In the Phase II experimental program, an effort was made to exclude combustor inlet airflow and pressure variations as additional variables to consider in evaluating design concepts for reducing undesirable exhaust emission concentrations during low-power operation. Consequently, a large plenum chamber was installed upstream of the burner and the burner itself was contained within a large-volume case to diffuse the supply air to low velocities and simulate static-fed operation. The external aerodynamics of the experimental arrangement were, therefore, completely repeatable from test to test.

However, in the initial five tests conducted with combustor B, Scheme 5-1A, locally nonuniform airflow was inadvertently produced by a blockage within the rig plenum. A thermocouple junction box used in the flashback monitoring system for the premixing tubes had been mounted in close proximity to the combustor, as shown in figure 142, obstructing the airflow into one of the premixing tubes. This arrangement caused the primary zone in the vicinity of the obstructed tube to be fuel rich, which resulted in locally high concentration levels of UHC and CO.

The data obtained with this arrangement are presented in the following paragraphs to illustrate the effects of a nonuniform inlet airflow on exhaust emission concentrations. In figure 143 the variations in UHC and CO concentrations with circumferential location are presented. Both curves exhibit a peak in the vicinity of the obstructed premixing tube. In addition, the high concentration levels diffuse into adjacent regions of the annulus with some of the high concentration influence still evident, in the case of CO, as far away as 90 deg.

In subsequent tests, the thermocouple junction box was removed from its initial location and was mounted at the rear of the rig plenum where no interference with the combustor inlet airflow pattern could occur. The circumferential profiles of UHC and CO obtained with this revised arrangement were uniform, with no concentration peaks present of the magnitudes previously observed. These profiles are shown in figure 144.

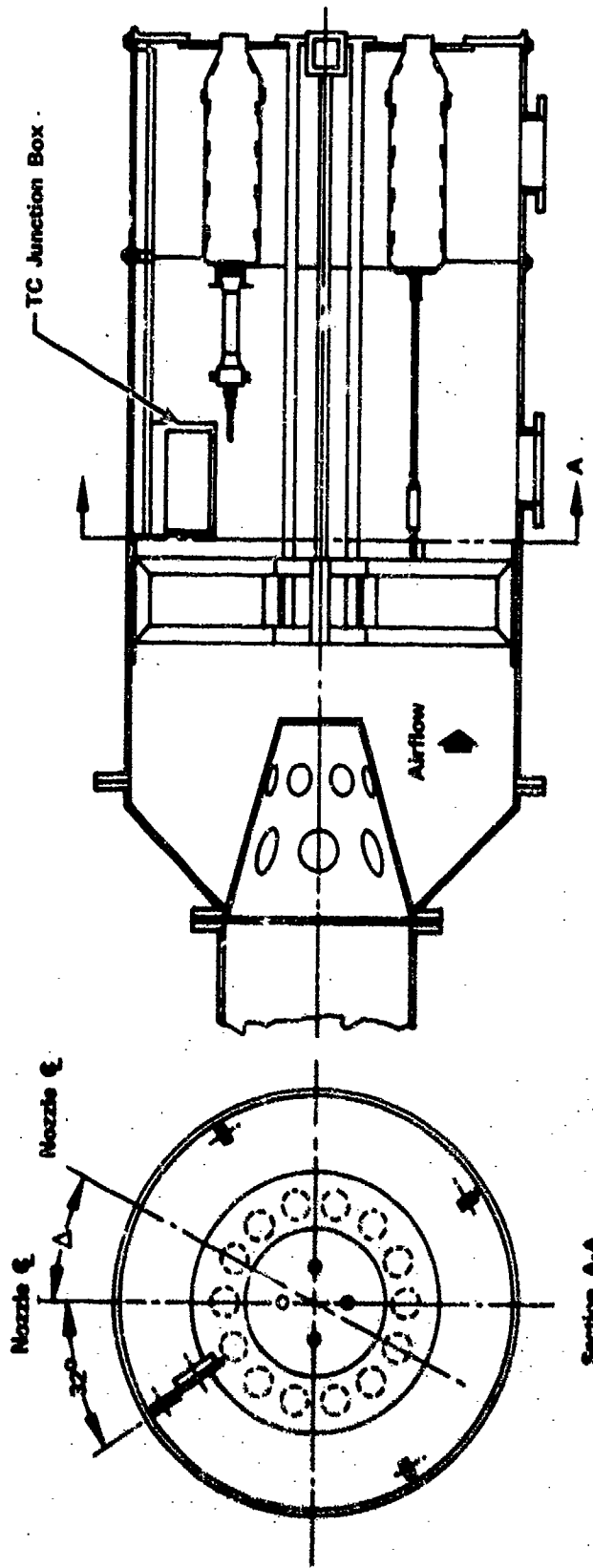
The locally high concentration levels that had been produced in the tests with the obstructed premixing tube resulted in significant increases in the overall average exit concentrations of UHC and CO. In figures 145 and 146, the variations in UHC and CO concentrations with fuel-air ratios are presented in tests with blockage and in tests without blockage. At an FA of 0.006, UHC concentration levels were in excess of 100 ppmv higher in the case with blockage; CO concentration levels were 150 ppmv higher.

The variation in NO_x concentration with FA is presented in figure 147. Concentration levels for the blocked and unblocked cases were comparable in the FA range from 0.005 to 0.006, but diverged at higher values of FA with lower levels being obtained in the tests with blockage. This result is charged to the slightly lower average reaction temperatures encountered in the tests with blockage.

The results obtained in these tests emphasize the need for developing methods for eliminating or counteracting the effects of inlet airflow distortion in future applications of low-emission combustors.

i. pH Measurements

For each full-traverse test conducted, the pH level of the combustor exhaust gas was determined. A portion of the gas that was abstracted for analysis from the exhaust stream at the exit plane of the combustor was condensed, removed from the condenser, and examined. Initially, pH paper, accurate to 0.1-pH unit, was used for analyses; later a Beckman Model SS-1 pH meter was added to the instrumentation system and used. Good agreement between the two methods was obtained when they were used to scrutinize a common sample.



$\Delta = 25^\circ 42' 51'' . 14$

Figure 142. Combustor Rig Case Showing Blockage

FD 72112

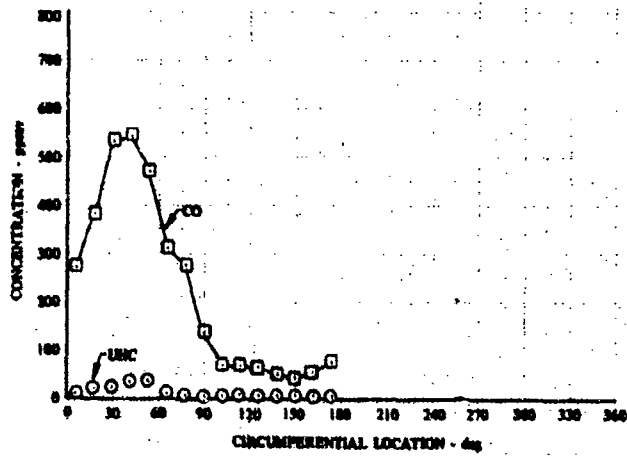


Figure 143. Variation in UHC and CO Concentrations DF 96111 with Circumferential Location for Tests with Blockage

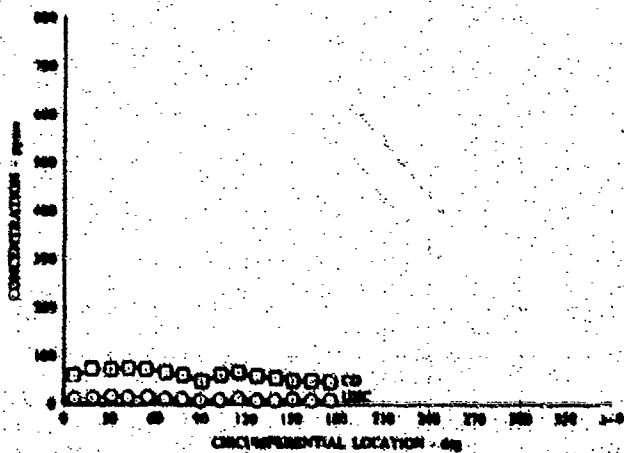


Figure 144. Variation in UHC and CO Concentrations DF 96112 with Circumferential Location for Tests with No Blockage

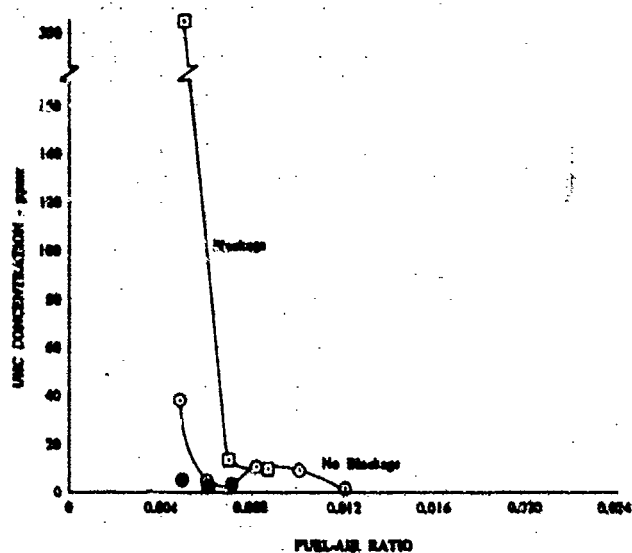


Figure 145. Comparison of Variations in UHC Concentration with Fuel-Air Ratio for Tests with Blockage and No Blockage DF 96113

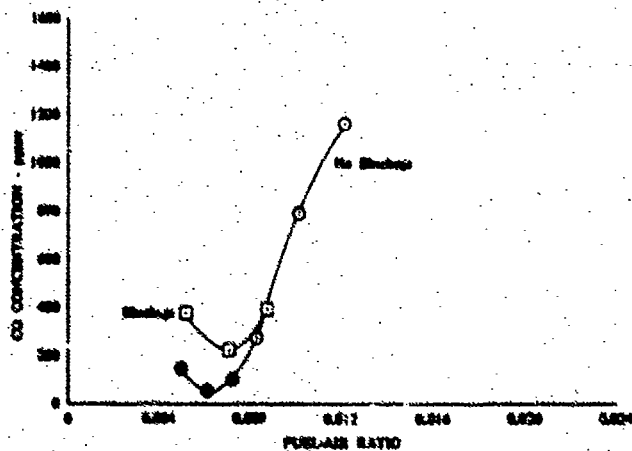


Figure 146. Comparison of Variations in CO Concentration with Fuel-Air Ratio for Tests with Blockage and No Blockage DF 96114

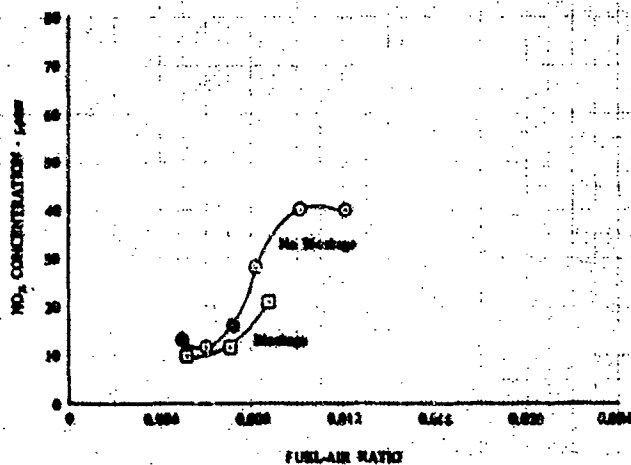


Figure 147. Comparison of Variations in NO_x Concentration with Fuel-Air Ratio for Tests with Blockage and No Blockage

DF 96115

The condensation and collection systems included a tightly coiled, 10-ft section of 1/4-in. OD stainless steel tubing and a small stainless steel bulb. The bulb was affixed to the tubing and served as a liquid collector. The tubing and bulb were located in a stainless steel container that, when filled with a mixture of water and ice, functioned as a batch condenser.

After each full-traverse test, the flow of exhaust gas into the condenser was halted, and the exhaust condensate was transferred from the condensation system, using gaseous nitrogen under pressure, into a polypropylene container for examination. The condensation system was then purged free of moisture using gaseous nitrogen until operating conditions for the next full-traverse test point were achieved. The condensate drain line was then closed; exhaust gas was allowed to enter the condenser; and liquefaction of the sample gas was again begun.

The basic system and procedure just described were incorporated into the experimental program prior to commencing the Scheme 1-1B test series. The system and procedure used in the Scheme 1-1A series was found to be unsatisfactory with respect to system cooling effectiveness and sample residence time in the condenser. This change in the modus operandi for obtaining exhaust gas condensate is considered to be the principal reason for the difference in pH level obtained in the seven tests of Scheme 1-1A and that obtained in the remaining tests of all other combustor schemes evaluated under Phase II.

The pH data obtained for all full-traverse tests conducted under Phase II are shown in Appendix IV and figure 148. Excluding the 1-1A test series, pH levels for tests conducted with combustors A and B ranged from 2.5 to 4.2

over a range of fuel-air ratios from 0.0038 through 0.0241. The only conclusions apparent are that the exhaust emissions were definitely acidic and that the acidity increased slightly as the overall fuel-air ratio was increased.

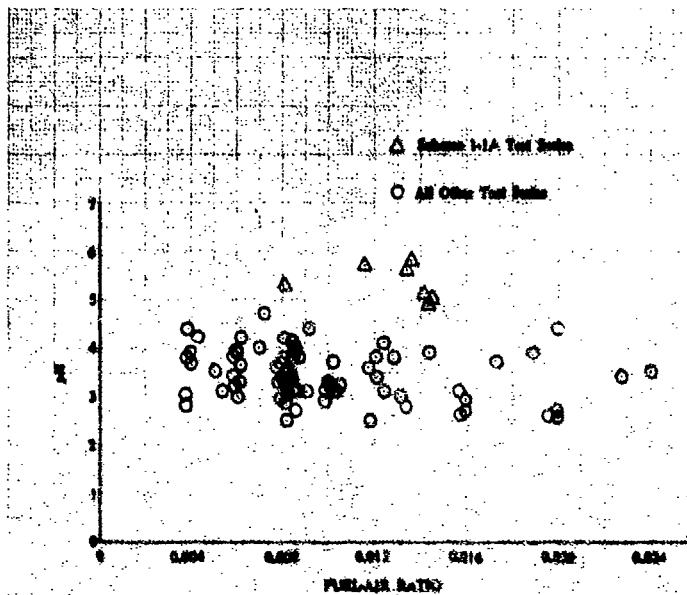


Figure 148. Variation in pH with FA for Full-
Traverse Tests of Combustors A
and B

DF 96116

SECTION V

COMPARISON OF PREDICTED AND MEASURED EMISSION CONCENTRATIONS

A. GENERAL

This section presents UHC and CO emissions concentration predictions obtained using the streamtube combustor model described in Section III. The combustor configurations and operating conditions chosen for input to the model corresponded to the JT8D probing test series (shown in table IV and figure 13), and to selected combustor A and B test points. (See Section IV.) The predicted CO and UHC concentrations have been compared with the corresponding experimental data. Examples from the parametric study were selected to correspond to test cases conducted under the combustor A test program insofar as possible, and the predicted results were compared with the experimental data where applicable. In the case of inlet pressure variation, no extensive experimental data exist for comparison with the predicted concentrations.

B. JT8D PROBING STUDIES

Predicted CO and UHC concentration profiles and FA profiles have been compared with the experimental probing data in figures 149 through 151 for the idle condition and in figures 152 through 154 for the approach condition. The profiles have been plotted at the correct axial locations, depicting the actual combustor geometry at each probe location. The predicted concentration levels are in general agreement with the measured values, particularly for the approach condition. Lack of detail in the central region of the burner is a consequence of the streamtube arrangement incorporated in the model. The discrepancy between predicted and measured FA profiles near the front of the burner, especially apparent in the idle case, is a measure of the difference between the total fuel flow rate, approximated by the measured values, and the amount of fuel vaporized and reacted (predicted values). The two values approached one another with movement down the burner. This is in qualitative agreement with the discrepancy between enthalpy-based and oxygen-deficiency-based combustion efficiencies found near the front of the burner. (See Section III.)

The measured and predicted exhaust-plane concentrations are shown in table XII. As indicated, there is only qualitative agreement with the UHC concentration levels and poor agreement with the CO values. The predicted exhaust levels, at the present state of model development responded relatively more strongly to changes in FA than to inlet temperature variations. This is contrary to the experimental trends. The values of FA reported in table XII exceed the set values of 0.0075 and 0.0131 since they represented midspan averages and hence did not include fuel-free wall cooling air at the periphery of the combustor.

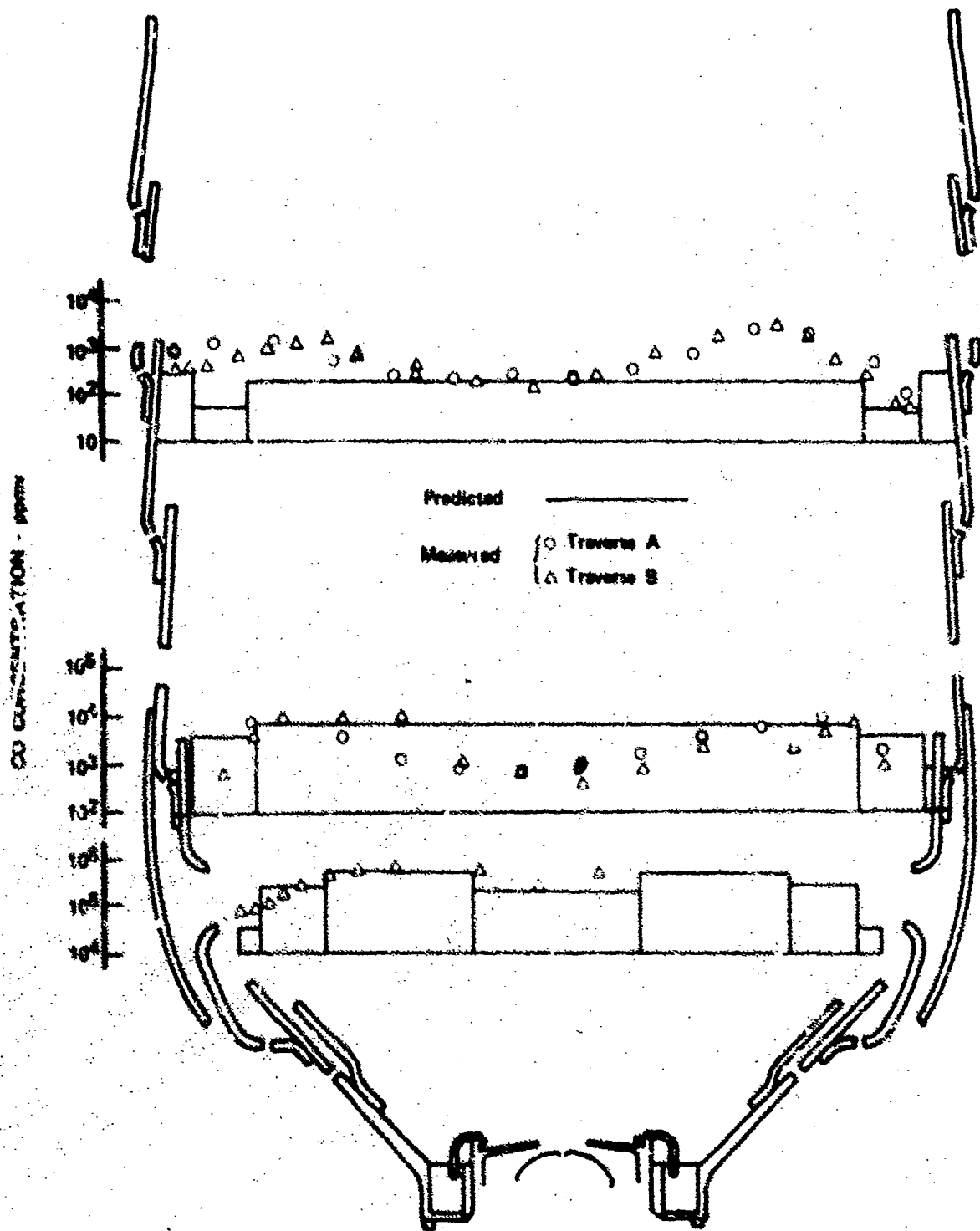


Figure 149. Variation in Predicted and Measured CO Concentrations within JT8D Burner (Idle Operation)

FD 72115

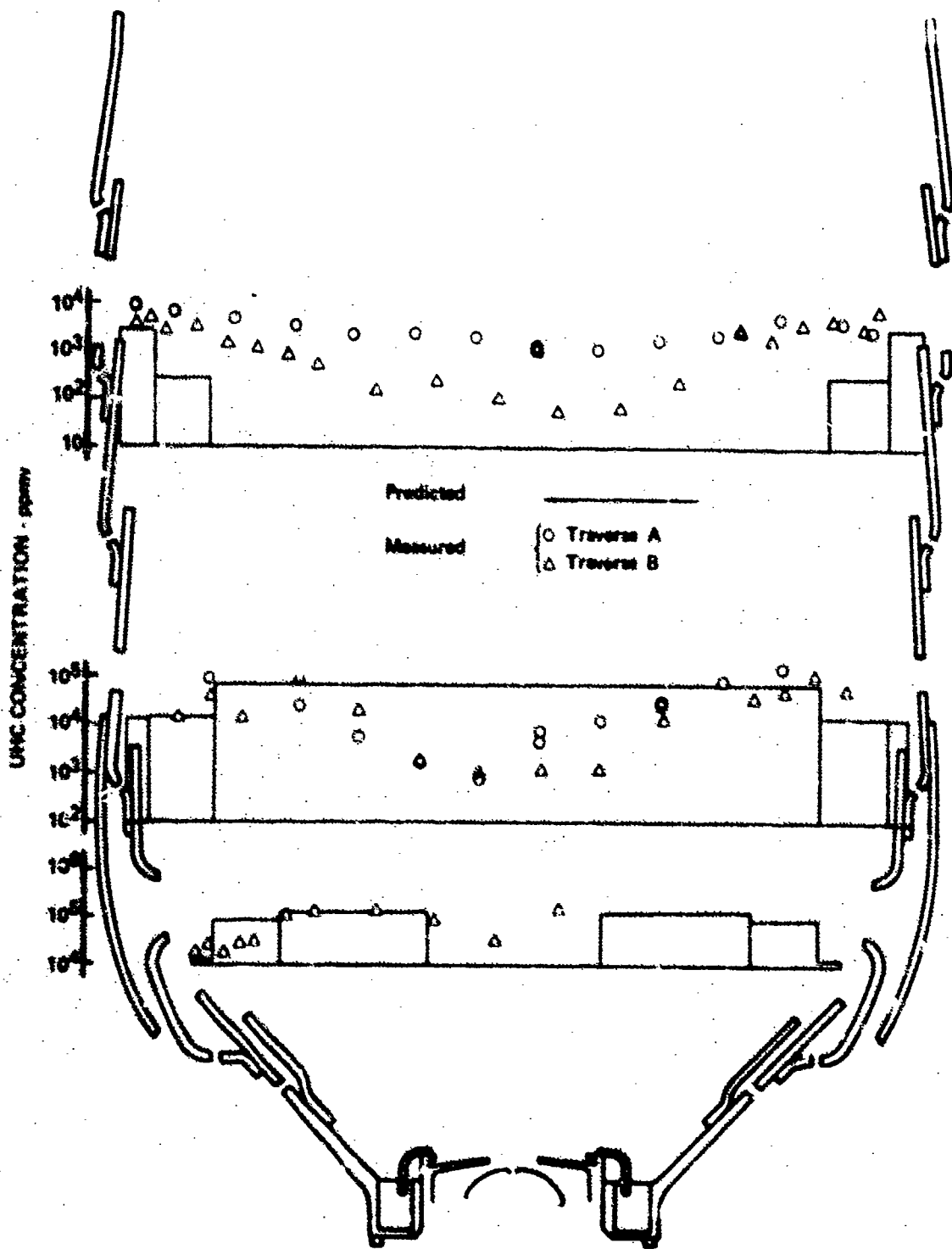


Figure 150. Variation in Predicted and Measured UHC Concentrations within JT8D Burner (Idle Operation)

FD 72116

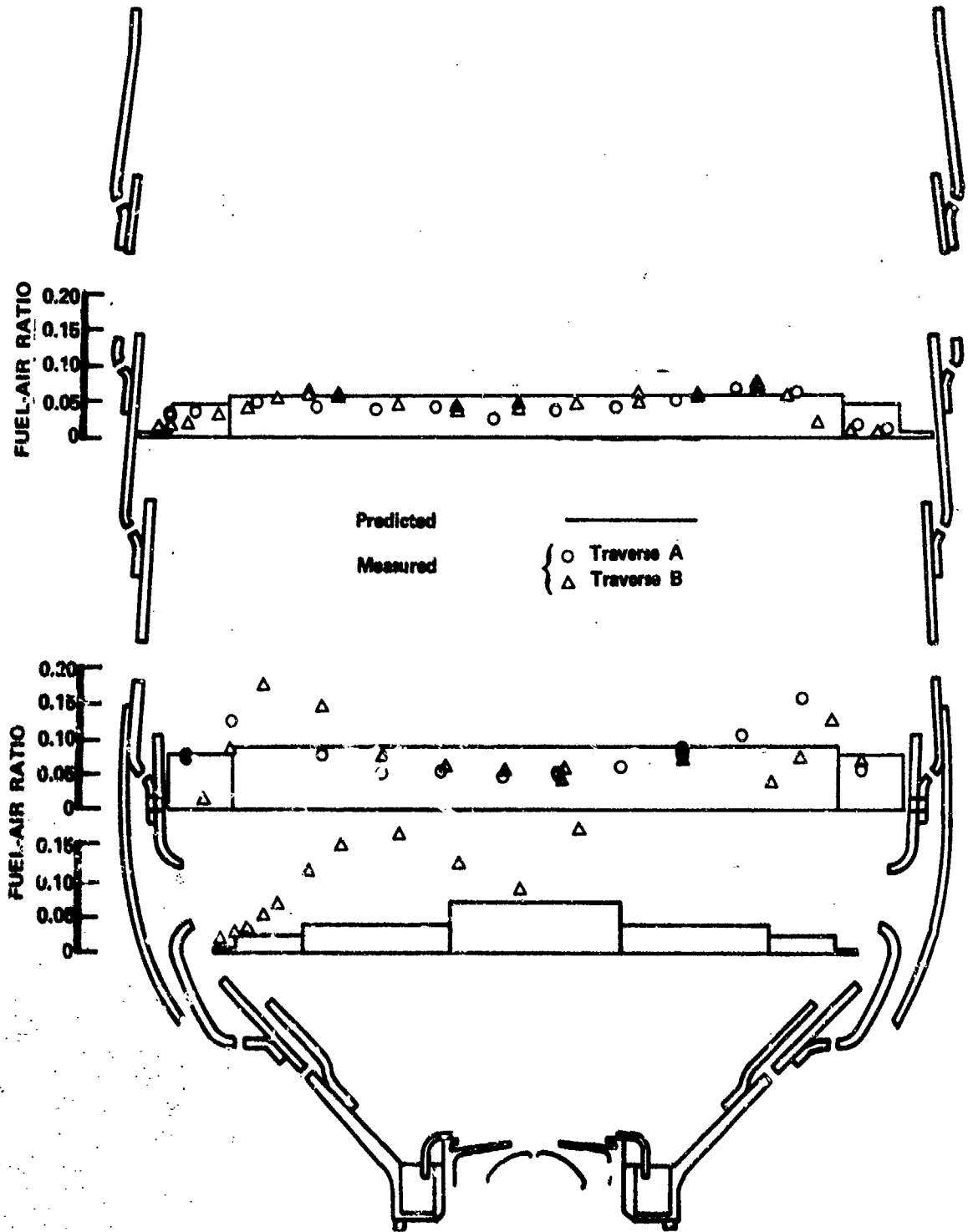


Figure 151. Variation in Predicted and Measured FA within JT8D Burner (Idle Operation)

FD 72117

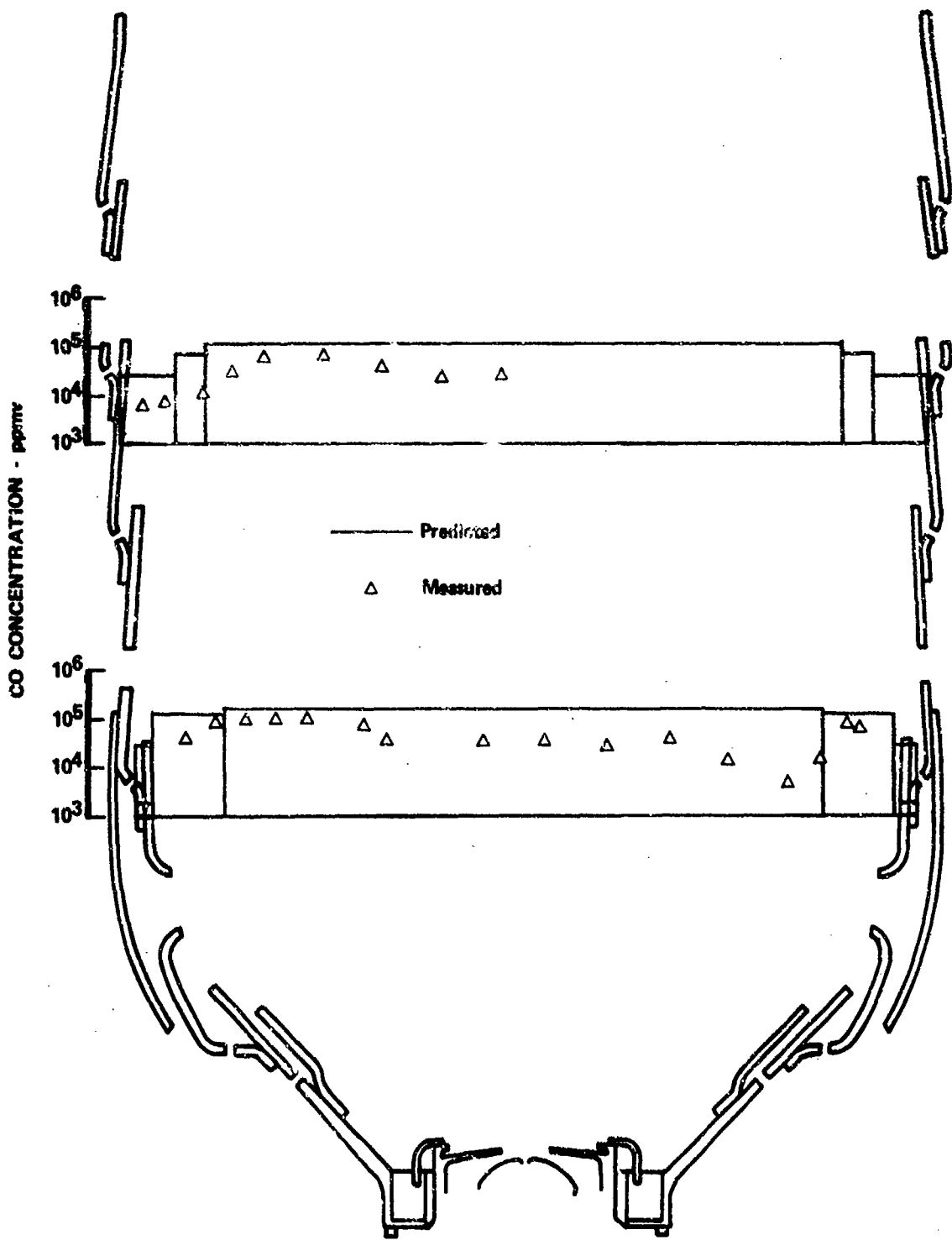


Figure 152. Variation in Predicted and Measured CO Concentrations within JT8D Burner (Approach Operation)

FD 72118

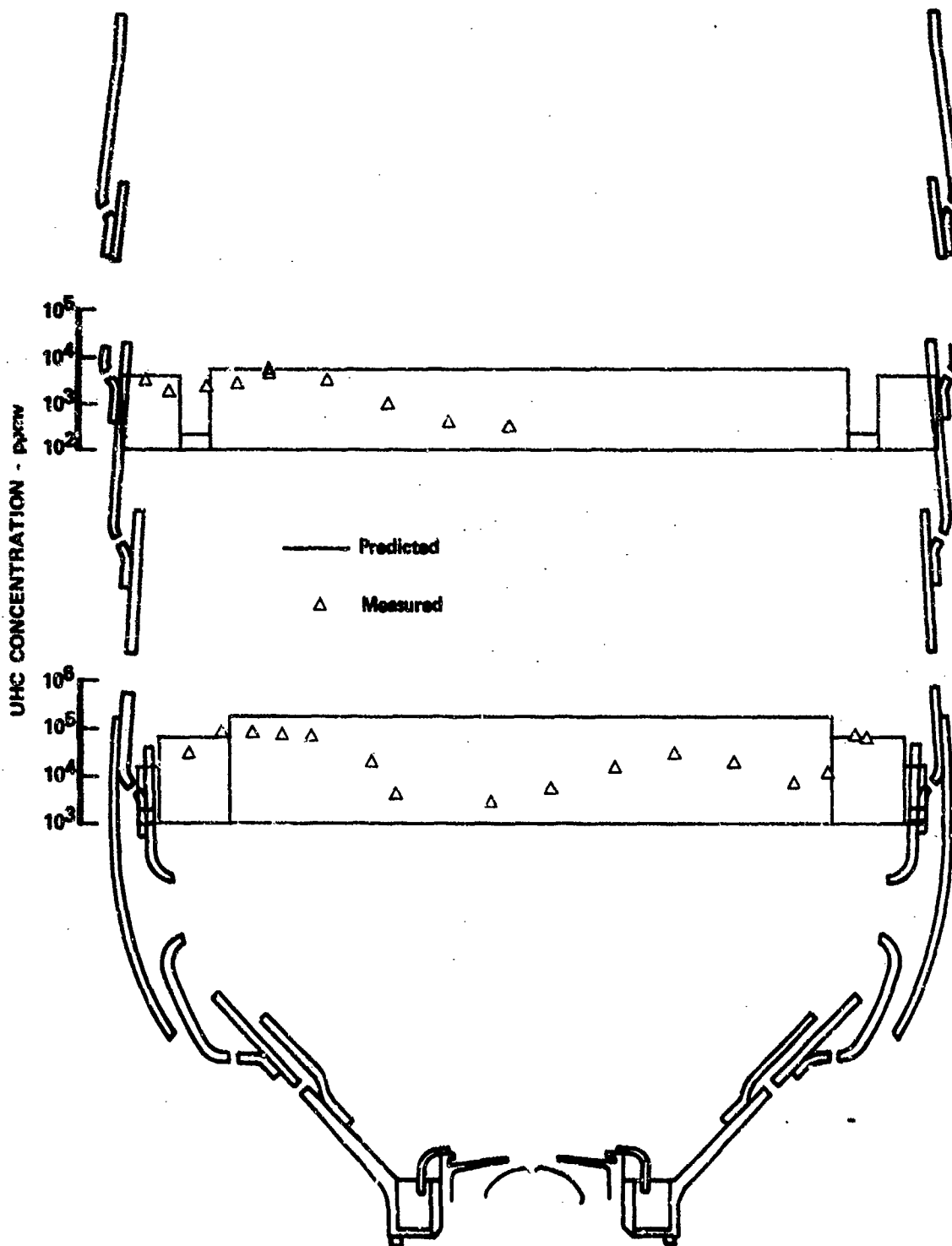


Figure 153. Variation in Predicted and Measured UHC Concentrations within JT8D Burner (Approach Operation)

FD 72119

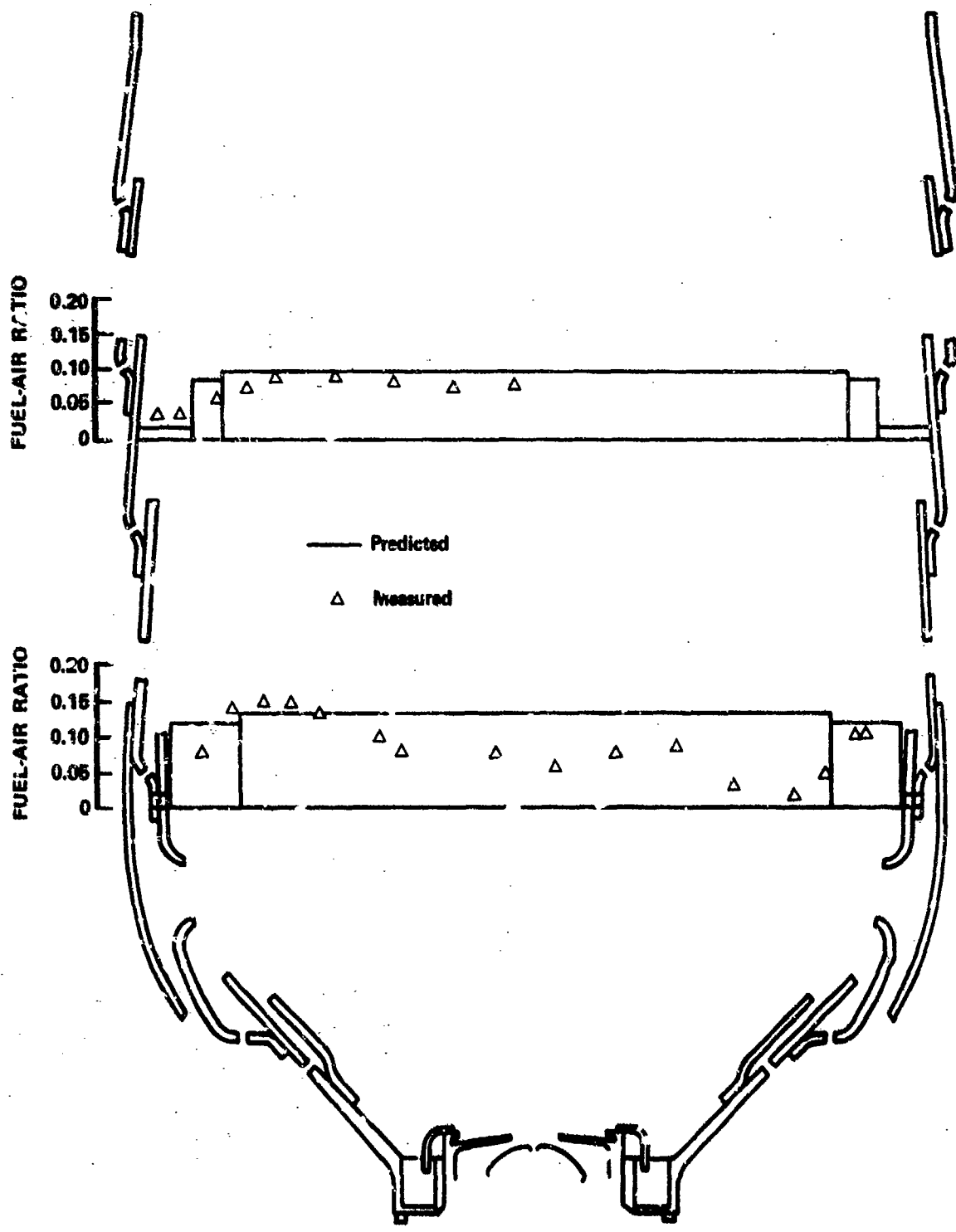


Figure 154. Variation in Predicted and Measured FA within JT8D Burner (Approach Operation) FD 72120

Table XII. Comparison of Predicted and Measured JT8D Probing Data

Condition	Exhaust Plane Emission Concentration					
	Experiment			Predicted		
	CO	UHC	FA	CO	UHC	FA
Idle	920	900	0.010	315	233	0.0088
Approach	320	0	0.018	1223	81	0.0150

C. PHASE II - COMBUSTOR A

Predicted values of CO and UHC concentrations were compared with the exhaust traverse data obtained from the tests conducted using combustor A in Phase II. Comparison of the predicted and experimental data are shown graphically as follows:

1. Figures 155 and 156 show comparisons of the effect of air staging using Schemes 1-1B, 2-1A, 3-1A, and 4-1A.
2. Figures 157 and 158 show comparisons of the effect of fuel staging using Scheme 2-1B. Scheme 2-1A results (unstaged) are shown for comparison.
3. Figures 159 and 160 show comparisons of the effect of fuel staging using Scheme 4-1A.

In all cases, as will be the convention for the remainder of this section, the predicted points have been indicated by darkened symbols that have been connected by straight lines. The fuel-staging cases have been confined to a single value of PHIP, 0.5.

With the exception of the 1-1B configuration, the predicted CO concentrations exhibited substantial agreement with the measured data. The UHC concentration predictions generally exceeded the measured values for those cases in which fuel was not staged, often by as much as an order of magnitude, and tended to underestimate the measured values in the fuel-staging cases. The predicted trends are generally correct, however. There is reason to believe that the UHC concentration predictions for the fuel-staging cases can be brought into line with the measured values by adjustment of the radial distribution of secondary fuel. The reason for the strong lack of agreement in the 1-1B case is not readily apparent.

D. PHASE II - COMBUSTOR B

Predicted CO and UHC exhaust concentrations were compared with the measured values for Scheme 5-1A of the premixed-tube combustor in figures 161 and 162. As observed for combustor A, there was reasonable agreement between the predicted and measured CO concentration values, while the predicted UHC concentration values exceeded the measured values by one and a half orders of magnitude. However, the predicted UHC concentration values for the premixed configuration were substantially below the corresponding predictions for the nonpremixed, exhibiting the correct qualitative trend.

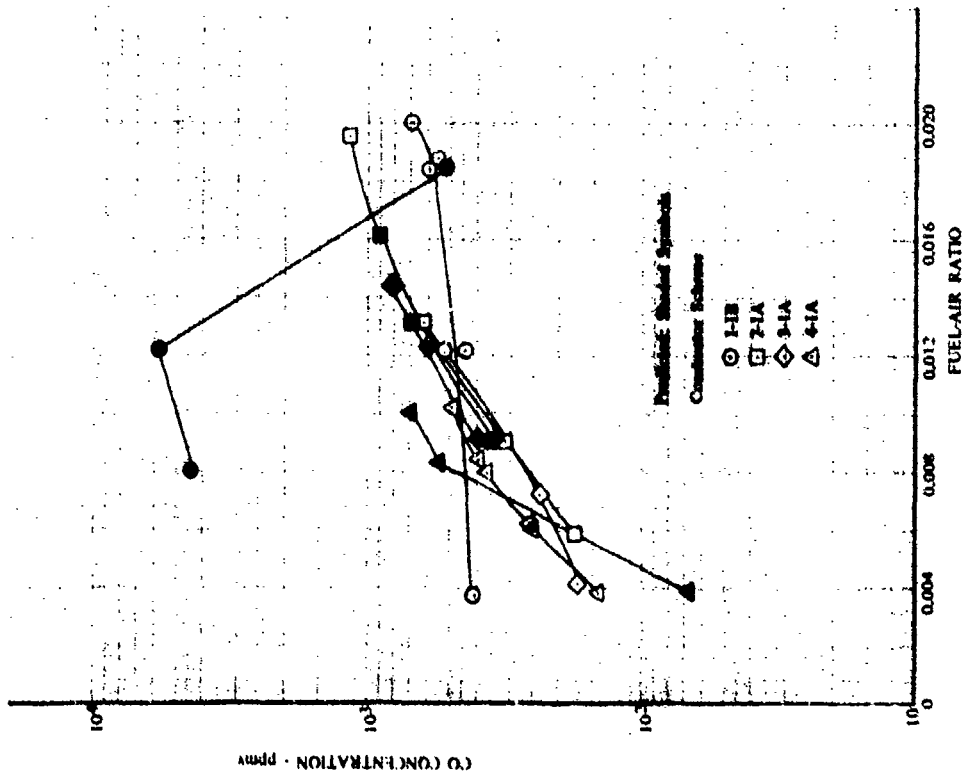


Figure 155. Comparison of Predicted and Measured Variations in CO Concentration with FA for Air-Staging Tests

DF 96117

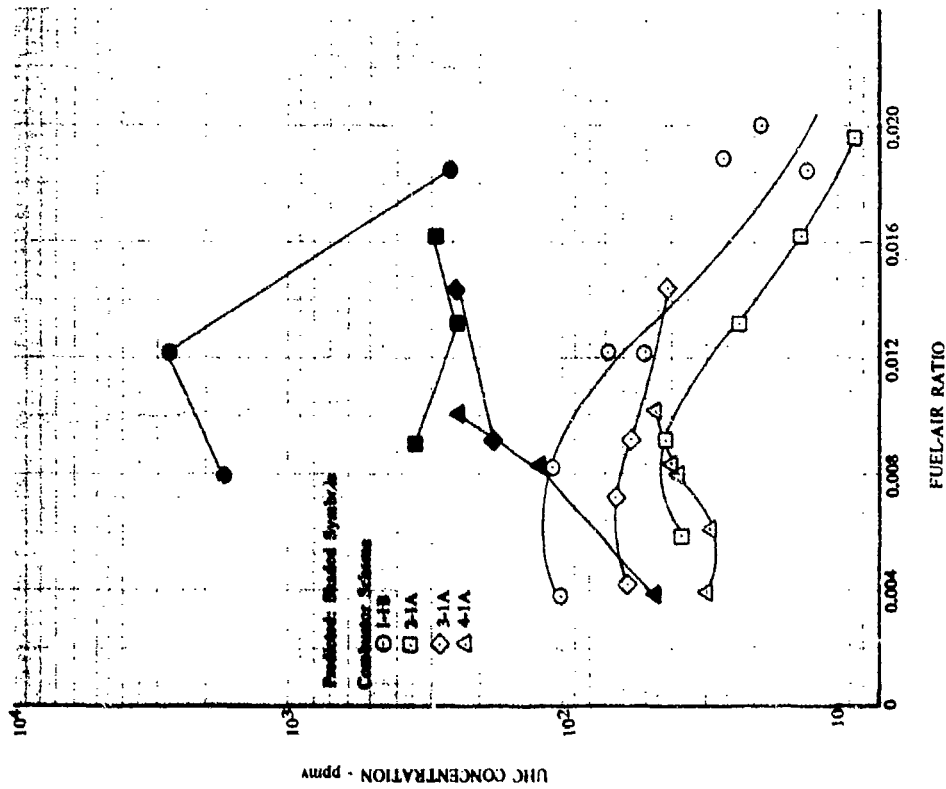


Figure 156. Comparison of Predicted and Measured Variations in UHC Concentration with FA for Air-Staging Tests

DF 96118

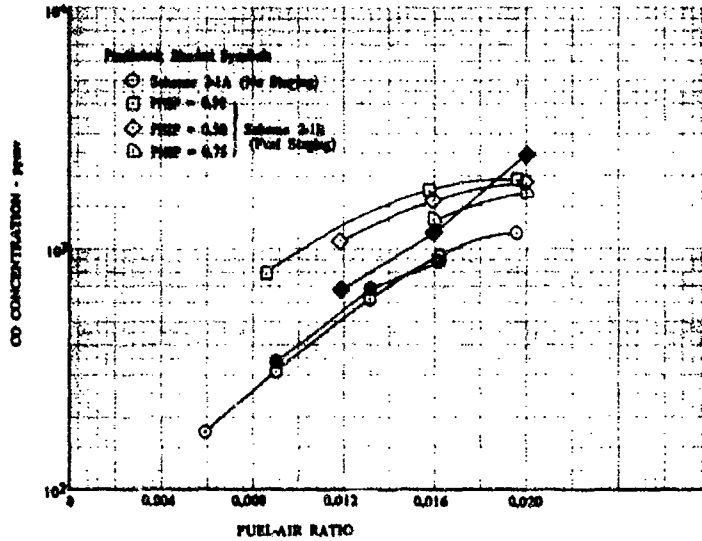


Figure 157. Comparison of Predicted and Measured Variations in CO Concentration with FA for Fuel-Staging Tests (Scheme 2-1A)

DF 96119

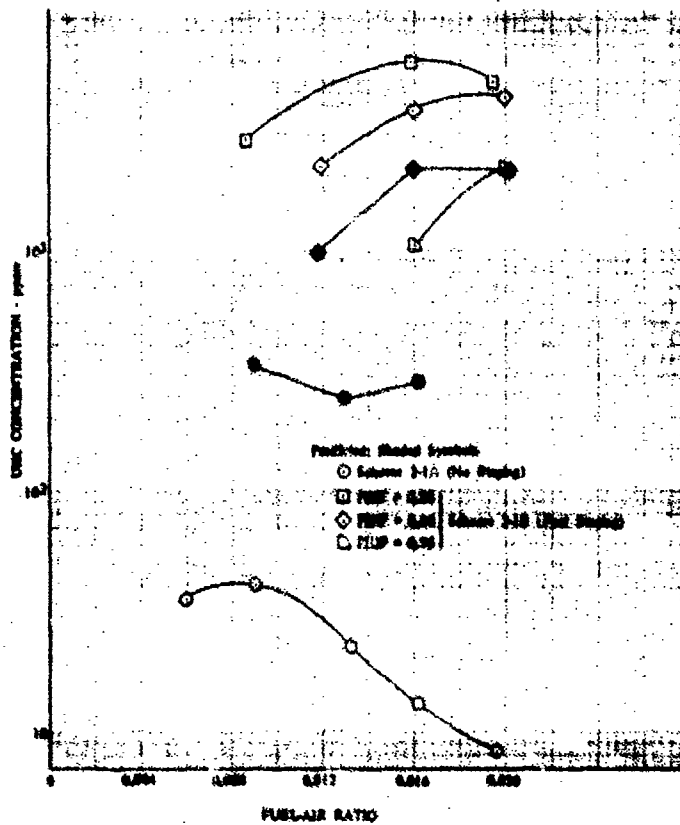


Figure 158. Comparison of Predicted and Measured Variations in UHC Concentration with FA for Fuel-Staging Tests (Scheme 2-1A, 4 gph Fuel Nozzles in Primary and Secondary)

DF 96120

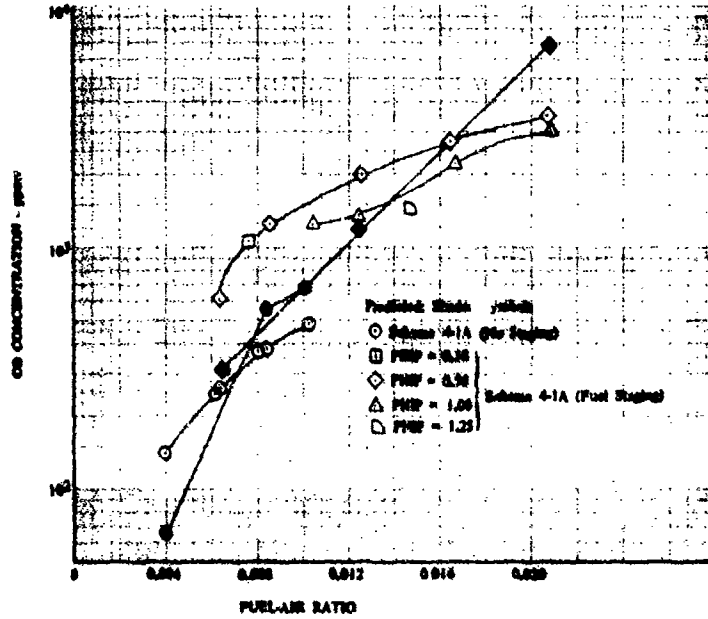


Figure 159. Comparison of Predicted and Measured Variations in CO Concentration with FA for Fuel-Staging Tests (Schemes 4-1A, 4 gph Fuel Nozzles in Primary and Secondary) DF 96121

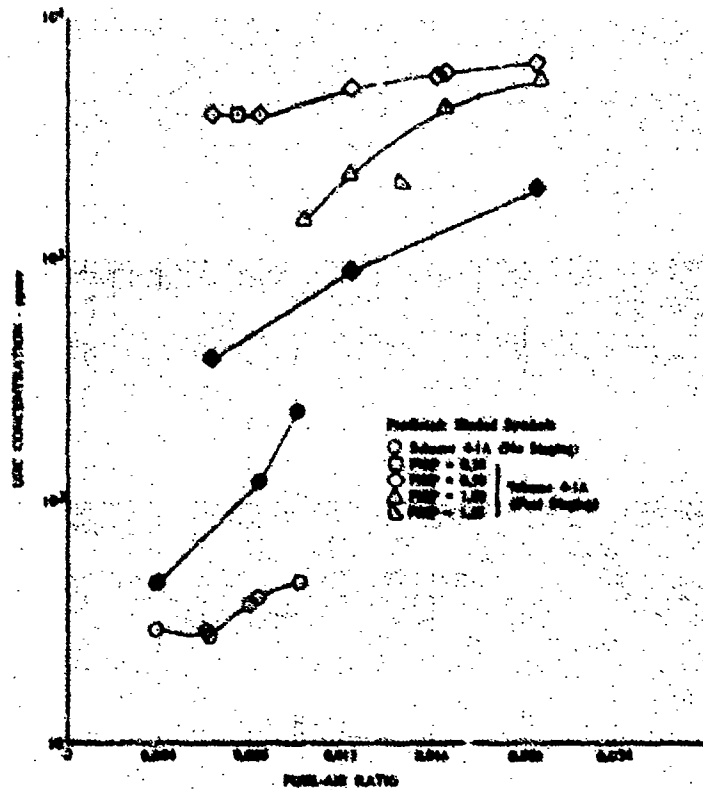


Figure 160. Comparison of Predicted and Measured Variations in UHC Concentration with FA for Fuel-Staging Tests (Scheme 4-1A, 4 gph Fuel Nozzles in Primary, Air Blast Nozzles in Secondary) DF 96122

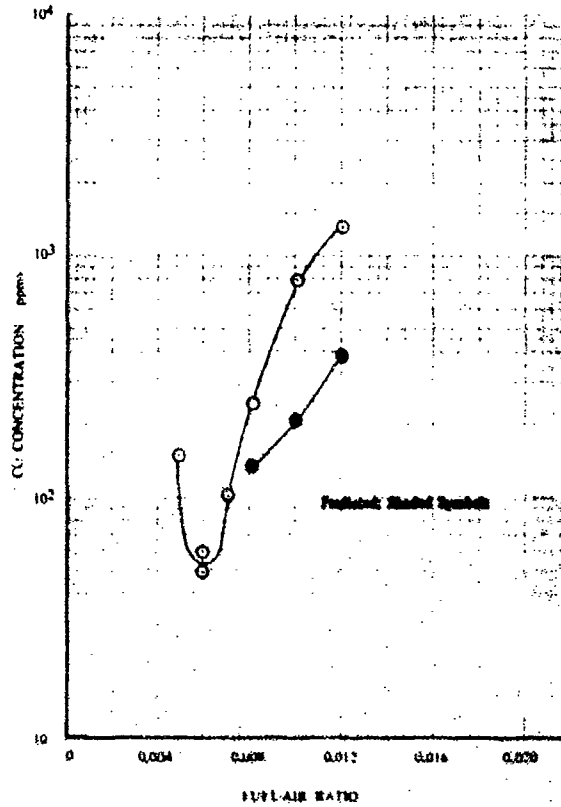


Figure 161. Comparison of Predicted and Measured Variations in CO Concentration with FA for Scheme 5-1A Tests

DF 96123

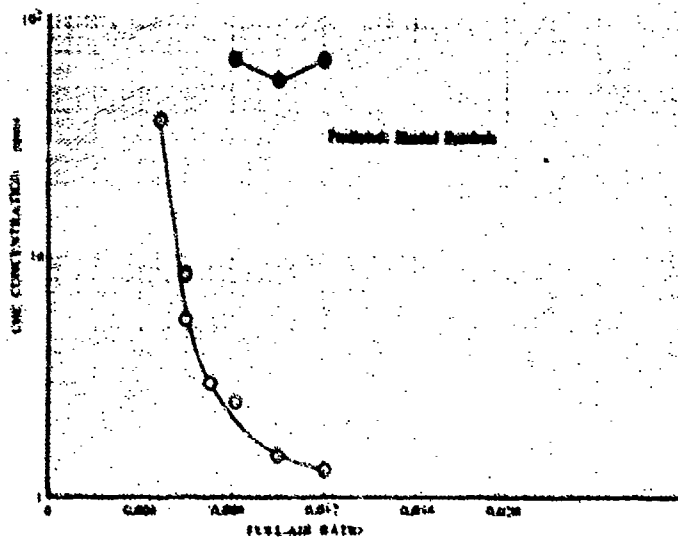


Figure 162. Comparison of Predicted and Measured Variations in UHC Concentration with FA for Scheme 5-1A Tests

DF 96124

E. PARAMETRIC STUDY

The parametric variation of predicted CO and UHC exhaust concentration was investigated with respect to the following input variables:

1. Figures 163 and 164 show comparisons of the effect of inlet air temperature using Scheme 1-1B at an inlet air pressure of 1 atm, FA of 0.0082, and reference velocity of 100 fps.
2. Figures 165 and 166 show comparisons of the effect of inlet air pressure using Scheme 1-1B at an inlet air temperature of 400°F, FA of 0.0082, and reference velocity of 100 fps.
3. Figures 167 and 168 show comparisons of the effect of reference velocity using Scheme 1-1B at an inlet air pressure of 1 atm, FA of 0.0082, and inlet air temperature of 400°F.
4. Figures 169 and 170 show comparisons of the effect of air-blast fuel injection (increased fuel droplet size) using Scheme 2-3A at an inlet air pressure of 1 atm, inlet air temperature of 400°F, and reference velocity of 100 fps. Data for Scheme 2-1A (pressure-atomizing fuel nozzles) are shown for reference.
5. Figures 171 and 172 show comparisons of the effect of dome cooling using Scheme 2-2A (reduced dome cooling) at an inlet air temperature of 400°F, inlet air pressure of 1 atm, and reference velocity of 100 fps. Data for Scheme 2-1A are shown for reference.

Analytical model input conditions were chosen to correspond to test points accomplished in the Phase II combustor A test program. This was done to provide experimental verification of the model predictions wherever possible. Only the cases involving variation of inlet pressure have been presented without corresponding experimental data.

In the cases of variation of inlet temperature and reference velocity, it was unfortunate that all testing was conducted utilizing the 1-1B configuration. This configuration exhibited the worst agreement between predicted and measured values of concentrations. The predicted effect of inlet temperature variation showed poor qualitative and quantitative agreement in the case of CO and only weak agreement in the case of UHC. The predicted effect of inlet pressure was quite strong, although the validity of the predictions cannot be determined with the limited data at hand. The predicted effect of reference velocity exhibited qualitative agreement with the measured values in the case of CO, but showed the reverse trend for UHC. The extent to which this lack of agreement was due to the difficulties with Scheme 1-1B, described above, has not been determined.

The air-blast fuel injectors used in Scheme 2-3A produced a relatively coarse spray. This was simulated in the model by an increased input value of initial fuel droplet size, 200 microns. As shown in figures 169 and 170, the model predictions indicate a reduction in CO concentration and essentially unchanged UHC concentration with increased fuel droplet size. The predicted UHC trend is in particularly

poor agreement with the experimental data. This poor agreement indicates that there is more involved than a simple increase in fuel droplet size, as a significant change in radial fuel distribution.

The effect of reduced dome cooling, in the configuration investigated, was both predicted and experimentally measured to be small. Returning to the pattern of the air and fuel-staging cases, the predicted CO concentration values showed good agreement with the corresponding measured values, while the UHC predictions exceed the measured values by approximately an order of magnitude.

F. DISCUSSION OF THE MODEL PREDICTIONS

Examination of the predicted CO and UHC concentrations within the combustor indicates that these emissions result from premature quenching of the respective chemical reaction mechanisms as the streamtube temperature was reduced by air addition. CO concentration level is controlled by the kinetic conversion to CO₂, while the UHC concentration level reflects both raw fuel, which has failed to ignite, and intermediate hydrocarbons, for which oxidation has been halted. Examination of the detailed predictions indicates that CO conversion is quenched at a higher temperature than the hydrocarbon oxidation reactions. Thus, continued hydrocarbon reaction produces CO below the temperature at which conversion to CO₂ can occur. With respect to the combustor internal flowfield CO is quenched in the downstream portions of the central streamtubes, following dilution air addition, and everywhere in the wall cooling streamtube. Quenched UHC is principally confined to the outer wall cooling air streamtube.

The increase in exit plane CO and, particularly, UHC concentrations with combustor wall fuel injection (fuel staging) is the result of severe quenching by dilution air addition downstream of the fuel injection site. Examination of the detailed model predictions indicates that for the particular configuration investigated, insufficient time has been provided for the rate limiting processes of fuel droplet vaporization and chemical reaction of the secondary fuel.

The degree of agreement obtained between the predicted and experimentally measured values of CO and UHC concentrations, both within the burner and at the exhaust plane, indicate that the modeling approach is fundamentally sound. In addition, the generally good agreement in absolute level obtained for CO concentration indicates that the CO mechanism incorporated in the model is correct. There are, however, significant instances where the model is unable to predict the observed levels and trends. The most serious shortcomings are the generally high predicted values of UHC in the exhaust and the lack of a strong trend with changes in inlet temperature. Extensive experimentation with the analytical model has indicated that these problems will not be rectified by simple changes in kinetic rates, fuel distribution, or other items that constitute the input data. Rather, the discrepancies noted in this section indicate a degree of inadequacy in the combustion models as presently formulated, particularly the physical model treating fuel-air mixture preparation prior to and during burning. Once identified, those aspects of the model requiring further development can be treated on an individual basis.

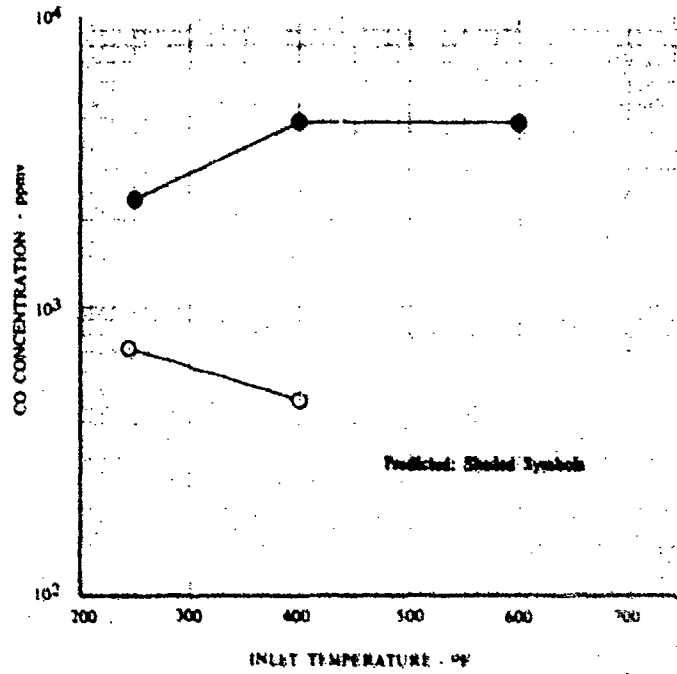


Figure 163. Comparison of Predicted and Measured Variations in CO Concentration with Inlet Air Temperature (Scheme 1-1B, FA = 0.0082, Reference Velocity = 100 fps) DF 96125

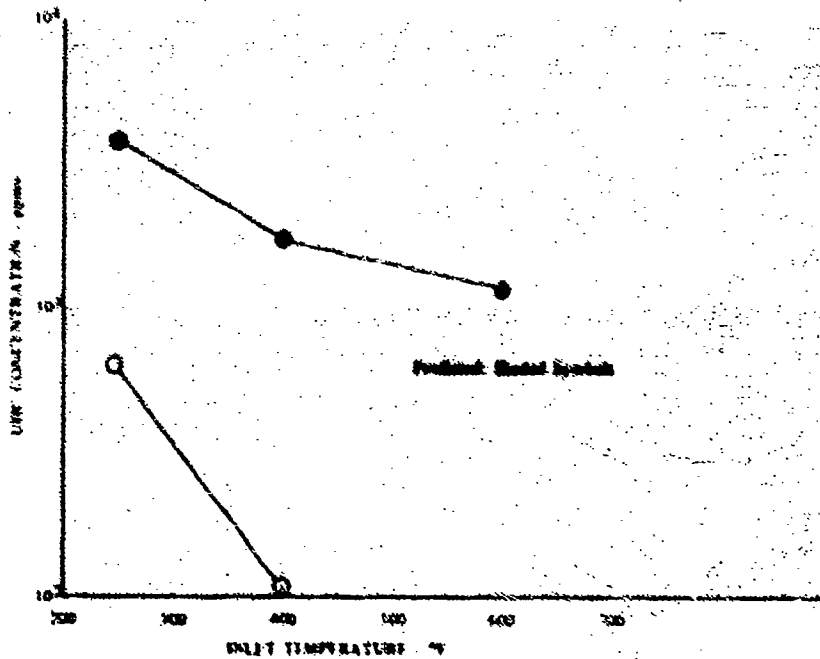


Figure 164. Comparison of Predicted and Measured Variations in UHC Concentration with Inlet Air Temperature (Scheme 1-1B, FA = 0.0082, Reference Velocity = 100 fps) DF 96126

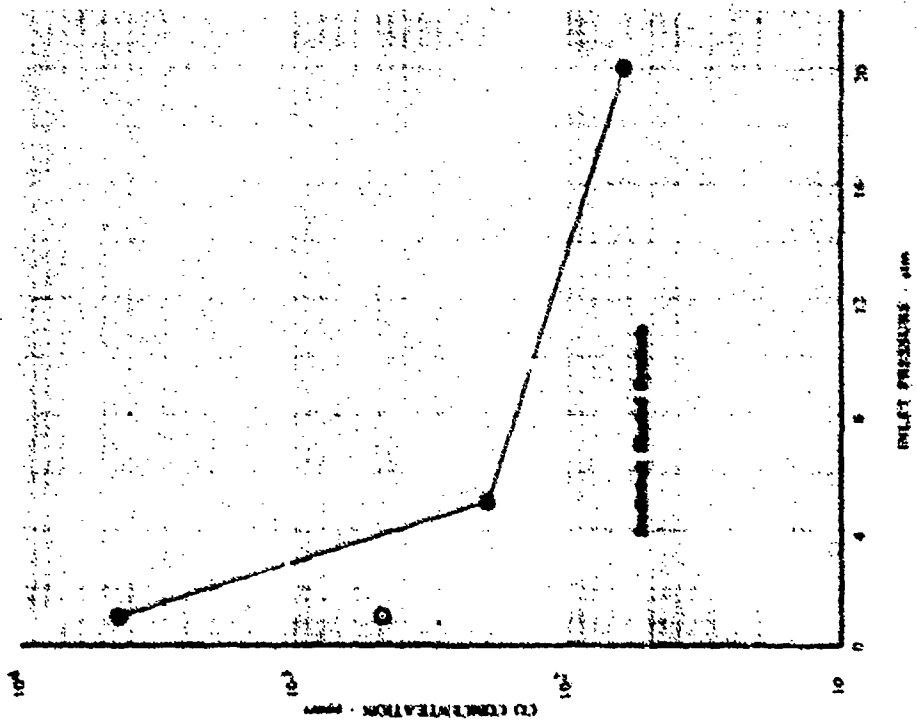


Figure 165. Comparison of Predicted and Measured Variations in CO Concentration with Inlet Air Pressure (Scheme 1-1B, FA = 0.0082, Reference Velocity = 100 fps)

DF 96127

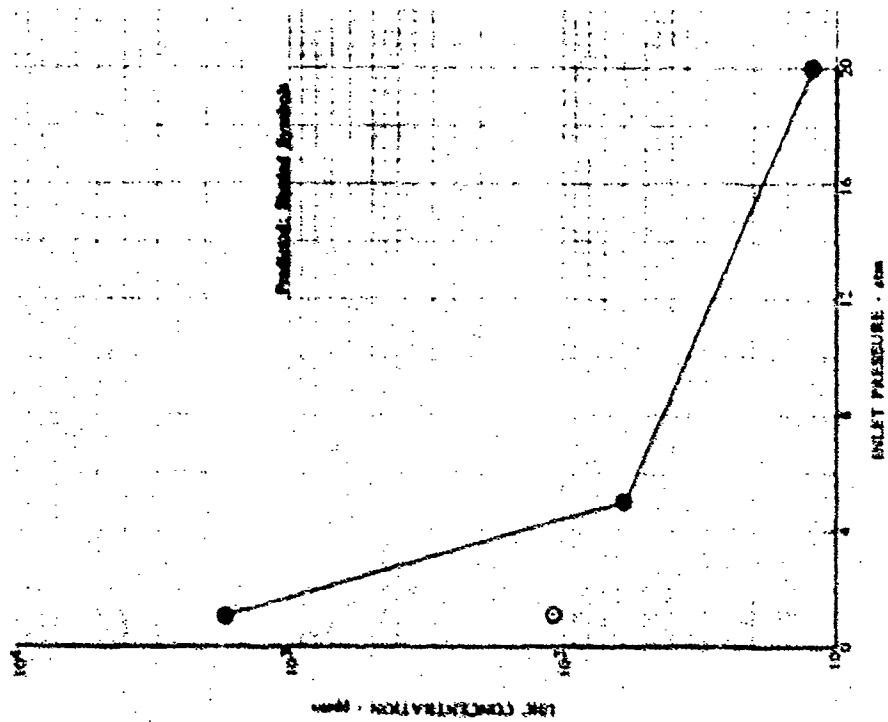


Figure 166. Comparison of Predicted and Measured Variations in UHC Concentration with Inlet Air Pressure (Scheme 1-1B, FA = 0.0082, Reference Velocity = 100 fps)

DF 96128

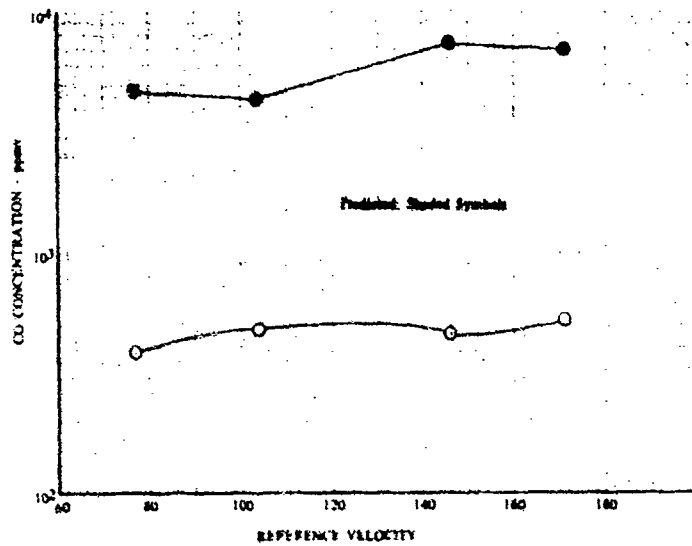


Figure 167. Comparison of Predicted and Measured Variations in CO Concentration with Reference Velocity (Scheme 1-1B, FA = 0.0082, Inlet Air Temp = 400° F) DF 96129

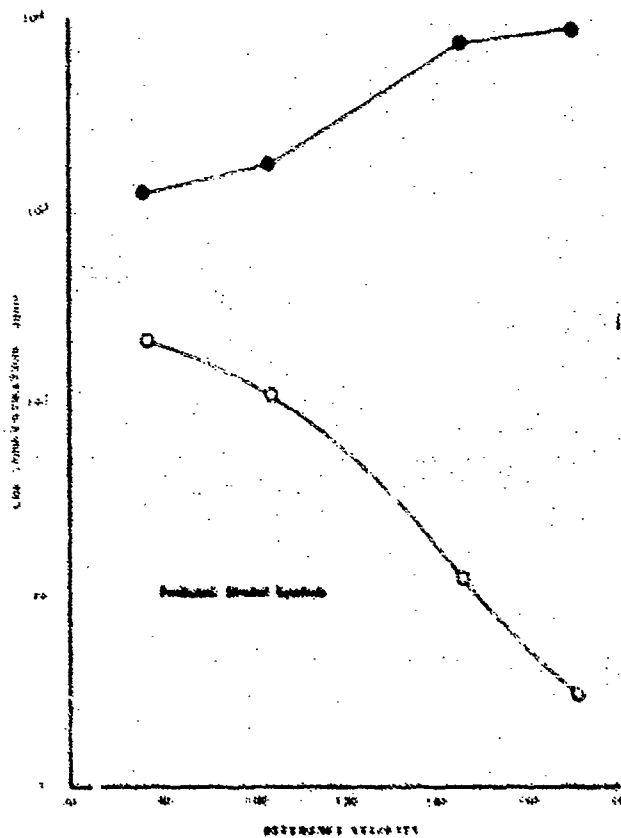


Figure 168. Comparison of Predicted and Measured Variations in UHC Concentration with Reference Velocity (Scheme 1-1B, FA = 0.0082, Reference Velocity = 100 fps) DF 96130

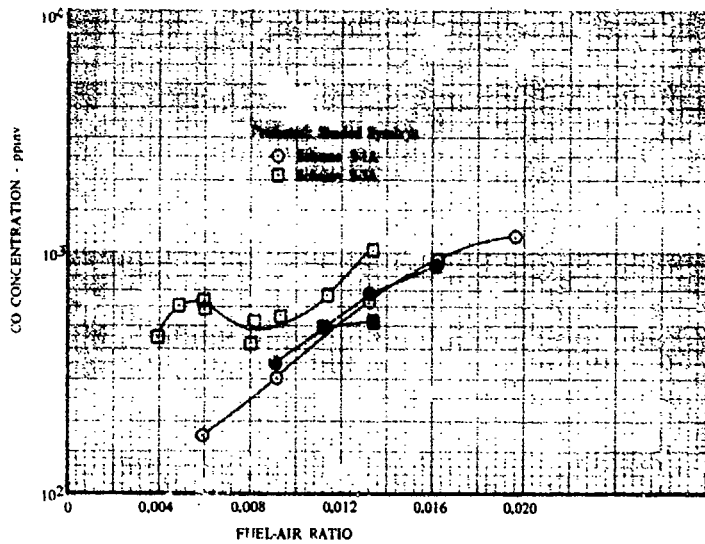


Figure 169. Comparison of Predicted and Measured Variations in CO Concentration with FA for Pressure-Atomizing and Air-Blast Fuel Nozzles DF 96131

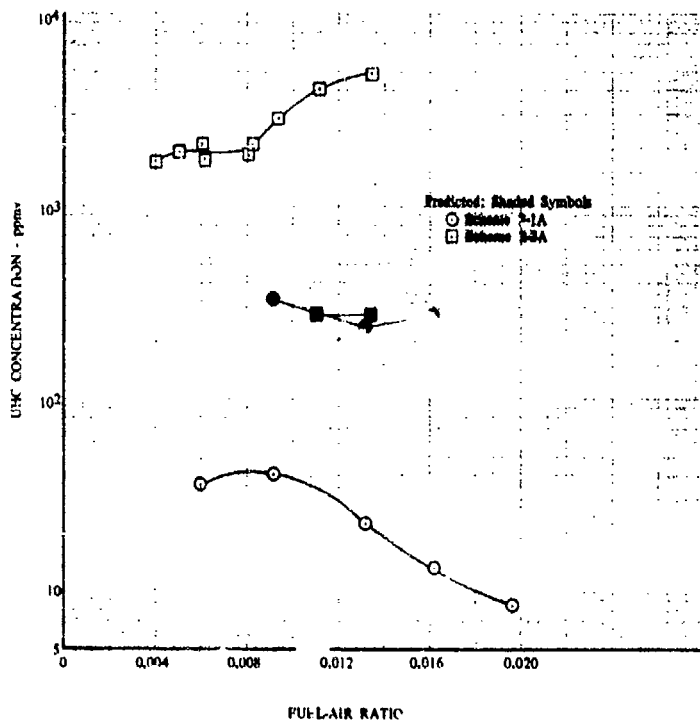


Figure 170. Comparison of Predicted and Measured UHC Concentration with FA for Pressure-Atomizing and Air-Blast Fuel Nozzles DF 96132

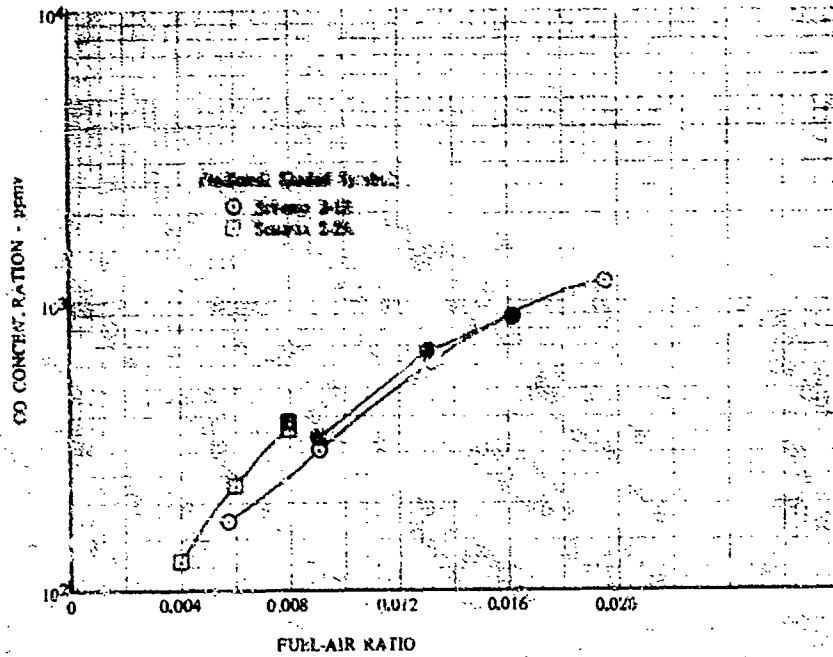


Figure 171. Comparison of Predicted and Measured CO Concentration with FA for Tests Demonstrating the Effect of Dome Cooling DF 96133

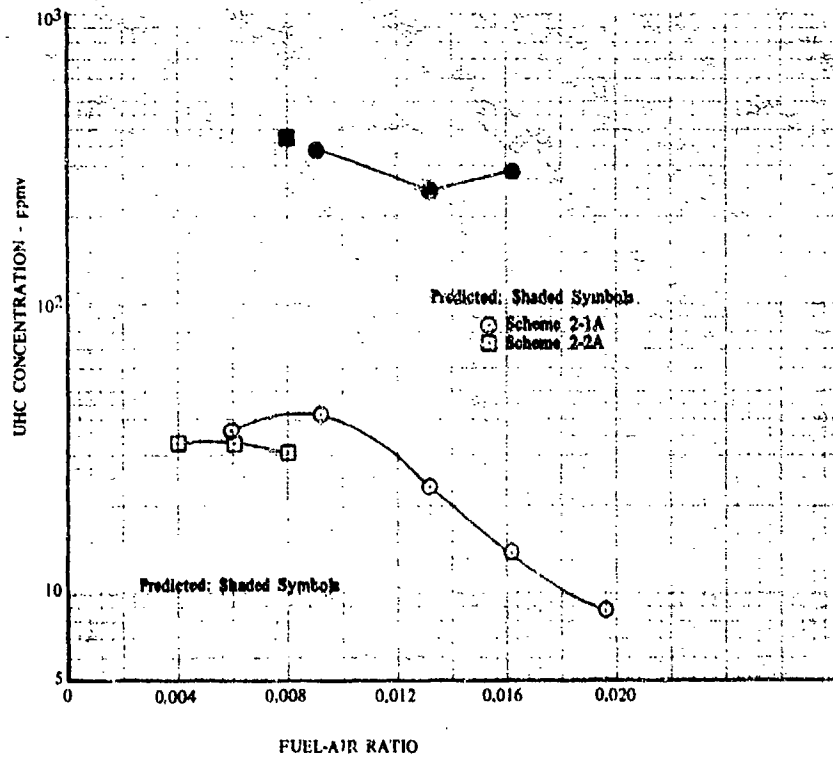


Figure 172. Comparison of Predicted and Measured UHC Concentration with FA for Tests Demonstrating the Effect of Dome Cooling DF 96134

SECTION VI

NOMENCLATURE FOR TEST DATA SUMMARY

The following nomenclature was used for the test data summary.

<u>Symbol</u>	<u>Definition</u>	<u>Units</u>
PSAR	Primary to secondary airflow ratio	-
FA	Overall fuel-air ratio	-
PHIP	Primary zone equivalence ratio	-
PSFR	Primary to secondary fuel flow ratio	-
PHINT	Intermediate zone equivalence ratio	-
TT3	Combustor inlet total temperature	°F
VREF	Combustor reference velocity	ft/sec
LPL	Combustor total pressure loss	%
EFFMB	Combustor efficiency from temperature measurements	%
EFFGA	Combustor efficiency from gas analysis measurements	%
PT3	Combustor inlet total pressure	psia
X	Mean absolute humidity	lb _m H ₂ O/lb _m dry air

The following symbols refer to overall average exit concentrations of the noted species.

HCTOA	UHC volumetric concentration	ppmv
HCTPW	UHC mass concentration	ppmw
HCTDX	UHC emission index	lb _m UHC/1000 lb _m JP-5
COOA	CO volumetric concentration	ppmv
COPW	CO mass concentration	ppmw
CODX	CO emission index	lb _m CO/1000 lb _m JP-5
NOOA	NO volumetric concentration	ppmv
NOPW	NO mass concentration	ppmw
NODX	NO emission index	lb _m NO/1000 lb _m JP-5
NO2OA	NO ₂ volumetric concentration	ppmv
NO2PW	NO ₂ mass concentration	ppmw
NO2DX	NO ₂ emission index	lb _m NO ₂ /1000 lb _m JP-5
NOXOA	NO _x volumetric concentration	ppmv
NOXPW	NO _x mass concentration	ppmw
NOXDX	NO _x emission index	lb _m NO _x /1000 lb _m JP-5
CO2OA	CO ₂ volumetric concentration	ppmv
CO2PW	CO ₂ mass concentration	ppmw
CO2DX	CO ₂ emission index	lb _m CO ₂ /1000 lb _m JP-5

APPENDIX I

JT8D COMBUSTOR CONCENTRATION AND FUEL-AIR RATIO PROFILES

Concentration and fuel-air ratio profiles obtained during probing tests on the JT8D combustor are shown in figures 173 through 184.

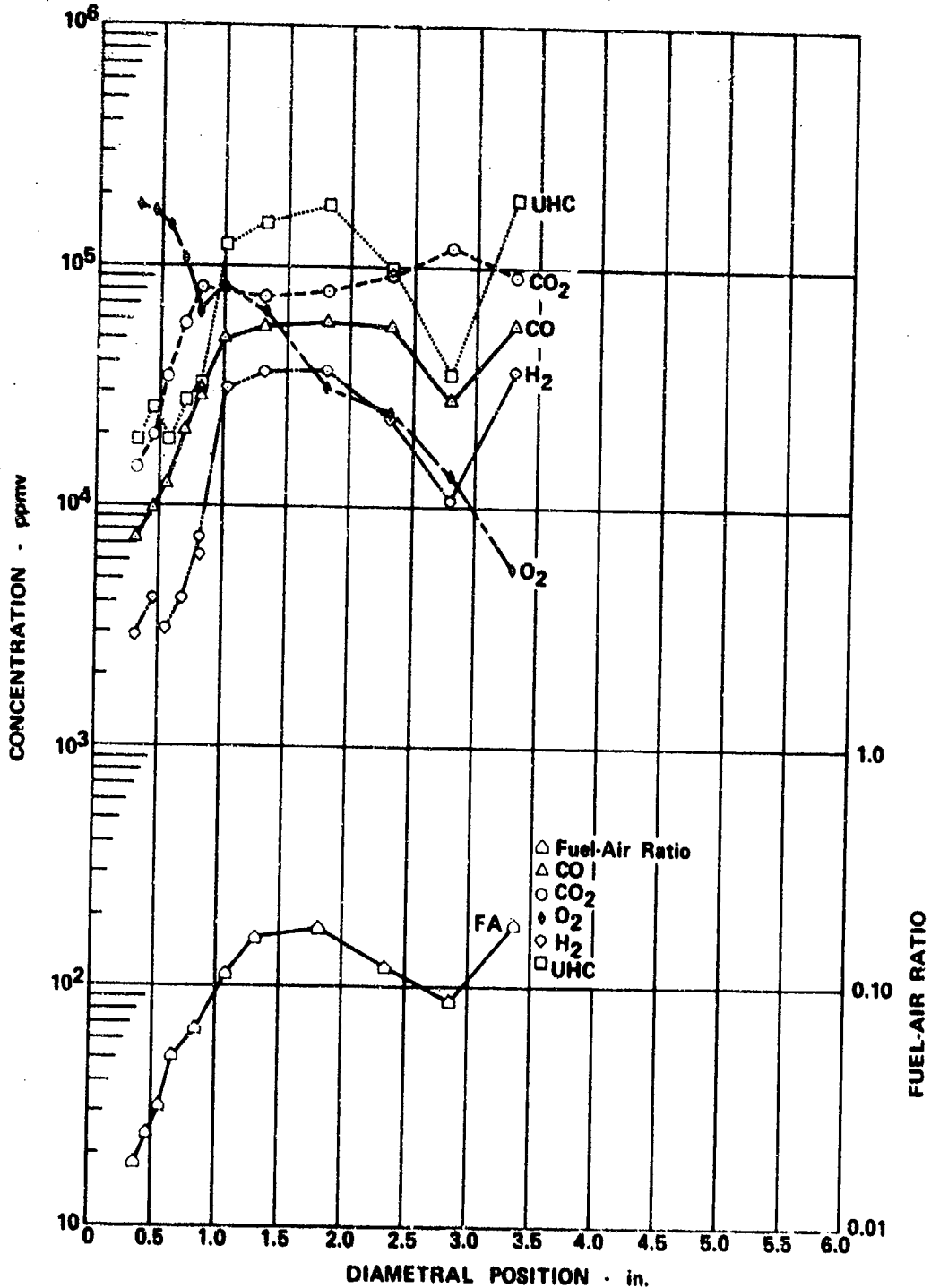


Figure 173. Variation in FA and Concentration of Combustion Products with Diametral Position (Position 1B, Idle Operation)

FD 72121

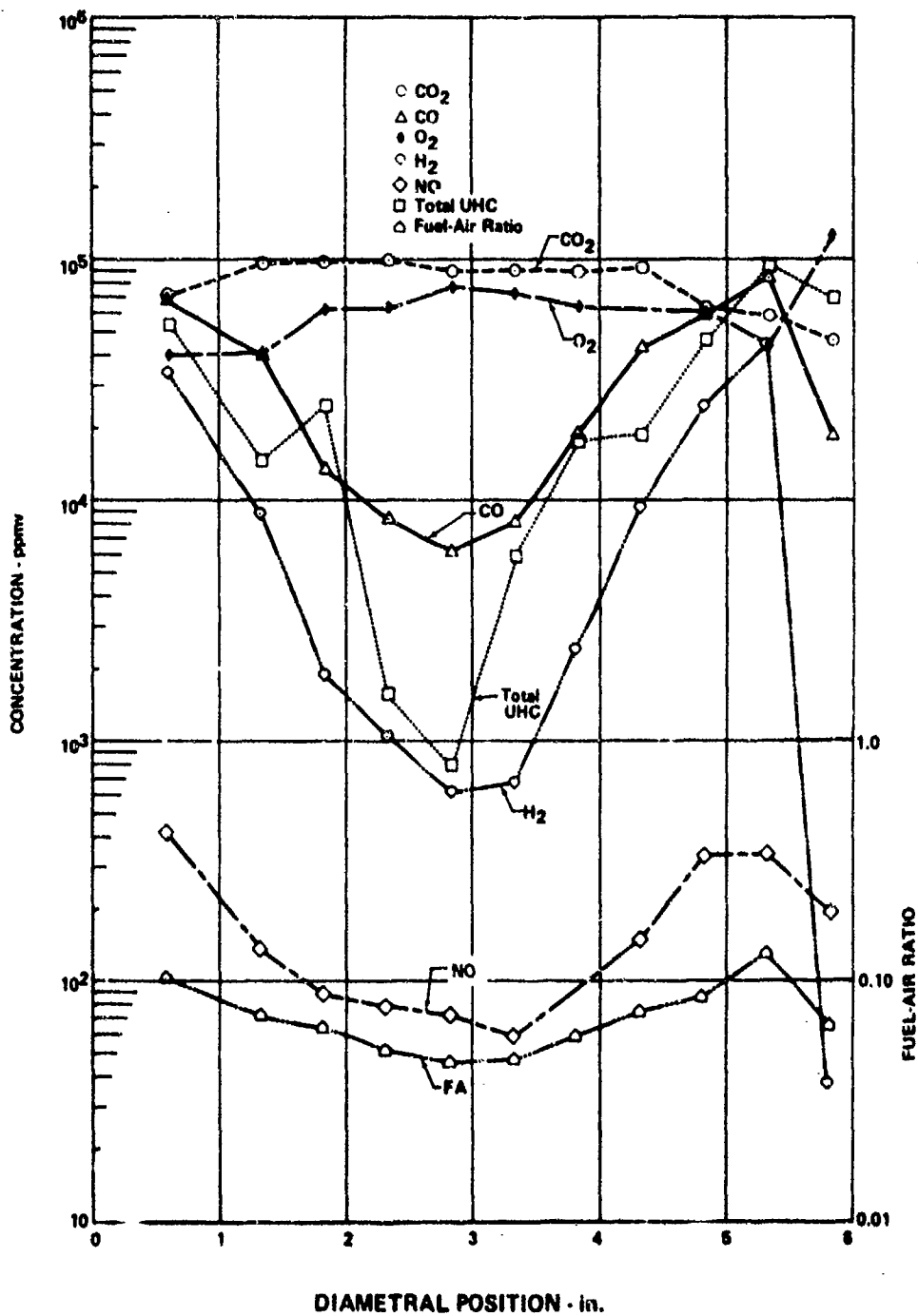


Figure 174. Variation in FA and Concentration of Combustion Products with Diametral Position (Positon 2A, Idle Operation)

FD 72122

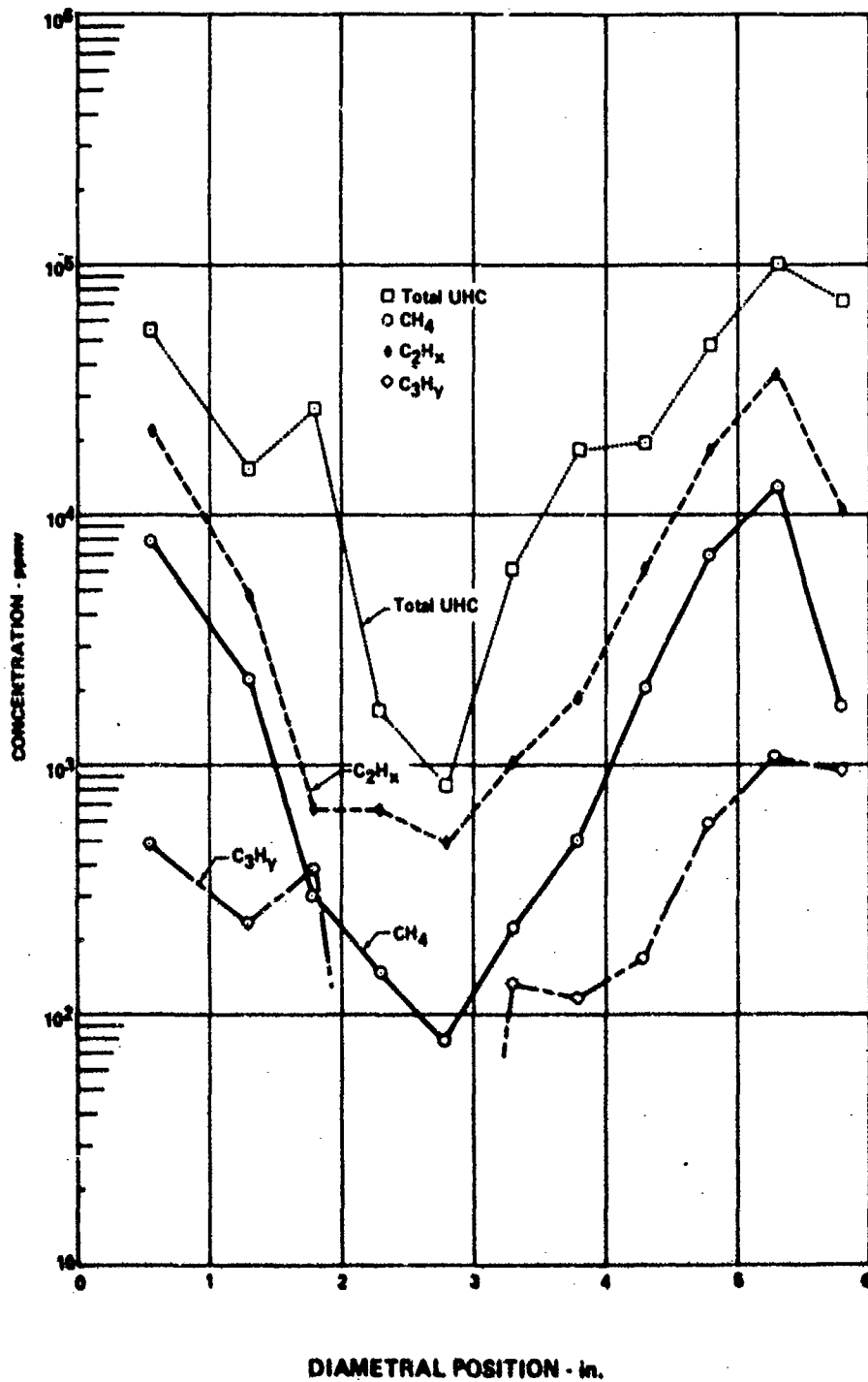


Figure 175. Variation in UHC Concentrations with Diametral Position (Position 2A, Idle Operation)

FD 72123

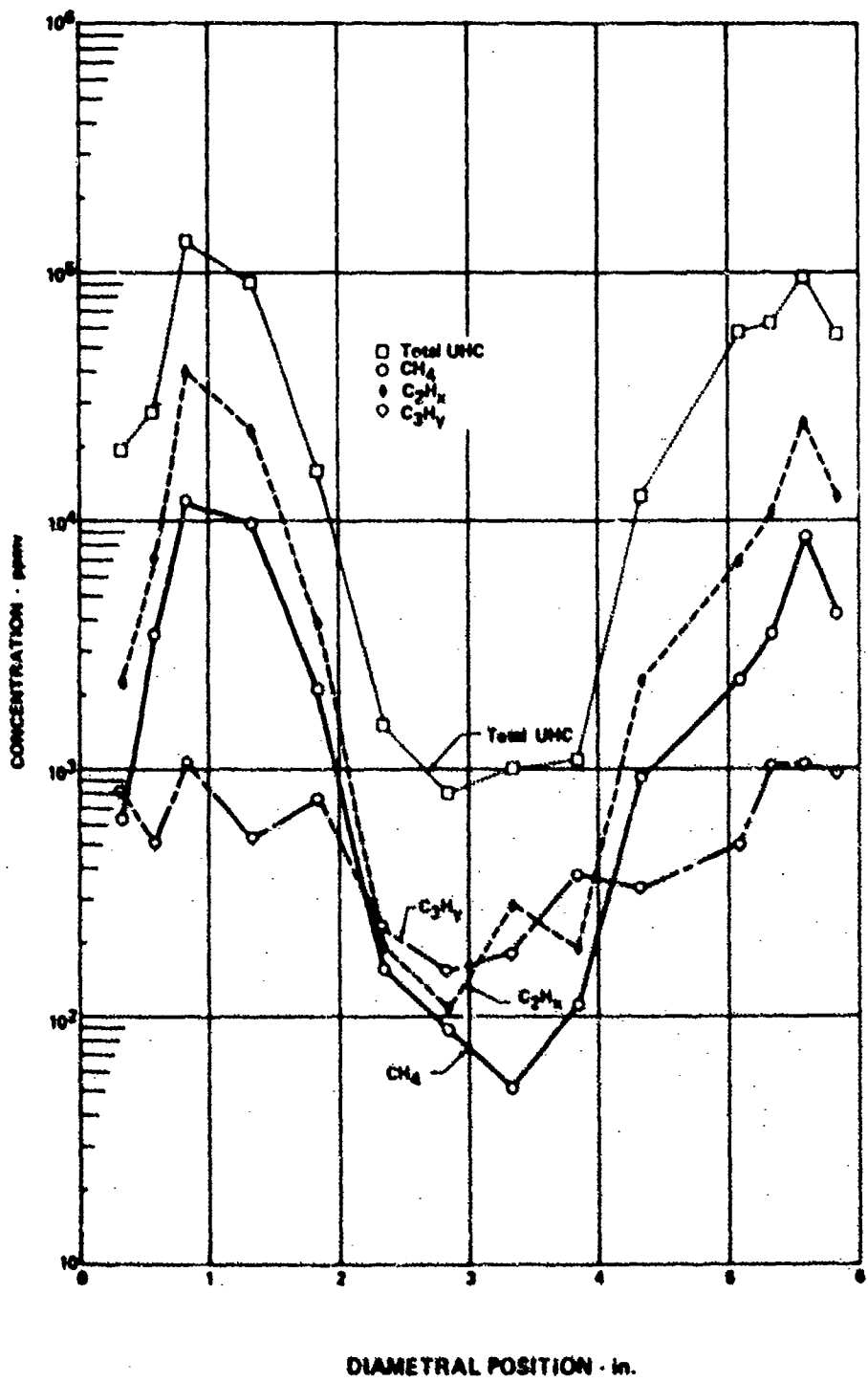


Figure 176. Variation in FA and Concentration of Combustion Products with Diametral Position (Position 2B, Idle Operation)

FD 72124

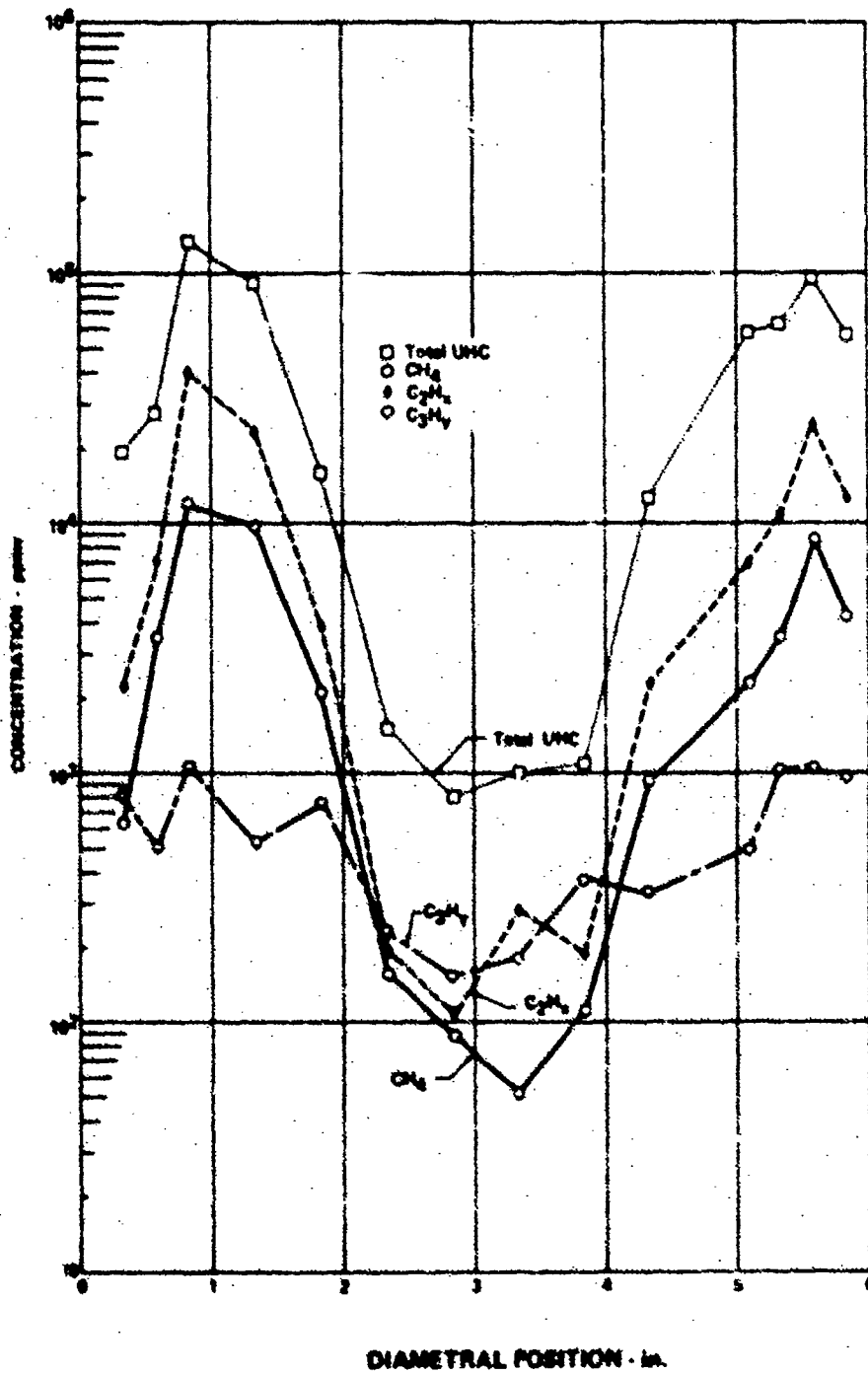


Figure 177. Variation in UHC Concentrations with Diametral Position (Position 2B, Idle Operation)

FD 72125

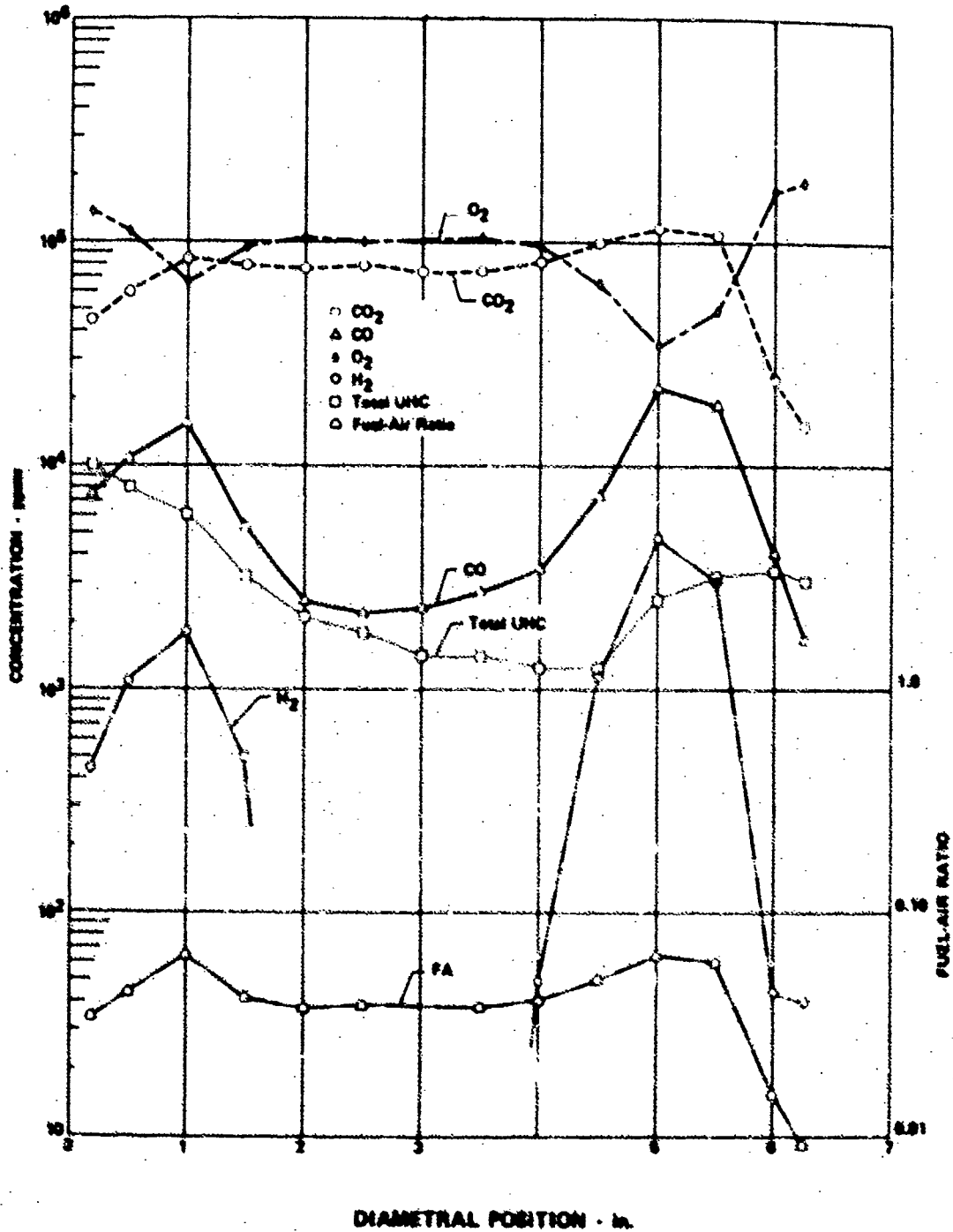


Figure 178. Variation in FA and Concentrations of Combustion Products with Diametral Position (Position 3A, Idle Operation)

FD 72126

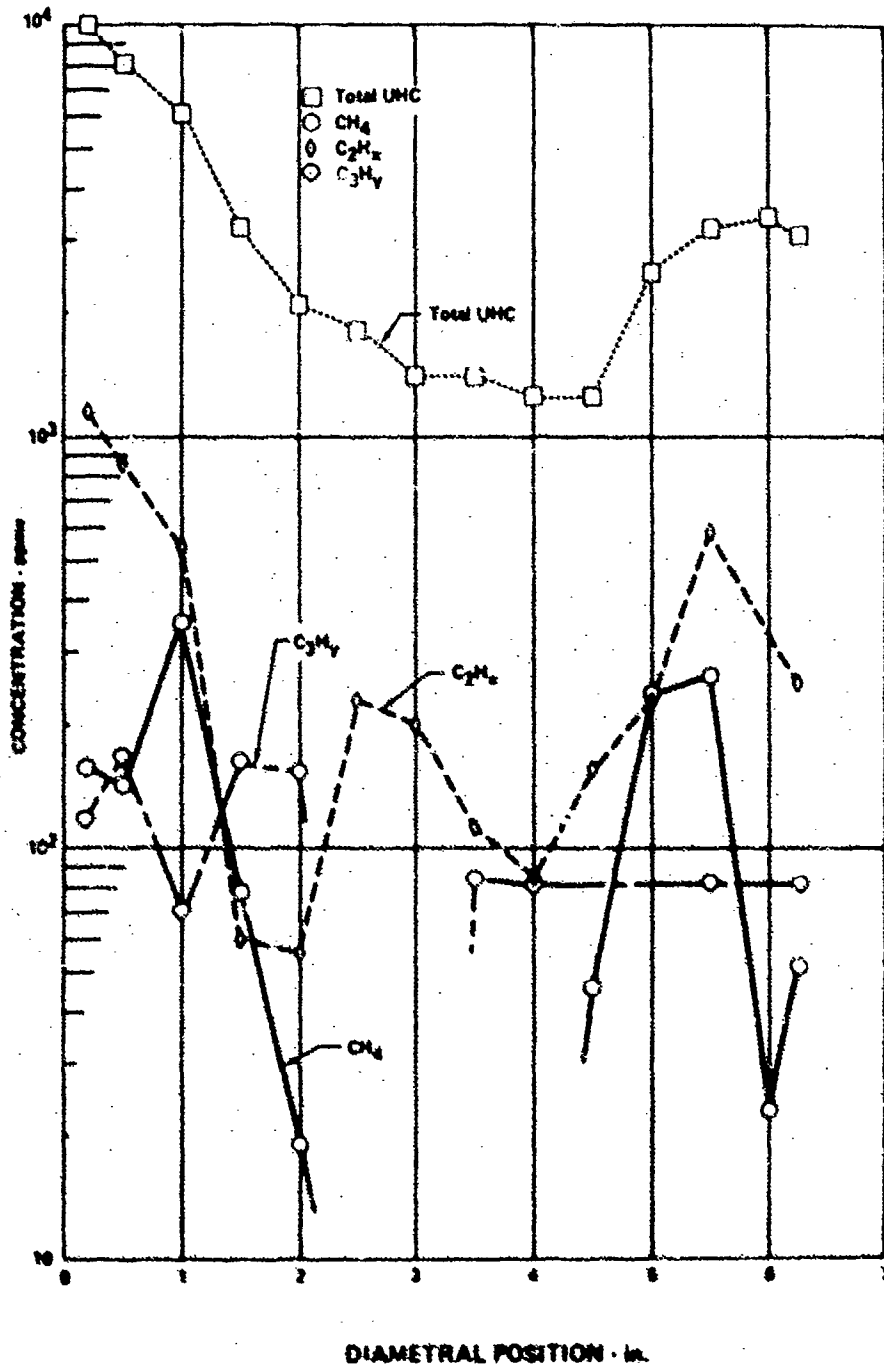


Figure 179. Variation in UHC Concentrations with Diametral Position (Position 3A, Idle Operation)

FD 72127

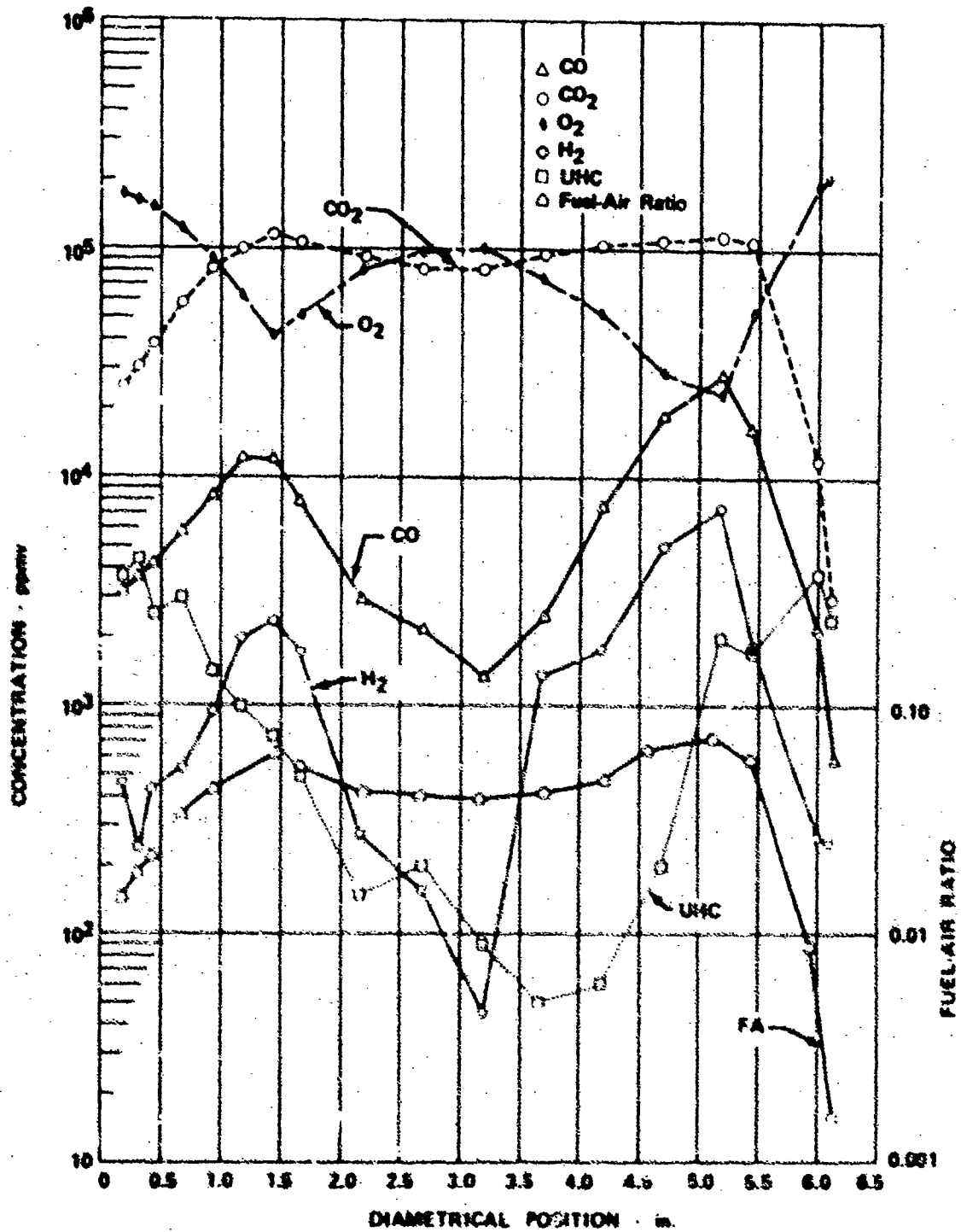


Figure 180. Variation in FA and Concentrations of Combustion Products with Diametral Position (Position 3B, Idle Operation)

FD 72128

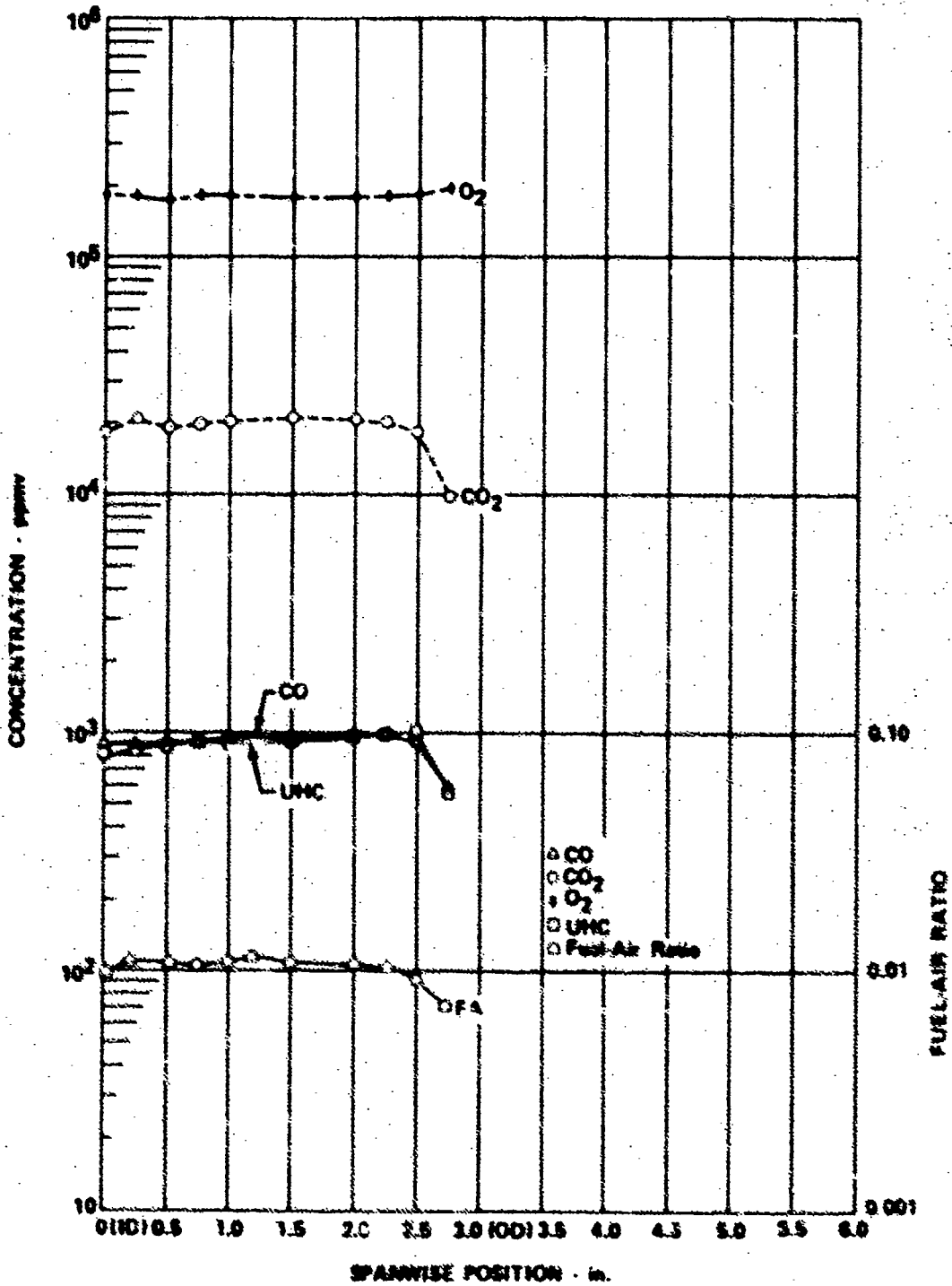


Figure 181. Variation in FA and Concentrations of Combustion Products with Spanwise Position (Exhaust Location, Idle Operation)

FD 73129

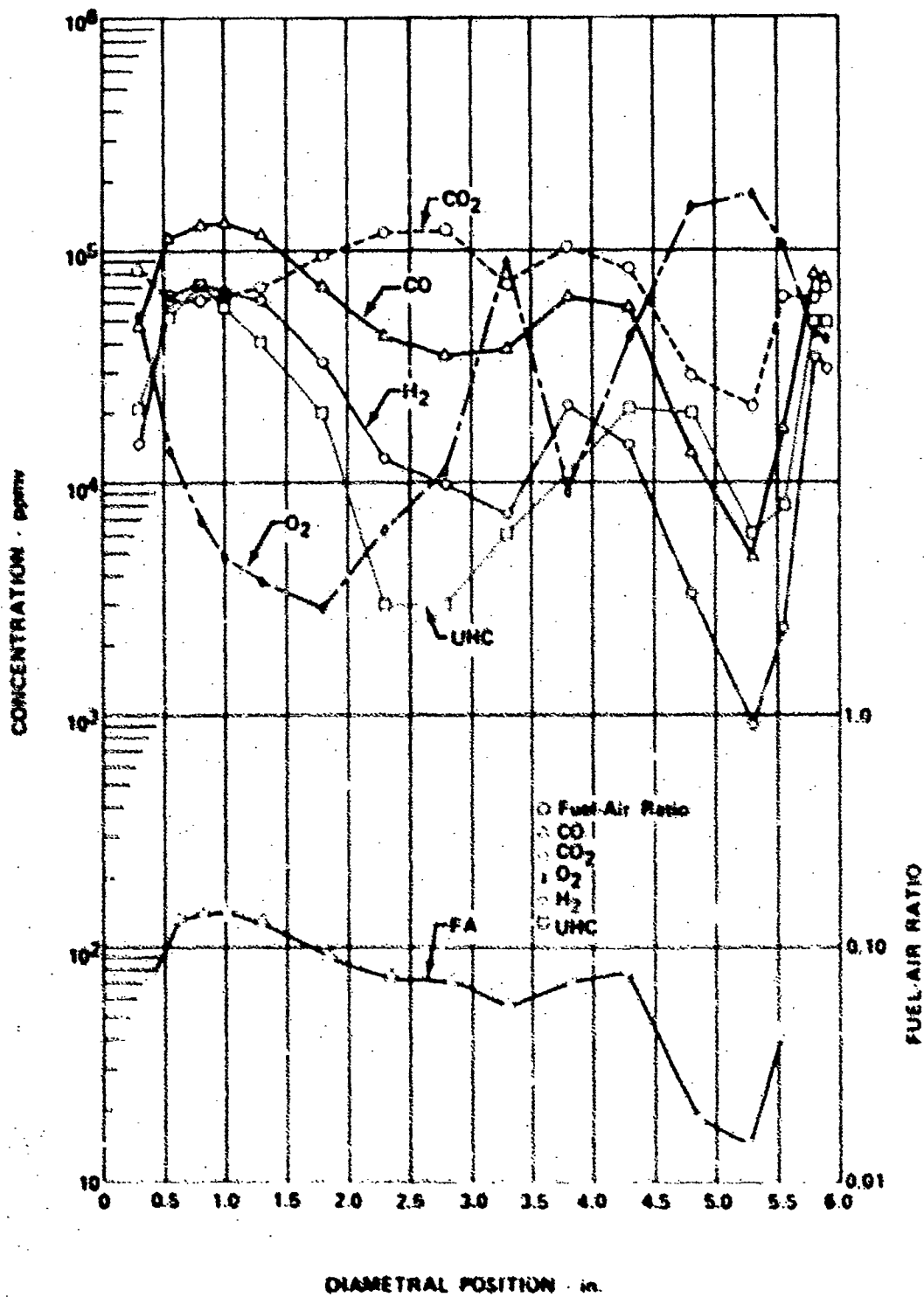


Figure 182. Variation in FA and Concentrations of Combustion Products with Diametral Position (Position 2E, Approach Operation)

FD 7:130

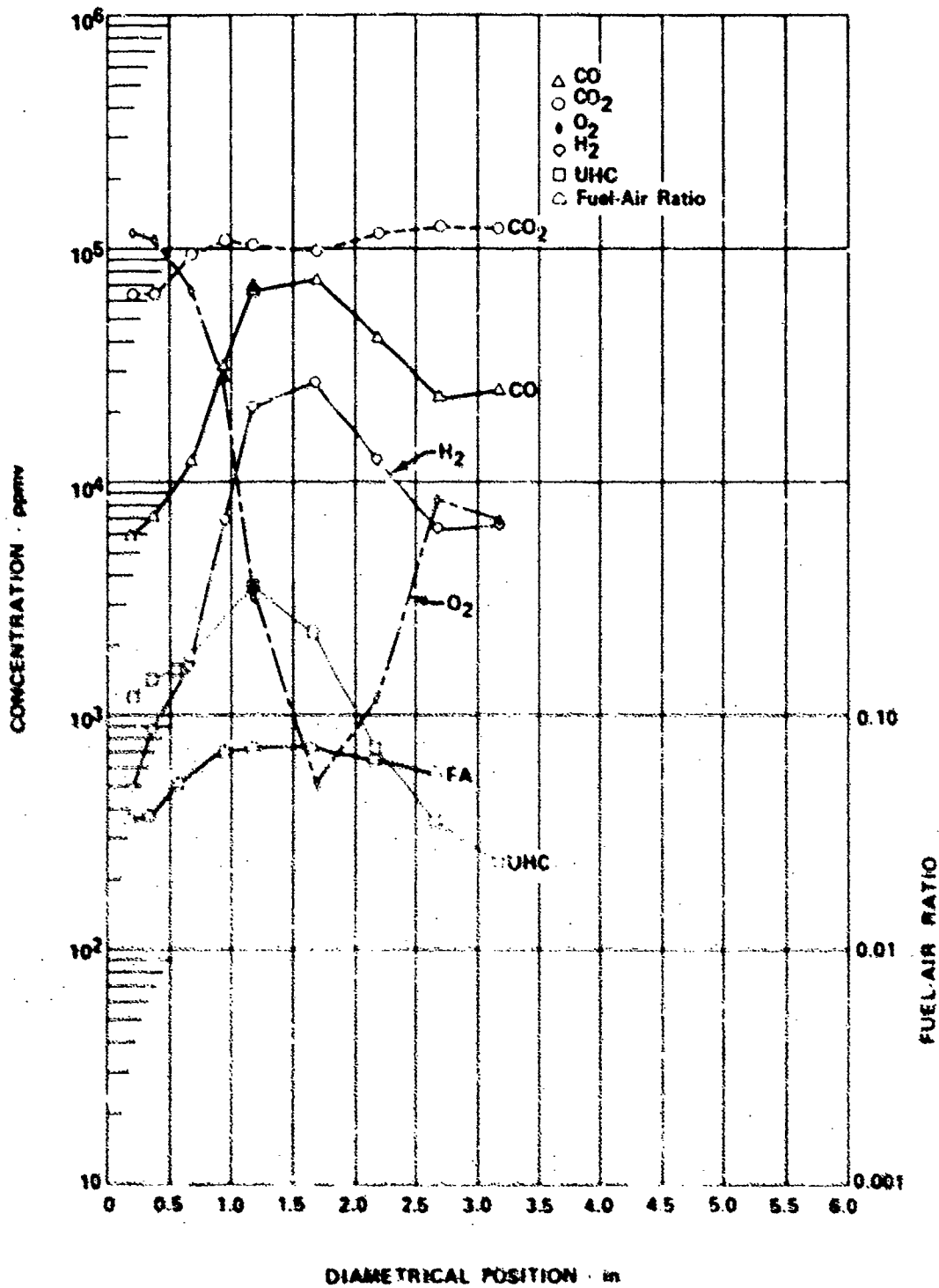


Figure 183. Variation in FA and Concentrations of Combustion Products with Diametral Position (Position 3B, Approach Operation) FD 72131

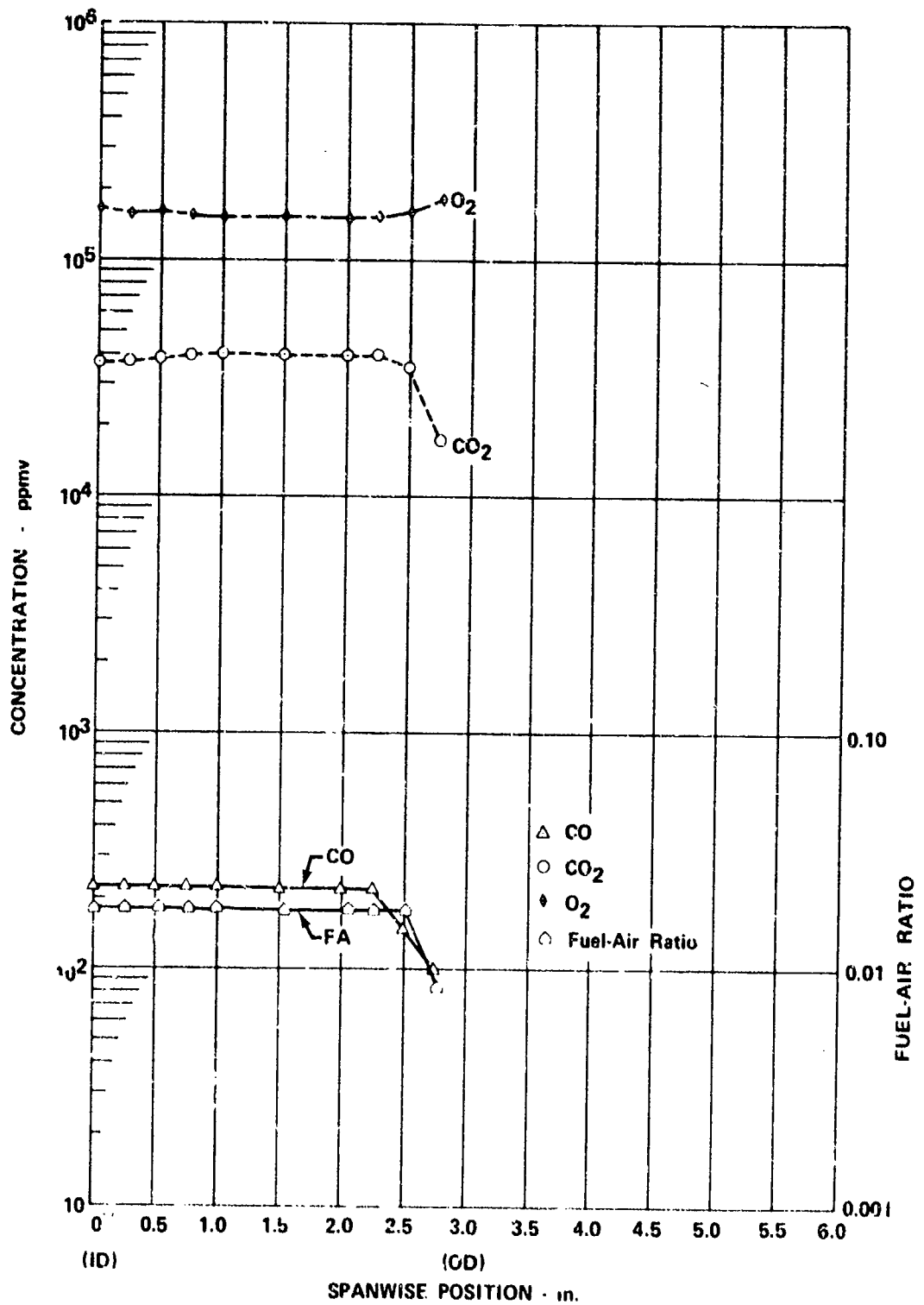


Figure 184. Variation in FA and Concentrations of Combustion Products with Spanwise Position (Exhaust Location, Approach Operation)

FD 72132

APPENDIX II

COMBUSTION EFFICIENCY AND TEMPERATURE PROFILES

Combustion efficiency and temperature profiles obtained during probing tests of the JT8D combustor are shown in figures 185 through 192.

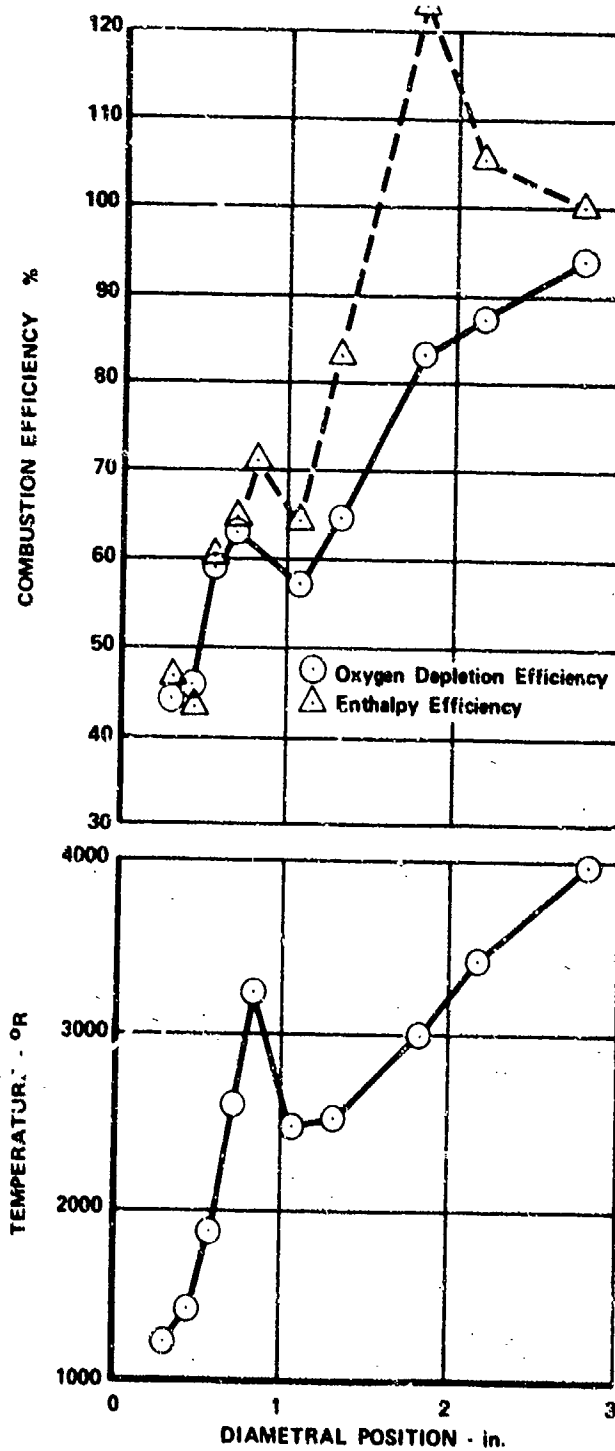


Figure 185. Variation in Combustion Efficiency and Temperature with Diametral Position (Probe Location 1B, Idle Operation)

FD 72133

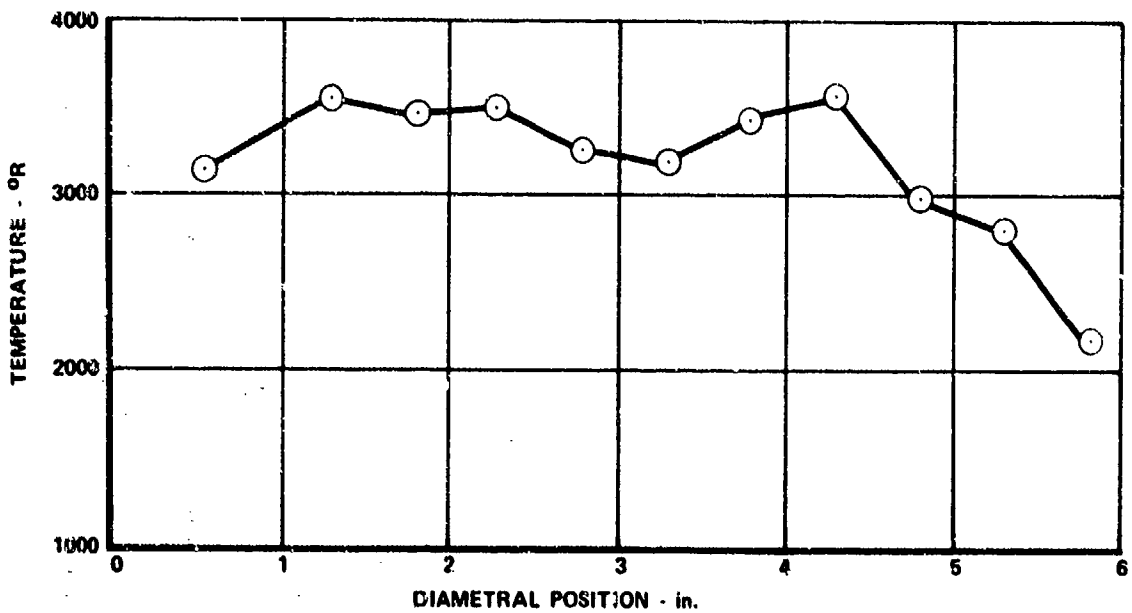
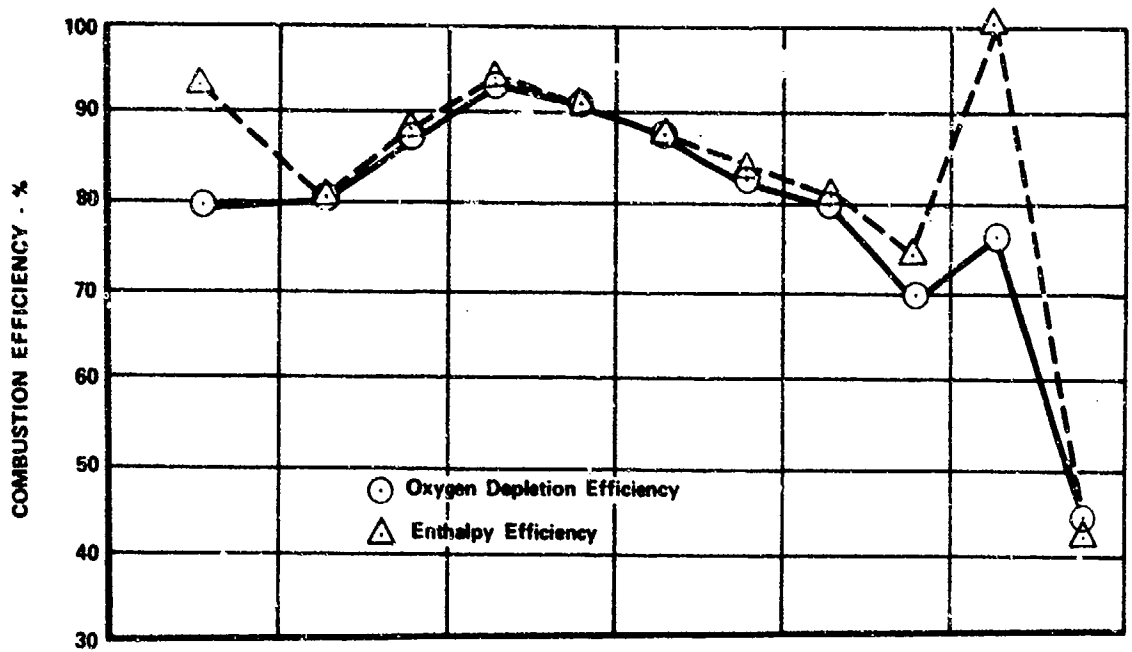


Figure 186. Variation in Combustion Efficiency and Temperature with Diametral Position (Probe Location 2A, Idle Operation)

FD 72134

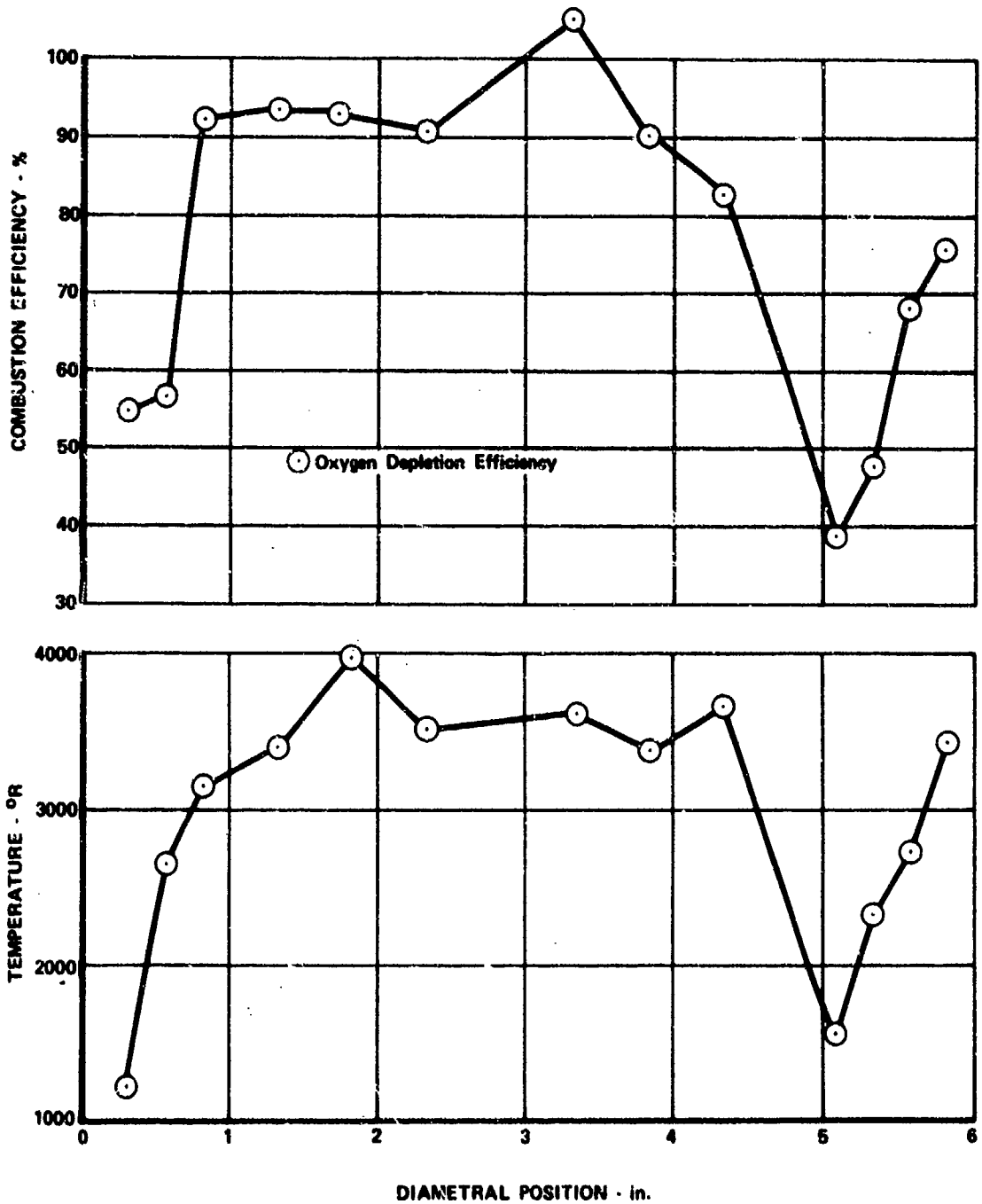


Figure 187. Variation in Combustion Efficiency and Temperature with Diametral Position (Probe Location 2B, Idle Operation)

FD 72135

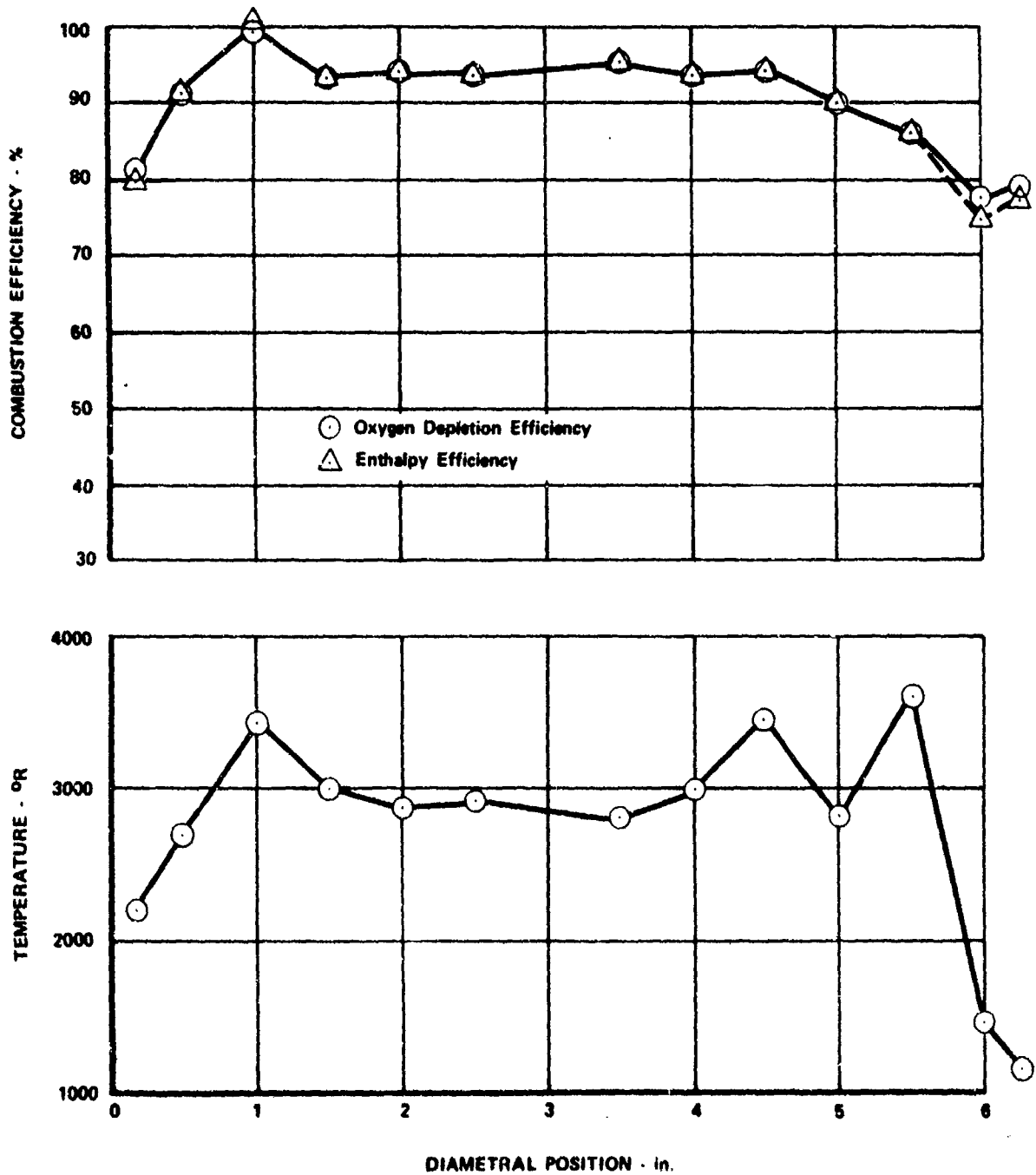


Figure 188. Variation in Combustion Efficiency and Temperature with Diametral Position (Probe Location 3A, Idle Operation)

FD 72136

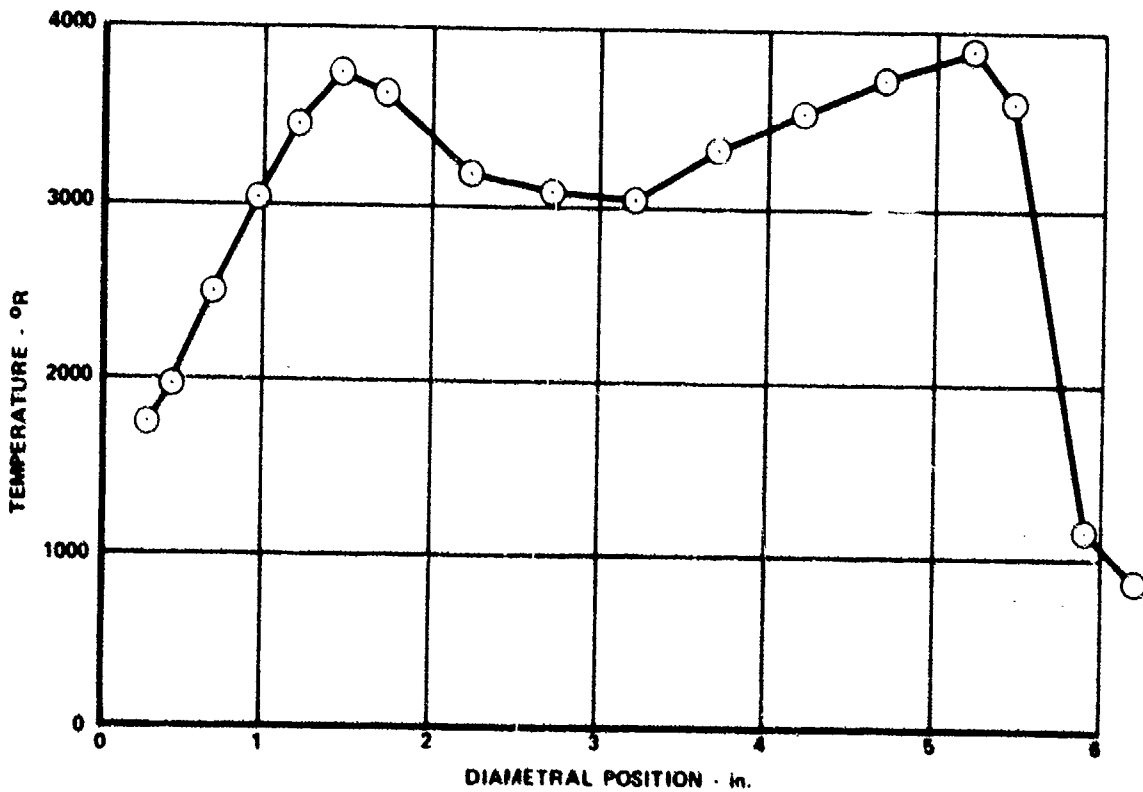
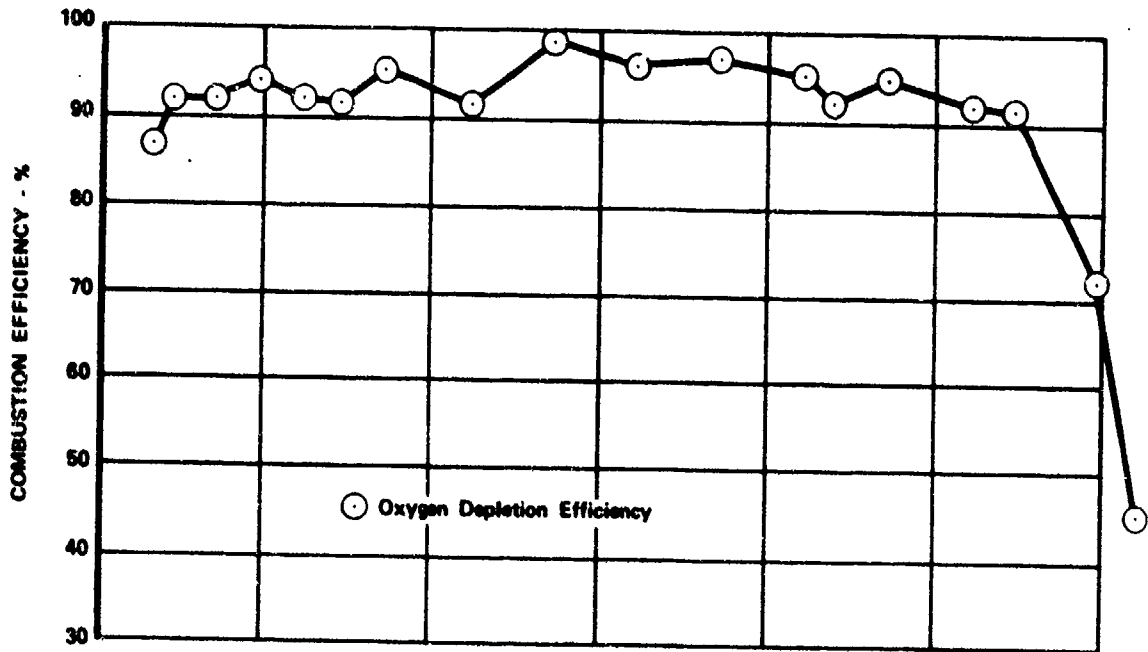


Figure 189. Variation in Combustion Efficiency and Temperature with Diametral Position (Probe Location 3B, Idle Operation)

FD 72137

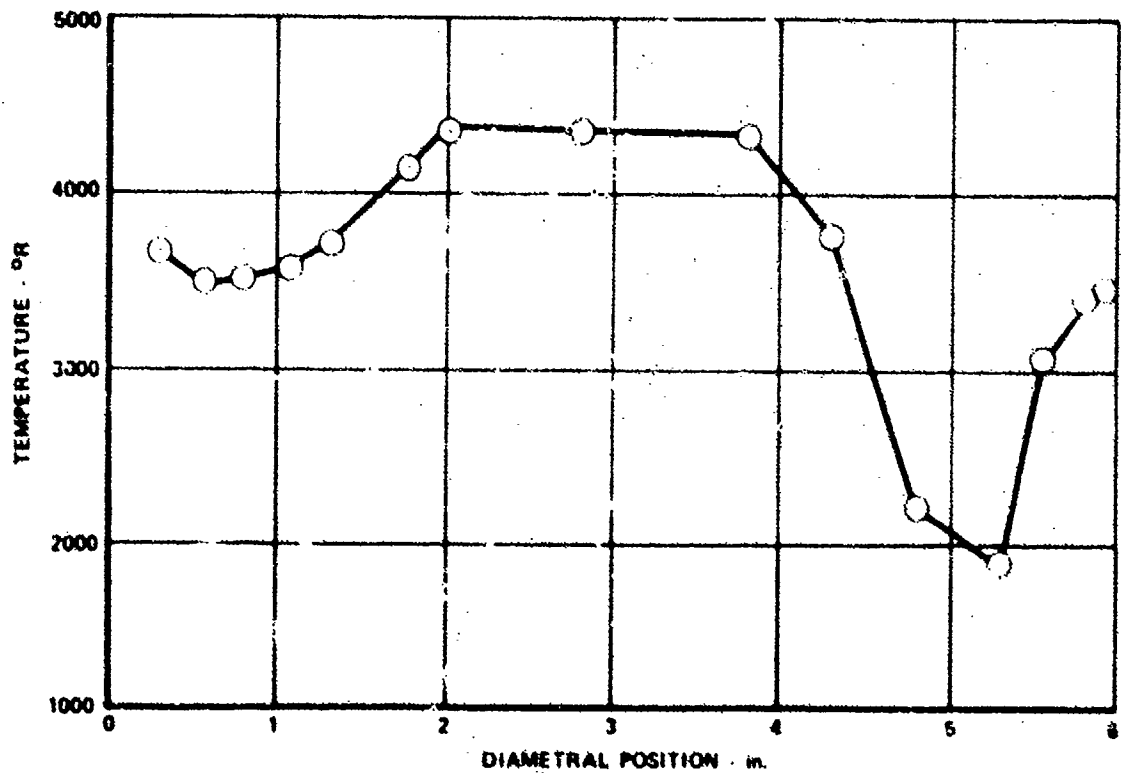
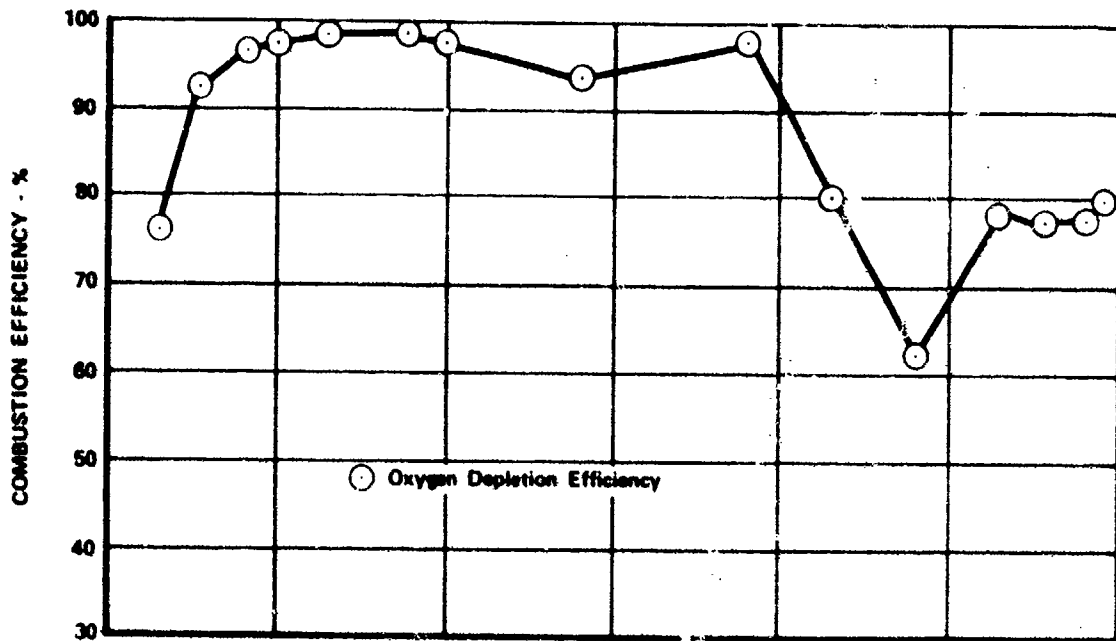


Figure 190. Variation in Combustion Efficiency and Temperature with Diametral Position (Probe Location 2B, Approach Operation)

FD 72138

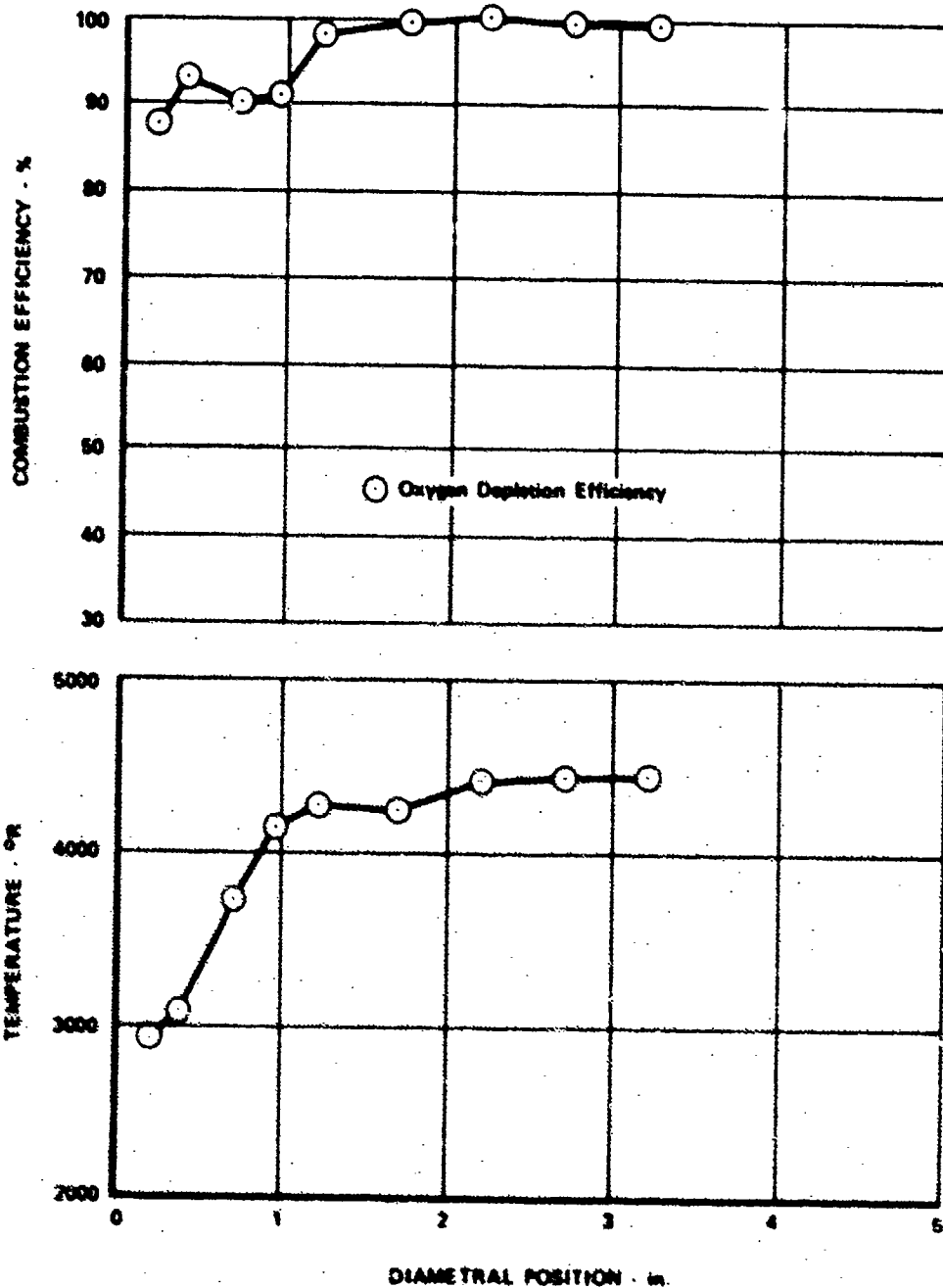


Figure 191. Variation in Combustion Efficiency and Temperature with Diametral Position (Probe Location 3B, Approach Operation)

FD 72139

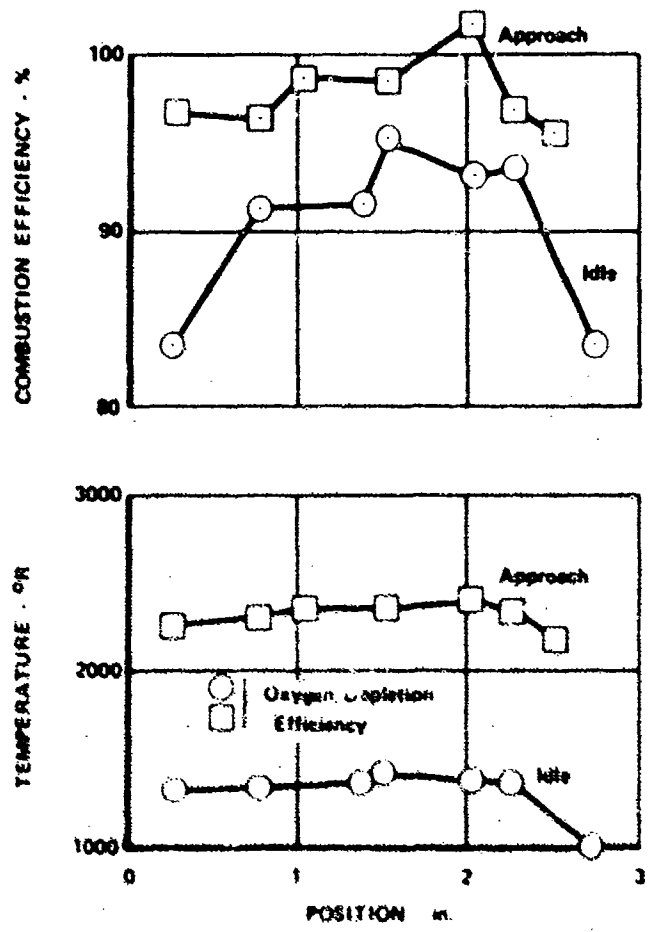


Figure 192. Variation in Combustion Efficiency and Temperature with Position at The Combustor Exit (Idle and Approach Operations)

FD 72140

APPENDIX III

PROCEDURE FOR CALCULATING REACTION RATES FOR FUEL AND CO

This appendix describes a procedure for calculating the reaction rates for fuel and CO as a part of the turbulent flame laboratory studies.

Reaction rates are first determined by solving the continuity expression, equation 33, below, for the particular species of interest. As will be shown, some simplification can be gained by solving for the reaction rate at points where at least one of the variables is known to be zero. With reference to the nomenclature of figure 193, the continuity expression for the species of interest (j) is

$$\rho U_x \frac{\partial C_j}{\partial x} + \rho U_y \frac{\partial C_j}{\partial y} + \rho U_z \frac{\partial C_j}{\partial z} - \left(\frac{\partial \epsilon}{\partial x} \frac{\partial C_j}{\partial x} + \frac{\partial \epsilon}{\partial y} \frac{\partial C_j}{\partial y} + \frac{\partial \epsilon}{\partial z} \frac{\partial C_j}{\partial z} \right) - \epsilon \left(\frac{\partial^2 C_j}{\partial x^2} + \frac{\partial^2 C_j}{\partial y^2} + \frac{\partial^2 C_j}{\partial z^2} \right) = Q_j \quad (33)$$

where

C_j = concentration of the species (j)

ϵ = turbulent diffusivity

ρ = density

U_x, U_y, U_z = are the velocities in X, Y, and Z directions

X = distance downstream of the flameholder

Y = direction normal to flow within the sampling plane

Z = direction normal to Y

Q_j = reaction rate for species j

Assuming that the flame is two dimensional, i.e., that no variation occurs in the Z direction, equation 33 becomes:

$$\rho U_x \frac{\partial C_j}{\partial x} + \rho U_y \frac{\partial C_j}{\partial y} - \left(\frac{\partial \epsilon}{\partial x} \frac{\partial C_j}{\partial x} + \frac{\partial \epsilon}{\partial y} \frac{\partial C_j}{\partial y} \right) - \epsilon \left(\frac{\partial^2 C_j}{\partial x^2} + \frac{\partial^2 C_j}{\partial y^2} \right) = Q_j \quad (34)$$

Some simplification is obtained by solving for Q_j at $\partial C_j / \partial y = 0$; then equation 34 becomes:

$$\rho U_x \frac{\partial C_j}{\partial x} - \frac{\partial \epsilon}{\partial x} \frac{\partial C_j}{\partial x} - \epsilon \frac{\partial^2 C_j}{\partial x^2} - \epsilon \frac{\partial^2 C_j}{\partial y^2} = Q_j \quad (35)$$

The various derivatives of C_j in equation 35 can be evaluated graphically from the species concentration profiles. The diffusivity terms, however, must be evaluated from the momentum equation as follows:

$$\frac{\partial P}{\partial x} + \frac{\partial(\rho U_x^2)}{\partial x} + \frac{\partial(\rho U_x U_y)}{\partial y} = \frac{\partial}{\partial y} \left(\epsilon \frac{\partial U_x}{\partial y} \right) \quad (36)$$

where P = static pressure.

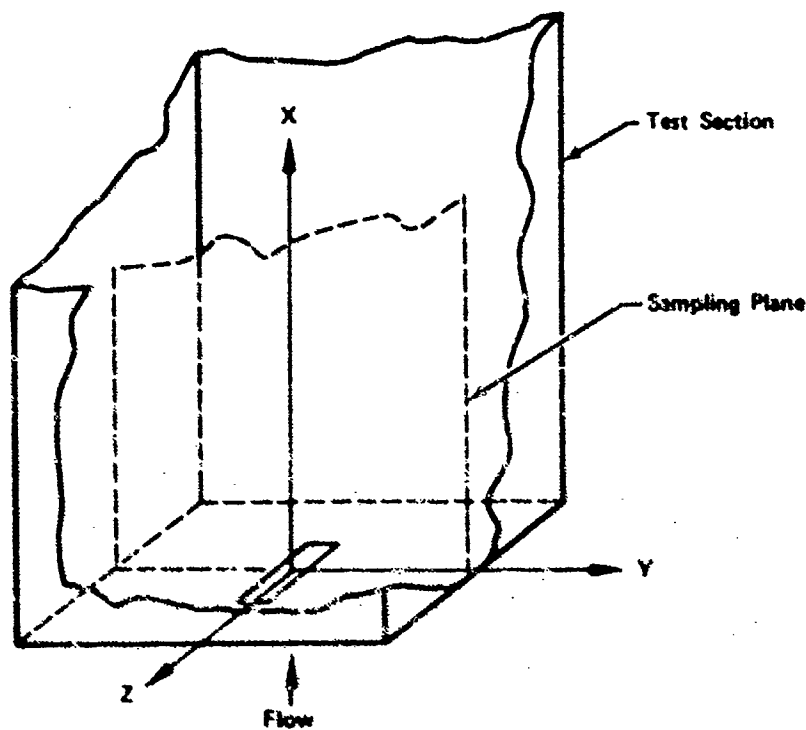


Figure 193. Schematic Diagram Showing Sampling Plane and Coordinate System for Turbulent Flame Rig

FD 72141

Integrating and simplifying,

$$\int_{Y_1}^{Y_2} \frac{\partial p}{\partial x} dy + \int_{Y_1}^{Y_2} \frac{\partial(\rho U_x^2)}{\partial x} dy + \rho U_x U_y \Big|_{Y_2} - \rho U_x U_y \Big|_{Y_1} + \epsilon_2 \frac{\partial U_x}{\partial y} \Big|_{Y_2} - \epsilon_1 \frac{\partial U_x}{\partial y} \Big|_{Y_1} \quad (37)$$

where

$$\left. \begin{array}{l} Y_1 = a(x) \\ Y_2 = b(x) \end{array} \right\} \text{are specified streamlines.}$$

Leibnitz' Theorem applied to the term $\int_{Y_1}^{Y_2} \frac{\partial(\rho U_x^2)}{\partial x} dy$

yields:

$$\int_{a(x)}^{b(x)} \frac{\partial}{\partial x} f(x,y) dy = \frac{d}{dx} \int_{a(x)}^{b(x)} f(x,y) dy + f(x, a(x)) \frac{da(x)}{dx} - f(x, b(x)) \frac{db(x)}{dx} \quad (38)$$

where:

$$\rho U_x^2 = f(x, y)$$

Therefore,

$$\int_{Y_1}^{Y_2} \frac{\partial(\rho U_x^2)}{\partial x} dy = \frac{d}{dx} \int_{Y_1}^{Y_2} \rho U_x^2 dy + \left[\rho U_x^2 \right]_{(x, Y_1)} \frac{dY_1}{dx} - \left[\rho U_x^2 \right]_{(x, Y_2)} \frac{dY_2}{dx} \quad (39)$$

But, along a streamline:

$$\tan \phi = \frac{U_y}{U_x} = \frac{dy}{dx}; \therefore U_y = U_x \frac{dy}{dx}$$

Therefore,

$$\int_{Y_1}^{Y_2} \frac{\partial(\rho U_x^2)}{\partial x} dy = \frac{d}{dx} \int_{Y_1}^{Y_2} \rho U_x^2 dy + \rho U_x U_y \Big|_{(x, Y_1)} - \rho U_x U_y \Big|_{(x, Y_2)} \quad (40)$$

Substituting equation 40 into 37 yields the final form:

$$\int_{Y_1}^{Y_2} \frac{\partial P}{\partial x} dy + \frac{d}{dx} \int_{Y_1}^{Y_2} \rho U_x^2 dy = \epsilon_2 \frac{\partial U_x}{\partial y} \Big|_{Y_2} - \epsilon_1 \frac{\partial U_x}{\partial y} \Big|_{Y_1} \quad (41)$$

Before solving equation 41 for the diffusivity, the streamlines for each flame (i.e., T, ϕ) are evaluated as follows:

The total mass flow at any X location = $\int_0^3 \rho U_x dy$

Therefore, the fraction of flow between 0 and Y_1 = $\frac{\int_0^{Y_1} \rho U_x dy}{\int_0^3 \rho U_x dy}$ (42)

for a duct 3 in. wide.

Equation 42 is used to define the desired streamlines (points in the X direction where the fraction of flow is constant) with integrations calculated graphically.

Equation 41 can now be evaluated between selected streamlines with integrations and differentiations done graphically. In each case, the upper limit of integration, Y_2 , corresponds to the 50% streamline, while the lower limit, Y_1 , corresponds to some other streamline between 0 and 50%. The values of diffusivity determined in this manner represent an average between the values at Y_2 and Y_1 .

In the limiting case, as Y_1 approaches Y_2 the value of diffusivity corresponds to the desired value at $dC/dy = 0$. However, in this case, the indeterminate form $0/0$ is obtained as shown in equation 43.

$$\text{Limit}_{Y_1 \rightarrow Y_2} \epsilon = \text{Limit}_{Y_1 \rightarrow Y_2} \frac{\int_{Y_1}^{Y_2} \frac{\partial P}{\partial z} dy + \frac{d}{dx} \int_{Y_1}^{Y_2} \rho U_x^2 dy}{\left. \frac{\partial U_x}{\partial y} \right|_{Y_2} - \left. \frac{\partial U_x}{\partial y} \right|_{Y_1}} = \frac{0}{0} \quad (43)$$

Application of L'Hospital's Rule allows evaluating the diffusivity in the limiting case by taking derivatives of both the numerator and denominator of equation 43 with respect to $Y_2 - Y_1$ and evaluating the resultant expression at $Y_1 = Y_2$. In our case, these derivatives are taken graphically using a sufficient number of points, values of numerator and denominator in equation 43, to define a smooth curve as the limit is approached.

The resulting values of diffusivity, when used in equation 35 to determine the reaction rates, accounted for less than 10% of the final answer. This relatively small gradient eliminates concern over the accuracy of the graphical approach used in generating values of diffusivity.

APPENDIX IV

FA, X, AND pH TEST DATA

Table XIII contains FA, X, and pH data obtained from tests conducted on combustors A and B during Phase II.

Humidity data are presented for each test, while pH data are presented for full-traverse tests only.

Table XIII. FA, X, and pH Test Data

TEST	FA	X	PH
1-1A-1	0.0039	0.0118	
1-1A-2	0.0080	0.0119	
1-1A-3	0.0083	0.0144	
1-1A-4	0.0039	0.0144	
1-1A-5	0.0122	0.0143	
1-1A-6	0.0183	0.0144	
1-1A-7	0.0120	0.0100	
1-1A-8	0.0121	0.0094	
1-1A-9	0.0123	0.0109	
1-1A-10	0.0040	0.0142	
1-1A-11	0.0039	0.0107	
1-1A-12	0.0027	0.0062	
1-1A-13	0.0067	0.0069	
1-1A-14	0.0080	0.0116	5.7000
1-1A-15	0.0060	0.0134	5.6000
1-1A-16	0.0039	0.0135	5.8000
1-1A-17	0.0123	0.0142	5.1000
1-1A-18	0.0165	0.0144	4.9000
1-1A-19	0.0188	0.0146	5.0000
1-1A-20	0.0081	0.0142	5.3000
1-1B-1	0.0082	0.0132	2.5000
1-1B-2	0.0038	0.0116	2.8000
1-1B-3	0.0122	0.0137	3.4000
1-1B-4	0.0041	0.0142	
1-1B-5	0.0083	0.0142	
1-1B-6	0.0125	0.0142	
1-1B-7	0.0189	0.0152	3.9000
1-1B-8	0.0200	0.0147	4.4000
1-1B-9	0.0122	0.0147	
1-1B-10	0.0185	0.0146	
1-1B-11	0.0084	0.0146	
1-1B-12	0.0082	0.0154	
1-1B-13	0.0083	0.0156	
1-1B-14	0.0084	0.0155	3.1000
1-1B-15	0.0082	0.0163	
1-1B-16	0.0081	0.0140	4.2000
1-1B-17	0.0061	0.0139	
1-1B-18	0.0102	0.0141	
1-1B-19	0.0092	0.0145	3.4000
1-1B-20	0.0062	0.0152	

Table XIII. FA, X, and pH Test Data (Continued)

TEST	FA	X	PH
4-1A-1	0.0062	0.0162	4.2000
4-1A-2	0.0084	0.0228	3.8000
4-1A-3	0.0039	0.0151	4.4000
4-1A-4	0.0102	0.0153	3.7000
4-1A-5	0.0080	0.0160	
4-1A-6	0.0039	0.0160	3.8000
4-1A-7	0.0102	0.0163	3.2000
4-1A-8	0.0061	0.0164	
4-1A-9	0.0085	0.0157	3.9000
4-1A-10	0.0125	0.0145	3.1000
4-1A-11	0.0166	0.0143	
4-1A-12	0.0206	0.0142	
4-1A-13	0.0064	0.0143	
4-1A-14	0.0104	0.0143	
4-1A-15	0.0163	0.0142	
4-1A-16	0.0124	0.0142	
4-1A-17	0.0166	0.0152	
4-1A-18	0.0208	0.0152	
4-1A-19	0.0146	0.0152	
4-1A-20	0.0075	0.0152	
3-1A-1	0.0072	0.0166	4.7000
3-1A-2	0.0092	0.0166	4.4000
3-1A-3	0.0124	0.0169	4.1600
3-1A-4	0.0144	0.0176	3.9000
3-1A-5	0.0042	0.0176	
3-1A-6	0.0133	0.0176	
2-1A-1	0.0059	0.0154	3.4000
2-1A-2	0.0091	0.0155	3.1000
2-1A-3	0.0132	0.0177	3.0000
2-1A-4	0.0162	0.0155	
2-1A-5	0.0196	0.0155	
2-2A-1	0.0040	0.0181	3.9000
2-2A-2	0.0060	0.0183	3.9000
2-2A-3	0.0080	0.0164	3.8000

Table XIII. FA, X, and pH Test Data (Continued)

TEST	FA	X	PH
2-3A-1	0.0061	0.0170	3.0000
2-3A-2	0.0082	0.0169	2.9000
2-3A-3	0.0134	0.0172	2.8000
2-3A-4	0.0113	0.0172	
2-3A-5	0.0093	0.0171	
2-3A-6	0.0081	0.0170	3.3000
2-3A-7	0.0040	0.0171	
2-3A-8	0.0050	0.0171	
2-3A-9	0.0060	0.0171	
2-1B-1	0.0039	0.0156	
2-1B-2	0.0086	0.0158	2.7000
2-1B-3	0.0158	0.0156	2.6000
2-1B-4	0.0196	0.0157	2.6000
2-1B-5	0.0119	0.0156	2.5000
2-1B-6	0.0160	0.0157	2.9000
2-1B-7	0.0200	0.0157	2.6000
2-1B-8	0.0160	0.0156	2.7000
2-1B-9	0.0200	0.0170	2.7000

Table XIII. FA, X, and pH Test Data (Continued)

TEST	FA	X	PH
5-1B-1	0.0040	0.0152	3.7000
5-1B-2	0.0081	0.0152	3.5000
5-1B-3	0.0101	0.0165	3.2000
5-1B-4	0.0061	0.0165	3.3000
5-1A-1	0.0070	0.0151	4.0000
5-1A-2	0.0087	0.0151	3.8000
5-1A-3	0.0100	0.0157	
5-1A-4	0.0051	0.0157	3.5000
5-1A-5	0.0060	0.0157	
5-1A-6	0.0082	0.0158	3.5000
5-1A-7	0.0071	0.0158	
5-1A-8	0.0060	0.0158	3.9000
5-1A-9	0.0101	0.0140	3.1000
5-1A-10	0.0121	0.0140	3.8000
5-1A-11	0.0060	0.0140	
5-1A-12	0.0049	0.0140	
5-2A-1	0.0081	0.0161	3.4000
5-2A-2	0.0100	0.0161	3.3000
5-2A-3	0.0059	0.0167	3.8000
5-2A-4	0.0079	0.0167	
5-2A-5	0.0068	0.0167	
5-2A-6	0.0055	0.0167	
5-2A-7	0.0063	0.0167	
5-3A-1	0.0083	0.0162	3.1000
5-3A-2	0.0062	0.0162	3.5500
5-3A-3	0.0102	0.0137	3.1000
5-3A-4	0.0054	0.0137	
5-3A-5	0.0057	0.0137	
5-3A-6	0.0067	0.0137	
5-4A-1	0.0080	0.0080	3.0000
5-4A-2	0.0099	0.0080	2.9000
5-4A-3	0.0050	0.0080	
5-4A-4	0.0054	0.0080	3.1000
5-4A-5	0.0059	0.0080	3.2000

Table XIII. FA, X, and pH Test Data (Continued)

TEST	FA	X	pH
5-5A-1	0.0084	0.0153	3.4000
5-5A-2	0.0105	0.0153	3.2000
5-5A-3	0.0073	0.0156	
5-5A-4	0.0075	0.0156	
5-5A-5	0.0076	0.0156	
5-5A-6	0.0078	0.0156	3.6000
5-7A-1	0.0080	0.0170	3.7000
5-7A-2	0.0118	0.0141	3.6000
5-7A-3	0.0157	0.0144	3.1000
5-7A-4	0.0228	0.0144	3.4000
5-7A-5	0.0086	0.0153	3.1000
5-7A-6	0.0043	0.0153	4.2000
5-7A-7	0.0086	0.0151	4.0000
5-7A-8	0.0079	0.0151	3.3000
5-7A-9	0.0050	0.0151	3.0000
5-8A-1	0.0085	0.0147	4.1000
5-8A-2	0.0129	0.0141	3.8000
5-8A-3	0.0173	0.0150	3.7000
5-8A-4	0.0241	0.0153	3.5000
5-8A-5	0.0075	0.0153	
5-8A-6	0.0072	0.0153	
5-8A-7	0.0066	0.0153	

APPENDIX V

TEST DATA FLOWPATH

Three types of data were recorded during combustor testing in Phase II, as shown in figure 194. Test stand data included those variables used to monitor overall stand conditions; rig data included those variables needed to determine operational and performance characteristics of the combustor configurations being evaluated; and gas analysis cart data included those variables needed to determine distribution and concentrations of exhaust emissions.

Each set of data taken included ambient readings that were used to correct instrument bias errors. In addition, the gas analysis cart data included a three-point prerun calibration (zero point, half span and full span) for each of the analyzers. The three-point prerun calibration was reinforced by conducting periodic multipoint calibrations for each analyzer.

All raw data were hand recorded on specially prepared forms to facilitate keypunching of the data on IBM computer cards. The keypunched cards were then processed using a data reduction computer program with which combustor operating and performance characteristics were calculated. A complete set of computer printouts for data obtained during the accomplishment of Test Matrix Point No. 5-8A-1, using Combustor Scheme 5-8A, is included in table XIV. The information shown in the data set is self-explanatory.

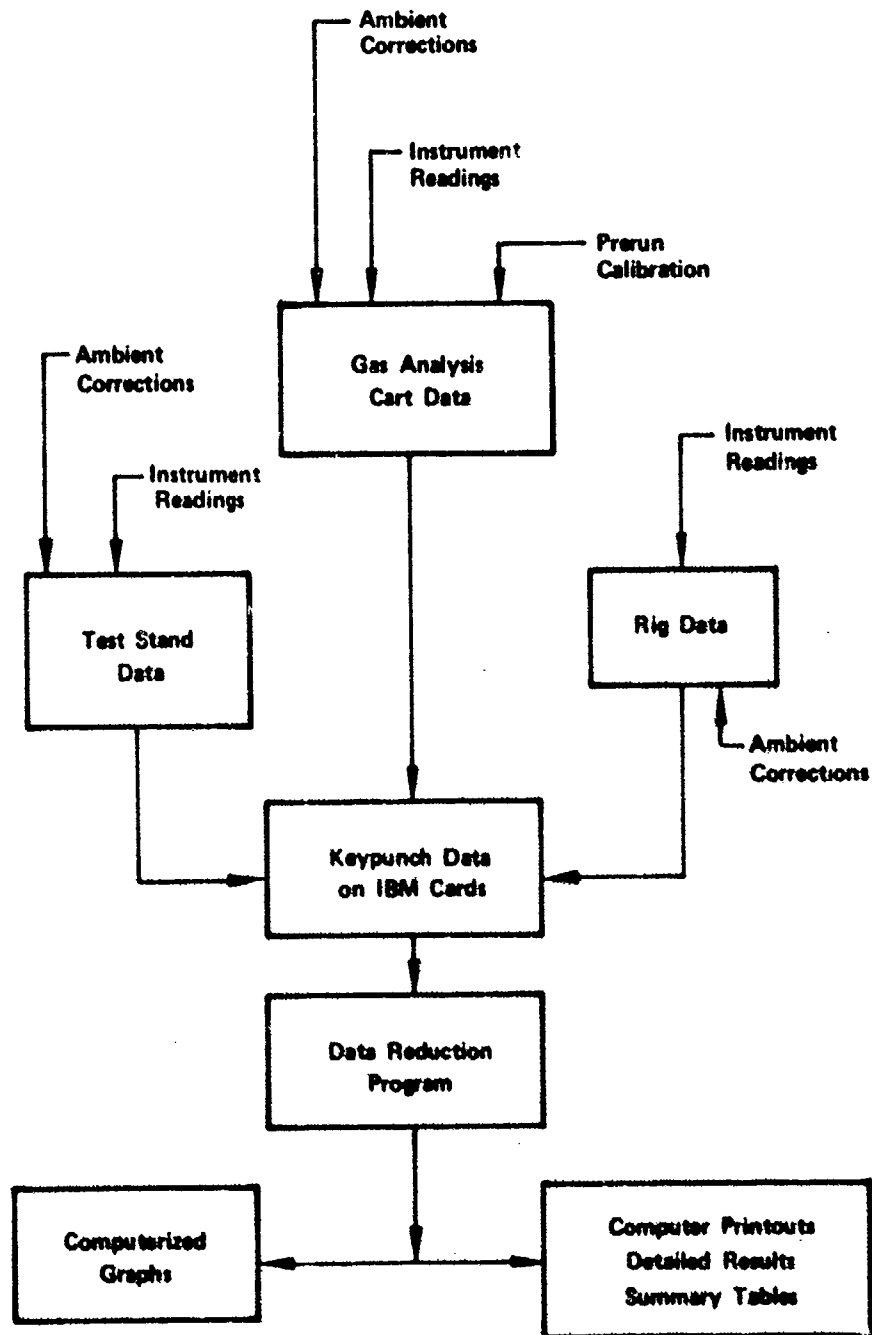


Figure 194. Test Data Flowpath

FD 72142

Table XIV. Combustor Rig Test Results

```

*****
* LOW POWER EMISSIONS STUDY CONTRACT AF F33619-71-C-1870 *
* COMBUSTOR A RIG TEST RESULTS *
*****
  
```

RUN NO.	DATE	SCHEME	PSAR	TEST MATRIX PT. NO.
103	12-12-72	3-8A	0000	3-8A-1

PURPOSE OF TEST

SCHEME 3-8A, FA = 0.000.

*****DESCRIPTIVE RESULTS*****

- NO YELLOW FLAME ANYWHERE IN BURNER EXCEPT APPROX. 5 PCT. AT ONE SITE WHERE BLUE FLAME INTERSECTS O.D. LINER.
- BLUE FLAME CORONA AT EACH TUBE EXTENDS FROM DEFLECTOR LIP AND INTERSECTS LINERS NEAR LOUVER UPSTREAM OF PRIMARY PENETRATION HOLES.
- BLUE FLAME NEAR WALL TERMINATED BY COOLING FILM FROM LOUVER UPSTREAM OF PRIMARY PENETRATION HOLES.
- BLUE FLAME IN MAINSTREAM EXTENDS TO LOUVER UPSTREAM OF INTERMEDIATE HOLES
- LOUVER UPSTREAM OF PRIM. PENETRATION HOLES IS RED AROUND MOST OF CIRCUM-FERENCE (LIP ONLY).
- BLUE FLAME JET FROM HOLE IN CENTERBODY DISTINGUISHABLE AT ONE SITE EXTENDING ABOUT 2 IN DOWNSTREAM.

Table XIV. Combustor Rig Test Results (Continued)

*****OPERATING AND PERFORMANCE PARAMETERS*****	
W-TOTAL WET AIR FLOWRATE (LBM/SEC)	9.067
WRFP-REFERENCE VELOCITY (FT/SEC)	96.23
WTI-INLET TOTAL TEMP. (DEG.F)	400.6
PTI-INLET TOTAL PRESS. (PSIA)	19.69
FA-OVERALL FUEL AIR RATIO	0.0089
PHIP-PRIMARY ZONE EQUIVALENCE RATIO	0.919
PPR-PRIMARY TO SECONDARY FUEL FLOW RATIO	INFINITE
EFFB-MAIN BURNER EFFICIENCY (PERCENT)	100.92
R-SPECIFIC HUMIDITY (LBM H2O/(LBM AIR+H2O))	0.0149
WPP-PRIMARY ZONE FUEL FLOW (PPM)	177.692
WPS-SECONDARY ZONE FUEL FLOW (PPM)	0.000
FAP-PRIMARY ZONE FUEL-AIR RATIO	0.0393
PAINT-INTERMEDIATE ZONE FUEL-AIR RATIO	0.0000
PAINT-INTERMEDIATE ZONE EQUIVALENCE RATIO	0.000
YTDI-IDEAL DRY EXIT TEMP. (DEG. F)	1007.9
YTEI-IDEAL WET EXIT TEMP. (DEG.F)	989.0
TTQA-OVERALL AVERAGE EXIT TEMP. (DEG. F)	992.0
DELTY-COMBUSTOR TEMPERATURE RISE (DEG.F)	991.3
THAI-MAXIMUM EXIT TEMP. LOCATED AT 1 = 27.0" (DEG. F)	1150.0
TFP-TEMPERATURE PATTERN FACTOR	0.267
TRMS-ROOT MEAN SQUARE TEMP. PATTERN FACTOR	0.787
PTAO-OVERALL AVERAGE TOTAL PRESSURE (PSIA)	19.07
LPL-COMBUSTOR TOTAL PRESSURE LOSS (ACT.)	3.723

Table XIV. Combustor Rig Test Results (Continued)

*****EXHAUST EMISSIONS PARAMETERS*****	
NO2O--OVERALL AVG. EXIT CONCENTRATION OF NO2 (PPM)	11.
NOO--OVERALL AVG. EXIT CONCENTRATION OF NO (PPM)	13.
NO2O--OVERALL AVG. EXIT CONCENTRATION OF NO2 (PPM)	20.
HCTO--OVERALL AVG. EXIT CONCENTRATION OF HCT (PPM)	4.
CO2O--OVERALL AVG. EXIT CONCENTRATION OF CO2 (PCY)	10.873
COO--OVERALL AVG. EXIT CONCENTRATION OF CO (PPM)	87.
H2OO--OVERALL AVG. EXIT CONCENTRATION OF H2O (PCY)	3.964
O2O--OVERALL AVG. EXIT CONCENTRATION OF O2 (PCY)	18.170
NOA1--SAMPLE TEMP. AT NO2 ANALYZER INLET (DEG.F)	90.
NOA2--SAMPLE TEMP. AT NO ANALYZER INLET (DEG.F)	90.
HCA1--SAMPLE TEMP. AT HCT ANALYZER INLET (DEG.F)	264.
COA1--SAMPLE TEMP. AT CO ANALYZER INLET (DEG.F)	92.
COA2--SAMPLE TEMP. AT CO ANALYZER INLET (DEG.F)	96.
H2OA1--SAMPLE TEMP. AT H2O ANALYZER INLET (DEG.F)	88.
O2A1--SAMPLE TEMP. AT O2 ANALYZER INLET (DEG.F)	92.
TSO1--SAMPLE GAS TEMP. IN TRAVERSE PROBE MAIN SHAFT (DEG.F)	426.
TSO2--SAMPLE GAS TEMP. AT PROBE - TRANSFER LINE CONNECTION (DEG.F)	338.
TSO3--SAMPLE GAS TEMP. AT END OF HEATED TRANSFER LINE (DEG.F)	306.
TSO4--SAMPLE GAS TEMP. AT INLET TO CART (DEG.F)	347.
TM1--TRANSFER MANIFOLD TEMPERATURE (DEG.F)	82.
EM1--EXHAUST MANIFOLD TEMPERATURE (DEG.F)	98.
CAT1--CART AIR TEMPERATURE (DEG.F)	83.

Table XIV. Combustor Rig Test Results (Continued)

*****EXHAUST EMISSIONS PARAMETERS*****	
NOA1-STATIC PRESSURE AT NO2 ANALYZER INLET (PSIA)	13.44
NOA2-STATIC PRESSURE AT NO ANALYZER INLET (PSIA)	13.38
NOA3-STATIC PRESSURE AT HCY ANALYZER INLET (PSIA)	13.55
COA1-STATIC PRESSURE AT CO2 ANALYZER INLET (PSIA)	13.18
COA2-STATIC PRESSURE AT CO ANALYZER INLET (PSIA)	13.16
HVA1-STATIC PRESSURE AT H2O ANALYZER INLET (PSIA)	13.37
ORA1-STATIC PRESSURE AT O2 ANALYZER INLET (PSIA)	13.22
YMP1-TRANSFER MANIFOLD STATIC PRESSURE (PSIA)	13.22
EMP1-EXHAUST MANIFOLD STATIC PRESSURE (PSIA)	6.17
*****COMBUSTOR & SPECIAL PARAMETERS*****	
DIAM-DEFLECTOR DIAMETER (INCHES)	1.00
ALREP-COMBUSTOR LINER TOTAL EFFECTIVE MOLE AREA (IN. SQ.)	43.97
WAP21-CARBURETION TUBE AIRFLOW, FRACTION BURNER TOTAL	0.078
VPR1-CARBURETION TUBE VELOCITY BASED ON AIR FLOW ONLY (FPS)	126.29
VPR2-CARBURETION TUBE VELOCITY BASED ON AIR AND FUEL FLOW (FPS)	127.26
PEPR-CARBURETION TUBE TO PRIMARY ZONE PENETRATION AIRFLOW RATIO	1.681
PHR1-CARBURETION TUBE EQUIVALENCE RATIO	1.850

Table XIV. Combustor Rig Test Results (Continued)

***** PARAMETERS *****

P11-VENTURI UPSTREAM STATIC PRESSURE (PSIA)	16.68
P11-VENTURI UPSTREAM TOTAL PRESSURE (PSIA)	16.74
T11-HEATER INLET TEMP. (DEG. F)	402.9
T11-VENTURI THROAT METAL TEMPERATURE (DEG. F)	356.5
P12-VENTURI THROAT STATIC PRESSURE (PSIA)	10.09
P12-VENTURI THROAT STATIC TO TOTAL PRESSURE RATIO	0.603
W02-TOTAL DRY AIR FLOWRATE (LBM/SEC)	9.764
P13-INLET STATIC PRESS. (PSIA)	13.64
MIN-INLET MACH NO.	0.0236
WREF-REFERENCE MACH NO.	0.0419
WF-MAIN BURNER FUEL FLOW (PPH)	177.692
TFP1-PRIMARY ZONE FUEL TEMP. AT FLOWMETER (DEG. F)	99.7
TFP2-PRIMARY ZONE FUEL TEMPERATURE AT RIG (DEG. F)	87.7
BT1-BURNER SKIN TEMP. ON OCME AT SOC (DEG. F)	668.7
BT2-BURNER SKIN TEMP. ON DOME AT 334 DEG FROM TDC (DEG. F)	548.7
BT3-BURNER SKIN TEMP. ON O.D. LINER, PRIM. ZONE, 39 DEG. FROM TDC (DEG. F)	517.5
BT4-BURNER SKIN TEMP. ON I.D., OPPOS. SEC. INJ., 77 DEG. FROM TDC (DEG. F)	420.0
WAP-PRIMARY ZONE AIRFLOW, FRACTION TOT. BURNER AIRFLOW	0.239
CAP-PRIMARY ZONE COOLING FLOW, FRACTION TOT. BURNER AIRFLOW	0.114
IDAR-INT. ZONE TO OIL. ZONE AIRFLOW RATIO	0.389
WAD1-OLLUTION ZONE AIRFLOW, FRACTION BURNER TOTAL	0.547
WAIN1-INT. ZONE AIRFLOW, FRACTION BURNER TOTAL	0.213
ODPIC-VENTURI DIAMETER (IN.)	5.00
WHRV-HEAT RELEASE RATE 0.0100 18TU/HR F1003 ATM.	2.6303
SAPP-SAPP-FUEL SPECIFIC GRAVITY-PRIMARY ZONE, SEC. ZONE	0.8033 0.0000

Table XIV. Combustor Rig Test Results (Continued)

EXHAUST EMISSIONS CONCENTRATIONS

TEST 5-84-1

ANG. LOC. REG.	NO ₂ PPMV	NO PPMV	CO PPMV	UHC PPMV	CO ₂ PCTW	ACTV EI	PPMV	CO PPMV	PCTW EI	MZO PCTV	EI
6	19.0	11.9	2.7	12.2	12.2	1.2	3.4	0.3	2.741	1.805	2176.6
18	18.6	11.7	2.7	12.7	12.3	1.6	3.4	0.3	2.661	1.752	2180.4
30	19.3	12.3	2.3	12.4	12.9	1.7	3.2	0.3	2.798	1.842	2203.9
42	19.4	12.3	2.3	13.0	14.5	1.7	3.0	0.3	2.910	1.916	2478.5
54	20.7	13.0	2.6	13.6	13.1	1.6	3.0	0.3	2.943	2.016	2461.4
64	17.3	10.9	2.0	11.3	11.1	1.3	2.8	0.2	2.878	1.899	2440.0
76	17.3	10.9	2.0	13.9	13.4	1.6	3.4	0.2	2.878	1.899	2440.0
90	17.3	10.9	2.0	15.0	14.9	1.7	3.4	0.2	2.844	1.873	2401.5
102	16.6	10.4	1.9	12.9	12.0	1.4	3.1	0.2	2.748	1.805	2276.4
116	15.9	10.0	1.9	11.6	11.0	1.3	2.9	0.2	2.802	1.847	2322.5
126	18.3	11.6	2.2	16.6	16.0	1.9	3.8	0.3	2.902	1.910	2448.9
138	18.1	11.4	2.1	12.6	12.2	1.5	3.5	0.3	2.915	1.985	2403.6
150	18.6	11.7	2.2	16.7	13.7	1.7	3.6	0.3	2.992	1.979	2491.6
162	18.1	11.6	2.1	13.9	13.6	1.6	3.2	0.3	2.854	1.879	2411.2
176	17.9	11.9	2.0	13.4	12.9	1.6	3.1	0.3	2.677	1.762	2199.8
186	19.0	11.9	2.2	13.6	12.2	1.5	3.1	0.3	2.761	1.875	2276.6
198	18.6	11.7	2.2	13.7	13.3	1.6	3.4	0.3	2.641	1.752	2180.6
210	19.3	12.3	2.3	14.6	12.8	1.7	3.2	0.3	2.798	1.842	2342.9
222	20.7	13.0	2.6	13.0	14.9	1.7	3.7	0.3	2.910	1.916	2478.5
234	20.7	13.0	2.6	13.6	13.1	1.6	3.4	0.3	2.963	2.016	2461.4
246	17.3	10.9	2.0	11.1	11.1	1.3	2.8	0.2	2.876	1.899	2440.0
258	17.3	10.9	2.0	13.9	13.4	1.6	3.4	0.2	2.876	1.899	2440.0
270	16.6	10.4	1.9	12.9	12.3	1.4	3.1	0.2	2.844	1.873	2401.5
282	16.6	10.4	1.9	12.3	12.3	1.4	3.1	0.2	2.741	1.805	2276.6
294	15.9	10.0	1.9	11.4	11.0	1.3	2.9	0.2	2.806	1.847	2322.5
304	16.9	11.6	2.2	16.6	16.0	1.9	3.8	0.3	2.902	1.910	2448.9
318	18.1	11.4	2.1	12.6	12.2	1.5	3.5	0.3	2.915	1.985	2403.6
330	18.6	11.7	2.2	16.7	13.7	1.7	3.6	0.3	2.992	1.979	2491.6
342	18.1	11.6	2.1	13.9	13.6	1.6	3.2	0.3	2.854	1.879	2411.2
354	17.3	10.9	2.0	13.4	12.9	1.6	3.1	0.3	2.677	1.762	2199.8

Table XIV. Combustor Rig Test Results (Continued)

EXHAUST EMIS IONS CONCENTRATIONS
TEST 5-8A-1

ANG. LOC. DEG.	- - 02 - -	PCTM	PCIV	F1
6	19.707	17.839	2351.5	
18	19.683	17.817	2352.3	
30	19.660	17.796	2349.1	
42	19.565	17.710	2338.2	
54	19.518	17.668	2325.8	
66	21.264	19.248	2541.1	
78	21.217	19.205	2535.8	
90	21.052	19.056	25158.5	
102	21.075	19.077	25186.7	
114	21.052	19.056	25158.5	
126	19.447	17.604	23241.1	
138	19.447	17.604	23241.1	
150	19.447	17.604	23241.1	
162	19.447	17.604	23241.1	
174	19.518	17.668	23325.8	
186	19.707	17.839	2351.5	
198	19.683	17.817	2352.3	
210	19.660	17.796	2349.1	
222	19.565	17.710	2338.2	
234	19.518	17.668	2325.8	
246	21.264	19.248	2541.1	
258	21.217	19.205	2535.8	
270	21.052	19.056	25158.5	
282	21.075	19.077	25186.7	
294	21.052	19.056	25158.5	
306	19.447	17.604	23241.1	
318	19.447	17.604	23241.1	
330	19.447	17.604	23241.1	
342	19.447	17.604	23241.1	
354	19.518	17.668	23325.8	

Table XIV. Combustor Rig Test Results (Continued)

RADIAL TEMPERATURE AVERAGES (DEG. F)---Y STATIONS		RADIAL TEMPERATURE AVERAGES (DEG. F)---X STATIONS			
1	2	3	4	5	6
887.	981.	1044.	1052.	993.	
2	3	4	5	6	
981.	971.	981.	1017.	1013.	993.
1009.	1039.	979.	975.	995.	1007.
1049.	981.	927.	919.	921.	929.
971.	993.	999.	973.	973.	947.
1021.	1027.	1073.	1011.	1037.	1009.
26	27	27	28	26	30

RADIAL PRESSURE AVERAGES (PSIA)		RADIAL PRESSURE AVERAGES (PSIA)---X STATIONS			
1	2	3	4	5	6
15.06	15.08	15.07	15.06		
2	3	4	5	6	
15.04	15.05	15.04	15.07	15.07	15.07
15.08	15.08	15.07	15.08	15.08	15.06
15.08	15.05	15.06	15.05	15.05	15.04
15.09	15.09	15.06	15.08	15.09	15.08
15.10	15.08	15.09	15.07	15.07	15.04
26	27	27	28	29	30

Table XIV. Combustor Rig Test Results (Continued)

SPECIAL PARAMETERS		
NO2DX-OVERALL AVG. EXIT EMISSION INDEX FOR NO2 (LBM/11000 LBM FUEL))		2.17
NODX-OVERALL AVG. EXIT EMISSION INDEX FOR NO (LBM/11000 LBM FUEL))		1.63
NOXDX-OVERALL AVG. EMISSION INDEX FOR NOX (LBM/11000 LBM FUEL))		3.80
HCTDX-OVERALL AVG. EXIT EMISSION INDEX FOR HCT (LBM/11000 LBM FUEL))		0.31
CO2DX-OVERALL AVG. EXIT EMISSION INDEX FOR CO2 (LBM/11000 LBM FUEL))		3400.36
CODX-OVERALL AVG. EXIT EMISSION INDEX FOR CO (LBM/11000 LBM FUEL))		10.07
H2O2DX-OVERALL AVG. EXIT EMISSION INDEX FOR H2O (LBM/11000 LBM FUEL))		2946.85
O2DX-OVERALL AVG. EXIT EMISSION INDEX FOR O2 (LBM/1000 LBM FUEL)		23989.33
WSNO2-NO2 SAMPLE FLOWRATE BASED ON NDAF1 AND EMP1 (SCFH)		3.93
WSNO-NO SAMPLE FLOWRATE BASED ON NOAP1 AND EMP1 (SCFH)		3.91
WSCO2-CO2 SAMPLE FLOWRATE BASED ON COAP1 AND EMP1 (SCFH)		3.85
WSCO-CO SAMPLE FLOWRATE BASED ON CHAP1 AND EMP1 (SCFH)		3.83
WSH2O-H2O SAMPLE FLOWRATE BASED ON WVAP1 AND EMP1 (SCFH)		3.92
WSO2-O2 SAMPLE FLOWRATE BASED ON OXAP1 AND EMP1 (SCFH)		5.56
T40AA-PROBE A AVERAGE EXIT TRAVERSE TEMP. (DEG.F)		1004.
T40AB-PROBE B AVERAGE EXIT TRAVERSE TEMP. (DEG.F)		979.
NO2PW-OVERALL AVG. EXIT WEIGHT CONC. OF NO2 (PPHM)		18.

Table XIV. Combustor Rig Test Results (Continued)

SPECIAL PARAMETERS

NOPW-OVERALL AVG. EXIT WEIGHT CONC. OF NO (PPMW)	13.
NOXPM-OVERALL AVG. EXIT WEIGHT CONC. OF NOX (PPMW)	31.
HCTPM-OVERALL AVG. EXIT WEIGHT CONC. OF HCT (PPMW)	2.
COZPM-OVERALL AVG. EXIT WEIGHT CONC. OF CO2 (PCTW)	2.845
COPW-OVERALL AVG. EXIT WEIGHT CONC. OF CO (PPMW)	84.
H2OPW-OVERALL AVG. EXIT WEIGHT CONC. OF H2O (PCTW)	2.465
O2PM-OVERALL AVG. EXIT WEIGHT CONC. OF O2 (PCTW)	20.073
FASAM-FUEL AIR RATIO FROM GAS ANALYSIS AS PER ARP 1256	0.0089
PH OF EXHAUST GAS BASED ON SAMPLE TAKEN FOR DURATION OF TRAVERSE	4.10
EFFGA-COMBUSTION EFFICIENCY BASED ON HCT AND CO READINGS ONLY (PCT.)	99.7262
HVL-FUEL LOWER HEATING VALUE (BTU/LBM)	18450.
FORMULA ASSUMED FOR JPS	C 12.88 H 25.02

Table XIV. Combustor Rig Test Results (Continued)

*****ELEMENT BALANCE PARAMETERS*****	
CFUEL-LBM CARBON IN FUEL PER LBM TOTAL RIG FLOW	0.00719907
CIN-TOTAL LBM CARBON INPUT PER LBM TOTAL RIG FLOW	0.00719907
MFUEL-LBM HYDROGEN IN FUEL PER LBM TOTAL RIG FLOW	0.00117279
MAIR-LBM HYDROGEN IN INLET AIR PER LBM TOT. RIG FLOW	0.00159396
MIN-TOTAL LBM HYDROGEN INPUT PER LBM TOTAL RIG FLOW	0.00276475
CCH4-LBM CARBON IN CH4 PER LBM TOT. RIG FLOW	0.00000197
CCO2-LBM CARBON IN CO2 PER LBM TOT. RIG FLOW	0.00776727
CCO-LBM CARBON IN CO PER LBM TOT. RIG FLOW	0.00003616
COUT-TOT. MEAS. CARBON OUTPUT PER LBM TOT. RIG FLOW	0.00780941
MCH4-LBM HYDROGEN IN CH4 PER LBM TOT. RIG FLOW	0.00000066
MH2O-LBM HYDROGEN IN H2O PER LBM TOT. RIG FLOW	0.00275934
MOUT-TOT. MEAS. HYDROG. OUTPUT PER LBM TOT. RIG FLOW	0.00276000
CFCH4-LBM CARBON IN CH4 PER TOT. LBM CARBON INPUT	0.00027911
CFCO2-LBM CARBON IN CO2 PER TOT. LBM CARBON INPUT	1.07992761
CFCO-LBM CARBON IN CO PER TOT. LBM CARBON INPUT	0.00902596
MFCH4-LBM HYDROGEN IN CH4 PER TOT. LBM HYDROGEN IN	0.00024034
MFH2O-LBM HYDROGEN IN H2O PER TOT. LBM HYDROGEN IN	0.99804091

Table XIV. Combustor Rig Test Results (Continued)

ELEMENT BALANCE PARAMETERS	
CFRAC-TOT. LBM CARBON OUT PER TOT. LBM CARBON IN	1.08462861
HFRAC-TOT. LBM HYDROGEN OUT PER TOT. LBM. HYDROG. IN	0.99828124
ACCO-ADDITIONAL CO REQUIRED TO ACHIEVE CARBON BALANCE (PPMV)	-1471.
ACCO2-ADDITIONAL CO2 REQUIRED TO ACHIEVE CARBON BALANCE (PCT.)	-0.147
ACCH-ADDITIONAL CH4 REQUIRED TO ACHIEVE CARBON BALANCE (PPMV)	-1471.
AHCH-ADDITIONAL CH4 REQUIRED TO ACHIEVE HYDROGEN BALANCE (PPMV)	14.
AH2O-ADDITIONAL H2O REQUIRED TO ACHIEVE HYDROGEN BALANCE (PCT.)	0.000
H2OCC-H2O CONCENTRATION FOR COMPLETE COMBUSTION WITH DRY AIR (PCTV.)	1.647
CO2TT-CO2 CONCENTRATION FOR COMPLETE COMBUSTION (PCT. BY VOL.)	1.770
H2OYT-TOTAL H2O CONC. FROM COMPLETE COMBUSTION AND INLET AIR HUMIDITY (PCTV.)	3.934
O2CC-O2 CONCENTRATION FOR COMPLETE COMBUSTION (PCTV)	18.355

Table XIV. Combustor Rig Test Results (Continued)

WET AND DRY BASIS EMISSIONS

(OVERALL AVG. EXIT CONCENTRATIONS)

	WET	DRY	IDEAL WET
NO ₂ (PPMV)	11.0	11.0	11.0
NO ₂ (PPHM)	18.0	18.0	18.0
NO (PPMV)	12.0	13.0*	12.0
NO (PPHM)	13.0	13.0	13.0
HCT (PPMV)	4.0	4.0	4.0
HCT (PPHM)	2.0	2.0	2.0
CO ₂ (PCTV)	1.799	1.873	1.841
CO ₂ (PCTW)	2.797	2.827	2.797
CO (PPMV)	83.0	87.0	85.0
CO (PPHM)	81.0	83.0	82.0

* BASIS ON WHICH MEASUREMENTS ARE ACTUALLY MADE.

COMPUTATIONS BASED ON MEASURED AMBIENT H₂O AND THEORETICAL H₂O DUE TO COMBUSTION

WET BASIS - CONCENTRATION WITH ALL H₂O (AMBIENT AND COMBUSTION) PRESENT IN SAMPLE BULK.

DRY BASIS - CONCENTRATION AFTER REMOVAL OF ALL H₂O FROM SAMPLE BULK.

IDEAL WET BASIS - CONCENTRATION AFTER REMOVAL OF AMBIENT H₂O ONLY FROM SAMPLE BULK.

HCTDM-DRY BASIS HCT CONC. COMPUTED USING MEASURED EXHAUST H₂O (PPMV) 4.0

HCTIM-IDEAL WET BASIS HCT CONC. COMPUTED USING MEASURED EXHAUST H₂O (PPMV) 4.0

Table XIV. Combustor Rig Test Results (Continued)

STATISTICAL PARAMETERS

(OVERALL AVG. EXIT CONCENTRATIONS)

	AVG.	MAX.	MIN.	SIGMA
NO ₂ (PPMV)	11.46	13.05	10.05	0.77
NO ₂ (PPMV)	18.27	20.91	16.10	1.24
NO ₂ (EI)	2.19	2.49	1.92	0.14
NO (PPMV)	13.16	16.05	11.00	1.32
NO (PPMV)	13.57	16.32	11.32	1.36
NO (EI)	1.62	1.97	1.35	0.16
HCT (PPMV)	4.77	5.68	3.83	0.55
HCT (PPMV)	2.66	3.17	2.14	0.30
HCT (EI)	0.31	0.37	0.25	0.03
CO ₂ (PCTV)	1.87	2.01	1.75	0.07
CO ₂ (PCTV)	2.82	3.04	2.64	0.11
CO ₂ (EI)	3379.01	3638.42	3160.71	133.51
CO (PPMV)	87.20	92.28	84.05	3.12
CO (PPMV)	83.78	88.35	80.75	2.99
CO (EI)	10.01	10.59	9.65	0.35
H ₂ O (PCTV)	3.96	4.04	3.85	0.05
H ₂ O (PCTV)	2.48	2.53	2.41	0.03
H ₂ O (EI)	2972.33	3030.09	2891.92	43.84

APPENDIX VI
CONTROLLED AND MEASURED
TEST DATA

Table XV contains controlled and measured data for tests conducted on combustors A and B during Phase II. Specific data presented, where applicable, for each test are Test No., FA, PSAR, PSFR, EFFMB and EFFGA.

EFFMB and EFFGA are presented for full-traverse tests conducted using combustors A and B. EFFGA is also presented for the partial-traverse tests conducted using combustor B.

Table XV. Controlled and Measured Test Data

TEST	FA	PSAR	PSFR	EFFMB	EFFGA
1-1A-1	0.0039	0.1300	-	95.3707	
1-1A-2	0.0080	0.1300	-	97.2642	
1-1A-3	0.0083	0.8600	-	97.9572	
1-1A-4	0.0039	0.8600	-	95.3076	
1-1A-5	0.0122	0.8600	-	100.6059	
1-1A-6	0.0183	0.8600	-	96.8054	
1-1A-7	0.0120	0.8600	-	96.3939	
1-1A-8	0.0121	0.8600	-	97.3765	
1-1A-9	0.0123	0.8600	-	97.8921	
1-1A-10	0.0040	0.8600	-	95.1156	96.5187
1-1A-11	0.0039	0.8600	-	94.2456	95.7597
1-1A-12	0.0027	0.8600	-	91.4564	95.8919
1-1A-13	0.0067	0.8600	-	97.3486	99.2110
1-1A-14	0.0080	0.8600	-	96.3593	99.1183
1-1A-15	0.0060	0.8600	-	96.3392	98.5600
1-1A-16	0.0039	0.8600	-	92.7296	96.4868
1-1A-17	0.0123	0.8600	-	96.8093	99.1554
1-1A-18	0.0165	0.8600	-	96.9268	99.1109
1-1A-19	0.0188	0.8600	-	97.3378	99.1675
1-1A-20	0.0081	0.8600	-	97.1934	98.9859
1-1B-1	0.0082	0.8600	-	98.3389	97.8067
1-1B-2	0.0038	0.8600	-	95.0533	95.8203
1-1B-3	0.0122	0.8600	-	98.4827	98.6296
1-1B-4	0.0041	0.8600	-		
1-1B-5	0.0083	0.8600	-		
1-1B-6	0.0125	0.8600	-		
1-1B-7	0.0189	0.8600	-	99.6490	99.2104
1-1B-8	0.0200	0.8600	-	98.7894	99.1272
1-1B-9	0.0122	0.8600	-		
1-1B-10	0.0185	0.8600	-		
1-1B-11	0.0084	0.8600	-		
1-1B-12	0.0082	0.8600	-		
1-1B-13	0.0083	0.8600	-		
1-1B-14	0.0084	0.8600	-		
1-1B-15	0.0082	0.8600	-		
1-1B-16	0.0081	0.8600	-	98.2068	95.9935
1-1B-17	0.0061	0.8600	-		
1-1B-18	0.0102	0.8600	-		
1-1B-19	0.0082	0.8600	-	106.3314	98.2989
1-1B-20	0.0062	0.8600	-		

Table XV. Controlled and Measured Test Data (Continued)

TEST	FA	PSAR	PSFR	EFFMB	EFFGA
4-1A-1	0.0062	0.1300	-	98.6618	98.7589
4-1A-2	0.0084	0.1300	-	98.6543	98.5832
4-1A-3	0.0039	0.1300	-	97.3776	
4-1A-4	0.0102	0.1300	-	97.6430	
4-1A-5	0.0080	0.1300	-		
4-1A-6	0.0039	0.1300	-	97.7924	98.6482
4-1A-7	0.0102	0.1300	-	98.2758	98.5987
4-1A-8	0.0061	0.1300	-		
4-1A-9	0.0085	0.1300	0.9408	80.0106	66.1069
4-1A-10	0.0125	0.1300	0.4798	86.4386	69.3337
4-1A-11	0.0166	0.1300	0.3218		
4-1A-12	0.0206	0.1300	0.2447		
4-1A-13	0.0064	0.1300	1.6580		
4-1A-14	0.0104	0.1300	3.3018		
4-1A-15	0.0163	0.1300	0.3251		
4-1A-16	0.0124	0.1300	1.8609		
4-1A-17	0.0166	0.1300	0.9655		
4-1A-18	0.0208	0.1300	0.6449		
4-1A-19	0.0146	0.1300	2.2904		
4-1A-20	0.0075	0.1300	0.6963		
3-1A-1	0.0072	0.2100	-	98.2579	98.6738
3-1A-2	0.0092	0.2100	-	98.5368	98.7387
3-1A-3	0.0124	0.2100	-	97.9891	98.5880
3-1A-4	0.0144	0.2100	-	97.6891	98.4946
3-1A-5	0.0042	0.2100	-		
3-1A-6	0.0133	0.2100	2.2954		
2-1A-1	0.0059	0.3100	-	98.6618	98.9140
2-1A-2	0.0091	0.3100	-	97.8522	98.9049
2-1A-3	0.0132	0.3100	-	97.6687	98.7852
2-1A-4	0.0162	0.3100	-	92.3248	98.6658
2-1A-5	0.0196	0.3100	-	90.9037	98.5688
2-2A-1	0.0040	0.3100	-	95.3216	98.7278
2-2A-2	0.0060	0.3100	-	95.3974	98.7505
2-2A-3	0.0080	0.3100	-	95.3289	98.6519

Table XV. Controlled and Measured Test Data (Continued)

TEST	FA	PSAR	PSFR	EFFNB	EFFGA
2-3A-1	0.0061	0.3100	-	88.0620	78.6367
2-3A-2	0.0082	0.3100	-	91.2547	81.3607
2-3A-3	0.0134	0.3100	-	93.6552	73.5601
2-3A-4	0.0113	0.3100	-		
2-3A-5	0.0093	0.3100	-		
2-3A-6	0.0081	0.3100	-	93.2044	83.6889
2-3A-7	0.0040	0.3100	-		
2-3A-8	0.0050	0.3100	-		
2-3A-9	0.0060	0.3100	-		
2-1H-1	0.0039	0.3100	-		
2-1H-2	0.0086	0.3100	2.3927	97.5510	75.2164
2-1H-3	0.0158	0.3100	0.6278	98.3736	72.1284
2-1H-4	0.0196	0.3100	0.4479	99.5859	80.3401
2-1H-5	0.0119	0.3100	2.1558	99.3048	85.3204
2-1H-6	0.0160	0.3100	1.0493	97.8245	81.2969
2-1H-7	0.0200	0.3100	0.7013	98.3780	83.1815
2-1H-8	0.0160	0.3100	3.2359	98.0406	93.5684
2-1H-9	0.0200	0.3100	1.5762	97.7283	90.4346

Table XV. Controlled and Measured Test Data (Continued)

TEST	FA	PSAR	PSFR	EFFMB	EFFGA
5-1H-1	0.0040	0.1300	-	97.4302	98.9169
5-1H-2	0.0081	0.1300	-	97.3160	98.3266
5-1H-3	0.0101	0.1300	-	98.4252	98.1795
5-1H-4	0.0061	0.1300	-	98.5180	98.7462
5-1A-1	0.0070	0.1625	-	98.5524	99.1343
5-1A-2	0.0087	0.1613	-	99.5990	98.8823
5-1A-3	0.0100	0.1638	-	-	98.9937
5-1A-4	0.0051	0.1608	-	95.7084	93.3359
5-1A-5	0.0060	0.1608	-	-	99.6574
5-1A-6	0.0082	0.1636	-	99.1168	99.2040
5-1A-7	0.0071	0.1643	-	-	99.6455
5-1A-8	0.0060	0.1639	-	99.6948	99.6820
5-1A-9	0.0101	0.1618	-	99.2402	98.1760
5-1A-10	0.0121	0.1617	-	98.8810	97.7500
5-1A-11	0.0080	0.1628	-	-	99.7563
5-1A-12	0.0049	0.1621	-	-	98.8136
5-2A-1	0.0081	0.1761	-	100.9863	99.4869
5-2A-2	0.0100	0.1730	-	99.4943	98.8602
5-2A-3	0.0059	0.1738	-	99.9223	99.8584
5-2A-4	0.0079	0.1746	-	-	99.6242
5-2A-5	0.0068	0.1740	-	-	99.8175
5-2A-6	0.0055	0.1742	-	-	98.3659
5-2A-7	0.0063	0.1746	-	-	99.7821
5-3A-1	0.0083	0.1799	-	97.2020	99.4947
5-3A-2	0.0062	0.1793	-	99.4070	99.8545
5-3A-3	0.0102	0.1780	-	99.1559	98.9021
5-3A-4	0.0054	0.1798	-	-	99.6242
5-3A-5	0.0057	0.1791	-	-	99.6724
5-3A-6	0.0067	0.1797	-	-	99.8478
5-4A-1	0.0080	0.1740	-	100.0661	99.3585
5-4A-2	0.0099	0.1736	-	100.3360	98.8399
5-4A-3	0.0050	0.1737	-	-	99.2448
5-4A-4	0.0054	0.1738	-	100.5635	99.5168
5-4A-5	0.0054	0.1733	-	101.7747	99.7900

Table XV. Controlled and Measured Test Data (Continued)

TEST	FA	PSAR	PSFR	EFFA'B	EFFGA
5-5A-1	0.0084	0.1647	-	101.8504	99.5687
5-5A-2	0.0105	0.1646	-	101.2500	98.9647
5-5A-3	0.0073	0.1652	-		99.3473
5-5A-4	0.0075	0.1653	-		99.4893
5-5A-5	0.0076	0.1651	-		99.5234
5-5A-6	0.0078	0.1649	-	101.1874	99.5762
5-7A-1	0.0080	0.8531	-	95.3143	92.5278
5-7A-2	0.0118	0.8533	-	97.4836	98.2584
5-7A-3	0.0157	0.8545	-	98.2366	98.3170
5-7A-4	0.0228	0.8551	-	95.1056	98.9066
5-7A-5	0.0086	0.8538	-	107.3376	98.2019
5-7A-6	0.0043	0.8534	-	105.6458	98.7887
5-7A-7	0.0086	0.8537	-	107.1973	98.4050
5-7A-8	0.0079	0.8543	-	97.0589	94.9266
5-7A-9	0.0050	0.8545	-	96.1388	96.3381
5-8A-1	0.0085	0.3141	-	100.5203	99.7262
5-8A-2	0.0129	0.3134	-	99.9342	99.6742
5-8A-3	0.0173	0.3136	-	99.6078	99.5698
5-8A-4	0.0241	0.3146	-	99.8095	99.2956
5-8A-5	0.0075	0.3088	-		99.7096
5-8A-6	0.0072	0.3092	-		99.7357
5-8A-7	0.0066	0.3091	-		99.6532

APPENDIX VII
SAMPLE-GAS TRANSFER LINE
TEMPERATURE DATA

Table XVI contains sample-gas transfer line temperature data obtained from tests conducted on combustors A and B during Phase II. (See Section IV, paragraph B.5 for a discussion of the traverse and gas sample transfer systems.)

Table XVI. Sample-Gas Transfer Line Temperature Data

TEST	FA	TSG1	TSG2	TSG3	TSG4
1-1A-1	0.0039	465.2500	340.5000	81.7500	
1-1A-2	0.0080	496.2500	348.7500	83.7500	
1-1A-3	0.0083	445.0000	322.5000	355.0000	
1-1A-4	0.0039	410.0000	315.0000	350.0000	342.5000
1-1A-5	0.0122	480.0000	333.7500	351.2500	343.7500
1-1A-6	0.0183	530.0001	353.7500	355.0000	342.5000
1-1A-7	0.0120	479.0000	328.2500	332.0000	336.7500
1-1A-8	0.0121	550.0001	386.2500	333.0000	349.2500
1-1A-9	0.0123	486.2500	335.0000	327.5000	354.2500
1-1A-10	0.0040	493.7500	382.5000		365.0000
1-1A-11	0.0039	427.5000	328.7500		325.0000
1-1A-12	0.0027	452.5000	317.5000		325.0000
1-1A-13	0.0067	433.7500	310.0000		323.7500
1-1A-14	0.0080	471.2500	328.7500		328.7500
1-1A-15	0.0060	447.5000	313.7500		377.5000
1-1A-16	0.0039	433.7500	317.5000		353.7500
1-1A-17	0.0123	473.7500	318.7500		373.7500
1-1A-18	0.0165	512.5001	341.2500		380.0000
1-1A-19	0.0188	536.2501	347.5000		322.5000
1-1A-20	0.0081	446.2500	320.0000		348.7500

Table XVI. Sample-Gas Transfer Line Temperature Data (Continued)

TEST	FA	TSG1	TSG2	TSG3	TSG4	HCA11
1-1B-1	0.0082	526.2501	347.5000	353.7500	323.0000	316.6951
1-1B-2	0.0038	455.0000	342.0000	354.5000	334.2500	336.6898
1-1B-3	0.0122	487.5000	345.0000	332.0000	316.0000	309.6317
1-1B-4	0.0041	420.0000	310.0000	360.0000	335.0000	315.6084
1-1B-5	0.0083	465.0000	320.0000	375.0000	350.0000	316.0431
1-1B-6	0.0125	510.0000	330.0000	350.0000	330.0000	313.0005
1-1B-7	0.0189	548.7501	348.7500	350.0000	325.0000	304.6331
1-1B-8	0.0200	568.0001	366.2500	353.0000	323.7500	331.6912
1-1B-9	0.0122	505.0000	350.0000	317.0000	270.0000	294.7444
1-1B-10	0.0185	555.0001	360.0000	350.0000	315.0000	329.5178
1-1B-11	0.0084	472.0000	347.0000	355.0000	325.0000	304.7260
1-1B-12	0.0082	455.0000	320.0000	390.0000	350.0000	298.6564
1-1B-13	0.0083	475.0000	330.0000	395.0000	355.0000	298.2217
1-1B-14	0.0084	431.7500	320.0000	357.5000	327.5000	328.3224
1-1B-15	0.0082	440.0000	325.0000	337.0000	335.0000	366.0299
1-1B-16	0.0081	460.0000	327.5000	343.7500	303.7500	324.9537
1-1B-17	0.0061	415.0000	310.0000	345.0000	310.0000	322.9978
1-1B-18	0.0102	480.0000	335.0000	350.0000	320.0000	312.1311
1-1B-19	0.0032	455.6666	330.0000	361.6666	313.3333	319.5204
1-1B-20	0.0062	470.0000	330.0000	350.0000	300.0000	312.1311
4-1A-1	0.0062	471.2500	322.5000	310.0000	321.2500	288.9850
4-1A-2	0.0084	482.5000	327.5000	307.5000	313.7500	298.2217
4-1A-3	0.0039	485.0000	283.7500	318.7500	327.5000	313.3264
4-1A-4	0.0102	553.7501	303.7500	318.7500	333.7500	289.6370
4-1A-5	0.0080	450.0000	325.0000	315.0000	310.0000	293.4403
4-1A-6	0.0039	413.7500	315.0000	317.5000	333.7500	295.1790
4-1A-7	0.0102	471.2500	327.5000	317.5000	332.5000	297.8958
4-1A-8	0.0061	430.0000	315.0000	315.0000	360.0000	302.5684
4-1A-9	0.0085	451.2500	305.0000	313.7500	338.7500	278.9877
4-1A-10	0.0125	500.0000	328.7500	318.7500	301.2500	286.3770
4-1A-11	0.0166	505.0000	335.0000	320.0000	350.0000	284.7470
4-1A-12	0.0206	555.0001	360.0000	320.0000	340.0000	293.0057
4-1A-13	0.0064	485.0000	336.0000	315.0000	300.0000	293.8750
4-1A-14	0.0104	450.0000	310.0000	310.0000	350.0000	289.9630
4-1A-15	0.0163	505.0000	330.0000	310.0000	345.0000	305.6111
4-1A-16	0.0124	475.0000	315.0000	310.0000	340.0000	300.3950
4-1A-17	0.0166	505.0000	330.0000	310.0000	345.0000	292.1364
4-1A-18	0.0208	550.0001	350.0000	310.0000	345.0000	301.6991
4-1A-19	0.0146	495.0000	340.0000	310.0000	350.0000	302.1338
4-1A-20	0.0075	425.0000	295.0000	310.0000	350.0000	286.9203

Table XVI. Sample-Gas Transfer Line Temperature Data (Continued)

TEST	FA	TSG1	TSG2	TSG3	TSG4	HCA1
3-1A-1	0.0072	462.5000	308.7500	332.5000	308.7500	300.7211
3-1A-2	0.0092	456.2500	305.0000	323.7500	310.0000	307.2411
3-1A-3	0.0124	492.5000	331.2500	315.0000	328.7500	310.7184
3-1A-4	0.0144	480.0000	331.2500	318.7500	288.7500	306.9151
3-1A-5	0.0042	440.0000	315.0000	315.0000	260.0000	302.1338
3-1A-6	0.0133	480.0000	340.0000	315.0000	310.0000	312.5658
2-1A-1	0.0059	418.7500	306.2500	288.7500	336.2500	312.4570
2-1A-2	0.0091	445.0000	322.5000	300.0000	328.7500	314.8478
2-1A-3	0.0132	465.0000	343.7500	311.2500	327.5000	307.5670
2-1A-4	0.0162	475.0000	355.0000	330.0000	335.0000	310.8270
2-1A-5	0.0196	485.0000	360.0000	330.0000	340.0000	323.4325
2-2A-1	0.0040	365.0000	311.2500	316.2500	328.7500	330.7131
2-2A-2	0.0060	388.7500	318.7500	325.0000	321.2500	309.1970
2-2A-3	0.0080	422.5000	325.5000	323.7500	309.5000	303.5464
2-3A-1	0.0061	412.5000	316.2500	310.0000	320.0000	315.6084
2-3A-2	0.0082	422.5000	328.7500	290.0000	306.2500	326.2578
2-3A-3	0.0134	453.7500	337.5000	301.2500	320.0000	311.3704
2-3A-4	0.0113	435.0000	330.0000	305.0000	335.0000	307.3497
2-3A-5	0.0093	410.0000	315.0000	310.0000	330.0000	305.1764
2-3A-6	0.0081	420.0000	313.7500	318.7500	328.7500	302.8944
2-3A-7	0.0040	375.0000	294.0000	300.0000	295.0000	296.0484
2-3A-8	0.0050	380.0000	297.0000	315.0000	310.0000	292.1364
2-3A-9	0.0060	392.0000	305.0000	318.0000	315.0000	302.5684
2-1B-1	0.0039	385.0000	325.0000	305.0000	345.0000	285.6163
2-1B-2	0.0086	396.2500	315.0000	305.0000	343.7500	323.8671
2-1B-3	0.0158	436.2500	333.7500	307.0000	336.2500	302.0250
2-1B-4	0.0196	411.2500	326.2500	303.7500	333.7500	306.6978
2-1B-5	0.0119	397.2500	311.2500	300.0000	335.0000	300.2864
2-1B-6	0.0160	416.2500	330.0000	297.5000	317.5000	303.1117
2-1B-7	0.0200	407.5000	326.2500	300.0000	331.2500	305.3937
2-1B-8	0.0160	371.2500	297.5000	296.2500	318.7500	303.4378
2-1B-9	0.0200	407.5000	332.5000	295.0000	330.0000	305.5023

Table XVI. Sample-Gas Transfer Line Temperature Data (Continued)

TEST	FA	TSG1	TSG2	TSG3	TSG4	HCAT1
5-1B-1	0.0040	416.2500	313.7500	331.2500	346.2500	280.2916
5-1B-2	0.0081	455.7500	330.7500	310.0000	308.7500	331.4738
5-1B-3	0.0101	477.5000	345.5000	290.0000	291.2500	347.6652
5-1B-4	0.0061	442.5000	321.2500	307.5000	303.7500	332.7778
5-1A-1	0.0070	366.5000	298.0000	347.2500	349.0000	284.6383
5-1A-2	0.0087	381.2500	334.5000	315.7500	323.0000	301.8078
5-1A-3	0.0100	360.0000	290.0000	290.0000	252.0000	304.3070
5-1A-4	0.0051	362.5000	297.5000	300.0000	315.5000	302.1337
5-1A-5	0.0060	370.0000	300.0000	300.0000	315.0000	303.8724
5-1A-6	0.0082	416.2500	321.2500	300.0000	352.5000	283.1170
5-1A-7	0.0071	405.0000	315.0000	280.0000	335.0000	324.3018
5-1A-8	0.0060	396.2500	310.0000	275.0000	344.5000	315.0651
5-1A-9	0.0101	450.0000	345.0000	286.2500	362.5000	313.7611
5-1A-10	0.0121	455.0000	370.0000	303.3333	333.3333	320.3898
5-1A-11	0.0060	365.0000	280.0000	300.0000	325.0000	303.4378
5-1A-12	0.0049	350.0000	270.0000	300.0000	325.0000	294.3097
5-2A-1	0.0081	393.7500	307.5000	328.0000	392.5000	232.5868
5-2A-2	0.0100	405.2500	306.7500	339.5000	363.0000	232.1522
5-2A-3	0.0059	399.2500	315.0000	346.0000	326.0000	247.0395
5-2A-4	0.0079	400.0000	305.0000	325.0000	310.0000	268.2296
5-2A-5	0.0068	395.0000	300.0000	330.0000	320.0000	277.3577
5-2A-6	0.0055	390.0000	290.0000	330.0000	325.0000	260.8402
5-2A-7	0.0063	400.0000	305.0000	337.0000	325.0000	269.0990
5-3A-1	0.0083	422.5000	321.2500	332.5000	326.2500	242.9101
5-3A-2	0.0062	400.0000	310.0000	342.5000	352.5000	270.4030
5-3A-3	0.0102	440.2500	335.5000	338.0000	330.2500	315.6084
5-3A-4	0.0054	390.0000	290.0000	330.0000	330.0000	314.7391
5-3A-5	0.0057	400.0000	285.0000	335.0000	330.0000	316.4778
5-3A-6	0.0067	405.0000	295.0000	335.0000	330.0000	313.0005
5-4A-1	0.0080	417.0000	315.0000	310.2500	353.0000	280.2916
5-4A-2	0.0099	428.2500	335.5000	321.5000	334.2500	336.2551
5-4A-3	0.0050	374.0000	300.0000	323.5000	326.0000	313.8698
5-4A-4	0.0054	383.7500	315.0000	324.7500	326.2500	286.9203
5-4A-5	0.0059	379.2500	321.2500	326.2500	332.0000	283.2257

Table XVI. Sample-Gas Transfer Line Temperature Data (Continued)

TEST	FA	TSG1	TSG2	TSG3	TSG4	HCAT1
5-5A-1	0.0084	419.0000	330.5000	331.7500	240.0000	268.4469
5-5A-2	0.0105	443.0000	345.0000	325.7500	233.7500	293.8750
5-5A-3	0.0073	407.0000	320.0000	325.0000	235.0000	297.3524
5-5A-4	0.0075	407.0000	320.0000	325.0000	240.0000	299.0911
5-5A-5	0.0076	407.0000	320.0000	330.0000	260.0000	292.1364
5-5A-6	0.0078	413.0000	325.0000	326.2500	375.0000	293.0057
5-7A-1	0.0080	402.5000	308.7500	288.7500	357.5000	242.2582
5-7A-2	0.0118	406.7500	319.7500	306.5000	340.0000	300.1777
5-7A-3	0.0157	440.0000	339.2500	309.2500	319.2500	337.0805
5-7A-4	0.0228	442.5000	341.7500	308.0000	297.5000	344.1878
5-7A-5	0.0086	412.5000	343.0000	293.7500	296.2500	283.5516
5-7A-6	0.0043	367.5000	310.0000	295.0000	325.0000	286.0510
5-7A-7	0.0086	408.7500	342.5000	297.0000	329.2500	290.7236
5-7A-8	0.0079	393.0000	331.2500	286.2500	300.0000	317.5645
5-7A-9	0.0050	373.7500	315.5000	296.2500	327.5000	315.9345
5-8A-1	0.0085	426.2500	338.7500	306.2500	347.5000	264.2090
5-8A-2	0.0129	442.5000	341.2500	317.5000	355.0000	286.8117
5-8A-3	0.0173	451.2500	351.2500	322.5000	350.0000	246.4962
5-8A-4	0.0241	528.7501	391.2500	325.0000	340.0000	238.5635
5-8A-5	0.0075	265.0000	215.0000	315.0000	335.0000	243.0189
5-8A-6	0.0072	260.0000	210.0000	315.0000	335.0000	237.8028
5-8A-7	0.0066	255.0000	205.0000	315.0000	335.0000	230.8481

Table XVI. Sample-Gas Transfer Line Temperature Data (Continued)

TEST	FA	SIT1	HCA11
1-1A-1	0.0039	373.8539	389.9367
1-1A-2	0.0080	404.1720	387.3286
1-1A-3	0.0083	326.3665	306.9151
1-1A-4	0.0039	312.5657	302.8944
1-1A-5	0.0122	313.0004	306.8064
1-1A-6	0.0183	317.0211	312.2398
1-1A-7	0.0120	358.8579	301.8076
1-1A-8	0.0121	275.0757	342.8838
1-1A-9	0.0123	353.4246	336.4724
1-1A-10	0.0040	352.0119	351.5772
1-1A-11	0.0039	335.0598	333.4298
1-1A-12	0.0027	329.7351	357.4452
1-1A-13	0.0067	339.0805	326.5838
1-1A-14	0.0080	274.4236	314.7390
1-1A-15	0.0060	314.6304	336.6898
1-1A-16	0.0039	356.0325	321.5851
1-1A-17	0.0123	356.7932	364.9432
1-1A-18	0.0165	340.6018	344.7311
1-1A-19	0.0188	323.9757	330.9304
1-1A-20	0.0081	318.5424	318.2164

APPENDIX VIII

MEASURED TEST DATA

Table XVII contains measured data for tests conducted on combustors A and B during Phase II. The operating variables listed are Test No., FA, TT3, PT3, VREF, and LPL.

APPENDIX VIII

MEASURED TEST DATA

Table XVII contains measured data for tests conducted on combustors A and B during Phase II. The operating variables listed are Test No., FA, TT3, PT3, VREF, and LPL.

Table XVII. Measured Test Data

TEST	FA	TT3	PT3	VREF	LPL
1-1A-1	0.0039	397.5000	14.8071	109.0100	1.5607
1-1A-2	0.0080	399.1666	14.7071	109.5554	1.9018
1-1A-3	0.0083	400.0000	15.2066	104.5762	1.8201
1-1A-4	0.0039	396.6666	15.2068	105.2934	1.8188
1-1A-5	0.0122	396.6666	15.3068	105.4227	1.8838
1-1A-6	0.0183	396.6666	15.4067	104.1490	1.9671
1-1A-7	0.0120	402.3333	15.4068	105.2706	1.8801
1-1A-8	0.0121	400.0000	15.4067	103.9805	1.8113
1-1A-9	0.0123	397.5833	15.3442	103.9606	1.8202
1-1A-10	0.0040	403.3333	15.2067	105.1596	1.7892
1-1A-11	0.0039	400.0000	15.2068	106.0094	1.8463
1-1A-12	0.0027	395.0000	15.2067	104.6763	1.7541
1-1A-13	0.0067	390.0000	15.1068	104.9614	1.7767
1-1A-14	0.0080	400.0000	15.2565	103.2986	1.7924
1-1A-15	0.0060	407.0833	15.2067	105.3431	1.7926
1-1A-16	0.0039	404.5833	15.1317	105.6971	1.7892
1-1A-17	0.0123	400.0000	15.2067	104.8283	1.8357
1-1A-18	0.0165	400.0000	15.3066	104.0760	1.8875
1-1A-19	0.0188	406.6666	15.5066	103.3529	1.8873
1-1A-20	0.0031	400.0000	15.3068	105.0962	1.8407
1-1B-1	0.0082	400.0000	15.4066	103.5378	1.7934
1-1B-2	0.0038	400.0000	15.2319	106.5658	1.8156
1-1B-3	0.0122	395.2500	15.4068	104.5276	1.8330
1-1B-4	0.0041	395.0000	16.0142	147.9809	3.4306
1-1B-5	0.0083	395.0000	16.0639	146.1865	3.3984
1-1B-6	0.0125	395.0000	16.1890	146.0898	3.4955
1-1B-7	0.0189	400.0000	15.6064	101.3933	1.8161
1-1B-8	0.0200	400.0000	15.5066	103.0721	1.8789
1-1B-9	0.0122	402.0000	15.4068	104.9705	1.8279
1-1B-10	0.0185	400.0000	15.5066	103.3026	1.8880
1-1B-11	0.0084	405.0000	16.7196	171.2228	4.5136
1-1B-12	0.0082	250.0000	15.1545	78.5513	1.2579
1-1B-13	0.0083	395.0000	15.0035	76.9858	1.0082
1-1B-14	0.0084	245.7500	15.4074	99.2096	1.9248
1-1B-15	0.0082	245.0000	16.0134	130.5596	3.3383
1-1B-16	0.0081	400.0000	15.4067	104.0196	1.7355
1-1B-17	0.0061	410.0000	15.4066	104.2829	1.7172
1-1B-18	0.0102	400.0000	15.4067	104.4922	1.7405
1-1B-19	0.0082	400.0000	15.4066	103.6038	1.7690
1-1B-20	0.0062	400.0000	15.4066	103.6258	1.7596

Table XVII. Measured Test Data (Continued)

TEST	FA	TT3	PT3	VREF	LPL
4-1A-1	0.0062	398.7500	15.4066	103.3657	1.5984
4-1A-2	0.0084	400.0000	15.4066	103.9347	1.6184
4-1A-3	0.0039	393.7500	15.2318	105.7094	1.6326
4-1A-4	0.0102	395.0000	15.3317	104.3135	1.6489
4-1A-5	0.0080	405.0000	15.4067	104.9061	1.6284
4-1A-6	0.0039	405.0000	15.3068	105.5062	1.6301
4-1A-7	0.0102	405.0000	15.3318	105.3779	1.6769
4-1A-8	0.0061	400.0000	15.4069	105.7051	1.6483
4-1A-9	0.0085	402.5000	15.3067	104.7816	1.6319
4-1A-10	0.0125	400.0000	15.4066	103.8295	1.6934
4-1A-11	0.0166	405.0000	15.4067	104.9174	1.7940
4-1A-12	0.0206	405.0000	15.6066	102.9732	1.9017
4-1A-13	0.0064	405.0000	15.2068	106.0195	1.6265
4-1A-14	0.0104	405.0000	15.4068	105.4024	1.6889
4-1A-15	0.0163	405.0000	15.4068	105.4024	1.8355
4-1A-16	0.0124	405.0000	15.4068	105.4290	1.7168
4-1A-17	0.0166	400.0000	15.4066	103.7283	1.7537
4-1A-18	0.0208	400.0000	15.5066	103.0598	1.8485
4-1A-19	0.0146	400.0000	15.4066	103.8499	1.7054
4-1A-20	0.0075	400.0000	15.4066	103.8499	1.5984
3-1A-1	0.0072	400.0000	15.3066	104.2314	1.6146
3-1A-2	0.0092	400.0000	15.3067	104.4951	1.6299
3-1A-3	0.0124	400.0000	15.3067	104.5189	1.6631
3-1A-4	0.0144	400.0000	15.4066	103.8627	1.6800
3-1A-5	0.0092	400.0000	15.3067	104.5366	1.6342
3-1A-6	0.0132	400.0000	15.3067	104.5366	1.6888
2-1A-1	0.0054	405.0000	15.3318	105.6529	1.6888
2-1A-2	0.0091	395.0000	15.4067	103.6851	1.6546
2-1A-3	0.0102	395.0000	15.4066	103.6938	1.7028
2-1A-4	0.0162	395.0000	15.5066	102.9525	1.7654
2-1A-5	0.0196	395.0000	15.5066	102.9525	1.8303
2-2A-1	0.0040	395.0000	15.1880	105.6865	1.6453
2-2A-2	0.0060	395.4166	15.2067	104.8535	1.6563
2-2A-3	0.0080	406.6666	15.2818	106.1722	1.6903

Table XVII. Measured Test Data (Continued)

TEST	FA	TT3	PT3	VREF	LPL
2-3A-1	0.0061	402.5000	15.2067	104.9825	1.6654
2-3A-2	0.0082	405.0000	15.2817	104.9861	1.6962
2-3A-3	0.0134	406.6666	15.4566	103.7096	1.6982
2-3A-4	0.0113	405.0000	15.5065	103.0750	1.7084
2-3A-5	0.0093	409.0000	15.5065	103.4675	1.6652
2-3A-6	0.0081	487.9166	15.2054	99.2510	1.3369
2-3A-7	0.0040	394.3333	15.2067	104.5940	1.6684
2-3A-8	0.0050	394.3333	15.2067	104.6146	1.6735
2-3A-9	0.0060	394.3333	15.2067	104.6146	1.6888
2-1H-1	0.0039	405.0000	15.2068	106.3324	1.7253
2-1H-2	0.0086	406.2500	15.2067	105.7647	1.7218
2-1H-3	0.0158	410.0000	15.5254	104.0019	1.8054
2-1H-4	0.0196	407.2500	15.5816	103.3556	1.7524
2-1H-5	0.0119	405.5000	15.4566	103.7404	1.7198
2-1H-6	0.0160	405.0000	15.5065	102.7303	1.7845
2-1H-7	0.0200	405.0000	15.5065	102.8559	1.8723
2-1H-8	0.0160	405.0000	15.4066	103.8304	1.7948
2-1H-9	0.0200	405.0000	15.5066	103.3342	1.8698

Table XVII. Measured Test Data (Continued)

TEST	FA	TT3	PT3	VREF	LPL
5-1A-1	0.0040	400.0000	15.5067	104.2614	3.5231
5-1A-2	0.0081	400.0000	15.6067	103.5184	3.4811
5-1A-3	0.0101	398.7500	15.7066	102.6464	3.4583
5-1A-4	0.0061	395.0000	15.6066	102.5407	3.4112
5-1A-1	0.0070	399.0833	15.7089	118.9504	3.5852
5-1A-2	0.0087	396.4166	15.7340	119.0971	3.5709
5-1A-3	0.0100	398.3333	15.7089	118.8355	3.6252
5-1A-4	0.0051	396.0000	15.6715	119.2710	3.5418
5-1A-5	0.0060	395.0000	15.7089	118.5803	3.5331
5-1A-6	0.0082	409.8333	15.7590	120.1705	3.6238
5-1A-7	0.0071	393.3333	15.7091	119.6024	3.5952
5-1A-8	0.0060	392.0833	15.7091	119.6420	3.5906
5-1A-9	0.0101	390.0000	15.7090	119.0698	3.6153
5-1A-10	0.0121	392.2222	15.8090	118.9251	3.6220
5-1A-11	0.0060	390.0000	15.7089	118.2182	3.6155
5-1A-12	0.0049	390.0000	15.7089	118.2536	3.5923
5-2A-1	0.0081	405.7500	16.0091	119.5149	4.1419
5-2A-2	0.0100	394.2500	15.8077	109.7797	3.5627
5-2A-3	0.0059	397.2500	15.7077	110.5034	3.6156
5-2A-4	0.0079	395.0000	15.7079	111.7301	3.6912
5-2A-5	0.0068	395.0000	15.7079	111.6636	3.6550
5-2A-6	0.0055	395.0000	15.7079	111.7301	3.6715
5-2A-7	0.0063	393.0000	15.7079	111.4710	3.6944
5-3A-1	0.0083	420.0000	15.6823	109.3746	3.4879
5-3A-2	0.0062	420.0000	15.6323	109.6704	3.4525
5-3A-3	0.0132	408.0000	15.7423	107.9442	3.4177
5-3A-4	0.0054	405.0000	15.6073	108.6714	3.5098
5-3A-5	0.0037	410.0000	15.8073	108.2104	3.4816
5-3A-6	0.0067	410.0000	15.8073	107.9809	3.5075
5-4A-1	0.0080	393.3333	15.6138	109.4012	3.5255
5-4A-2	0.0099	393.1666	15.7075	108.8217	3.4972
5-4A-3	0.0050	396.8333	15.6076	109.8727	3.5015
5-4A-4	0.0054	394.9166	15.6075	108.8903	3.4853
5-4A-5	0.0059	396.7500	15.7074	108.2406	3.4346

Table XVII. Measured Test Data (Continued)

TEST	FA	IT3	PT3	VREF	LPL
5-5A-1	0.0084	401.2500	16.1810	96.2724	7.0805
5-5A-2	0.0105	401.6666	16.2060	96.1657	7.0729
5-5A-3	0.0073	401.6666	16.1060	96.7063	7.1198
5-5A-4	0.0075	401.6666	16.1060	96.5345	7.1100
5-5A-5	0.0075	401.6666	16.1060	96.8191	7.1199
5-5A-6	0.0078	400.4166	16.1059	96.2650	7.0656
5-7A-1	0.0080	404.0000	15.6574	109.2226	3.6855
5-7A-2	0.0118	404.3333	15.7074	109.1231	3.7070
5-7A-3	0.0157	405.0000	15.8072	107.0960	3.7202
5-7A-4	0.0228	405.0000	16.0073	106.9393	3.7971
5-7A-5	0.0086	400.0000	15.6136	108.8954	3.7208
5-7A-6	0.0043	400.0000	15.6075	109.2928	3.7118
5-7A-7	0.0046	405.0000	15.6074	108.6929	3.7069
5-7A-8	0.0079	400.0000	15.6074	109.0070	3.7512
5-7A-9	0.0052	400.0000	15.6074	109.2567	3.7702
5-8A-1	0.0089	400.6666	15.6560	98.2307	3.7237
5-8A-2	0.0129	400.0000	15.7058	95.9301	3.6092
5-8A-3	0.0173	400.0000	15.7807	95.0536	3.5967
5-8A-4	0.0241	398.7500	15.9057	95.0483	3.6845
5-8A-5	0.0075	395.0000	15.8068	103.6189	3.8313
5-8A-6	0.0072	395.0000	15.8069	103.8766	3.8477
5-8A-7	0.0066	395.0000	15.8069	103.9801	3.8511

APPENDIX IX

UHC EMISSION CONCENTRATION DATA

Table XVIII contains data on UHC emission concentrations obtained during tests on combustors A and B during Phase II.

Table XVIII. UHC Emission Concentration Data

TEST	FA	HCTOA	HCTPW	HCTDX
1-1A-1	0.0039			
1-1A-2	0.0080			
1-1A-3	0.0083			
1-1A-4	0.0039			
1-1A-5	0.0122			
1-1A-6	0.0183			
1-1A-7	0.0120			
1-1A-8	0.0121			
1-1A-9	0.0123			
1-1A-10	0.0040	61.6251	34.1080	8.5427
1-1A-11	0.0039	56.9303	31.5095	8.0023
1-1A-12	0.0027	80.5619	44.5891	16.2092
1-1A-13	0.0067	9.8200	5.4351	0.8161
1-1A-14	0.0080	3.7074	2.0519	0.2585
1-1A-15	0.0060	14.2497	7.8869	1.3281
1-1A-16	0.0039	59.1249	32.7242	8.3887
1-1A-17	0.0123	2.1137	1.1699	0.0975
1-1A-18	0.0165	11.7593	6.5085	0.4054
1-1A-19	0.0188	5.6521	3.1283	0.1711
1-1A-20	0.0061	3.9825	2.2042	0.2760
1-1B-1	0.0082	107.5631	59.5336	7.3294
1-1B-2	0.0038	102.8424	56.9208	15.0356
1-1B-3	0.0122	69.2340	38.3194	3.2194
1-1B-4	0.0041	65.6944	36.3602	8.8365
1-1B-5	0.0083	12.8180	7.0944	0.8710
1-1B-6	0.0125	2.5706	1.4227	0.1165
1-1B-7	0.0189	26.4870	14.6599	0.8021
1-1B-8	0.0200	19.3743	10.7232	0.5520
1-1B-9	0.0122	51.3671	28.4304	2.3763
1-1B-10	0.0185	13.0184	7.2054	0.4011
1-1B-11	0.0084	3.9476	2.1849	0.2650
1-1B-12	0.0082	948.3106	524.8675	65.3201
1-1B-13	0.0083	210.8014	116.6735	14.2596
1-1B-14	0.0084	637.7398	352.9739	42.8674
1-1B-15	0.0082	264.2197	146.2393	18.2194
1-1B-16	0.0081	192.4040	106.4911	13.2804
1-1B-17	0.0061	295.3423	163.4649	26.9386
1-1B-18	0.0102	138.7717	76.8068	7.7120
1-1B-19	0.0082	19.6973	10.9020	1.3547
1-1B-20	0.0062	35.6102	19.7094	3.2456

Table XVIII. UHC Emission Concentration Data (Continued)

TEST	FA	HCTOA	HCTPW	HCTDX
4-1A-1	0.0062	28.5400	15.7962	2.5913
4-1A-2	0.0084	40.7383	22.5477	2.7644
4-1A-3	0.0039	41.4849	22.9609	5.9570
4-1A-4	0.0102	82.5923	45.7128	4.5836
4-1A-5	0.0080	38.1838	21.1338	2.6723
4-1A-6	0.0039	30.8475	17.0733	4.4129
4-1A-7	0.0102	46.4606	25.7148	2.5777
4-1A-8	0.0061	29.2213	16.1733	2.6994
4-1A-9	0.0085	3943.8813	2182.8452	261.6429
4-1A-10	0.0125	5097.1836	2821.1704	231.2247
4-1A-11	0.0166	5992.8759	3316.9150	205.9362
4-1A-12	0.0206	6521.4423	3609.4638	180.6336
4-1A-13	0.0064	4002.3051	2215.1816	348.0082
4-1A-14	0.0104	1462.2795	809.3371	79.5130
4-1A-15	0.0163	5773.3759	3195.4272	200.8321
4-1A-16	0.0124	2292.8461	1269.0361	104.6342
4-1A-17	0.0166	4278.4550	2368.0234	146.5152
4-1A-18	0.0208	5500.8320	3044.5800	150.9718
4-1A-19	0.0146	2052.6923	1136.1167	80.0016
4-1A-20	0.0075	4013.8549	2221.5737	301.3622
3-1A-1	0.0072	64.0760	35.4645	4.9763
3-1A-2	0.0092	57.2497	31.6863	3.5061
3-1A-3	0.0124	52.3652	28.9829	2.4047
3-1A-4	0.0144	41.9885	23.2396	1.6615
3-1A-5	0.0042	58.4228	32.3356	7.8324
3-1A-6	0.0133	1154.9492	639.2369	49.2080
2-1A-1	0.0059	36.7522	20.3414	3.4871
2-1A-2	0.0091	42.0802	23.2904	2.6174
2-1A-3	0.0132	23.3322	12.9138	1.0048
2-1A-4	0.0162	13.6196	7.5381	0.4781
2-1A-5	0.0196	8.7457	4.8405	0.2554
2-2A-1	0.0040	33.2044	18.3778	4.6613
2-2A-2	0.0060	33.5082	18.5460	3.1319
2-2A-3	0.0080	31.2009	17.2690	2.1930

Table XVIII. UHC Emission Concentration Data (Continued)

TEST	FA	HCTOA	HCTPW	HCTDX
2-3A-1	0.0061	1794.0285	992.9523	164.9206
2-3A-2	0.0082	2139.3466	1184.0776	147.3393
2-3A-3	0.0134	4985.0976	2759.1337	211.2952
2-3A-4	0.0113	4177.0966	2311.9238	208.9642
2-3A-5	0.0093	2900.6347	1605.4328	176.6095
2-3A-6	0.0081	1872.2080	1036.2229	129.7994
2-3A-7	0.0040	1772.7624	981.1821	248.2805
2-3A-8	0.0050	1969.6835	1090.1733	219.2986
2-3A-9	0.0060	2124.5312	1175.8776	198.0233
2-1B-1	0.0039	39.8226	22.0408	5.6666
2-1B-2	0.0086	2964.1074	1640.5634	194.3981
2-1B-3	0.0158	6020.2588	3332.0708	217.0537
2-1B-4	0.0196	5115.9082	2831.5336	148.9452
2-1B-5	0.0119	2273.1157	1258.1157	108.1560
2-1B-6	0.0160	3946.9589	2184.5483	140.1850
2-1B-7	0.0200	4367.7597	2417.4516	125.1784
2-1B-8	0.0160	1087.0524	601.6578	38.6364
2-1B-9	0.0200	2260.2548	1250.9975	64.6360

Table XVIII. UHC Emission Concentration Data (Continued)

TEST	FA	HCTCA	HCTPW	HCTDX
5-1H-1	0.0040	14.6459	8.1062	2.0598
5-1H-2	0.0081	3.4013	1.8825	0.2365
5-1H-3	0.0101	2.7831	1.5404	0.1550
5-1H-4	0.0061	3.5222	1.9494	0.3238
5-1A-1	0.0070	13.3096	7.3666	1.0736
5-1A-2	0.0087	9.0132	4.9886	0.5848
5-1A-3	0.0100	0.9322	0.5159	0.0526
5-1A-4	0.0051	390.0789	215.8994	42.6446
5-1A-5	0.0060	10.1085	5.5948	0.9380
5-1A-6	0.0082	2.8729	1.5901	0.1976
5-1A-7	0.0071	3.0592	1.6932	0.2410
5-1A-8	0.0060	8.5623	4.7390	0.7965
5-1A-9	0.0101	1.5277	0.8455	0.0853
5-1A-10	0.0121	1.3538	0.7493	0.0635
5-1A-11	0.0060	5.0665	2.8042	0.4754
5-1A-12	0.0049	38.2738	21.1836	4.3476
5-2A-1	0.0081	1.8261	1.0107	0.1271
5-2A-2	0.0100	0.2474	0.1369	0.0140
5-2A-3	0.0059	1.4982	0.8292	0.1421
5-2A-4	0.0079	2.2493	1.2449	0.1604
5-2A-5	0.0068	2.0760	1.1490	0.1710
5-2A-6	0.0055	55.1486	30.5234	5.6414
5-2A-7	0.0063	8.2011	4.5391	0.7261
5-3A-1	0.0083	2.7599	1.5275	0.1980
5-3A-2	0.0062	3.1727	1.7560	0.2877
5-3A-3	0.0102	2.5807	1.4283	0.1427
5-3A-4	0.0054	19.2937	10.6786	2.0121
5-3A-5	0.0057	2.9650	1.6411	0.2907
5-3A-6	0.0067	2.2249	1.2314	0.1859
5-4A-1	0.0080	1.9248	1.0653	0.1343
5-4A-2	0.0099	1.3915	0.7701	0.0786
5-4A-3	0.0050	27.0068	14.9476	3.0073
5-4A-4	0.0054	17.0128	9.4162	1.7495
5-4A-5	0.0059	1.3444	0.7441	0.1258

Table XVIII. UHC Emission Concentration Data (Continued)

TEST	FA	HCTOA	HCTPW	HCTDX
5-5A-1	0.0084	1.3475	0.7458	0.0906
5-5A-2	0.0105	0.4589	0.2540	0.0246
5-5A-3	0.0073	18.6228	10.5073	1.4306
5-5A-4	0.0075	11.0179	6.0981	0.8227
5-5A-5	0.0076	8.3981	4.6481	0.6209
5-5A-6	0.0078	3.8806	2.1478	0.2782
5-7A-1	0.0080	4.6276	2.5613	0.3274
5-7A-2	0.0118	31.7289	17.5612	1.5215
5-7A-3	0.0157	38.5893	21.3582	1.3937
5-7A-4	0.0228	13.2895	7.3554	0.3333
5-7A-5	0.0086	62.1974	34.4248	4.0745
5-7A-6	0.0043	10.2758	5.6874	1.3422
5-7A-7	0.0086	37.3513	20.6730	2.4551
5-7A-8	0.0079	262.4821	145.2776	18.6332
5-7A-9	0.0050	93.2510	51.6122	10.4697
5-8A-1	0.0085	4.7737	2.6421	0.3157
5-8A-2	0.0129	6.6659	3.6894	0.2936
5-8A-3	0.0173	8.4945	4.7015	0.2795
5-8A-4	0.0241	12.1430	6.7208	0.2890
5-8A-5	0.0075	5.2859	2.9256	0.3943
5-8A-6	0.0072	4.5969	2.5443	0.3605
5-8A-7	0.0066	7.5090	4.1561	0.6340

APPENDIX X

CO EMISSION CONCENTRATION DATA

Table XIX contains data on the CO emission concentrations obtained during tests on combustors A and B during Phase II.

Table XIX. CO Emission Concentration Data

TEST	FA	COOA	COPW	CODX
1-1A-1	0.0039			
1-1A-2	0.0080			
1-1A-3	0.0089			
1-1A-4	0.0039			
1-1A-5	0.0122			
1-1A-6	0.0183			
1-1A-7	0.0120			
1-1A-8	0.0121			
1-1A-9	0.0123			
1-1A-10	0.0040	436.4757	421.9194	105.6740
1-1A-11	0.0039	572.7857	553.6835	140.6161
1-1A-12	0.0027	268.4751	259.5216	94.3424
1-1A-13	0.0067	203.1857	196.4096	29.4945
1-1A-14	0.0080	297.1625	287.2523	36.1978
1-1A-15	0.0060	335.6276	324.4346	54.6336
1-1A-16	0.0039	435.0118	420.5043	107.7944
1-1A-17	0.0123	439.0335	424.3919	35.4045
1-1A-18	0.0165	594.3217	574.5013	35.7853
1-1A-19	0.0188	653.1143	631.3332	34.5418
1-1A-20	0.0081	344.7686	333.2708	41.7410
1-1H-1	0.0082	478.3499	462.3872	56.9276
1-1H-2	0.0038	404.1546	390.6762	103.1967
1-1H-3	0.0122	520.9436	503.5702	42.3080
1-1H-4	0.0041	520.4455	503.0888	122.2646
1-1H-5	0.0083	464.0108	448.5363	55.0694
1-1H-6	0.0125	560.7419	542.0413	44.4070
1-1H-7	0.0189	559.4598	540.8021	29.5925
1-1H-8	0.0200	690.6225	667.5905	34.3691
1-1H-9	0.0122	443.8099	429.0090	35.8586
1-1H-10	0.0185	600.3560	580.3343	32.3075
1-1H-11	0.0084	529.0128	511.3704	62.0334
1-1H-12	0.0082	747.6822	722.7474	89.9463
1-1H-13	0.0083	387.7640	374.8322	45.8113
1-1H-14	0.0084	716.5463	692.6499	84.1199
1-1H-15	0.0082			
1-1H-16	0.0081	867.1156	838.1976	104.5312
1-1H-17	0.0061	750.1453	725.1284	119.4996
1-1H-18	0.0102	971.6640	939.2594	94.3098
1-1H-19	0.0082	546.1646	527.9503	65.6038
1-1H-20	0.0062	491.5258	475.1336	78.2437

Table XIX. CO Emission Concentration Data (Continued)

TEST	FA	COOA	COPW	CODX
4-1A-1	0.0062	251.7602	243.3641	39.9234
4-1A-2	0.0084	392.6242	379.5303	46.5318
4-1A-3	0.0039			
4-1A-4	0.0102			
4-1A-5	0.0080	371.2796	358.8976	45.3817
4-1A-6	0.0039	142.5090	137.7563	35.6057
4-1A-7	0.0102	482.9884	466.8809	46.8016
4-1A-8	0.0061	246.8308	238.5991	39.8244
4-1A-9	0.0085	1248.7553	1207.1098	144.6881
4-1A-10	0.0125	1996.8090	1930.2163	158.2016
4-1A-11	0.0166	2783.9072	2691.0649	167.0793
4-1A-12	0.0206	3450.4516	3335.3803	166.9173
4-1A-13	0.0064	607.7718	587.5029	92.2975
4-1A-14	0.0104	1121.1391	1083.7495	106.4726
4-1A-15	0.0163	2753.1528	2661.3359	167.2645
4-1A-16	0.0124	1318.6818	1274.7043	105.1015
4-1A-17	0.0166	2220.3295	2146.2822	132.7955
4-1A-18	0.0208	3029.7924	2928.7500	145.2282
4-1A-19	0.0146	1418.3413	1371.0402	96.5442
4-1A-20	0.0075	1053.4670	1018.3342	138.1396
3-1A-1	0.0072	233.8909	226.0907	31.7246
3-1A-2	0.0092	338.8951	327.5930	36.2487
3-1A-3	0.0124	599.8973	579.8909	48.1136
3-1A-4	0.0144	806.8754	779.9665	59.7649
3-1A-5	0.0042	169.0589	163.4208	39.5841
3-1A-6	0.0133	1190.2858	1150.5903	88.5716
2-1A-1	0.0099	174.3501	168.5356	28.8924
2-1A-2	0.0091	309.1412	298.8314	33.5835
2-1A-3	0.0132	620.3923	599.7025	46.6637
2-1A-4	0.0162	886.3471	856.7878	54.3479
2-1A-5	0.0196	1167.8024	1128.8966	59.5773
2-2A-1	0.0040	126.3979	122.1825	30.9902
2-2A-2	0.0060	230.3230	222.6418	37.5989
2-2A-3	0.0080	376.3322	369.7150	46.4437

Table XIX. CO Emission Concentration Data (Continued)

TEST	FA	COOA	COPW	CODX
2-3A-1	0.0061	567.9292	548.9888	91.1822
2-3A-2	0.0082	519.4078	502.6857	62.4764
2-3A-3	0.0134	1043.6650	1008.8591	77.2587
2-3A-4	0.0113	675.1102	652.5955	58.9851
2-3A-5	0.0093	554.0106	535.5345	58.9127
2-3A-6	0.0081	416.1895	402.3097	50.3941
2-3A-7	0.0040	445.0803	430.2370	108.8681
2-3A-8	0.0050	608.4742	588.1818	118.3183
2-3A-9	0.0060	626.3504	605.4619	101.9626
2-18-1	0.0039	244.8340	236.6689	60.8474
2-18-2	0.0086	790.5710	764.2058	90.5943
2-18-3	0.0158	1740.4938	1682.4492	107.5960
2-18-4	0.0196	1925.5141	1861.2990	97.9086
2-18-5	0.0119	1062.0209	1026.6030	88.2536
2-18-6	0.0160	1622.2895	1568.1070	100.6324
2-18-7	0.0200	1895.0461	1831.8471	94.8551
2-18-8	0.0160	1321.2287	1277.1662	82.0152
2-18-9	0.0200	1730.6635	1672.9467	86.4370

Table XIX. CO Emission Concentration Data (Continued)

TEST	FA	COOA	COPW	COUX
5-1H-1	0.0040	145.9021	141.0364	35.8389
5-1H-2	0.0081	576.1145	556.9012	69.9666
5-1H-3	0.0101	787.2430	760.9287	76.6213
5-1H-4	0.0061	321.9171	311.1812	51.6966
5-1A-1	0.0070	223.4650	216.0135	31.4819
5-1A-2	0.0087	393.7067	380.5767	44.6174
5-1A-3	0.0100	431.0436	416.6685	42.5161
5-1A-4	0.0051	377.3182	364.7348	72.0428
5-1A-5	0.0040	61.1816	59.1413	9.9160
5-1A-6	0.0082	273.5105	264.3890	32.8573
5-1A-7	0.0071	100.8013	97.4396	13.8741
5-1A-8	0.0060	58.9200	56.9550	9.5727
5-1A-9	0.0101	790.8087	764.4355	77.1181
5-1A-10	0.0121	1163.2614	1124.4670	95.3367
5-1A-11	0.0060	43.8238	47.1955	8.0019
5-1A-12	0.0069	145.6502	140.7928	28.8959
5-2A-1	0.0081	174.1286	168.3215	21.1801
5-2A-2	0.0100	489.4195	473.0975	48.3851
5-2A-3	0.0059	32.0711	31.0016	5.3139
5-2A-4	0.0075	120.1452	116.1384	14.9675
5-2A-5	0.0068	48.0040	46.4031	6.9091
5-2A-6	0.0055	232.3897	224.6396	41.5165
5-2A-7	0.0063	36.6226	35.4012	5.6636
5-3A-1	0.0083	172.7024	166.9429	20.5464
5-3A-2	0.0062	28.7038	27.7466	4.5471
5-3A-3	0.0102	475.7958	459.9292	45.9656
5-3A-4	0.0054	64.4789	62.3285	11.7446
5-3A-5	0.0057	23.2362	22.4613	3.9800
5-3A-6	0.0067	37.9971	36.7299	5.5474
5-4A-1	0.0080	218.3160	211.0353	26.6038
5-4A-2	0.0099	495.7892	479.2548	48.9272
5-4A-3	0.0050	88.4738	85.5233	17.2064
5-4A-4	0.0054	66.1083	63.9036	11.8737
5-4A-5	0.0059	50.7797	49.0862	6.3031

Table XIX. CO Emission Concentration Data (Continued)

TEST	FA	COOA	COPW	CODX
5-5A-1	0.0084	152.2807	147.2022	17.8848
5-5A-2	0.0105	467.4956	451.9049	43.8862
5-5A-3	0.0073	153.9501	148.8159	20.6559
5-5A-4	0.0073	135.2193	130.7098	17.5349
5-5A-5	0.0076	133.0521	128.6149	17.1817
5-5A-6	0.0078	132.8690	128.4379	16.6365
5-7A-1	0.0080	458.8861	443.3824	56.7119
5-7A-2	0.0118	793.9854	767.5063	66.4970
5-7A-3	0.0157	1024.7023	990.5289	64.6386
5-7A-4	0.0228	1023.1857	989.0629	44.8294
5-7A-5	0.0086	491.6796	475.2823	56.2547
5-7A-6	0.0043	196.5562	190.0011	44.8423
5-7A-7	0.0086	484.6944	468.5301	55.6424
5-7A-8	0.0079	995.0571	961.8723	123.2691
5-7A-9	0.0050	529.3753	511.7208	103.8042
5-8A-1	0.0085	87.2095	84.3011	10.0743
5-8A-2	0.0129	161.0811	155.7091	12.3928
5-8A-3	0.0173	308.8959	298.5943	17.7526
5-8A-4	0.0241	726.6977	702.4626	30.2127
5-8A-5	0.0075	79.7546	77.0948	10.3916
5-8A-6	0.0072	68.9513	66.6518	9.4463
5-8A-7	0.0066	78.6739	76.0502	11.6020

APPENDIX XI

NITROGEN OXIDE EMISSION CONCENTRATION DATA

Table XX contains data on the oxides of nitrogen (NO, NO₂ and NO_x) emission concentrations obtained during tests on combustors A and B during Phase II.

Table XX. Nitrogen Oxide Emission Concentration Data

TEST	FA	NOCA	NOPI	NOGX
1-1A-1	0.0039			
1-1A-2	0.0080			
1-1A-3	0.0083			
1-1A-4	0.0039			
1-1A-5	0.0122			
1-1A-6	0.0183			
1-1A-7	0.0120			
1-1A-8	0.0121			
1-1A-9	0.0123			
1-1A-10	0.0040			
1-1A-11	0.0039	15.6731	16.2369	4.1236
1-1A-12	0.0027	7.8369	8.1188	2.9513
1-1A-13	0.0067	13.4913	13.9767	2.0988
1-1A-14	0.0080	18.6834	19.5627	2.4651
1-1A-15	0.0060	13.8772	14.3764	2.4210
1-1A-16	0.0039	10.1333	10.4978	2.6910
1-1A-17	0.0123	24.3397	25.2153	2.1035
1-1A-18	0.0165	30.6460	31.7485	1.9775
1-1A-19	0.0188	29.8328	30.9059	1.6909
1-1A-20	0.0081	17.4496	18.0773	2.2641
1-1B-1	0.0082	6.0525	6.2702	0.7719
1-1B-2	0.0038	0.9524	0.9857	0.2606
1-1B-3	0.0122	7.4903	7.7597	0.6519
1-1B-4	0.0041	1.7968	1.8615	0.4524
1-1B-5	0.0083	11.8935	12.3214	1.5127
1-1B-6	0.0125	13.7640	14.2591	1.1581
1-1B-7	0.0189	21.3159	22.0827	1.2083
1-1B-8	0.0200	23.1245	23.9564	1.2333
1-1B-9	0.0122	14.2380	14.7502	1.2328
1-1B-10	0.0185	22.5111	23.3209	1.2982
1-1B-11	0.0084	7.3081	7.5710	0.9184
1-1B-12	0.0082	4.1075	4.2552	0.5295
1-1B-13	0.0083	12.1843	12.6226	1.5427
1-1B-14	0.0084	3.2641	3.3815	0.4106
1-1B-15	0.0082	1.6126	1.6707	0.2081
1-1B-16	0.0081	11.0407	11.4379	1.4264
1-1B-17	0.0061	8.4069	8.7093	1.4352
1-1B-18	0.0102	12.1879	12.6264	1.2678
1-1B-19	0.0082	13.6717	14.1636	1.7599
1-1B-20	0.0062	14.0653	14.5713	2.3995

Table XX. Nitrogen Oxide Emission Concentration Data (Continued)

TEST	FA	NOOA	NOPW	NODX
4-1A-1	0.0052	17.5143	18.1443	2.9765
4-1A-2	0.0084	27.1161	28.0915	3.4441
4-1A-3	0.0039	12.5317	12.9825	3.3682
4-1A-4	0.0102	23.1847	24.0187	2.4083
4-1A-5	0.0080	16.5687	17.1648	2.1704
4-1A-6	0.0039	11.4490	11.8609	3.0656
4-1A-7	0.0102	21.8703	22.6570	2.2712
4-1A-8	0.0061	12.9473	13.4130	2.2387
4-1A-9	0.0085	7.4861	7.7554	0.9295
4-1A-10	0.0125	11.9565	12.3866	1.0152
4-1A-11	0.0166	20.9832	21.7380	1.3496
4-1A-12	0.0206	29.6347	30.7007	1.5364
4-1A-13	0.0064	5.1386	5.3235	0.8363
4-1A-14	0.0104	12.0913	12.5262	1.2306
4-1A-15	0.0163	42.6461	44.1802	2.7767
4-1A-16	0.0124	62.9704	65.2357	5.3788
4-1A-17	0.0166	81.8829	84.8285	5.2485
4-1A-18	0.0208	98.8605	102.4168	5.0785
4-1A-19	0.0146	104.0420	107.7847	7.5898
4-1A-20	0.0075	108.9818	112.9022	15.3154
3-1A-1	0.0072	12.8544	13.3168	1.8685
3-1A-2	0.0092	14.9576	15.4957	1.7146
3-1A-3	0.0124	18.2728	18.9302	1.5706
3-1A-4	0.0144	19.5469	20.2501	1.4478
3-1A-5	0.0042	10.6968	11.0816	2.6842
3-1A-6	0.0133	13.3650	13.8458	1.0658
2-1A-1	0.0059	10.9438	11.3375	1.9436
2-1A-2	0.0091	14.9358	15.4731	1.7389
2-1A-3	0.0132	23.7938	24.6498	1.9180
2-1A-4	0.0162	22.7619	23.5807	1.4957
2-1A-5	0.0196	24.6429	25.5294	1.3473
2-2A-1	0.0040	4.6881	4.8568	1.2318
2-2A-2	0.0060	6.4283	6.6595	1.1246
2-2A-3	0.0080	10.8049	11.1936	1.4215

Table XX. Nitrogen Oxide Emission Concentration Data (Continued)

TEST	FA	NOOA	NOPW	NOGX
2-3A-1	0.0061	2.8818	2.9855	0.4958
2-3A-2	0.0082	3.8795	4.0191	0.5001
2-3A-3	0.0134	6.0736	6.2921	0.4818
2-3A-4	0.0113	7.7615	8.0408	0.7267
2-3A-5	0.0093	8.7491	9.0638	0.9970
2-3A-6	0.0081	3.7778	3.9137	0.4902
2-3A-7	0.0040	5.0478	5.2294	1.3232
2-3A-8	0.0050	6.5113	6.7455	1.3569
2-3A-9	0.0060	7.7687	8.0481	1.3553
2-1B-1	0.0039	3.8423	3.9805	1.0234
2-1B-2	0.0086	4.9072	5.0837	0.6024
2-1B-3	0.0158	6.6832	6.9236	0.4510
2-1B-4	0.0133	8.6146	8.9244	0.4694
2-1B-5	0.0119	9.9118	10.2684	0.8827
2-1B-6	0.0160	14.7978	15.3301	0.9837
2-1B-7	0.0200			
2-1B-8	0.0160			
2-1B-9	0.0200			

Table XX. Nitrogen Oxide Emission Concentration Data (Continued)

TEST	FA	NOOA	NCPW	NODX
5-1B-1	0.0040	8.2721	8.5697	2.1776
5-1B-2	0.0081	17.6586	18.2938	2.2983
5-1B-3	0.0101	20.4019	21.1358	2.1280
5-1B-4	0.0061	14.5134	15.0355	2.4978
5-1A-1	0.0070	8.3522	8.6527	1.2610
5-1A-2	0.0087	14.8075	15.3402	1.7984
5-1A-3	0.0100	24.4038	25.2817	2.5797
5-1A-4	0.0051	5.4049	5.5993	1.1059
5-1A-5	0.0060	5.1130	5.2969	0.8881
5-1A-6	0.0082	21.3164	22.0832	2.7444
5-1A-7	0.0071	12.7318	13.1898	1.8780
5-1A-8	0.0060	9.5260	9.8687	1.6586
5-1A-9	0.0101	31.1849	32.3068	3.2591
5-1A-10	0.0121	28.0162	29.0241	2.4607
5-1A-11	0.0060	14.2012	14.7121	2.4944
5-1A-12	0.0049	10.7295	11.1155	2.2813
5-2A-1	0.0081	20.3814	21.1146	2.6568
5-2A-2	0.0100	25.9526	26.8862	2.7497
5-2A-3	0.0059	10.0455	10.4069	1.7838
5-2A-4	0.0079	23.9250	24.7856	3.1942
5-2A-5	0.0068	17.5156	18.1457	2.7018
5-2A-6	0.0055	6.4586	6.6910	1.2366
5-2A-7	0.0063	12.7521	13.2109	2.1135
5-3A-1	0.0083	19.4522	20.1520	2.4802
5-3A-2	0.0062	10.4277	10.8028	1.7703
5-3A-3	0.0102	27.0658	28.0394	2.8022
5-3A-4	0.0054	13.0529	13.5275	2.5480
5-3A-5	0.0057	15.3695	15.9224	2.8213
5-3A-6	0.0067	22.3356	23.1390	3.4947
5-4A-1	0.0080	22.4289	23.2358	2.9291
5-4A-2	0.0099	28.3525	29.3724	2.9986
5-4A-3	0.0050	13.0653	13.5353	2.7231
5-4A-4	0.0054	14.0008	14.5045	2.6950
5-4A-5	0.0059	18.3910	19.0526	3.2226

Table XX. Nitrogen Oxide Emission Concentration Data (Continued)

TEST	FA	NOOA	NOPW	NODX
5-5A-1	0.0084	16.4530	17.0448	2.0709
5-5A-2	0.0105	35.0695	36.3311	3.5282
5-5A-3	0.0073	15.7437	16.3101	2.2638
5-5A-4	0.0075	15.2936	15.8438	2.1376
5-5A-5	0.0076	16.7790	17.3826	2.3221
5-5A-6	0.0078	17.1948	17.8133	2.3073
5-7A-1	0.0080			
5-7A-2	0.0118			
5-7A-3	0.0157			
5-7A-4	0.0228			
5-7A-5	0.0086			
5-7A-6	0.0043			
5-7A-7	0.0086			
5-7A-8	0.0079			
5-7A-9	0.0050			
5-8A-1	0.0085	13.1890	13.6635	1.6328
5-8A-2	0.0129	25.6025	26.5235	2.1110
5-8A-3	0.0173	30.6088	31.7099	1.8852
5-8A-4	0.0241	40.4871	41.9436	1.8039
5-8A-5	0.0075	16.8073	17.4119	2.3469
5-8A-6	0.0072	13.6358	14.1263	2.0020
5-8A-7	0.0066	10.6230	11.0051	1.6789

Table XX. Nitrogen Oxide Emission Concentration Data (Continued)

TEST	FA	NO2OA	NO2PW	NO2DX
1-1A-1	0.0039			
1-1A-2	0.0080			
1-1A-3	0.0083			
1-1A-4	0.0039			
1-1A-5	0.0122			
1-1A-6	0.0183			
1-1A-7	0.0120			
1-1A-8	0.0121			
1-1A-9	0.0123			
1-1A-10	0.0040			
1-1A-11	0.0039	1.8184	2.8882	0.7335
1-1A-12	0.0027			
1-1A-13	0.0067	6.1496	9.7676	1.4668
1-1A-14	0.0080	3.1722	5.0385	0.6349
1-1A-15	0.0060	4.0696	6.4640	1.0885
1-1A-16	0.0039	5.8696	9.3230	2.3899
1-1A-17	0.0123	8.6249	13.6993	1.1428
1-1A-18	0.0165	12.6161	20.0387	1.2482
1-1A-19	0.0188	12.9611	20.5867	1.1263
1-1A-20	0.0081	9.1906	14.5979	1.8283
1-1B-1	0.0082	6.1296	9.7360	1.1986
1-1B-2	0.0038	5.1633	8.2012	2.1663
1-1B-3	0.0122	9.9832	15.8568	1.3322
1-1B-4	0.0041	1.7409	2.7652	0.6720
1-1B-5	0.0083	1.3801	2.1920	0.2691
1-1B-6	0.0125			
1-1B-7	0.0189			
1-1B-8	0.0200	4.8286	7.6695	0.3948
1-1B-9	0.0122	3.1560	5.0128	0.4189
1-1B-10	0.0185	4.6754	7.4262	0.4134
1-1B-11	0.0084	2.9554	4.6942	0.5694
1-1B-12	0.0082	10.3701	16.4713	2.0498
1-1B-13	0.0083	10.6498	16.9156	2.0674
1-1B-14	0.0084	10.2311	16.2505	1.9735
1-1B-15	0.0082	10.0892	16.0252	1.9965
1-1B-16	0.0081	7.9617	12.6460	1.5770
1-1B-17	0.0061	7.7470	12.3049	2.0278
1-1B-18	0.0102	8.7085	13.8322	1.3888
1-1B-19	0.0082	5.5988	8.8928	1.1050
1-1B-20	0.0062	4.6590	7.7178	1.2709

Table XX. Nitrogen Oxide Emission Concentration Data (Continued)

TEST	FA	NO2OA	NO2PW	NO2DX
4-1A-1	0.0062	24.6979	39.2287	6.4354
4-1A-2	0.0084	26.0380	41.3574	5.0705
4-1A-3	0.0039			
4-1A-4	0.0102			
4-1A-5	0.0080	17.7627	28.2133	3.5675
4-1A-6	0.0039	16.7775	26.6485	6.8878
4-1A-7	0.0102	17.0400	27.0654	2.7131
4-1A-8	0.0061	19.9336	31.6614	5.2846
4-1A-9	0.0085	35.7050	56.7118	6.7976
4-1A-10	0.0125	73.6254	116.9425	9.5846
4-1A-11	0.0166	199.1040	316.2459	19.6346
4-1A-12	0.0206	434.6595	690.3890	34.5501
4-1A-13	0.0064	45.5441	72.3398	11.3646
4-1A-14	0.0104	56.6476	90.2936	8.8708
4-1A-15	0.0163	90.5174	143.7728	9.0361
4-1A-16	0.0124	57.6272	91.5319	7.5469
4-1A-17	0.0166	84.3219	133.9322	8.2867
4-1A-18	0.0208	112.3058	178.3803	8.8453
4-1A-19	0.0146	79.6220	126.4672	8.9054
4-1A-20	0.0075	80.7684	128.2881	17.4026
3-1A-1	0.0072	20.4125	32.4221	4.5494
3-1A-2	0.0092	25.3370	40.2438	4.4530
3-1A-3	0.0124	28.2169	44.8181	3.7185
3-1A-4	0.0144	32.1380	51.0463	3.6496
3-1A-5	0.0042	27.4441	43.5907	10.5586
3-1A-6	0.0133	41.0304	65.1704	5.0167
2-1A-1	0.0059	15.0099	23.8409	4.0871
2-1A-2	0.0091	18.2228	28.9441	3.2528
2-1A-3	0.0132	26.6288	42.2957	3.2911
2-1A-4	0.0162	25.6889	40.8029	2.5882
2-1A-5	0.0196	25.8120	40.9984	2.1637
2-2A-1	0.0040	8.7118	13.8373	3.5096
2-2A-2	0.0060	12.0056	19.0691	3.2203
2-2A-3	0.0080	11.7693	18.6937	2.3740

Table XX. Nitrogen Oxide Emission Concentration Data (Continued)

TEST	FA	NO2OA	NO2PW	NO2DX
2-3A-1	0.0061	16.4407	26.1135	4.3372
2-3A-2	0.0082	23.1777	36.8142	4.5809
2-3A-3	0.0134	79.5245	126.3123	9.6730
2-3A-4	0.0113	66.7496	106.0213	9.5827
2-3A-5	0.0093	39.3562	62.5113	6.8767
2-3A-6	0.0081	35.8852	56.9981	7.1367
2-3A-7	0.0040	12.7187	20.2017	5.1119
2-3A-8	0.0050	15.5931	24.7672	4.9821
2-3A-9	0.0060	17.6985	28.1113	4.7340
2-1B-1	0.0039	19.4624	30.9130	7.9477
2-1B-2	0.0086	22.6597	35.9914	4.2647
2-1B-3	0.0158	29.5283	46.9012	3.0551
2-1B-4	0.0196	32.6198	51.8115	2.7254
2-1B-5	0.0119	23.8749	37.9215	3.2599
2-1B-6	0.0160	25.1286	39.9129	2.5612
2-1B-7	0.0200	29.3029	46.5431	2.4100
2-1B-8	0.0160	25.2862	40.1632	2.5791
2-1B-9	0.0200	29.6693	47.1568	2.4364

Table XX. Nitrogen Oxide Emission Concentration Data (Continued)

TEST	FA	NO2OA	NO2PW	NO2DX
5-1B-1	0.0040	14.1342	22.4501	5.7048
5-1B-2	0.0081	40.4526	64.2527	8.0724
5-1B-3	0.0101	26.5051	42.0992	4.2388
5-1B-4	0.0061	19.1095	30.3524	5.0424
5-1A-1	0.0070	3.2611	5.1798	0.7549
5-1A-2	0.0087	5.3754	8.5381	1.0009
5-1A-3	0.0100	7.1054	11.2858	1.1515
5-1A-4	0.0051	4.0101	6.3694	1.2581
5-1A-5	0.0060	2.9791	4.7318	0.7933
5-1A-6	0.0082	6.6169	10.5100	1.3061
5-1A-7	0.0071	3.3086	5.2553	0.7482
5-1A-8	0.0060	2.1661	3.4406	0.5782
5-1A-9	0.0101	9.0709	14.4077	1.4534
5-1A-10	0.0121	11.4587	18.2003	1.5431
5-1A-11	0.0060	2.5144	3.9938	0.6771
5-1A-12	0.0049	2.2121	3.5136	0.7211
5-2A-1	0.0081	8.6106	13.6767	1.7209
5-2A-2	0.0100	12.3839	19.6700	2.0117
5-2A-3	0.0059	6.1868	9.8268	1.6843
5-2A-4	0.0079	9.2527	14.6965	1.8940
5-2A-5	0.0068	7.9790	12.6735	1.8670
5-2A-6	0.0055	6.5981	10.4801	1.9369
5-2A-7	0.0063	7.8799	12.5160	2.0023
5-3A-1	0.0083	10.2304	16.2494	1.9998
5-3A-2	0.0062	7.1373	11.3366	1.8578
5-3A-3	0.0102	13.0859	20.7849	2.0772
5-3A-4	0.0054	6.7670	10.7483	2.0253
5-3A-5	0.0057	7.5612	12.0098	2.1280
5-3A-6	0.0067	8.6638	13.7611	2.0783
5-4A-1	0.0080	8.1736	12.9826	1.6366
5-4A-2	0.0099	12.2853	19.5134	1.9921
5-4A-3	0.0050	5.0059	7.9511	1.5996
5-4A-4	0.0054	5.8340	9.2664	1.7217
5-4A-5	0.0059	7.1918	11.4231	1.9322

Table XX. Nitrogen Oxide Emission Concentration Data (Continued)

TEST	FA	NO2OA	NO2PW	NO2DX
5-5A-1	0.0084	11.5595	18.3605	2.2307
5-5A-2	0.0105	20.1938	32.0747	3.1149
5-5A-3	0.0073	10.3468	16.4343	2.2811
5-5A-4	0.0075	10.6957	16.9885	2.2920
5-5A-5	0.0076	10.1523	16.1253	2.1541
5-5A-6	0.0078	10.8552	17.2418	2.2333
5-7A-1	0.0080	9.2220	14.6477	1.8727
5-7A-2	0.0118	14.1491	22.4736	1.9471
5-7A-3	0.0157	18.4487	29.3029	1.9122
5-7A-4	0.0228	16.3410	25.9552	1.1764
5-7A-5	0.0086	393.6335	625.2257	74.0021
5-7A-6	0.0043	24.1904	38.4227	4.0681
5-7A-7	0.0086	29.4167	46.7240	5.5489
5-7A-8	0.0079	21.1111	33.5317	4.3007
5-7A-9	0.0050	16.8127	26.7044	5.4170
5-8A-1	0.0085	11.4689	18.2166	2.1769
5-8A-2	0.0129	16.0479	25.4896	2.0287
5-8A-3	0.0173	20.8413	33.1032	1.9681
5-8A-4	0.0241	24.7009	37.2335	1.6874
5-8A-5	0.0075	14.0060	22.2464	2.9986
5-8A-6	0.0072	13.8953	22.0705	3.1279
5-8A-7	0.0066	12.5641	19.9561	3.0444

Table XX. Nitrogen Oxide Emission Concentration Data (Continued)

TEST	FA	NOXOA	NOXPW	NOXDX
1-1A-1	0.0039			
1-1A-2	0.0080			
1-1A-3	0.0083			
1-1A-4	0.0039			
1-1A-5	0.0122			
1-1A-6	0.0183			
1-1A-7	0.0120			
1-1A-8	0.0121			
1-1A-9	0.0123			
1-1A-10	0.0040			
1-1A-11	0.0039	17.4915	19.1252	4.8571
1-1A-12	0.0027			
1-1A-13	0.0067	19.6410	23.7444	3.5656
1-1A-14	0.0080	22.0556	24.6012	3.1001
1-1A-15	0.0060	17.9469	20.8405	3.5096
1-1A-16	0.0039	16.0030	19.8209	5.0810
1-1A-17	0.0123	32.9646	38.9146	3.2464
1-1A-18	0.0165	43.2621	51.7872	3.2257
1-1A-19	0.0188	42.7939	51.4927	2.8172
1-1A-20	0.0081	26.6402	32.6752	4.0924
1-18-1	0.0082	12.1822	16.0063	1.9706
1-18-2	0.0038	6.1158	9.1879	2.4269
1-18-3	0.0122	17.4733	23.6166	1.9841
1-18-4	0.0041	3.3378	4.6268	1.1244
1-18-5	0.0083	13.2737	14.5135	1.7819
1-18-6	0.0125			
1-18-7	0.0189			
1-18-8	0.0200	27.9532	31.5260	1.6281
1-18-9	0.0122	17.3940	19.7630	1.6516
1-18-10	0.0185	27.1865	30.7471	1.7117
1-18-11	0.0084	10.2635	12.2652	1.4378
1-18-12	0.0082	14.4776	20.7266	2.5794
1-18-13	0.0083	22.8342	29.5383	3.6101
1-18-14	0.0084	13.4952	19.6321	2.3842
1-18-15	0.0082	11.7019	17.6939	2.2046
1-18-16	0.0081	19.0025	24.0839	3.0039
1-18-17	0.0061	16.1539	21.0143	3.4631
1-18-18	0.0102	20.8966	26.4586	2.6566
1-18-19	0.0082	19.2706	23.0564	2.8650
1-18-20	0.0062	18.9244	22.2892	3.6705

Table XX. Nitrogen Oxide Emission Concentration Data (Continued)

TEST	FA	NOXOA	NOXPW	NOXDZ
4-1A-1	0.0062	42.2122	57.3731	9.4119
4-1A-2	0.0084	53.1541	69.4490	8.5147
4-1A-3	0.0039			
4-1A-4	0.0102			
4-1A-5	0.0080	34.3315	45.3781	5.7379
4-1A-6	0.0039	28.2266	38.5094	9.9535
4-1A-7	0.0102	38.9103	49.7224	4.9843
4-1A-8	0.0061	32.8809	43.0745	7.5233
4-1A-9	0.0085	43.1912	64.4673	7.7272
4-1A-10	0.0125	65.5819	129.3291	10.5998
4-1A-11	0.0166	220.0873	337.9839	20.9843
4-1A-12	0.0206	464.2942	721.0897	36.0865
4-1A-13	0.0064	50.6828	77.6633	12.2010
4-1A-14	0.0104	68.9389	102.8198	10.1015
4-1A-15	0.0163	133.1636	187.9531	11.8128
4-1A-16	0.0124	120.5977	156.7676	12.9257
4-1A-17	0.0166	166.2048	218.7608	13.5352
4-1A-18	0.0208	211.1663	280.7971	13.9239
4-1A-19	0.0166	183.6640	234.2519	16.4952
4-1A-20	0.0075	189.7502	241.1903	32.7180
3-1A-1	0.0072	33.2669	45.7389	6.4180
3-1A-2	0.0092	40.2947	55.7396	6.1676
3-1A-3	0.0124	46.4897	63.7483	5.2892
3-1A-4	0.0164	51.6850	71.2964	5.0974
3-1A-5	0.0042	38.1409	54.6723	13.2428
3-1A-6	0.0133	54.3955	79.0163	6.0826
2-1A-1	0.0039	25.9537	35.1784	6.0307
2-1A-2	0.0091	33.1586	44.4172	4.9917
2-1A-3	0.0132	50.4227	66.9456	5.2091
2-1A-4	0.0162	48.4509	64.3837	4.0840
2-1A-5	0.0196	50.4550	66.5279	3.5111
2-2A-1	0.0040	13.3999	18.6941	4.7415
2-2A-2	0.0060	18.4340	25.7287	4.3449
2-2A-3	0.0080	22.5743	29.8874	3.7955

Table XX. Nitrogen Oxide Emission Concentration Data (Continued)

TEST	FA	NOXOA	NOXPW	NOXDX
2-3A-1	0.0061	19.3226	29.0991	4.8331
2-3A-2	0.0082	27.0573	40.8333	5.0810
2-3A-3	0.0134	85.5982	132.6045	10.1548
2-3A-4	0.0113	74.5111	114.0621	10.3099
2-3A-5	0.0093	48.1053	71.5751	7.8738
2-3A-6	0.0081	39.6631	60.9119	7.6299
2-3A-7	0.0040	17.7665	25.4311	6.4351
2-3A-8	0.0050	22.1044	31.5128	6.3391
2-3A-9	0.0060	25.4672	36.1595	6.0894
2-1B-1	0.0039	23.3047	34.8936	8.9711
2-1B-2	0.0086	27.5669	41.0752	4.8671
2-1B-3	0.0158	36.2115	53.8248	3.5061
2-1B-4	0.0196	41.2344	60.7360	3.1948
2-1B-5	0.0119	33.7867	48.1899	4.1427
2-1B-6	0.0160	39.9264	55.2431	3.5450

Table XX. Nitrogen Oxide Emission Concentration Data (Continued)

TEST	FA	NOXOA	NOXPW	NOXDX
5-1B-1	0.0040	22.4064	31.0198	7.8824
5-1B-2	0.0081	58.1112	82.5466	10.3708
5-1B-3	0.0101	46.9070	63.2350	6.3669
5-1B-4	0.0061	33.6229	45.3880	7.5403
5-1A-1	0.0070	11.6133	13.8325	2.0159
5-1A-2	0.0087	20.1830	23.8783	2.7994
5-1A-3	0.0100	31.5092	36.5676	3.7313
5-1A-4	0.0051	9.4150	11.9688	2.3641
5-1A-5	0.0060	8.0921	10.0288	1.6815
5-1A-6	0.0082	27.9333	32.5932	4.0505
5-1A-7	0.0071	16.0405	18.4451	2.6263
5-1A-8	0.0060	11.6922	13.3093	2.2369
5-1A-9	0.0101	40.2558	46.7145	4.7126
5-1A-10	0.0121	39.4749	47.2245	4.0038
5-1A-11	0.0060	15.7157	18.7059	3.1715
5-1A-12	0.0049	12.9417	14.6292	3.0024
5-2A-1	0.0081	28.9921	34.7913	4.3778
5-2A-2	0.0100	38.3366	46.5562	4.7614
5-2A-3	0.0059	16.2323	20.2337	3.4682
5-2A-4	0.0079	33.1777	39.4822	5.0833
5-2A-5	0.0068	25.4947	30.8193	4.5888
5-2A-6	0.0055	13.0508	17.1712	3.1736
5-2A-7	0.0063	20.6320	25.7269	4.1159
5-3A-1	0.0083	29.6827	36.4014	4.4801
5-3A-2	0.0062	17.5651	22.1395	3.6282
5-3A-3	0.0102	40.1517	48.8244	4.8795
5-3A-4	0.0054	19.8199	24.2709	4.5733
5-3A-5	0.0057	22.9307	27.9322	4.9494
5-3A-6	0.0067	30.9994	36.9002	5.5731
5-4A-1	0.0080	30.6026	36.2184	4.5658
5-4A-2	0.0099	40.6378	48.8858	4.9907
5-4A-3	0.0050	18.0713	21.4865	4.3228
5-4A-4	0.0054	19.8348	23.7709	4.4168
5-4A-5	0.0059	25.5828	30.4757	5.1551

Table XX. Nitrogen Oxide Emission Concentration Data (Continued)

TEST	FA	NOXOA	NOXPW	NOXDX
5-5A-1	0.0084	28.0125	35.4054	4.3017
5-5A-2	0.0105	55.2633	68.4058	6.6431
5-5A-3	0.0073	26.0906	32.7444	4.5449
5-5A-4	0.0075	25.9894	32.8324	4.4296
5-5A-5	0.0076	26.9313	33.5079	4.4763
5-5A-6	0.0078	28.0500	35.0552	4.5407
5-7A-1	0.0080			
5-7A-2	0.0118			
5-7A-3	0.0157			
5-7A-4	0.0228			
5-7A-5	0.0086			
5-7A-6	0.0043			
5-7A-7	0.0086			
5-7A-8	0.0079			
5-7A-9	0.0050			
5-8A-1	0.0085	24.6580	31.8801	3.8098
5-8A-2	0.0129	41.6504	52.0131	4.1397
5-8A-3	0.0173	51.4502	64.8132	3.8534
5-8A-4	0.0241	65.1881	81.1772	3.4914
5-8A-5	0.0075	30.8133	39.6583	5.3455
5-8A-6	0.0072	27.5311	36.1969	5.1300
5-8A-7	0.0066	23.1871	30.9613	4.7233

APPENDIX XI

CO₂ EMISSION CONCENTRATION DATA

Table XXI contains data on CO₂ emission concentrations obtained during tests on combustors A and B during Phase II.

Table XXI. CO₂ Emission Concentration Data

TEST	FA	CO2OA	CO2PW	CO2DX
1-1A-1	0.0039			
1-1A-2	0.0080			
1-1A-3	0.0083			
1-1A-4	0.0039			
1-1A-5	0.0122			
1-1A-6	0.0183			
1-1A-7	0.0120			
1-1A-8	0.0121			
1-1A-9	0.0123			
1-1A-10	0.0040	0.8387	1.2740	3191.0527
1-1A-11	0.0039	0.8505	1.2920	3281.3828
1-1A-12	0.0027	0.7552	1.1473	4170.7265
1-1A-13	0.0067	1.6076	2.4419	3667.1191
1-1A-14	0.0080	1.8166	2.7595	3477.3994
1-1A-15	0.0060	1.4203	2.1574	3633.2622
1-1A-16	0.0039	0.9716	1.4759	3783.5517
1-1A-17	0.0123	2.7460	4.1713	3479.9204
1-1A-18	0.0165	3.6052	5.4764	3411.2710
1-1A-19	0.0188	3.7098	5.6352	3083.2036
1-1A-20	0.0081	1.7053	2.5904	3244.4760
1-1B-1	0.0082	1.7539	2.6643	3280.1748
1-1B-2	0.0038	0.8156	1.2389	3272.6523
1-1B-3	0.0122	2.5862	3.9286	3300.6630
1-1B-4	0.0041	0.8792	1.3355	3245.8530
1-1B-5	0.0083	1.8089	2.7478	3373.7514
1-1B-6	0.0125	2.7532	4.1822	3426.3559
1-1B-7	0.0189	3.9272	5.9655	3264.3242
1-1B-8	0.0200	4.0947	6.2200	3202.2387
1-1B-9	0.0122	2.5732	3.9088	3267.2260
1-1B-10	0.0185	3.8408	5.8343	3248.0210
1-1B-11	0.0084	1.8842	2.8622	3472.1752
1-1B-12	0.0082	1.5802	2.4003	2987.3115
1-1B-13	0.0083	1.6800	2.5519	3118.9658
1-1B-14	0.0084	1.6342	2.4824	3014.8432
1-1B-15	0.0082	1.6064	2.4402	3040.2153
1-1B-16	0.0081	1.6845	2.5588	3191.0976
1-1B-17	0.0061	1.1708	1.7785	2930.9355
1-1B-18	0.0102	2.0725	3.1482	3161.0781
1-1B-19	0.0082	1.8249	2.7721	3444.6904
1-1B-20	0.0062	1.2190	1.8518	3049.5327

Table XXI. CO₂ Emission Concentration Data (Continued)

TEST	FA	CO2OA	CO2PW	CO2DX
4-1A-1	0.0062	1.2853	1.9524	3202.8808
4-1A-2	0.0084	1.6718	2.5395	3113.5874
4-1A-3	0.0039			
4-1A-4	0.0102			
4-1A-5	0.0080	1.9056	2.8947	3660.3750
4-1A-6	0.0039	0.8269	1.2562	3246.9453
4-1A-7	0.0102	2.0051	3.0459	3053.3120
4-1A-8	0.0061	1.2171	1.8489	3085.9921
4-1A-9	0.0085	1.3736	2.0866	2501.1259
4-1A-10	0.0125	2.1256	3.2288	2646.3798
4-1A-11	0.0166	2.7409	4.1635	2584.9858
4-1A-12	0.0206	3.6281	5.5112	2758.0546
4-1A-13	0.0064	0.9168	1.3926	2187.8676
4-1A-14	0.0104	1.6152	2.4536	2410.5932
4-1A-15	0.0163	2.7687	4.2057	2643.3061
4-1A-16	0.0124	2.3349	3.5467	2924.3784
4-1A-17	0.0166	3.0432	4.6227	2860.1801
4-1A-18	0.0208	3.8787	5.8919	2921.6269
4-1A-19	0.0146	2.7553	4.1853	2947.2060
4-1A-20	0.0075	1.0788	1.6388	2223.1611
3-1A-1	0.0072	1.3791	2.0950	2939.6919
3-1A-2	0.0092	1.7147	2.6046	2882.1206
3-1A-3	0.0124	2.2645	3.4398	2854.0615
3-1A-4	0.0144	3.0708	4.6643	3335.0542
3-1A-5	0.0042	1.1082	1.6834	4077.6821
3-1A-6	0.0133	2.7521	4.1806	3218.2128
2-1A-1	0.0059	1.2774	1.9404	3326.5996
2-1A-2	0.0091	1.9606	2.9782	3347.0361
2-1A-3	0.0132	2.7899	4.2379	3297.5986
2-1A-4	0.0162	3.2031	4.8656	3086.3623
2-1A-5	0.0196	3.7462	5.6907	3003.3642
2-2A-1	0.0040	0.9369	1.4232	3610.0371
2-2A-2	0.0060	1.1999	1.8227	3078.2421
2-2A-3	0.0080	1.5670	2.3804	3023.0195

Table XXI. CO₂ Emission Concentration Data (Continued)

TEST	FA	CO2OA	CO2PW	CO2DX
2-3A-1	0.0061	1.0971	1.6665	2767.9926
2-3A-2	0.0082	1.4523	2.2061	2745.2251
2-3A-3	0.0134	2.5094	3.8118	2919.1298
2-3A-4	0.0113	1.9502	2.9625	2677.6850
2-3A-5	0.0093	1.5768	2.3953	2635.0336
2-3A-6	0.0081	1.6878	2.5638	3211.4936
2-3A-7	0.0040	0.6486	0.9853	2493.4223
2-3A-8	0.0050	0.8538	1.2970	2609.0810
2-3A-9	0.0060	1.0738	1.6312	2747.0507
2-1B-1	0.0039	0.7851	1.1926	3066.1850
2-1B-2	0.0086	1.6775	2.5482	3019.5253
2-1B-3	0.0158	3.1121	4.7274	3079.4682
2-1B-4	0.0196	4.0474	6.1481	3234.0766
2-1B-5	0.0119	2.4946	3.7893	3257.5927
2-1B-6	0.0160	3.3083	5.0254	3224.9082
2-1B-7	0.0200	4.0507	6.1532	3186.2202
2-1B-8	0.0160	3.2901	4.9978	3209.4458
2-1B-9	0.0200	4.0945	6.2196	3213.5595

Table XXI. CO₂ Emission Concentration Data (Continued)

TEST	FA	CO2OA	CO2PW	CO2DX
5-1B-1	0.0040	0.8772	1.3325	3386.1196
5-1B-2	0.0081	1.6890	2.5656	3223.4199
5-1B-3	0.0101	2.0244	3.0751	3096.2524
5-1B-4	0.0061	1.3235	2.0105	3340.0644
5-1A-1	0.0070	1.4013	2.1286	3102.3457
5-1A-2	0.0087	1.7206	2.6136	3064.1704
5-1A-3	0.0100	1.8149	2.7569	2813.1855
5-1A-4	0.0051	1.0144	1.5410	3043.8129
5-1A-5	0.0060	1.1106	1.6870	2828.6079
5-1A-6	0.0082	1.7504	2.6590	3304.5268
5-1A-7	0.0071	1.5454	2.3475	3342.6416
5-1A-8	0.0060	1.3264	2.0149	3386.6357
5-1A-9	0.0101	2.1086	3.2030	3231.3252
5-1A-10	0.0121	2.4455	3.7148	3149.5595
5-1A-11	0.0040	1.2816	1.9468	3300.7959
5-1A-12	0.0049	1.0771	1.6361	3358.0434
5-2A-1	0.0081	1.6597	2.5212	3172.5581
5-2A-2	0.0100	1.9637	2.9829	3050.7211
5-2A-3	0.0059	1.2432	1.8885	3237.0537
5-2A-4	0.0079	1.5837	2.4057	3100.4536
5-2A-5	0.0068	1.4295	2.1714	3233.1899
5-2A-6	0.0055	1.1498	1.7466	3228.1977
5-2A-7	0.0063	1.3364	2.0300	3247.7309
5-3A-1	0.0083	1.6703	2.5372	3122.6787
5-3A-2	0.0062	1.3003	1.9751	3236.9809
5-3A-3	0.0102	2.0110	3.0548	3053.0107
5-3A-4	0.0054	1.2270	1.8638	3512.1147
5-3A-5	0.0057	1.2862	1.9538	3462.0971
5-3A-6	0.0067	1.4696	2.2324	3371.6933
5-4A-1	0.0080	1.6941	2.5735	3244.2631
5-4A-2	0.0099	2.0137	3.0589	3122.8393
5-4A-3	0.0050	1.1679	1.7741	3569.4721
5-4A-4	0.0054	1.1599	1.7619	3273.8735
5-4A-5	0.0059	1.2662	1.9235	3253.7294

Table XXI. CO₂ Emission Concentration Data (Continued)

TEST	FA	CO2OA	CO2PW	CO2DX
5-5A-1	0.0084	1.8106	2.7504	3341.6953
5-5A-2	0.0105	2.2001	3.3421	3245.6899
5-5A-3	0.0073	1.4964	2.2731	3155.2353
5-5A-4	0.0075	1.5306	2.3251	3136.9780
5-5A-5	0.0076	1.5526	2.3584	3150.6787
5-5A-6	0.0078	1.6834	2.5572	3312.4350
5-7A-1	0.0080	1.5161	2.3030	2944.3823
5-7A-2	0.0118	2.2916	3.4809	3015.9443
5-7A-3	0.0157	3.0356	4.6111	3009.1167
5-7A-4	0.0228	4.3952	6.6765	3026.1489
5-7A-5	0.0086	1.5520	2.3576	2790.4853
5-7A-6	0.0043	0.7978	1.2119	2860.3056
5-7A-7	0.0086	1.5750	2.3925	2841.3642
5-7A-8	0.0079	1.6405	2.4919	3196.2172
5-7A-9	0.0050	1.1442	1.7381	3525.8193
5-8A-1	0.0085	1.8731	2.8453	3400.3813
5-8A-2	0.0129	2.7588	4.1907	3335.3999
5-8A-3	0.0173	3.5725	5.4268	3226.4687
5-8A-4	0.0241	5.0232	7.6304	3281.8261
5-8A-5	0.0075	1.8538	2.8160	3795.7065
5-8A-6	0.0072	1.7741	2.6950	3819.5463
5-8A-7	0.0066	1.6695	2.3360	3868.8598

APPENDIX XIII

H₂O EMISSION CONCENTRATION DATA

Table XXII contains data on H₂O emission concentrations obtained during tests on combustors A and B during Phase II.

Table XXII. H₂O Emission Concentration Data

TEST	FA	H200A	H20PW	H20DX
1-1A-1	0.0039			
1-1A-2	0.0080			
1-1A-3	0.0083			
1-1A-4	0.0039			
1-1A-5	0.0122			
1-1A-6	0.0183			
1-1A-7	0.0120			
1-1A-8	0.0121			
1-1A-9	0.0123			
1-1A-10	0.0040	2.7317	1.6990	4255.5507
1-1A-11	0.0039	2.1584	1.3425	3409.5068
1-1A-12	0.0027	2.5087	1.5603	5672.2158
1-1A-13	0.0067	2.4097	1.4987	2250.7060
1-1A-14	0.0080	3.4491	2.1452	2703.3730
1-1A-15	0.0060	3.1491	1.9905	3298.4272
1-1A-16	0.0039	2.8537	1.7749	4549.9345
1-1A-17	0.0123	4.1118	2.5574	2133.5444
1-1A-18	0.0165	4.3680	2.7168	1692.2810
1-1A-19	0.0168	4.9532	3.0807	1685.5827
1-1A-20	0.0081	3.1055	1.9315	2419.2065
1-1B-1	0.0082	4.0210	2.5009	3079.0561
1-1B-2	0.0038	2.4708	1.5367	4059.3535
1-1B-3	0.0122	5.0583	3.1461	2643.2641
1-1B-4	0.0041	2.8138	1.7501	4253.2998
1-1B-5	0.0083	3.9929	2.4834	3049.1215
1-1B-6	0.0125	4.8267	3.0021	2459.5087
1-1B-7	0.0189	5.3950	3.3555	1836.1389
1-1B-8	0.0200	4.5691	2.8419	1463.0813
1-1B-9	0.0122	4.0104	2.4944	2084.9438
1-1B-10	0.0185	4.1316	2.5697	1430.6152
1-1B-11	0.0084	4.0042	2.4905	3021.2280
1-1B-12	0.0082	4.4512	2.7685	3445.5009
1-1B-13	0.0083	4.4335	2.7575	3370.1928
1-1B-14	0.0084	5.7865	3.5990	4370.9248
1-1B-15	0.0082	5.7619	3.5837	4464.9150
1-1B-16	0.0081	4.6694	2.9042	3621.8955
1-1B-17	0.0061	3.5629	2.2160	3652.0297
1-1B-18	0.0102	3.9502	2.4569	2466.9550
1-1B-19	0.0082	3.7716	2.3458	2914.9692
1-1B-20	0.0062	4.2626	2.6512	4365.9453

Table XXII. H₂O Emission Concentration Data (Continued)

TEST	FA	H200A	H20PW	H20DX
4-1A-1	0.0062	4.4342	2.7579	4524.3935
4-1A-2	0.0084	4.7521	2.9556	3623.7627
4-1A-3	0.0039			
4-1A-4	0.0102			
4-1A-5	0.0080			
4-1A-6	0.0039			
4-1A-7	0.0102			
4-1A-8	0.0061			
4-1A-9	0.0085			
4-1A-10	0.0125			
4-1A-11	0.0166			
4-1A-12	0.0206			
4-1A-13	0.0064			
4-1A-14	0.0104			
4-1A-15	0.0163			
4-1A-16	0.0124			
4-1A-17	0.0166			
4-1A-18	0.0208			
4-1A-19	0.0146			
4-1A-20	0.0075			
3-1A-1	0.0072			
3-1A-2	0.0092			
3-1A-3	0.0124			
3-1A-4	0.0144			
3-1A-5	0.0042			
3-1A-6	0.0133			
2-1A-1	0.0059			
2-1A-2	0.0091			
2-1A-3	0.0132			
2-1A-4	0.0162			
2-1A-5	0.0196			
2-2A-1	0.0040			
2-2A-2	0.0060			
2-2A-3	0.0080			

Table XXII. H₂O Emission Concentration Data (Continued)

TEST	FA	H200A	H20PW	H20DX
2-3A-1	0.0061			
2-3A-2	0.0082			
2-3A-3	0.0134			
2-3A-4	0.0113			
2-3A-5	0.0093			
2-3A-6	0.0081			
2-3A-7	0.0040			
2-3A-8	0.0050			
2-3A-9	0.0060			
2-18-1	0.0039			
2-18-2	0.0086			
2-18-3	0.0158			
2-18-4	0.0196			
2-18-5	0.0119			
2-18-6	0.0160			
2-18-7	0.0200			
2-18-8	0.0160			
2-18-9	0.0200			

Table XXII. H₂O Emission Concentration Data (Continued)

TEST	FA	H200A	H20PW	H20DX
5-1B-1	0.0040	3.0487	1.8962	4818.5527
5-1B-2	0.0081	3.7429	2.3280	2924.8276
5-1B-3	0.0101	3.8357	2.3857	2402.1059
5-1B-4	0.0061	3.7607	2.3390	3885.8950
5-1A-1	0.0070	3.6878	2.2937	3342.8857
5-1A-2	0.0087	3.9373	2.4489	2871.0361
5-1A-3	0.0100	4.0891	2.5433	2595.1762
5-1A-4	0.0091	3.3973	2.1130	4173.7627
5-1A-5	0.0060	3.4984	2.1759	3648.2817
5-1A-6	0.0082	6.6682	4.1474	5154.3134
5-1A-7	0.0071	3.3388	2.0766	2956.8496
5-1A-8	0.0060	3.3429	2.0792	3494.6347
5-1A-9	0.0101	4.0933	2.5459	2568.3842
5-1A-10	0.0121	4.4086	2.7420	2324.8398
5-1A-11	0.0060	3.2296	2.0087	3405.7451
5-1A-12	0.0049	3.0642	1.9058	3911.5190
5-2A-1	0.0081	4.0231	2.5035	3150.2334
5-2A-2	0.0100	4.4834	2.7761	2839.2421
5-2A-3	0.0059	3.8079	2.3684	4059.6308
5-2A-4	0.0079	4.1190	2.5619	3301.7153
5-2A-5	0.0068	4.0089	2.4934	3712.6088
5-2A-6	0.0055	3.7515	2.3333	4312.5791
5-2A-7	0.0063	3.8611	2.4014	3842.0307
5-3A-1	0.0083	3.7782	2.3499	2892.2158
5-3A-2	0.0062	3.3457	2.0809	3410.2919
5-3A-3	0.0102	4.0557	2.5225	2521.0752
5-3A-4	0.0054	3.1819	1.9790	3729.1709
5-3A-5	0.0057	3.2046	1.9932	3531.8691
5-3A-6	0.0067	3.5178	2.1879	3304.5639
5-4A-1	0.0080	2.4919	1.5498	1953.8479
5-4A-2	0.0099	2.6667	1.6586	1693.7900
5-4A-3	0.0050	2.4268	1.5094	3036.4086
5-4A-4	0.0054	2.2772	1.3852	2573.8994
5-4A-5	0.0059	2.2603	1.4058	2378.1054

Table XXII. H₂O Emission Concentration Data (Continued)

TEST	FA	H200A	H20PW	H20DX
5-5A-1	0.0084	4.0724	2.5329	3077.5053
5-5A-2	0.0105	4.6000	2.8611	2778.5488
5-5A-3	0.0073	4.0929	2.5456	3533.4404
5-5A-4	0.0075	4.1776	2.5984	3505.6928
5-5A-5	0.0076	4.1479	2.5799	3446.5195
5-5A-6	0.0078	4.1884	2.5050	3374.3564
5-7A-1	0.0080	3.7079	2.3062	2948.5341
5-7A-2	0.0118	4.3813	2.7250	2361.0219
5-7A-3	0.0157	4.8579	3.0215	1971.7475
5-7A-4	0.0228	4.8022	2.9868	1353.8017
5-7A-5	0.0086	3.4330	2.1352	2527.3154
5-7A-6	0.0043	3.0346	1.8874	4454.5908
5-7A-7	0.0086	3.3103	2.0589	2445.1977
5-7A-8	0.0079	3.6294	2.2573	2893.3149
5-7A-9	0.0050	3.4886	2.1698	4401.5556
5-8A-1	0.0085	3.9646	2.4658	2946.8525
5-8A-2	0.0129	4.3736	2.7202	2165.0629
5-8A-3	0.0173	4.5400	2.8237	1678.8613
5-8A-4	0.0241	4.8958	2.9206	1256.1826
5-8A-5	0.0075	4.4258	2.7527	3710.4199
5-8A-6	0.0072	4.4172	2.7473	3893.7710
5-8A-7	0.0066	4.3310	2.6938	4109.5918

APPENDIX XIV

PERFORMANCE PARAMETERS

Table XXIII contains derived performance parameters in tabular form for tests conducted using combustors A and B. The parameters listed are FA, PSAR, PHIP, PSFR, and PHINT.

Table XXIII. Performance Parameters

TEST	FA	PSAR	PHIP	PSFR	PHINT
1-1A-1	0.0039	0.1300	0.1236	-	-
1-1A-2	0.0080	0.1300	0.2527	-	-
1-1A-3	0.0083	0.8600	0.2606	-	-
1-1A-4	0.0039	0.8600	0.1250	-	-
1-1A-5	0.0122	0.8600	0.3828	-	-
1-1A-6	0.0183	0.8600	0.5755	-	-
1-1A-7	0.0120	0.8600	0.3796	-	-
1-1A-8	0.0121	0.8600	0.3833	-	-
1-1A-9	0.0123	0.8600	0.3875	-	-
1-1A-10	0.0040	0.8600	0.1275	-	-
1-1A-11	0.0039	0.8600	0.1258	-	-
1-1A-12	0.0027	0.8600	0.0878	-	-
1-1A-13	0.0067	0.8600	0.2133	-	-
1-1A-14	0.0080	0.8600	0.2546	-	-
1-1A-15	0.0060	0.8600	0.1901	-	-
1-1A-16	0.0039	0.8600	0.1246	-	-
1-1A-17	0.0123	0.8600	0.3861	-	-
1-1A-18	0.0165	0.8600	0.5193	-	-
1-1A-19	0.0188	0.8600	0.5926	-	-
1-1A-20	0.0081	0.8600	0.2561	-	-
1-1B-1	0.0082	0.8600	0.2606	-	-
1-1B-2	0.0038	0.8600	0.1209	-	-
1-1B-3	0.0122	0.8600	0.3834	-	-
1-1B-4	0.0041	0.8600	0.1315	-	-
1-1B-5	0.0083	0.8600	0.2613	-	-
1-1B-6	0.0125	0.8600	0.3933	-	-
1-1B-7	0.0189	0.8600	0.5925	-	-
1-1B-8	0.0200	0.8600	0.6305	-	-
1-1B-9	0.0122	0.8600	0.3854	-	-
1-1B-10	0.0185	0.8600	0.5822	-	-
1-1B-11	0.0084	0.8600	0.2645	-	-
1-1B-12	0.0082	0.8600	0.2578	-	-
1-1B-13	0.0083	0.8600	0.2625	-	-
1-1B-14	0.0084	0.8600	0.2642	-	-
1-1B-15	0.0082	0.8600	0.2575	-	-
1-1B-16	0.0081	0.8600	0.2573	-	-
1-1B-17	0.0061	0.8600	0.1943	-	-
1-1B-18	0.0102	0.8600	0.3202	-	-
1-1B-19	0.0082	0.8600	0.2582	-	-
1-1B-20	0.0062	0.8600	0.1944	-	-

Table XXIII. Performance Parameters (Continued)

TEST	FA	FSAR	PHIP	PSFR	PHINT
4-1A-1	0.0062	0.1300	0.7643	-	
4-1A-2	0.0084	0.1300	1.0248	-	
4-1A-3	0.0039	0.1300	0.4822	-	
4-1A-4	0.0102	0.1300	1.2554	-	
4-1A-5	0.0080	0.1300	0.9934	-	
4-1A-6	0.0039	0.1300	0.4840	-	
4-1A-7	0.0102	0.1300	1.2557	-	
4-1A-8	0.0061	0.1300	0.7511	-	
4-1A-9	0.0085	0.1300	0.5082	0.9408	0.1831
4-1A-10	0.0125	0.1300	0.4991	0.4798	0.3516
4-1A-11	0.0166	0.1300	0.4967	0.3218	0.5212
4-1A-12	0.0206	0.1300	0.4996	0.2447	0.6901
4-1A-13	0.0054	0.1300	0.4980	1.6580	0.1014
4-1A-14	0.0104	0.1300	0.9836	3.3018	0.1204
4-1A-15	0.0163	0.1300	0.4944	0.3251	0.5131
4-1A-16	0.0174	0.1300	0.9952	1.8609	0.2171
4-1A-17	0.0166	0.1300	1.0057	0.9655	0.4248
4-1A-18	0.0208	0.1300	1.0057	0.6449	0.6359
4-1A-19	0.0146	0.1300	1.2497	2.2904	0.2471
4-1A-20	0.0075	0.1300	0.3799	0.6963	0.1772
3-1A-1	0.0072	0.2100	0.5997	-	
3-1A-2	0.0092	0.2100	0.7620	-	
3-1A-3	0.0124	0.2100	1.0193	-	
3-1A-4	0.0144	0.2100	1.1852	-	
3-1A-5	0.0042	0.2100	0.3463	-	
3-1A-6	0.0133	0.2100	0.7660	2.2954	0.2357
2-1A-1	0.0059	0.3100	0.3671	-	
2-1A-2	0.0091	0.3100	0.5618	-	
2-1A-3	0.0132	0.3100	0.8146	-	
2-1A-4	0.0162	0.3100	1.0023	-	
2-1A-5	0.0196	0.3100	1.2086	-	
2-2A-1	0.0040	0.3100	0.2476	-	
2-2A-2	0.0060	0.3100	0.3727	-	
2-2A-3	0.0080	0.3100	0.4966	-	

Table XXIII. Performance Parameters (Continued)

TEST	FA	PSAR	PHIP	PSFR	PHINT
2-3A-1	0.0061	0.3100	0.3790	-	
2-3A-2	0.0082	0.3100	0.5069	-	
2-3A-3	0.0134	0.3100	0.8279	-	
2-3A-4	0.0113	0.3100	0.7000	-	
2-3A-5	0.0093	0.3100	0.5740	-	
2-3A-6	0.0081	0.3100	0.5035	-	
2-3A-7	0.0040	0.3100	0.2482	-	
2-3A-8	0.0050	0.3100	0.3126	-	
2-3A-9	0.0060	0.3100	0.3738	-	
2-1B-1	0.0039	0.3100	0.2443	-	
2-1B-2	0.0086	0.3100	0.3756	2.3927	0.1352
2-1B-3	0.0158	0.3100	0.3763	0.6278	0.5167
2-1B-4	0.0196	0.3100	0.3751	0.4479	0.7213
2-1B-5	0.0119	0.3100	0.5031	2.1558	0.2259
2-1B-6	0.0160	0.3100	0.5072	1.0493	0.4697
2-1B-7	0.0200	0.3100	0.5079	0.7013	0.7044
2-1B-8	0.0160	0.3100	0.7562	3.2359	0.2996
2-1B-9	0.0200	0.3100	0.7556	1.5762	0.6142

Table XXIII. Performance Parameters (Continued)

TEST	FA	PSAR	PHIP	PSFK	PHINT
5-1B-1	0.0040	0.1300	0.4923	-	-
5-1B-2	0.0081	0.1300	0.9999	-	-
5-1B-3	0.0101	0.1300	1.2501	-	-
5-1B-4	0.0061	0.1300	0.7547	-	-
5-1A-1	0.0070	0.1625	0.7264	-	-
5-1A-2	0.0087	0.1613	0.9104	-	-
5-1A-3	0.0100	0.1638	1.0337	-	-
5-1A-4	0.0051	0.1608	0.5401	-	-
5-1A-5	0.0060	0.1608	0.6367	-	-
5-1A-6	0.0082	0.1636	0.8480	-	-
5-1A-7	0.0071	0.1643	0.7368	-	-
5-1A-8	0.0060	0.1609	0.6347	-	-
5-1A-9	0.0101	0.1618	1.0566	-	-
5-1A-10	0.0121	0.1617	1.2605	-	-
5-1A-11	0.0060	0.1628	0.6230	-	-
5-1A-12	0.0049	0.1621	0.5161	-	-
5-2A-1	0.0081	0.1761	0.7864	-	-
5-2A-2	0.0100	0.1730	0.9842	-	-
5-2A-3	0.0059	0.1738	0.5826	-	-
5-2A-4	0.0079	0.1746	0.7735	-	-
5-2A-5	0.0068	0.1740	0.6708	-	-
5-2A-6	0.0055	0.1742	0.5390	-	-
5-2A-7	0.0063	0.1746	0.6220	-	-
5-3A-1	0.0083	0.1799	0.7898	-	-
5-3A-2	0.0062	0.1793	0.5937	-	-
5-3A-3	0.0102	0.1780	0.9834	-	-
5-3A-4	0.0054	0.1798	0.5146	-	-
5-3A-5	0.0057	0.1791	0.5493	-	-
5-3A-6	0.0067	0.1797	0.6432	-	-
5-4A-1	0.0080	0.1740	0.7931	-	-
5-4A-2	0.0099	0.1736	0.9830	-	-
5-4A-3	0.0050	0.1737	0.4961	-	-
5-4A-4	0.0054	0.1738	0.5371	-	-
5-4A-5	0.0059	0.1733	0.5918	-	-

Table XXIII. Performance Parameters (Continued)

TEST	FA	PSAR	PHIP	PSFR	PHINT
5-5A-1	0.0084	0.1647	0.8628	-	-
5-5A-2	0.0105	0.1646	1.0821	-	-
5-5A-3	0.0073	0.1652	0.7525	-	-
5-5A-4	0.0075	0.1653	0.7741	-	-
5-5A-5	0.0076	0.1651	0.7825	-	-
5-5A-6	0.0078	0.1649	0.8080	-	-
5-7A-1	0.0080	0.8531	0.2518	-	-
5-7A-2	0.0118	0.8533	0.3729	-	-
5-7A-3	0.0157	0.8545	0.4966	-	-
5-7A-4	0.0228	0.8551	0.7197	-	-
5-7A-5	0.0086	0.8538	0.2720	-	-
5-7A-6	0.0043	0.8534	0.1358	-	-
5-7A-7	0.0086	0.8537	0.2711	-	-
5-7A-8	0.0079	0.8543	0.2508	-	-
5-7A-9	0.0050	0.8545	0.1581	-	-
5-8A-1	0.0085	0.3141	0.5191	-	-
5-8A-2	0.0129	0.3134	0.7840	-	-
5-8A-3	0.0173	0.3136	1.0536	-	-
5-8A-4	0.0241	0.3148	1.4618	-	-
5-8A-5	0.0075	0.3088	0.4657	-	-
5-8A-6	0.0072	0.3092	0.4424	-	-
5-8A-7	0.0066	0.3091	0.4108	-	-

REFERENCES

1. Roberts, et al. An Analytical Model for Nitric-Oxide Formation in a Gas Turbine Combustion Chamber, AIAA Paper 71-715, 1971.
2. Clark, J. S., "The Relation of Specific Heat Release to Pressure Drop in Aero-Gas-Turbine Combustion Chambers," Proceedings of the 1955 IME-ASME Conference on Combustion, 1955, pp 354-361.
3. Kind, C., and T. Youssef, "Calculating the Flow in the Combustion Chamber of Gas Turbines," Brown Boveri Review, Vol 51, 1964, pp 808-816.
4. Wise, H., J. Lorell, and B. J. Wood, "The Effects of Chemical and Physical Parameters on the Burning Rate of a Liquid Droplet," Fifth Symposium (International) on Combustion, The Combustion Institute, 1955, pp 132-141.
5. Wood, B. J., W. A. Rosser, and H. Wise, "Combustion of Fuel Droplets," AIAA Journal, Vol 1, 1963, pp 1076-1081.
6. Brinkley, S. R., "Computational Methods in Combustion Calculations," Combustion Processes, Sect C: High Speed Aerodynamics and Jet Propulsion, Vol 2, B. Lewis, R. S. Pease, and H. S. Taylor, Editors, Princeton University Press, Princeton, New Jersey, 1956.
7. Brinkley, S. R., "Calculation of the Thermodynamic Properties of Multi-Component Systems and Evaluation of Propellant Performance Parameters," Proceedings of the First Conference on Kinetics, Equilibrium and Performance of High Temperature Systems, G. S. Bahá and E. E. Zukowski, Editors, The Combustion Institute, 1960, pp 74-81.
8. Winterfeld, G., "On Processes of Turbulent Exchange Behind Flameholders," 10th Symposium (International) on Combustion, The Combustion Institute, 1965, pp 1265-1275.
9. Alptekin, L. J., "Turbulent Mixing of Coaxial Jets," AIAA Journal, Vol 2, No. 9, 1964, pp 1560-1567.
10. Computer Program for the Analysis of Annular Combustors, Volume I: Computational Procedures, Report 1111-1, 1968, Northern Research and Engineering Corp, Cambridge, Massachusetts.
11. Abramovich, G. N., The Theory of Turbulent Jets, MIT Press, Cambridge, Massachusetts, Chapter 12, Section 4, 1963.

12. Williams, F. A., Combustion Theory, Addison-Wesley, Reading, Massachusetts, 1965, pp 56-57.
13. Dickerson, R. A., and M. D. Schuman, "Rate of Aerodynamic Atomization of Droplets," Journal of Spacecraft, Vol 2, 1965, pp 99-100.
14. Edelman, R. B., and O. F. Fortune, A Quasi-Global Chemical Kinetic Model for the Finite Rate Combustion of Hydrocarbon Fuels with Application to Turbulent Burning and Mixing in Hypersonic Engines and Nozzles, AIAA Paper 69-86, New York, New York, 1969.
15. Browne, W. G., R. P. Porter, J. D. Verline, and A. H. Clark, "A Study of Acetylene-Oxygen Flames," Twelfth Symposium (International) on Combustion, The Combustion Institute, 1969, pp 1035-1047.
16. Cooke, D. F., and A. Williams, "Shock-Tube Studies of the Ignition and Combustion of Ethane and Slightly Rich Methane Mixtures with Oxygen," Thirteenth Symposium (International) on Combustion, The Combustion Institute, 1971, pp 757-766.
17. Sorensen, S. C., P. S. Myers, and O. A. Uyehara, "Ethane Kinetics in Spark-Ignition Engine Exhaust Gases," Thirteenth Symposium (International) on Combustion, The Combustion Institute, 1971, pp 451-459.
18. Baker, R. R., R. R. Balwin, R. W. Walker, "The Use of the $H_2 \cdot O_2$ Reaction in Determining the Velocity Constants of Elementary Reactions in Hydrocarbon Oxidation," Thirteenth Symposium (International) on Combustion, The Combustion Institute, 1971, pp 291-299.
19. Benson, S. W., and G. R. Haugen, "Mechanisms for Some High-Temperature Gas-Phase Reactions of Ethylene, Acetylene, and Butadiene," J. Phys Chem, Vol 71, 1967, pp 1735-1746.
20. Camac, M., and R. M. Feinberg, "Formation of NO in Shock-Heated Air," Eleventh Symposium (International) on Combustion, The Combustion Institute, 1966, pp 137-145.
21. Bauleh, D. L., D. D. Drysdale, D. G. Horne, and A. C. Lloyd, Critical Evaluation of Rate Data for Homogeneous, Gas Phase Reactions of Interest in High-Temperature Systems, No. 1-1, 1968-1969, Department of Physical Chemistry, Leeds University, England.
22. Franklin, J. L., "Mechanisms and Kinetics of Hydrocarbon Combustion," Annual Review of Physical Chemistry, edited by H. Eyring, C. J. Christensen, and H. S. Johnston, Annual Reviews, Inc., Palo Alto, California, 1967, pp 261-282.
23. Drysdale, D. D., and A. C. Lloyd, "Gas Phase Reactions of the OH Radical," Oxidation and Combustion Revs, Vol 4, 1970, pp 157-250.

24. Bogdan, L., and H. T. McAdams, Analysis of Aircraft Exhaust Emissions Measurements, CAL Report No. NA-5007-K-1, Cornell Aeronautical Laboratory, Inc., Buffalo, New York, 1971.
25. Shipman, C. W., and N. M. Howe, Jr., "A Tentative Model for Rates of Combustion in Confined Turbulent Flames," Tenth Symposium (International) on Combustion, The Combustion Institute, 1965, pp 1139-1149.
26. Dugger, G. L., D. M. Simon, and M. Gerstein, Laminar Flame Propagation, NACA Report 1300, Chapter IV, 1957.
27. Fenimore, C. P., and G. W. Jones, "Water Catalyzed Oxidation of Carbon Monoxide by Oxygen at High Temperature," Journal of Physical Chemistry, Vol 61, 1957, pp 651-654.
28. "Procedure for the Continuous Sampling and Measurement of Gaseous Emissions from Aircraft Turbine Engines," Aerospace Recommended Practice (ARP) 1256, Society of Automotive Engineers, 1971.
29. The Design and Performance Analysis of Gas-Turbine Combustion Chambers, Volume II, NREC Report No. 1082-2, Northern Research and Engineering Corporation, Cambridge, Massachusetts, and London, England, 1964.
30. Briebl, D. and L. Papathakos, Use of An Air-Assist Fuel Nozzle to Reduce Exhaust Emissions from a Gas-Turbine Combustor at Simulated Idle Conditions, NASA TN D-6404, August 1971.
31. Blazowski, W. S. and R. E. Henderson, Assessment of Pollution Measurement and Control Technology and Development of Pollution Reduction Goals for Military Aircraft Engines, AFAP1-TT-72-102, Air Force Aero Propulsion Laboratory, Wright Patterson Air Force Base, Ohio, 1972.